



Experimental Study of Single Sided Ventilation Through a Multi-Configuration Slotted Louvre System

by

Paul D. O'Sullivan

A thesis submitted in partial fulfillment for the
degree of Doctor of Philosophy

in the
College of Engineering, Design and Physical Sciences
Department of Mechanical, Aerospace and Civil Engineering

June 2018

“The time you enjoy wasting is not wasted time.”

Bertrand Russell

Abstract

Evidence based performance of novel ventilation systems in existing low energy buildings is invaluable as it provides data on the system operation in a real dynamic environment. This thesis presents the outcomes from research involving a number of experimental field studies of a single sided ventilation system installed in a single cell office space as part of a building retrofit pilot project in Cork, Ireland. The solution consists of a purpose provided, multi configuration opening, comprising a narrow slotted architectural louvre component split across a low level manual opening section and a high level automated opening section. A review of published research found that little experimental data exists on the performance of such systems and airflow rate correlations developed for plain openings are currently used by designers to make predictions about their performance. Three experimental campaigns were designed and carried out. First, in order to quantify performance of the system, long term and short term monitoring of the internal thermal and airflow environment at the experimental building was completed. Second, ventilation rate measurements in existing and retrofit spaces were completed using a tracer gas concentration decay technique. Thirdly, airflow through the single sided slot louvre opening was investigated. In addition, the annual cooling potential of the multi-configuration system was investigated computationally. Results show there was a significant difference between both thermal environments with the retrofit space consistently displaying lower air temperatures over the cooling season and throughout all Air Change Rate measurement periods. Lower levels of vertical thermal stratification and diurnal temperature variation were also observed. On average, across a wide range of boundary conditions, lower ventilation rates were observed for the slotted louvre system with a narrower spread of values when compared with the existing building. The dominant driving force was either buoyancy or wind depending on the opening configuration adopted in the slotted louvre system. The slot louvre was found to be wind dominant for lower opening heights when compared with a plain opening of the same dimensions. Existing single sided correlations were found to perform better when predicting airflow rates through a plain opening when compared with the slot louvre system and a new dimensionless exchange rate parameter is proposed for predicting wind driven airflow through the slot louvre. Simulations indicate that 80% of annual occupied hours required an enhanced ventilative cooling airflow rate to achieve internal thermal comfort. Using a combination of configurations the system was able to provide the required cooling airflow rate for 93% of the occupied hours.

Acknowledgements

The completion of this thesis would not have been possible without the continued support, advice and patience of many people. Undertaking a PhD part time, while trying to maintain a balanced approach to the different demands of life outside study, is challenging and near impossible at best.

Firstly and most importantly, my supervisor Prof. Maria Kolokotroni who consistently displayed great patience and experience throughout the entire 6 years of research and continuously provided valuable and necessary advice and guidance, keeping me on the straightest path to the end goal, despite my endless attempts to drift off beat and into uncertainty scorched desert of distraction. Studying remotely from your supervisor puts an increased importance on being able to engage in tricky and nuanced discussions by telephone and email without losing focus and Prof. Kolokotroni guided the work superbly in this regard. I have learnt a lot from her.

I would like to acknowledge the support of my employer and source of funding Cork Institute of Technology. In particular, Dr Matt Cotterall, Head of School for Mechanical, Electrical and Process Engineering, who provided much support and encouragement, facilitating the investment of time and finances in the research project. My thanks also go to my colleague Dr. Michael D Murphy, who provided valuable advice during the experimental design and setup stage and was the sounding board for various ideas on many a dark winter evening in the offices at CIT.

I would also like to extend my acknowledgements to my colleagues from IEA-EBC Annex 62, in particular Prof. Per Heiselberg, Dr Guilherme Carrilho da Graca and the late Prof. Hisashi Kotani, for many a lively discussion about ventilative cooling and single sided ventilation applications amongst other topics. There is much to learn in such company.

To Damien Ryan, Ger Rasmussen and Liam Carroll for their support with the development of instrumentation supports and cabling solutions for experimental measuring campaigns. To members of the zero2020 research team, Fergus Delaney, Adam O'Donovan and Daithi Fallon who shared and continue to share in solutions to many teething problems at the testbed in CIT.

My deepest gratitude is extended to my parents, Terry and Colette, their boundless source of understanding was a great help when progress was slow or things weren't going as planned. Another lifelong student finally out of their hair. My thanks to my brothers for their support and in particular Ian for sharing in the frustrations and challenges associated with doctoral research along the way. To Sarah, who made more sacrifices than anyone else and who is the only one that has accompanied me on the journey from the outset, entertaining my many failings as well as reminding me of my strengths when I was struggling. To Karen, for being Chuffin and for all the late night conversations, support and advice on the home stretch to see it safely over the line, hah.

Finally, to my beautiful children Maximilian and Beatrice, who will now have a Father that has the head-space to respond sooner than the seventh "daaaaddy!" call.

Contents

Abstract	ii
Acknowledgements	iii
List of Figures	vii
List of Tables	xiii
Abbreviations	xv
Symbols	xvi
1 Introduction	1
1.1 Research Motivation	1
1.1.1 Research context	1
1.1.2 IEA-EBC Annex 62 and VC at zero2020, CIT	3
1.2 Research Objectives	5
1.3 Research Methods	6
1.3.1 Full Scale performance: Long Term Overheating	6
1.3.2 Full Scale Performance: Air Change Rate (ACR)	7
1.3.3 Mapping and Prediction of the Airflow Rate with the Slot Louvre	7
1.3.4 Demonstration of Component Cooling Potential	8
1.4 Thesis Structure	9
1.5 Publications	11
1.5.1 Journal Articles	11
1.5.2 Conferences	11
1.5.3 Additional Related Co-Authored Publications	12
2 Single Sided VC in Building Retrofit	13
2.1 Delivering Energy Performance in Existing Buildings	13
2.1.1 Energy performance in commercial Offices	14
2.1.2 Motivation and barriers to deep building retrofit	16
2.1.3 Strategies for deep building retrofit	16
2.1.4 Thermal comfort and low energy building retrofits	19
2.2 Overheating in free running Low energy buildings	19
2.2.1 Evidence of overheating in the existing building stock	19
2.2.2 Quantifying the effects of overheating	20
2.2.3 Method for Defining Long Term Overheating	22
2.3 VC as a Mitigation Strategy	24
2.3.1 Definition and justification for passive VC	24

2.3.2	Extending the performance of VC	25
2.3.3	Estimating cooling potential	27
2.3.4	Barriers to the adoption of passive VC	29
2.4	Single Sided Ventilation	32
2.5	Driving Forces in Single Sided Ventilation	33
2.5.1	Single sided ventilation from buoyancy alone	34
2.5.2	Single sided ventilation from wind alone	36
2.5.3	Combined Wind and Buoyancy	42
2.6	Existing Single Sided Empirical Correlations	45
2.6.1	de Gids & Pfaff	46
2.6.2	Warren	46
2.6.3	Dascalaki & Argiriou	47
2.6.4	Larsen	47
2.6.5	Caciolo	48
2.6.6	Tang	49
2.6.7	FprEN 16798-7	49
2.7	Slotted Architectural Ventilation Openings	49
2.7.1	Recent Investigations of airflow through slotted openings	52
2.8	Characterising unsteady air movement	53
2.8.1	Spectral Analysis	55
2.8.2	Air movement and Thermal Comfort	59
2.9	Conclusions of the Literature Review	61
3	Experimental Field Studies	63
3.1	Description of the Building Retrofit Solution	63
3.1.1	Design criteria	64
3.1.2	zero2020 Architectural Concept	65
3.1.3	Envelope Components	66
3.1.4	Installation	70
3.1.5	Energy Performance	70
3.2	Description of the MCSL System	71
3.3	Description of Experimental Field Studies	72
3.3.1	Full Scale OH Performance: Experimental Setup	74
3.3.2	Full Scale ACR performance: Experiment Setup	75
3.3.3	Mapping and Prediction of Airflow with the Slotted Louvre: Experiment Setup	81
3.4	Processing of raw experimental data	90
3.4.1	General Data Storage structure	90
3.4.2	2013 testing	91
3.4.3	2014 testing	92
4	Pre and Post Retrofit Ventilation Performance	96
4.1	Full Scale Performance: Long term overheating	96
4.1.1	Percentage Hours above static threshold	97
4.1.2	Assessment using CIBSE adaptive Criteria	97
4.1.3	Discussion	100
4.2	Full Scale Performance: ACR	100
4.2.1	Wind Boundary Conditions	100
4.2.2	Internal Environment Measurements	101
4.2.3	ACR Measurements	104
4.2.4	Analysis	106
4.3	Conclusion	115

5	Mapping and Prediction of Airflow Rate with the Slot Louvre System	117
5.1	U_i/U_r measurements	117
5.2	ACR Measurements	118
5.3	Analysis	120
5.3.1	Non-Dimensional Analysis	120
5.3.2	Sensitivity Study of Influential Boundary Parameters	121
5.3.3	Airflow Characteristics at the Opening	122
5.3.4	Performance of Existing Correlations	125
5.3.5	Discussion	127
5.4	Airflow Characteristics at the Occupant Location	130
5.4.1	Occupant location temperature data	130
5.4.2	Airflow Characteristics at the occupant location	131
5.5	Conclusion	138
6	Ventilative Cooling Potential of the Slot Louvre System	141
6.1	Introduction	141
6.2	Methodology: Component Cooling Potential	142
6.2.1	ACR for RS.02	143
6.2.2	ACR for RS.04	144
6.2.3	ACR for RS.03	144
6.3	Results	145
6.3.1	Model Inputs	145
6.3.2	Climate VC potential	146
6.3.3	ACR Profiles: Required and Predicted	148
6.4	Analysis	151
6.4.1	ACR profile matching, N_{re} vs N_{pr}	152
6.4.2	Optimum Opening Schedule	154
6.4.3	Parametric Analysis	156
6.5	Conclusion	159
7	Overall Conclusion & Future Work	161
7.1	General Overview	161
7.1.1	Primary Conclusions	162
7.2	Practical Implications for Designers and Researchers	165
7.3	Future Work	165
7.3.1	Future Research ideas	165
A	Single Sided Ventilation Measurement Techniques	184
A.1	Properties of Tracer Gases	185
A.2	Mixing	186
A.3	Tracer Gas Analysers	186
A.4	Analytical Methods	187
A.4.1	Tracer Decay, Two Point Average Decay Method	188
A.4.2	Tracer Decay, Regression Method	189
A.4.3	Constant Concentration	191
B	IEA-EBC Annex 62 VC Potential Analysis	193
B.1	Calculate Heat Gains	194
B.2	Thermal Comfort Threshold Temperatures	195
B.3	VC modes	196

List of Figures

1.1	zero2020 retrofit testbed at CIT. The slot louvre ventilation openings are visible along the fenestration sections.	4
1.2	Control and retrofit spaces used for ACR and Internal Thermal Environment measuring campaign during summer 2013	5
1.3	Data logging equipment and typical indoor space used for full scale overheating performance measuring campaign during May - September 2013	8
1.4	Examples of experimental set up in the cellular office for measuring campaign during summer 2014. Refer to Figure 3.22, page 86 for details on the layout shown in (A) above. For the 2013 testing layout see Figure 3.16, page 79	8
1.5	Information flowchart outlining the structure of the thesis and how individual chapters link with work carried out. Details regarding the scope at each stage are also included	10
2.1	Commercial and Public Services final energy use by fuel for Ireland - 1990 to 2015 [26]	14
2.2	Percentage split for various VC operating modes for annual occupied hours . . .	15
2.3	Reported Motivating factors and barriers in decision making for building energy retrofits. reproduced from [32]	17
2.4	Worker productivity performance as a function of indoor temperature and mean thermal sensation vote. Reproduced from [38] and [39]	18
2.5	Scatter plot of relationship between MTSV and operative temperature ramp from the start to the finish of a test. Colour indicates the operative temperature at the end of the test using an arithmetic mean of the last two minutes. [72]	27
2.6	Ranges for heating, free-cooling and mechanical cooling when the free running temperature is higher than the outdoor temperature. The left side shows how the indoor temperature will track along the comfort ranges. [74]	28
2.7	Map of mean climatic cooling potential (Kh/night) in July based on Meteonorm data	29
2.8	Various interactions between urban climate and canyons [85]	31
2.9	Various single sided strategies for cooling purposes. Reproduced from CIBSE AM 10 [90]	34
2.10	Single Sided ventilation with one opening driven by buoyancy alone	35
2.11	Two way symmetrical exchange of entrained air in a turbuent shear mixing layer. 38	
2.12	Velocity distributions inside a single opening; aspect ratio of opening is 2, external free stream velocity is $6m/s$, [94]	39
2.13	Ratio of local wind velocity to reference wind velocity from measurements by Warren [97]	40
2.14	Ratio of local wind velocity to reference wind velocity from measurements by Warren [97]	41
2.15	Variation of density with temperature according to the ideal gas law and the boussinesq approximation	44
2.16	Warren Plot of F_r versus $Ar^{0.5}$ used for differentiating ventilation rate measurements depending on the dominate force generating airflow. Buoyancy asymptote shown in red. data close to this are generally driven by buoyancy forces alone. [97] 45	

2.17	Passivent Purpose Provided Aircool Ventilator using external louvre, multileaf damper and internal grille	51
2.18	Purpose provided louvre solution at St Patricks Place, Cork City, Ireland	51
2.19	Swiss prison Champ-Dollon incorporating slat type slotted louvres and internal insulated doors for single sided ventilation	52
2.20	EPFL GC Building in Switzerland utilising PPO design for natural ventilation purposes.	52
2.21	Schematic illustration of the different layers of the planetary boundary layer above an urban area. The urban boundary layer (UBL) is divided into a mixed layer (ML), inertial sublayer (IS) and surface layer (SL), which in turn is divided into a roughness sublayer (RS) and an urban canopy layer (UCL). [125]	54
2.22	The time history of the axial component of velocity on the centreline of a turbulent jet. [126]	54
2.23	Time series of air velocity and power spectrum for the different samples. [134]	58
2.24	Relationship between power spectrum fluctuations and the frequency exponent β [134]	58
2.25	Variation of β with velocity for different sources of natural and mechanical wind [133]	59
2.26	Reproduced from CIBSE TM52. EN15251 allowance for elevated air speed effects on thermal comfort [21]	60
3.1	External view of the zero2020 testbed envelope upgrade	64
3.2	Plan layout for the zero2020 testbed space at CIT. First floor only. Room used for experimental work shown in red border. Further details of experimental setup for different measurement campaigns in Chapters 4 & 5	65
3.3	Left: Waterford campus 1969, Middle: existing structure table concept, Right: existing structure grid concept	66
3.4	External retrofit opaque wall construction build up. (reproduced courtesy of Henry J Lyons Architects)	67
3.5	External retrofit opaque roof construction build up. (reproduced courtesy of Henry J Lyons Architects)	67
3.6	External retrofit glazing module build up. (reproduced courtesy of Henry J Lyons Architects)	69
3.7	External retrofit glazing module build up. (reproduced courtesy of Henry J Lyons Architects)	70
3.8	Energy consumption data for 2013 to 2016 categorised according to user type.	71
3.9	Purpose Provided Narrow Slotted Architectural Louvres and Insulated Ventilation Doors. Left: Detail section of openings, Right: Installed Combined glazing and ventilation modules.	72
3.10	Part site map of cork institute of technology. Location of control and retrofit spaces shown in red and orange respectively.	75
3.11	Dimensioned locations for control space and retrofit space chosen for field study. Overall facade width approximately 22m	76
3.12	3D obstacle study of control and retrofit space. Surrounding obstacles included in calculation of C_p values shown in yellow	76
3.13	C_p generator polar plots of obstacle correction factors	76
3.14	C_p characteristics for control and retrofit spaces as a function of wind incidence angle	77
3.15	NDIR sensor being installed into protective housing for external mounting	78
3.16	Instrument and equipment positioning for July-August 2013 measurement campaign. (Legend: Orange - CO_2 NDIR; Green - Vertical precision thermistors; Grey - External CO_2 NDIR; Blue - Corridor CO_2 NDIR; Red - CO_2 Cylinder and Injection point)	79
3.17	Roof mounted weather station with recommissioned Campbell Scientific instrumentation. See Table 3.7 for instrument specifications	80

3.18	Plain Opening in retrofit space used for comparing with slotted louvre. The existing individual louvre sections normally screwed into the facade frame (see figure 3.9) were removed and replaced with a single mock up louvre shown in Figure 3.19	82
3.19	Left: Louvre module used for testing. Middle: louvre opening. Right: External facade of the testbed building showing the pre and post retrofit (see www.zero2020energy.com for more details). Integrated vertical slotted louvre banks also visible	83
3.20	Plan and elevation drawings of various opening types measured including main dimensioning. Net free opening area for each case, A_o , shown coloured, with the m^2 value below each plan drawing. Slot louvre, L, with 2 cases, L1 & L2. Plain opening, P, with 3 cases, P1, P2 & P3. Blanking plates used to create reduced H_o, W_o dimensions shown in dark grey	84
3.21	Typical CO ₂ decay profiles (Test 35, 11th Sept 2014, case P2). Test start time, Optimum decay Time and data collection end time shown as vertical red lines. CO is adjacent corridor CO ₂ sensor and EX is external CO ₂ sensor. Figure 3.22 shows sensor locations	85
3.22	Experiment setup details. Left: Building section showing heights and depths of instrument positions. Right top: Overall testbed first floor plan with test room marked in red. Right bottom: Dimensions of CO ₂ and Temperature measuring locations	86
3.23	experimental room setup showing internal instrument layout and cylinder injection location with mixing fan used for CO ₂ dispersion	86
3.24	Alphasense CO ₂ NDIR sensors used for measurement of concentration levels during TGCD ACR testing.	87
3.25	3D Ultrasonic anemometer measuring boundary conditions.	88
3.26	Opening Anemometers shown for a Plain opening test in differing positions for differing wind directions. Slot Louvre configuration also shown	88
3.27	Experimental setup details for occupant location measurements. Temperature and RH measurement locations shown as red in section. Anemometers shown in green.	89
3.28	Schiltknecht Omni Directional Anemometers used to capture high speed air velocity data at a typical occupant location within the single zone office.	90
3.29	The framework concept which was broadly followed for filing, accessing and processing data. The folder structure for each experimental field study is also shown	91
3.30	Matrix showing the different sub sets of data depending on parameter and testing configuration	92
3.31	Structured filenames used for all .csv data to allow an efficient callign system within the analysis environment	93
3.32	R code used to process raw data files into working data files and eventually cleaned data for use in analysis	93
3.33	R code used to import cleaned data, assign to a dataframe, add to a list and begin applying analysis functions	94
4.1	Heat-map of indoor air temperature in open plan office B294 (taken as operative temperature as discussed earlier)	98
4.2	Exceedance of overheating limits in open plan office B294 (taken as operative temperature as discussed earlier.)	98
4.3	Indoor Air Temperature as function of exponentially weighted running mean for B294)	99
4.4	Polar frequency plots of mean wind speed and direction for all 38 tests categorised according to configuration. Wind speed is plotted on the polar axis. For each data point shown, data is averaged over the test period using 5 minute recordings of wind speed and wind direction.	101

4.5	Mean vertical temperature profiles during different ACR tests for different configuration categorised according to whether STR was greater than 1.0 (bottom) or ACR was greater than 4.0 (Top)	102
4.6	Histogram for STR values for control and retrofit spaces categorised according to occupied and unoccupied hours	103
4.7	Boxplot of mean ACR, (h^{-1}), for each configuration	106
4.8	Natural logarithm of CN as a function of elapsed time for each test	107
4.9	Scatterplot of mean ventilation rates (h^{-1}) vs wind direction, (classified with ΔT_{ie} & σ_c)	108
4.10	Scatterplot of mean ventilation rates (h^{-1}) vs wind speed, (classified with ΔT_{ie} & σ_c)	109
4.11	e_c for all X combinations grouped according to F_R (vertical axis) and Ar (horizontal axis). Negative e_c values represent a modal shift with $F_{th,c}$ passing through F_R giving the critical C_D/β combination causing change in contribution from wind forces. Magnitude of e_c represents scale of modal shift.	112
4.12	Warren Plot for all CS and RS configurations varying F_{th} asymptotes included as dashed lines	114
4.13	Warren Plots for wind directions	115
5.1	Wind data for individual tests. Top Left: Mean wind speed, U_l and incidence angle, θ_l , measured local to the opening taken as local conditions at the opening. Top Right: U_r and θ_r measured at 6.0 metres above roof level (shown in red) and data taken from the nearby met station, Cork Airport (shown in blue), for the same 44 test periods. Bottom: Ratio of U_l/U_r for each test according to θ_r , with size of point proportional to U_r . Warren wind tunnel measurements shown in green, Adams equation for estimating U_l/U_r shown in orange.	118
5.2	Measured mean ACR values presented using discrete categories according to opening type and case (see Figure 3.20). Also shown is the sample mean (red square), standard deviation (red diamond).	119
5.3	Non-Dimensional Flow Number, F_r Vs adjusted Archimedes Number, $Ar^{0.5}$. Data categorised according to opening type and case (Figure 3.20)	120
5.4	Non-Dimensional Local Flow Number, F_l Vs Local wind speed, U_l for all plain opening cases only.	121
5.5	Elevations of openings selected in Table 5.2 showing dimensions of anemometer locations during windward and leeward tests. Dimensions were taken from inside of room facing outwards. Note: the origin (0,0) represents the south corner of the opening when considered in plan, i.e. the bottom right corners in Figure 3.20	124
5.6	Power spectra for wind velocity measured at the opening for high turbulence (windward) and low turbulence (leeward) tests. Opening boundary spectra (U_l) shown to the left. Top: Comparison of spectra for leeward tests & cases L1 and P1. Bottom: Windward tests. Axes are log transformed.	125
5.7	β for all velocity measuring positions within the opening according to mean test opening velocity categorised according to opening case tested. Size of each data point relative to mean boundary wind speed, U_l . Values used to calculate mean opening conditions in Table 5.2 coloured darker. Kernel density estimates for each case also shown	126
5.8	Comparison of existing correlations with measured ACR values for all tests. Axes are log transformed to accommodate large spread of predictions in some correlations. 25% error ranges shown as red dashed lines.	127
5.9	Section of slot louvre showing concave profile, with flow travelling normal to this profile when parallel along envelope. Airflow path shown coloured.	128
5.10	Time series data for velocities at the occupant location for different tests and opening cases.	131

5.11	Percentage opening area to floor area ratio, POF, for various non domestic buildings using VC in different countries. Buildings represented are case studies from IEA-EBC Annex 62. Case P1 shown in Blue. [172]	132
5.12	Histogram of all air speeds measured at all three locations for plain opening cases tested (shown as separate distributions). Each measuring location shown with gradient transparency and substantial overlapping exists for each.	133
5.13	Histogram of all air speeds measured at all three locations for Louvre opening cases tested (shown as separate distributions). Each measuring location shown with gradient transparency and substantial overlapping exists for each.	134
5.14	Empirical and theoretical density plots, Quantile-Quantile plots, probability-probability plots and cumulative distribution functions for air speed data at the occupant location during all L1 case tests.	134
5.15	Empirical and theoretical density plots, Quantile-Quantile plots, probability-probability plots and cumulative distribution functions for air speed data at the occupant location during all L2 case tests.	135
5.16	Box plot of 10 minute turbulence intensities calculated for all tests categorised according to case type and grouped into, from left to right; seated chest height, seated head height and standing head height.	135
5.17	Power spectra for air velocity measured at the three occupancy vertical locations for high boundary turbulence (windward) tests (see Table 5.6). Top: Comparison of spectra for L1. Bottom: Comparison of spectra for P1. Axes are log transformed.	136
5.18	Power spectra for air velocity measured at the three occupancy vertical locations for low boundary turbulence (Leeward) tests (see Table 5.2). Top: Comparison of spectra for L1. Bottom: Comparison of spectra for P1. Axes are log transformed.	138
5.19	Power spectra for air velocity measured at the three occupancy vertical locations for high indoor air temperature , test No. 17 of 44. Solid grey lines show the "fluctuation zone" important to human perception while the dashed lines represent the narrow zone shown to provide cooling at elevated temperatures.	138
5.20	Beta values for room air velocities at all occupancy measuring locations. All 3 vertical heights included. Data is categorised based on test case and grouped according to opening type.	139
6.1	Percentage split for various ventilative cooling operating modes for each individual month	147
6.2	Percentage split for various ventilative cooling operating modes for annual occupied hours	147
6.3	N_{re} probability distributions for 12 months based on results from equation 6.7 in VC Potential analysis tool. (converted from mass flowrate to ACR)	149
6.4	Mean monthly required ACR values, $\hat{N}_{re}(i)$ for month i including all 12 months in the annual calender, (A) Mean monthly ACR, (B) Annual normal distribution for \hat{N}_{re}	150
6.5	mean monthly required ACR values, \hat{N}_i for month i including all months in the annual calender	151
6.6	Ventilative Cooling State for January to April	152
6.7	Ventilative Cooling State for May to August	153
6.8	Ventilative Cooling states for September to December	153
6.9	Percentage of monthly occupied hours where the required ventilative cooling ACR rate is met with the predicted ACR for the particular configuration	155
6.10	Percentage of monthly occupied hours where the required ventilative cooling ACR rate is met with the predicted ACR for the particular configuration	156
6.11	Percentage of monthly occupied hours where the required ventilative cooling ACR rate is met with the predicted ACR for the particular configuration	156
6.12	Percentage of monthly occupied hours where the required ventilative cooling ACR rate is met with the predicted ACR for the particular configuration	156

6.13	Total percentage hours with N_{re} either met (grey) or not met (red) for the integrated system using optimum N_{pr} values from each configuration. Two scenarios shown, one incorporating a low limit constraint for T_e of $12^\circ C$ for RS.04, the other with a constraint of $0^\circ C$ (Note: individual configuration contributions shown with shaded borders)	157
6.14	Effect the external ambient temperature limit has on the number of hours where no VC is possible due to the un-availability of RS.04	157
6.15	Density distribution of Percentage difference between the required ACR values and the predicted ACR values for RS.04 during the months of June, July & August, (Only instances where the predicted ACR value was less than the required ACR value are shown)	158
6.16	N_{pr} as a function of both opening height, H and envelope temperature difference, ΔT . N_{pr} vs H curves shown for two different slot louvre section opening widths, 0.3m and 0.4m, Effectively a 30% increase in available opening area. Proposed Upper limit for ACR shown in orange based on measurements. Current opening height also shown in orange.	159
A.1	concentrations and estimate of concentrations plotted logarithmically against elapsed time. [156]	189

List of Tables

1.1	Research Objectives and methodologies matrix	6
2.1	Dimensionless exchange rate F_r of a building with a single opening	41
3.1	Key Building Information	64
3.2	Retrofit External Wall Components and Thickness's	67
3.3	Retrofit External Roof Components and Thickness's	68
3.4	Thermal characteristics of retrofit external envelope opaque elements	68
3.5	Ventilation Opening Configurations for Control space and Retrofit Space. Note: CS=Control Space; RS= Retrofit Space; M = Manual; A=Automated with manual override (flow schematics not to scale)	73
3.6	Tracer gas test characteristics for TGCD tests, categorised according to opening location or configuration	78
3.7	Roof mounted weather station instrumentation specifications.	81
3.8	Geometric dimensioning information for each of the opening cases measured in the field study. Aspect Ratio, AR, based on individual louvre slots for L cases with 17 slots in total within the louvre for airflow passage making up the available free opening area. subscript 's' denotes slot	83
3.9	Summary statistics for CO ₂ uniformity of concentration across all 44 tests in accordance with ASTM E741-11. (% difference between individual location and spatially averaged concentration). Also shown for windward and leeward tests separately. See Figure 3.22 for sensor positioning	85
3.10	Summary of external weather conditions during testing categorised according to each opening case. Conditions during testing for each case were comparatively equal for all boundary conditions.	89
4.1	Climate data for summer period May to September 2013	97
4.2	Summary of CIBSE overheating criteria for all internal spaces in zero2020	100
4.3	Sample of Stratification Factors with a range of low and high values and corresponding test conditions	103
4.4	Measured Peak $T_{\frac{H}{2}}$, Time Lag during week 8th-14th July 2013.(*Denotes night cooling present the previous night. †, denotes using RS-4.0; ‡, denotes using RS-3.0) 104	
4.5	Descriptive Statistics for ACR tests	105
5.1	Results from stepwise selection process for four boundary parameters U_l , U_r , θ and δT with three different sets of experimental test results, All wind directions, windward only & leeward only	123
5.2	Test summary data for L1 & P1 tests with similar high and medium/low turbulence boundary conditions	124
5.3	Model metrics for existing correlations fit to measured ACR data.	126
5.4	Values for F_r according to different wind directions, windward and leeward (Parallel U_r taken as leeward or windward depending on θ_r). No windward tests for P2 were recorded. Values based on combining all L cases and all P cases also shown. All values rounded to two significant digits.	129

5.5	Change in F_r between different opening cases with comparable geometry characteristics. Wind direction used for each comparison based on available data from field study.	129
5.6	Summary of Occupancy Temperature Data for each test configuration	130
5.7	Summary of Occupancy Air Speed Data for each test case	132
5.8	Summary of Occupancy Turbulence Data for each test case	136
6.1	Location and Building data	146
6.2	Technical Specifications	146
6.3	Summary statistics of N_{re} (VC mode 2, see equation B.8) for each month individually calculated using equation B.7 in the VC potential analysis tool	150
A.1	Characteristics of commonly used tracer gases [157]	185

Abbreviations

ACR	A ir C hange R ate
ACH	A ir C hanges P er H our
AR	A spect R atio
CS	C ontrol S pace
L	L eeward
L(1,2)	L ouvre case
mape	m ean a bsolute p ercent
MCSL	M ulti C onfiguration S lot L ouvre
MLR	M ultiple L R egression
mse	m ean s quared e rror
NDIR	N on D ispersive I nfrared S ensor
OLS	O rdinary L east S quares
P(1,2,3)	P lain opening case
P	P arallel
POF	P ercentage O penable A rea to F loor A rea
PPO	P urpose P rovided O pening
rmse	r oot m ean s quared e rror
RS	R etrofit S pace
SS	S ingle S ided
STR	S T R atification F actor
TGCD	T racer G as C oncentration D ecay
TI	T urbulence I ntensity
W	W indward,
WD	W ind D irection
WS	W ind S peed
VC	V entilative C ooling

Symbols

Roman Symbols

a	regression intercept	-
A	Area	m^2
Ar	Archimedes Number	-
b	flow constant, regression predictor variable	-
C	Concentration	ppm
C_d	Orifice Discharge Coefficient	-
C_p	Wind pressure coefficient	-
c_p	Specific heat capacity	$KjKg^{-1}K^{-1}$
CF	Dascalaki Correction factor	-
d	Fourier transform	$(ms)^{-2}$
E	Heat Energy	W
F	Non-dimensional Flow Number	-
\vec{f}	Power Spectrum	ms^{-2}
g	Acceleration due to gravity	ms^{-2}
G	Solar Irradiation	Wm^{-2}
Gr	Grashof Number	-
h	Hour	h
H	Height of opening	m
I	1D Turbulence Intensity	%
L	Characteristic Length	m
m	Mass flow rate	$kg s^{-1}$
N	Air Changes per Hour	h^{-1}
n	Total samples, measurement points, quantity	-
p	Total pressure, pressure	Pa ($kg m^{-1}s^2$)
P	Reference pressure	Pa ($kg m^{-1}s^2$)
Q	Mean volumetric flow rate	m^3s^{-1}
Re	Reynolds Number	-
r	2D unit vector	-

R^2	Goodness of fit	-
T	Temperature	$^{\circ}C, K$
t	Time interval, t-table value	s
U	Mean velocity, mean wind speed	ms^{-1}
u, v, w	3-Dimensional Wind Vectors	ms^{-1}
V	Volume	m^3
w	Width	m
wf	Weighting factor	-
W_e	Weighted Exceedence	-
x	Parameter, discrete sample	-

Greek Symbols

α	Empirical flow coefficient, jet spread rate	-
β	Flow exponent, frequency power exponent	-
Δ	Delta, difference	-
ϵ	Residual error	-
φ	Thermal Admittance	$(Wm^{-2}K^{-1})$
θ	Wind incidence angle	Deg ($^{\circ}$)
σ	Variance, root mean square, fluctuation -	
ϕ	Wind azimuth angle	Deg ($^{\circ}$)
ω	Frequency	Hz (s^{-1})

Subscripts

bp	balance point	-
b	buoyancy	-
c	comfort, combination, concentration	-
cl	lower thermal comfort limit	-
cu	upper thermal comfort limit	-
e	external, eddy	
f	floor	-
g	glass	-
i	internal, series term	
l	local, boundary	
m	measured, measurement	-
mn	minimum	-
n	normalised, network	-
o	opening	-
oc	occupancy	-

<i>op</i>	operative, optimum	-
<i>pr</i>	predicted	-
<i>r</i>	reference, roof	-
<i>re</i>	required	-
<i>rm</i>	running mean	-
<i>sp</i>	set point	-
<i>s</i>	stratification, slot	-
<i>t</i>	tracer	-
<i>vc</i>	ventilative cooling	-
<i>w</i>	wind	-
<i>z</i>	zone	-

Accents

\bar{x}	Mean of parameter x	-
\hat{x}	adjusted parameter, transform	-

To Maximilian and Beatrice.

Chapter 1

Introduction

This chapter provides an introduction to the thesis. It outlines the context and motivation for undertaking the research work. It defines the problem the research aims to address, the objectives of the research, the techniques applied in achieving the objectives and provides an outline of the thesis structure.

1.1 Research Motivation

1.1.1 Research context

The energy efficiency of existing supply chains is widely accepted as integral to any climate change mitigation strategy developed to deal with greenhouse emissions reductions. To this end, on 25th October 2012, the EU adopted the Energy Efficiency Directive 2012/27/EU in order to achieve the 2020 headline target of 20% improvement in energy efficiency [1] at all stages in the supply chain from production to final consumption. This reduction is based on the average energy demand during the period 2001 to 2005. The need for a sustainable, high energy performance building stock is generally identified as having strategic importance to tackling such energy security and climate change challenges. Naturally the existing building stock will play a key role in delivering on this. In fact Marnay et al [2] estimated that half of the buildings in use in 2050 have already been constructed. In Europe, these existing buildings already account for 40% of energy consumption [3]. In Ireland this contribution is 27% [4]. The salience of the existing built environment in improving an economy's energy efficiency and developing lasting, sustainable solutions to minimising societal energy consumption is self-evident. For countries with climates where energy consumption is predominantly required for heating, tackling the thermal fossil fuel energy consumption of older buildings is something that, realistically, can only be effectively addressed through deep retrofit upgrades to the external envelope; Such upgrades will improve the thermal resistance of the building exterior, enhance the dynamic response of the structure and minimise air permeability to levels that are in line with future energy performance targets. In general, any product or service, when finished and put to use, should satisfactorily

provide the functions for which it was intended without catalysing additional adverse or unwanted effects. This is also true for solutions developed to address energy efficiency challenges in the built environment. However, there are already examples where, solutions that have successfully reduced the energy consumption required to maintain comfortable indoor conditions in buildings during winter, have, in turn, resulted in an unacceptable indoor environment for its occupants during summer [5–8]. Building retrofit strategies must offer solutions without negative consequences for the indoor environment year round and must not be designed solely based on an energy reduction brief.

It is in this context that more knowledge is needed of approaches that can tackle heating energy consumption while at the same time providing an enhanced indoor thermal environment year round at no additional energy cost for cooling. This requires integrated thinking of how components and solutions can be more responsive to the local climate and offer the optimum balance of energy supply and demand to a buildings interior spaces. There is sufficient potential in Northern European climates to provide these types of solutions without the need for supplementary energy for cooling by using the cooling potential of ambient air [9].

The ability of a natural or mechanical ventilation system to provide cooling to an interior space is conditional on the external ambient temperature both in terms of its instantaneous value as well as the amplitude of its diurnal variation. Passive and hybrid cooling through the integration of natural and mechanical ventilation principles with the building morphology and materials has long been championed as a viable alternative to mechanical cooling [10]. However, the basic premises under which mechanical and natural approaches operate are fundamentally different and this has led to a scepticism from building owners regarding the ability of a natural ventilation system to adequately deliver acceptable internal conditions in buildings during the warmer months of the year. The criteria by which natural ventilation is assessed is often one suited only to mechanically controlled environments and this is diametrically opposed to the basic principles of the concept. Further, there are still many barriers to the effective adoption of natural ventilation for cooling related to climate change and increasing urban densification including amongst others; elevated ambient temperatures, external noise, air pollution and reduced local wind speeds [11].

The main negative consequence of a poorly performing Ventilative Cooling (VC) system is overheating leading to occupant dissatisfaction. Overheating poses a very real and validated challenge facing low energy buildings. This challenge is due to a number of reasons including the thermal and infiltration performance requirements imposed on buildings from regulation and policy to reduce heating energy consumption; consequences of climate change for the local ambient air temperatures; and the inability of low energy buildings to adequately dissipate heat build up from internal sources such as occupants, lighting and equipment. Such factors have resulted in significant deviations in energy use during operation which is usually termed the energy performance gap.

The outlook for warming will only compound efforts to control building overheating. The most recent IPCC Assessment Report AR5 has identified that each of the last three decades has been successively warmer at the Earth's surface than any preceding decade since 1850; 1983-2012 is likely the warmest 30 year period of the last 1400 years in the Northern Hemisphere

(see for example Fig SPM.1 in [12]), with Europe's human and managed systems providing a major contribution to climate change. Evidence already exists that current ambitious envelope and fabric oriented heating demand reduction strategies might result in an increased risk of extended periods of overheating in new buildings [13]. This is likely to also be an issue for ambitious building retrofits that focus on high levels of airtightness and very low thermal energy performance [14] which can result in a reduction in the heat removal potential when dealing with casual internal gains and incident solar gains. In most post-occupancy evaluations of low energy buildings and retrofits overheating is a frequently reported as a significant problem. If designed and operated correctly, passive VC can be a solution that avoids building overheating while delivering on legislative energy performance targets, in particular in low energy retrofits in Northern European climates where there is an opportunity to enhance performance of the existing approach. Demonstrated performance of new or novel VC solutions in real environments is key to ensuring solutions are better designed and specified as well as preventing their adoption due to misconceptions about their effectiveness as cooling solutions.

1.1.2 IEA-EBC Annex 62 and VC at zero2020, CIT

Under the auspices of the International Energy Agency (IEA) Energy in Buildings and Communities (EBC) program, an international project was initiated in 2014 on Ventilative Cooling. This project, due to be completed in 2017, addresses the existing challenges for VC applications and devises recommendations through development of design methods and compliance tools related to predicting, evaluating and eliminating the cooling need and the risk of overheating in buildings and through the development of new attractive energy efficient VC solutions [15]. IEA-EBC annex 62 State of the Art Review report recently defined VC as:

'The application of ventilation flow rates to reduce the cooling loads in buildings. VC utilizes the cooling and thermal perception potential of outdoor air. The air driving force can be natural, mechanical or a combination.'

The objective of the Annex work is to improve the prediction of cooling potential for new highly insulated and airtight low energy buildings, gather together knowledge of new solutions and strategies that can extend the range of applicability of VC considering the recent shift in building design and the effects of climate change and urbanisation and to publish results from well documented case studies that have successfully demonstrated the performance of VC systems.

To contribute to international efforts in addressing the challenges identified by Annex 62 and more generally, in the low energy building retrofit domain, in 2011, Cork Institute of Technology in Ireland decided to undergo an energy efficient upgrade with a small section of their existing 1974 campus building, comprising teaching and office facilities, known as the zero2020 project, see Figure 1.1(A). When developing the building upgrade scope additional funding was invested to produce a solution that included capabilities for generating data on the building performance to be used for research purposes. The strategy for retrofit was clear; the solution must offer a deep robust retrofit solution with scalable potential that delivered aggressive levels of low energy performance without compromising the quality of the occupant experience. The developed solution was installed in 2012 and this has afforded numerous studies on its performance since then.



(A) zero2020



(B) Multi-Configuration Slot Louvre system

FIGURE 1.1: zero2020 retrofit testbed at CIT. The slot louvre ventilation openings are visible along the fenestration sections.

An online data portal containing information about the zero2020 test-bed, data from various monitoring campaigns and modelling tools based on various projects under way there will be made available in early 2018. The author is currently based at Cork Institute of Technology as a lecturer and researcher and has been involved in the zero2020 project since its inception.

Contributing to, and within these larger research projects, the work presented in this thesis focuses on VC in non-residential buildings, with an emphasis on retrofit applications. The work entailed various full scale experimental investigations of the ventilation airflow performance and cooling potential of the single sided, Multi Configuration, Slotted Louvre (MCSL) VC solution installed at the zero2020 testbed in CIT (see Figure 1.1(B)). The multi-configuration nature of the system differs from a single configuration opening, i.e. a typical window, in that it can take on multiple different physical geometries within the facade with, subsequently, different opening heights and areas. This is achieved through the use of multiple ventilation doors. Reference to section 3.2 page 71 provides a fuller description of the dimensioning of the system while Table 3.5, page 73 defines each of the 3 possible configurations. The external slot louvre is fixed and has no modifiable geometry, only the internal ventilation doors are adjustable. The experimental field studies undertaken gathered valuable performance data for the natural ventilation system under real conditions, allowing an analysis and study of the effects of both the wind and buoyancy conditions to airflow rates through the newly designed ventilation openings, where the solution is single sided, there is no cross flow and air must exchange in and out of the same opening.

An extensive literature review has revealed that there is little published work relating to the performance of these systems under real operating conditions in single sided applications. There have been research studies into the theoretical nature of how slotted surfaces interact with airflow [16, 17] but these have generally been laboratory based and have not considered the configuration of parallel flow along a building envelope, driven by momentum and thermal forces, with the air exchange mechanisms present at the openings arising from the principles of single sided ventilation. Some studies have considered ventilation through louvred mechanisms but primarily with airflow normal to the opening surface and not necessarily in single sided ventilation modes, with aerofoil theory often adopted for the study [18]. Other studies have looked at grilles and louvres in applications such as vehicle radiator cooling grilles but the findings are not readily transferable [19]. Some studies have considered the effects of slat blinds used for



FIGURE 1.2: Control and retrofit spaces used for ACR and Internal Thermal Environment measuring campaign during summer 2013

shading on airflow through an opening but again the application is not directly related. There is a lack of experimental performance data for single sided VC under real conditions in recent literature. This type of information can be valuable for testing existing semi empirical airflow rate correlations and for comparing with measurements in other applications. Further, as very low energy buildings are a relatively recent development, there is a need for field measurements on the internal thermal environment in these buildings and evidence on how they perform can be invaluable to researchers and designers when making decisions regarding future projects.

The following section outlines the objectives of the research work while the subsequent section gives an overview of the methods employed to meet these objectives.

1.2 Research Objectives

The aim of the thesis is to investigate the effect of the ventilation performance (and subsequent cooling potential) of a single sided, natural ventilation opening when using a MCSL system that is designed to prevent rain ingress and burglary during night cooling. The work has the following objectives:

Objective 1. Assess the quality of the long term indoor thermal environment of a deeply refurbished experimental space quantifying the extent of overheating with slotted architectural louvre ventilation systems in a single sided configuration.

Objective 2. Investigate the full scale aeration potential of the integrated, multi-configuration, single sided natural ventilation system installed in the experimental building, compare its performance to the pre retrofit building and identify how the different opening types might result in a change in the dominant drivers of ventilation.

Objective 3. Quantify experimentally the specific effect of including the slot louvre component in a single sided ventilation opening under real conditions.

Objective 4. Assess the ability of existing single sided empirical correlations used in ventilation airflow rate calculations to adequately predict ventilation rates for the slot louvre component and propose a new correlation if applicable.

TABLE 1.1: Research Objectives and methodologies matrix

Obj.	Method	Technique	Study/Research
1	Experimental	Adaptive Thermal Comfort	Full Scale OH Performance
2, 4	Experimental	Tracer Gas Concentration Decay	Full Scale Air Change Rate Performance
3, 4	Experimental	Tracer Gas Concentration Decay	Mapping Airflow with the Slotted Louvre
5	Numerical	Energy balance model	Ventilative Cooling Potential

Objective 5. Demonstrate the component cooling potential of the VC system and identify whether the required ACR for cooling can be achieved.

1.3 Research Methods

The work presented in this thesis is largely experimental in its approach to meeting the objectives set out above. The methods adopted to achieve the objectives are outlined in detail in Chapter 3. Three separate field studies were completed to investigate the performance of the VC system installed at zero2020 and a modelling study was undertaken to demonstrate the cooling performance of the system using empirically derived data from the field studies. As the focus for the research was on single sided ventilation, a single cell isolated office space with ventilation from one external facade only was chosen for experimental measurements, see Figure 1.2(B). Findings from three separate studies are presented; a long term evaluation of indoor thermal environment and risk to overheating for the retrofit space, short term measurements of ACR for both the post retrofit office space and a pre retrofit space with similar characteristics and boundary conditions used for control purposes, (see Figure 1.2(A)), and finally, short term measurements of ACR and airflow characteristics in the zero2020 retrofit space with and without the slot louvre component. Table 1.1 summarises each the type of research undertaken and the method employed to meet the objectives above. The relevant part of the research is also identified.

1.3.1 Full Scale performance: Long Term Overheating

2013 was a particularly warm summer and during that year an investigation into the occurrence of overheating at the building was undertaken to establish whether the installed VC system was able to deliver a satisfactory environment during the cooling season. There are seven spaces within the testbed building. The method for assessing overheating outlined in EN15251 [20] and CIBSE TM52 [21] has been adopted in this study as this uses a variable threshold temperature based on the adaptive thermal comfort model when assessing overheating and has been shown to correlate better with the response of occupants in naturally ventilated buildings. The approach

outlined by CIBSE TM52 contains three criteria for assessment that capture the extent of hours of overheating, the amplitude of overheating when it does occur and the exposure time to a maximum allowable temperature. These three indices were calculated for each space and used to assess the performance of the system in maintaining an acceptable indoor environment without the need for supplementary cooling. Precision thermistors located in each room were used with a wireless radio based data logging system to measure and record air temperatures in the building from May to September 2013 that could then be used for calculating the various indices. Because of the data logging function thermistors were used instead of thermostats. A thermostat is useful for controlling at a set temperature but not suitable for continuous recording of air temperatures. Figure 1.3 shows a photo of the thermistor and data logger in-situ as well as an example of the interior space used for analysis of overheating. The details of the measurement set up are covered more fully in chapter three with results from the study presented in chapter four.

1.3.2 Full Scale Performance: Air Change Rate (ACR)

Empirically measuring single sided airflow rates in naturally ventilated buildings can be a challenging undertaking. This is often due to the bi directional nature of the flow through the opening and accounting for differences in localised air exchange at the opening with air exchange between the external air and the acquiescent air within the interior space. A technique often employed to overcome this is using a tracer gas to mark the air within the space when sealed prior to the test. Depending on the approach taken, the rate of dilution of the gas over time once the ventilation has been activated gives an indication of the amount of air that has been replaced by air from outside the space under consideration. The tracer gas concentration techniques have been shown to be efficient and reliable method to measure time averaged ACR in a naturally ventilated building. Appendix A includes details on the various methods available. For this field study the decay method was chosen. Carbon Dioxide (CO_2) was chosen as the tracer gas. Twenty five separate tests of the ACR in the retrofit office space was completed with 13 tests completed in the control space for comparative purposes. Both spaces are first floor, single cellular, west facing office, of similar dimensions, located in different sections of the same building. Each test duration varied depending on the ACR, driven by both wind and buoyancy forces across the openings. Boundary conditions were monitored and recorded using a weather station at roof level. The tests were completed during July and August in 2013. As well as measuring ACR internal temperatures were also monitored during each test. Internal thermal stratification was measured and compared within the control and retrofit spaces using eight individual thermistors equally spaced from floor to ceiling. Chapter 3 includes more details on the experimental set up and chapter 4 includes results and analysis from testing.

1.3.3 Mapping and Prediction of the Airflow Rate with the Slot Louvre

The final experimental field study was undertaken in the same single cellular isolated office space in zero2020. This study investigated how the slotted louvre device interacted with the boundary conditions at the opening and quantified how it modified ACR performance. Previous ACR measurements were sufficient for a comparison of performance between the pre and post retrofit

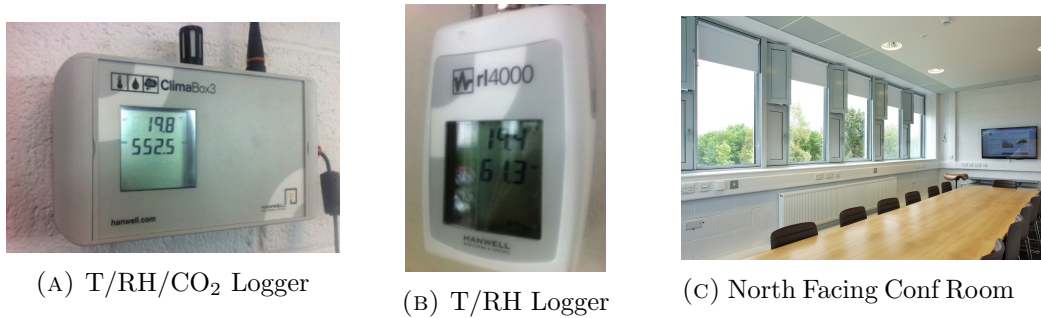


FIGURE 1.3: Data logging equipment and typical indoor space used for full scale overheating performance measuring campaign during May - September 2013

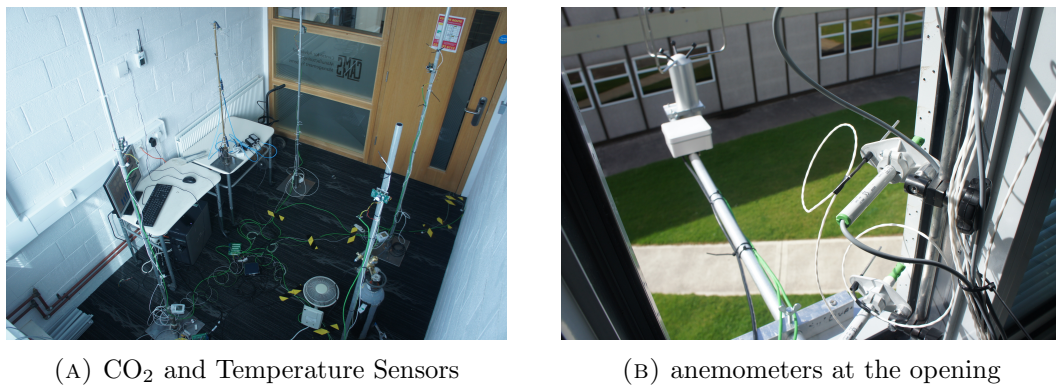


FIGURE 1.4: Examples of experimental set up in the cellular office for measuring campaign during summer 2014. Refer to Figure 3.22, page 86 for details on the layout shown in (A) above. For the 2013 testing layout see Figure 3.16, page 79

spaces but did not isolate the effects of the slotted nature of the opening. Little performance data in a real environment exists for such architectural louvres. Twenty ACR measurements were completed with the louvre in place using the tracer gas concentration decay technique while 24 ACR measurements in the same space and opening but without the slotted louvre were also completed to allow a comparison of performance, controlling for boundary conditions, see Figure 1.4(A). The local boundary conditions 1.0m from the opening were recorded during this measuring campaign as well as reference values at roof level, see Figure 1.4(B). Air speeds and temperatures within the opening and at the occupant location within the room were also logged during each ACR test. This allowed a deeper understanding of the local phenomena at the opening and how the opening configuration was affecting the characteristics of the airflow within the occupied space. The results were analysed using non dimensional analysis and a sensitivity study of the boundary conditions using multiple linear regression. A spectral analysis of the air in the opening and at the occupant location was also completed. Chapter 5 includes results and analysis from the study.

1.3.4 Demonstration of Component Cooling Potential

To investigate the cooling potential of the VC system the measured airflow performance of the system was used in combination with an approach developed within IEA-EBC Annex 62 for assessing performance of particular building and climate combinations. The required ACR

estimated numerically from the Annex 62 Climate Potential Analysis Tool was compared with a predicted ACR value based on measurement data using improved semi empirical correlations for wind and buoyancy driven scenarios. A parametric analysis to improve the system performance where it was unable to meet demand was also undertaken. This involved selecting the most suitable opening configuration for a given time interval as well as exploring the effects of the opening design. Appendix B includes an outline of the method applied. Results from the component cooling potential investigation and parametric analysis are included in chapter six.

1.4 Thesis Structure

Figure 1.5 below shows the structure of the thesis which comprises 5 research components described in seven chapters. The contents of each chapter are summarised below:

- **Chapter 1** This chapter presents the motivation and context for undertaking the research and the objectives. An overview of the research methods employed to meet the objectives is provided and the thesis structure is outlined.
- **Chapter 2** provides a review of published literature relevant to the research undertaken. A brief review of why building refurbishment is now an important sector for both industry and research is provided as well as the motivating factors for the need to consider non invasive ventilation strategies as part of retrofit solutions. Overheating as an indirect consequence of approaches to building refurbishment in heating dominated climates is addressed. Single sided ventilative cooling principles, strategies and applications are then discussed. Current knowledge regarding the barriers to its implementation is summarised. The underlying physics of single sided ventilation is presented along with a review of the semi empirical correlations currently used for predicting airflow rates through openings. Key developments pertaining to the state of the art are discussed.
- **Chapter 3** summarises the experimental setup for the three measuring campaigns. An outline of the design, manufacture and installation of the externally applied envelope retrofit solution at the case study building used for all experimental measurements herein, zero2020, is presented. The experimental setup for long term measurements in 2013, short term ACR measurements of the full scale operation in summer 2013 and the experimental investigation of the effects of the slot louvre component in summer 2014 are each described in detail along with the approach for processing measurement data.
- **Chapter 4** presents results from measurement and monitoring for the VC system under full scale operation. Data from the long term indoor thermal environment assessment during 2013 is first presented and discussed. Results from the field study of ACR performance for the normal operation of the VC system, completed during summer 2013, is subsequently presented. Work is summarised from experimental measurements of time averaged macroscopic ACR in a cellular isolated office space within the retrofit. The results are compared to a control space in the existing building. Results from measurements and analysis of the data is included. A sensitivity study of the non dimensional method used to analyse results is also included.



FIGURE 1.5: Information flowchart outlining the structure of the thesis and how individual chapters link with work carried out. Details regarding the scope at each stage are also included

- Chapter 5** presents results from the field study investigating the airflow effects of the slot louvre in order to infer any modifications to the local airflow exchange mechanisms at the opening. A comparison is made between the same opening in the same space, with and without the slotted louvre, allowing a direct investigation of phenomena. A non-dimensional analysis is employed to categorize tests according to driving forces; a spectral analysis of velocities at the opening is then used to investigate any changes in the wind characteristic in the opening and energy distribution with the addition of a slot louvre. Results from measurements of changes in airflow conditions within the opening are presented. The field study also assessed changes in the local air movement at the

occupant location specifically from the use of the slotted louvre component. A number of existing semi-empirical correlations were compared with measurement results and, following a discussion about potential causes for the pattern of measured ventilation rates, a new non-dimensional flow number is proposed for improved modelling of wind dominant macroscopic flow through the louvre components.

- **Chapter 6** presents an assessment of the climate cooling potential for the slot louvre system, effectively the component cooling potential, extending an approach developed within IEA-EBC Annex 62. The method of assessment is first outlined with the results then presented. Once the component cooling potential is known a parametric analysis is undertaken to extend the limits of performance for the louvre system.
- **Chapter 7** brings together the overall conclusions from the work and set outs recommendations for future work.

1.5 Publications

A list of refereed journal articles and conference papers, authored or co-authored by the thesis author, that have been published based on the work presented herein, are listed below.

1.5.1 Journal Articles

OSullivan, P.D., & Kolokotroni, M. (2016). A field study of wind dominant single sided ventilation through a narrow slotted architectural louvre system. *Energy and Buildings*, 138, 733747. <http://doi.org/10.1016/j.enbuild.2016.11.025>

OSullivan, P.D., & Kolokotroni, M. (2016). Non dimensional analysis and characterisation of driving forces for a single sided slot louver ventilation system. *International Journal of Ventilation*, 14(4), 335348. <http://doi.org/10.1080/14733315.2016.11684091>

OSullivan, P.D., & Kolokotroni, M. (2014). Time-averaged Single Sided Ventilation Rates and Thermal Environment in Cooling Mode for a Low Energy Retrofit Envelope. *International Journal of Ventilation*, 13(2), 153168. <http://doi.org/10.5555/2044-4044-13.2.153>

1.5.2 Conferences

O Sullivan, P. D., & Kolokotroni, M. (2014). Experimental Characterisation of Dominant Driving Forces and Fluctuating Ventilation Rates For a Single Sided Slot Louver Ventilation System. In AIVC Conference Proceedings, Poznan, Poland. **Conference Best Paper Award**

OSullivan, P., & Kolokotroni, M. (2013). Experimental analysis of different operational configurations for single sided ventilation as part of a low energy retrofit. In 34th AIVC - 3rd TightVent - 2nd Cool Roofs - 1st venticool Conference, Athens, Greece.

OSullivan, P., Delaney, F., ORiain, M., Clancy, T., OConnell, J., & Fallon, D. (2013). Design and Performance of an External Building Envelope Retrofit Solution For a Grid Optimised Concrete Structure: A Case Study. In IMC30 Conference Proceedings 2013, UCD, Dublin, Ireland.

1.5.3 Additional Related Co-Authored Publications

ODonovan, A., Murphy, M.D. and OSullivan, P.D. (2017) A long term parameter dataset for calibration of low energy building retrofit models for education and research. In PLEA 2017, Edinburgh, Scotland.

OSullivan, P.D., O'Donovan, A., Zhang, G. & Carrilho da Graca, G. (2017). Design and performance of ventilative cooling: a review of principals, strategies and components from International case studies. In 38th AIVC - 6rd TightVent - 4th venticool Conference, Nottingham, UK.

ODonovan, A., OSullivan, P.D., & Murphy, M. D. (2017). A field study of thermal comfort performance for a slotted louvre ventilation system in a low energy retrofit. *Energy and Buildings*, 135, 312323. <http://doi.org/10.1016/j.enbuild.2016.11.049>

O Donovan, A., O Sullivan, P.D., & Murphy, M. D. (2016). A field study on the thermal comfort performance of a ventilative cooling system in a retrofitted low energy building. In CLIMA2016.

Holzer, P., Psomas, T., & OSullivan, P.D. (2016). International Ventilation Cooling Application Database. In CLIMA 2016 - proceedings of the 12th REHVA World Congress.

Chapter 2

Single Sided VC in Building Retrofit

This chapter reviews the topic of VC, and more specifically single sided ventilation, as a potential technique to address the risk to overheating in low energy buildings, with a clear focus on its role in low energy building retrofits. A brief review of why building refurbishment is now an important sector for both industry and research is provided as well as the motivating factors for the need to consider non invasive ventilation strategies as part of retrofit solutions. Overheating as an indirect consequence of approaches to building refurbishment in Northern European climates is addressed. Single sided VC as an attractive component of building retrofit scopes and a climate change mitigation strategy is reviewed and current knowledge of the barriers to its implementation is summarised. Key developments pertaining to the state of the art are discussed. A literature review is presented, but only in so far as is necessary to sufficiently define the discipline to which the research belongs and the problem statement that the work aims to address. In this sense, the current context surrounding the adoption of VC strategies, important developments in the field are presented and key research findings are used to support the discussion that follows.

2.1 Delivering Energy Performance in Existing Buildings

The Irish Government has estimated that non behavioural measures such as external envelope upgrades can provide as much as 1.09 TWh of energy savings across public sector buildings [22]. Behavioural measures can further compliment such a strategy. The EU has identified 3% of total floor area of heated/cooled public sector buildings (with a floor area greater than $250m^2$ since July 2015) as the minimum amount of the building that should be refurbished each year to satisfy Article 5 of Directive 2010/31/EU, Energy Performance of Buildings (Recast) [23]. Article 9 of the EPBD Recast requires member states to ensure that all new buildings are nearly zero-energy by 31st December 2020 and new buildings occupied and owned by public authorities are nearly zero-energy after 31st December 2018. Article 9 also brings in existing

buildings under the near zero-energy umbrella by requiring member states to develop policies in order to stimulate the transformation of refurbished buildings into near zero-energy buildings (NZEB). Article 7 states that when buildings undergo major renovation, the energy performance of the building is upgraded in order to meet minimum energy performance requirements set in accordance with Article 4. The Irish Governments National Energy Efficiency Action Plan 2009-2020 3rd report [24] identified refurbishment of existing public sector buildings as a key area for focus with support for exemplar projects that demonstrate substantial reductions in energy consumption. There is huge potential for non-residential envelope retrofit works to form part of the solution in reducing energy consumption in the existing building stock. In 2009 it was estimated that there are 3,083 large public-sector buildings, of over $1,000m^2$ floor area, in Ireland [25]. Furthermore, based on data available from the Irish Central Statistics office, there is potentially over $20,000,000 m^2$ of existing non-residential building stock that was constructed before any national building regulations were in place. In this context, according to SEAI, the public body responsible for policy in the energy efficiency and building refurbishment sectors, between 1990 and 2015 final energy use in the commercial and public sector grew by 20% when corrected for weather fluctuations [4]. In recent times efforts to curtail the inefficient use of energy in Ireland over the period 2000 to 2014 resulted in a 19.4% improvement in energy efficiency in the overall economy [4].

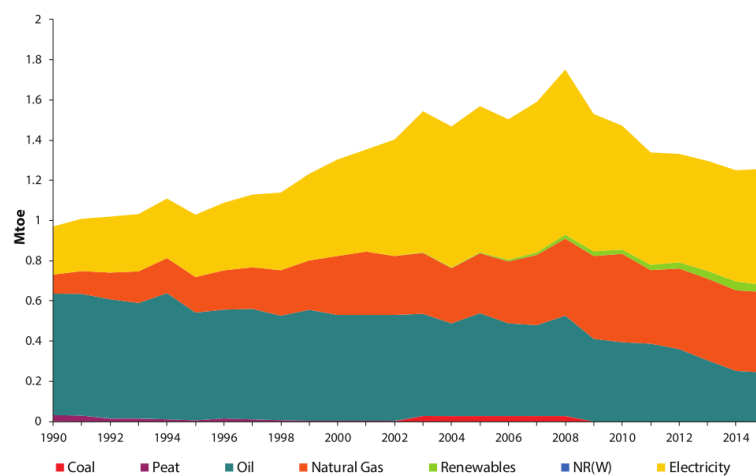


FIGURE 2.1: Commercial and Public Services final energy use by fuel for Ireland - 1990 to 2015 [26]

2.1.1 Energy performance in commercial Offices

The public sector in Ireland has been reporting on its energy efficiency improvements in line with the requirements of SI 426 of 2014 [26, 27] However, SI 426 does not require any reporting from the private sector. A survey of the non-public sector commercial buildings stock in Ireland was published recently by SEAI [28]. This is the first survey of its kind in Ireland. The study combined over 1500 site visits, a survey, the development of building archetypes and energy modelling using the Simplified Building Energy Model (SBEM). Some of the key findings for commercial offices can be summarised as follows:

- There are currently approximately 109,000 commercial buildings in Ireland. Of this there are 40,000 large offices (floor area greater than 1000 m^2) and 2,0000 small offices
- In almost 80% of commercial offices surveyed 80-100% of the glazing in these offices was either double glazing or triple glazing
- A range of different construction wall types exist depending on the building age. By 2006 commercial building were constructed using various methods including composite construction, cavity and solid masonry as the three main types with increasing examples of metal facades and non structural solutions.
- 50% of offices are heated using electricity, approximately 30% use oil and only 10% use natural gas for heating. In almost 50% of commercial offices surveyed there was 80-100% of the lighting installed as low energy lighting

Figure 2.2 presents a breakdown of HVAC solutions by sector. Specifically to offices we can see that 20% of offices use heating, mechanical cooling and mechanical ventilation, 60% use heating only with natural ventilation, while 10% of offices use heating only with mechanical ventilation and 10% are unheated and use natural ventilation.

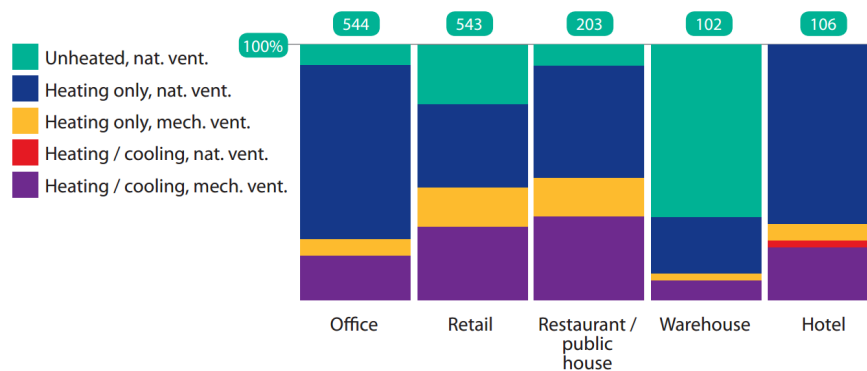


FIGURE 2.2: Percentage split for various VC operating modes for annual occupied hours

A report recently published investigating the energy efficiency potential for different sectors in the Irish economy considered the energy savings potential of various shallow, medium and deep energy performance improvement measures [29]. For the commercial buildings sector, which would include a large number of existing office spaces, they suggest roof insulation, energy efficient glazing and solid wall insulation combined could provide energy savings of 1.82 TWh, representing an 11% annual reduction for the sector. More efficient air conditioning was also identified as a recommended measure at 0.51 TWh annual savings for the national commercial building stock. However, natural ventilation as a viable alternative was not proposed, even when packages of measures, effectively combining different measures together into feasible groupings, were considered. This report, published by SEAI, identifies deep retrofit as a key component to an overall suite of measures but fails to identify the additional energy savings potential by utilising VC as part of the fabric upgrade strategy. There now exists a range of policy motivating measures and specific information that will allow the Irish Govt and SEAI propose further policies and regulations that aim to promote the uptake of commercial and public sector office

refurbishment. Before considering these strategies for retrofit projects and, subsequently, investigating the salience of ventilation and indoor environment in the scope of considerations for office retrofits, the motivating circumstances for advancing energy retrofitting is first discussed.

2.1.2 Motivation and barriers to deep building retrofit

Hoffman and Henn published a prominent paper in 2008 [30] discussing the social and psychological barriers to green building. They propose that there exists a complex interplay of individual, organizational and institutional perspectives on “green” building that creates biases resulting, semi consciously, in suboptimal decision making. At the individual level phenomena such as over discounting the future by perceiving reduced or delayed financial benefit from investing today in more energy efficient technologies, the effects of ego-centrism resulting in the self-reinforcing belief that positive personal decisions also have positive outcomes for the environment and society as a whole (e.g. each individual seeking larger gardens for their children resulting in unsustainable urban sprawl) and positive illusions, influencing the individual belief you are doing more than in reality. Hoffman and Henn suggest that at the organisational level cultural filters within the group can alter rational expectations and perspectives. In some organisations reward systems ostensibly aligned to the triple bottom line of sustainable development when in fact rewards are still ultimately linked with traditional metrics for promotion (economic productivity, profit et cetera). Further, the temporary nature of a building projects team structure, that, in themselves are enduring, structured role systems, can create counter productive cultures towards low energy and sustainable design. Institutional level biases and prejudices also exist in the form of social influences embodied in rules, laws, industry standards, best established practices and conventional wisdom. Overcoming the social and psychological barriers requires a massive systematic undertaking across institutions which in turn influence organisations and finally the individual. However this is not an easy challenge as effecting behavioural change is most difficult at the individual level. Other studies have also suggested the problems are very much at the cultural level when it comes to motivation to undertake energy retrofit projects [31]. In another recent study, Kontokosta [32] used a data set of 373 properties in North America to investigate what factors were the strongest motivators for building owners to initiate a retrofit program. He used a combination of owner surveying and a predictive model based on logistic regression using a binary out variable to account for a series of predictors. Fig 2.3, reproduced from Kontakosta, reports the motivating factors and barriers related to decision making for building retrofit.

The top four motivating factors are based on financial rewards, with reduced energy bills being the biggest motivating factor. Timing can also be an important criteria for the power of incentives given the prevalence of maintenance and repairs plans for existing systems and components as a motivating factor in almost 80% of retrofit projects surveyed.

2.1.3 Strategies for deep building retrofit

Once the culture exists for low energy retrofits to be considered as a viable project worthy of investment, choosing which strategy to adopt is a complex optimisation problem with many

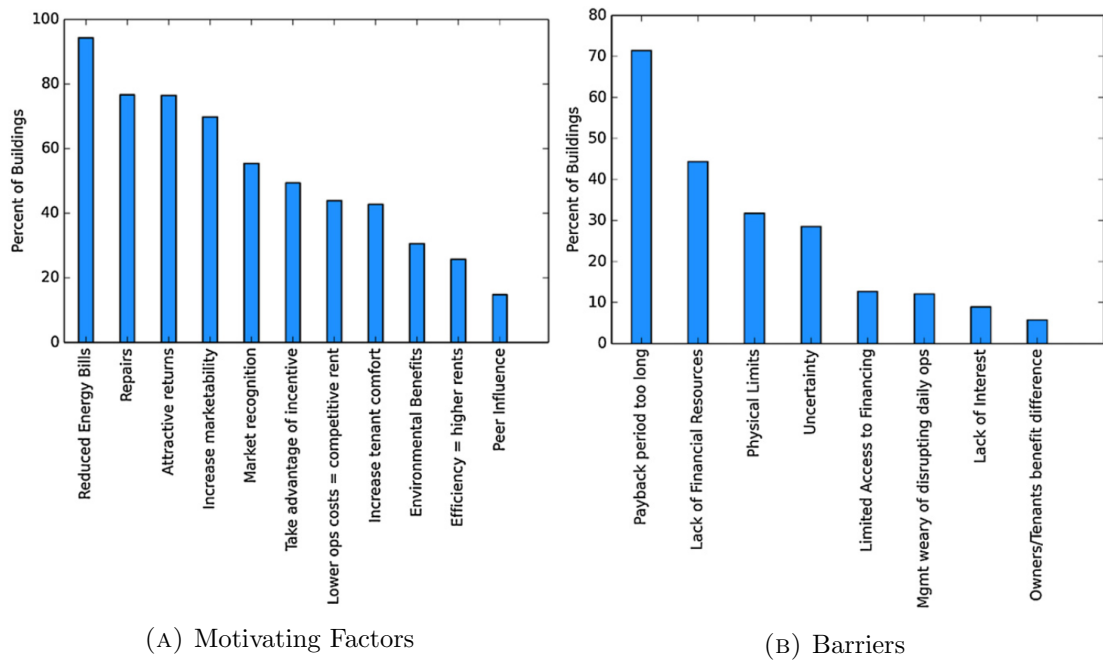


FIGURE 2.3: Reported Motivating factors and barriers in decision making for building energy retrofits. reproduced from [32]

parameters and constraints. Ma et al [33] present a systematic approach to retrofit that encompasses a model based approach to selection of energy conservation measures. In terms of categories for building retrofit technologies they list comfort requirements under human factors and natural ventilation as a low energy technology. To reduce energy consumption for cooling, natural ventilation or passive cooling techniques are often identified in recommended retrofit solutions for commercial office spaces. Dascalaki and Santamouris [34] investigated the effect of different scenarios of retrofitting, for different building typologies, including the use of various levels of passive and mechanical day-time and night-time ventilation, ceiling fans in major internal zones, improved ventilation controls and various shading devices. Using these passive techniques, depending on the building type, they were able to remove or reduce cooling energy demand by between 19% to 100% across a range of different climates, although the overall effect was negligible when the reduction on heating was taken into account. However, natural ventilation should be seen as viable cooling strategy when other interventions have already dealt with heating energy demand at the building. More generally there are a number of published studies summarised in Table 1 of [33] that present total energy savings potential in the range of 20% to 56% depending on retrofit interventions and building type. Amongst these the adoption of passive ventilation and solar shading techniques were identified as key.

In the context of ventilation strategies there are many factors to consider, the most significant being the effect on indoor environment and occupant experience. Achieving ambitious levels of energy reduction without compromising the thermal comfort performance of the building remains a major challenge. Delivering satisfactory thermal comfort has implications for many different parts of a building design and operation. In fact, a significant amount of energy consumption from the 1960s onwards resulted from a growing demand for control of thermal environment within a narrower comfort range though not necessarily delivering better thermal comfort for

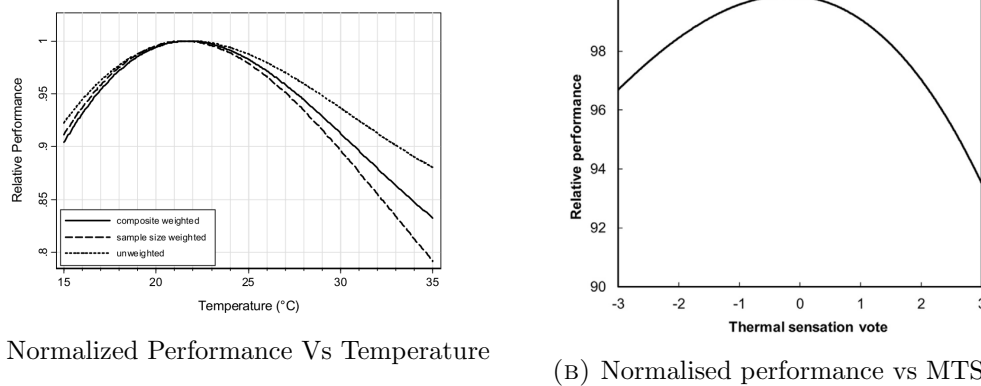


FIGURE 2.4: Worker productivity performance as a function of indoor temperature and mean thermal sensation vote. Reproduced from [38] and [39]

all. When undertaking refurbishment of an existing building the chosen ventilation strategies can have a large influence on the future energy performance of the building, depending on the amount of supplementary energy needed to maintain the required indoor environment, and whether or not the strategy is acceptable to occupants negating any future modifications or enhancements. Holistic sustainability strategies such as LEED [35] and BREEAM [36] do consider the consequences to indoor environment as part of the assessment of suitable retrofit approaches.

In principal improving thermal comfort and quality is seen as one of the objectives of successfully completed building refurbishment projects. Increasing the adaptive response potential of buildings and their occupants is a key criteria in ensuring low energy upgrades do not introduce negative consequences for thermal comfort. According to Barlow and Faiala [37] there are often different types of retrofit interventions, some that are passive-adaptive and focus on the upgrading of the building fabric and structure and others that are seen as active-adaptive interventions, focusing on ensuring there is an improvement in the occupants thermal experience of the new environment whilst also contributing to energy performance. Their study found that occupants surveyed voted positively for those active-adaptive refurbishment opportunities such as opening windows and manually controlled external solar shading. The adoption of passive VC strategies was seen as a favourable approach to low energy refurbishment. Free running low energy retrofit buildings are generally at increased risk to occupant dissatisfaction from the inability to mechanically control temperatures during summer months. Further, the range of acceptable thermal comfort conditions understandably has implications for energy efficiency refurbishment approaches. A wider range will result in less energy consumption and more likelihood of success of the retrofit project. Whilst energy performance is a tangible characteristic that is relatively easily verifiable, thermal comfort is more subjective and more difficult to measure. Building users will be the main source of determinant for success of retrofit projects so even when target energy savings are delivered if occupants are dissatisfied with the environment this can mean the project has failed overall in extending the life of the asset successfully. This is more acutely present in free running buildings where, although there is a wider acceptance range for thermal comfort there is also no opportunity to regulate the conditions to remain within the comfort ranges during periods of excessive warm weather.

2.1.4 Thermal comfort and low energy building retrofits

Improved energy performance and enhanced thermal comfort should not be perceived as a rigid dichotomy of concepts, depending on the approach adopted. Implementing energy efficiency measures that widen the range of acceptable internal conditions but do not materially change the building and systems can sometimes result in negative perceptions of the internal thermal environment by office occupants. A study in Japan that allowed higher indoor temperatures and lower lux levels during summer periods to reduce electricity consumption overall found that there was a negative effect on thermal satisfaction and self-assessed productivity of workers was down 6.6% [40]. While other researchers [41] have shown that the "need for comfort" can negatively influence energy savings intentions of individuals in low income housing, with a need for warmth being more impactful than a need for coolness, it is possible to deliver low energy spaces that also result in improved occupant thermal comfort. In other words by reducing the need to change or alter the thermal environment low energy buildings can remain low energy year round without increased cooling energy, offsetting reductions in heating energy savings. With deeper level retrofit and more visible solutions it is possible to achieve energy performance and overall occupant satisfaction. Zhang and Altan [42] suggested that, based on a comparative study of two buildings, a low energy building with advanced passive control of the indoor environment will lead to more satisfied occupants than a building constructed to poorly performing energy consumption concepts. Another study [43] investigated occupant satisfaction in two energy efficient buildings utilising natural ventilation strategies in a sub tropical climate. They found that between 55% and 58% of occupants agreed that the low energy designs improved the health and productivity of the staff and the advanced external facades were the main contributors to this improvement. Where offices that utilise natural or mechanical ventilation as their cooling strategy undergo a low energy retrofit the key to success is limiting the occurrence of overheating in these free running buildings, this is especially important given the increased risk of overheating and the restricted opportunity for dissipation of heat gains.

2.2 Overheating in free running Low energy buildings

2.2.1 Evidence of overheating in the existing building stock

In places like the UK and Ireland overheating and its perceived negative effects has become a recent phenomenon where traditionally there were no major concerns for the presence and effects of elevated temperatures in both residential and commercial buildings. Lomas and Porritt identify a number of key factors that have given rise to overheating issues in Northern European temperate climates [5]. The legislative and policy focus on winter heat retention in both refurbishment and new build design scopes combined with modern methods of construction such as airtight off site factory built walls and envelopes have reduced the heat dissipation potential of buildings, traditionally poor at retaining heat; increasingly warmer climates and occurrence of heat waves [44] also contribute to extended periods of overheating. Finally, the cultural unwillingness to accept that cooling in summer is now critical to maintaining conditions below risk

thresholds, particularly for the elderly. In Ireland 12% of the population is currently over 65. This is set to increase to 1.4m or 22% in 2041. An increase of 250% is expected by 2041 for those aged 80 or over. With the retirement age also likely to trend upwards towards 70 more severe health consequences of overheating in the workplace will need to shift centre stage in policy and legislation responsible for the indoor environment of our workplaces.

A number of recent studies in the UK have investigated the large scale existence of overheating in buildings related to both local climate and building characteristics. With regard to housing one study concluded that even during a cool summer in 2007 4% of 193 dwellings monitored had living room temperatures exceeding the recommended thresholds for overheating from the BRE with night time bedroom temperatures exceeding 26°C for more than 5% of the time in 21% of dwellings [45]. A second study of 200 dwellings reported that in 27% of these, indoor temperatures in living rooms exceeded 28°C for more than 1% of the occupied time [8]. A recent study by Mavrogianni et al [7] considered the effects of various building characteristics and future climate on the likelihood of overheating in dwellings in London. They found that while insulation retrofitting measures as a whole can potentially lead to a reduction in overheating risk, internal solid wall insulation may increase overheating risk during a warm period if no night time ventilation is provided. McLeod and Swainson [6] in a survey of issues exacerbating overheating not only in summer but also year round in a zero carbon building in London that uses natural ventilation as well as mechanical heat recovery ventilation identified differences with the design specified window opening area for ventilation and the reduced opening area of the installed window. This was due to opening restrictors put in place to meet health and safety and fire regulations. The resulting reduction in purge ventilation potential was seen as a source of both chronic year round overheating and seasonal overheating. In fact it seems that the development of energy regulations are out of sync with ventilation regulations and this should be addressed to prevent further examples of thermal discomfort from overheating in low energy spaces.

For naturally ventilated commercial buildings deWilde and Tian [46] demonstrated using probabilistic simulations the high likelihood of overheating risk in existing buildings when subjected to future weather conditions and the importance of corrective refurbishment measures to avoid substantial overheating during summer months with reductions in the likelihood of overheating varying according to renovation measure as well as whether the static or adaptive thermal comfort assessment method was used. Kolokotroni et al [47] showed using dynamic thermal simulations that for a typical office building overheating hours increase from 30% to 140% in 2050 in a rural location outside London and from 20% to 110% in the centre of London. Heavyweight construction with night cooling had the lowest number of overheating hours. When a building is retrofit with heating energy consumption in mind this can also lead to increased risk of overheating during warmer periods as no mechanical cooling is present to deal with the additional heat gains to the space and reduced heat losses.

2.2.2 Quantifying the effects of overheating

Overheating, characterised using various different indoor temperatures as a single value index, is often used as a measure of unacceptable long term indoor thermal environments. Carlucci and

Pagliano in a review of long term indices suggest there are almost 80 separate heat stress indices [48]. Specifically to buildings they identify fifteen separate indices with eleven of these based on comfort models and four on reference temperatures. Quantifying long term overheating risk is one of the objectives of these indices and is an important performance metric in free running buildings where there is no mechanical cooling. It allows alternative benchmark criteria to assess the performance of the design where energy consumption is either unavailable or unsuitable as an indicator. Overheating is a performance metric related to the quality of the indoor environment. In this regard existing research has investigated the link between overheating and the efficiency of the workers exposed to the indoor environment, utilising the space. When overheating is presented as such it is perceived as a negative consequence of both the improved thermal performance of a building, incorrect integration of ventilation systems and poor co-ordination between designers, builder and end users. This relationship between worker productivity and indoor thermal environment has been investigated by a number of researchers. Lan et al used an office in a real building with 12 volunteers undertaking various neuro-behavioural tasks while being exposed to different thermal conditions [39]. The objective was to investigate the quantitative relationship between worker performance and thermal sensation votes (a measure of acceptance with the thermal environment using a seven point scale about 0 [49]) as well as air temperature. They found that optimum performance is achieved when people feel slightly cool thereby setting the predicted mean vote (PMV) limits between -0.5 and 0. Earlier studies found similar results with values for PMV of around -1. This would suggest the best worker performance can be obtained when people are slightly cool. More recently Wargocki and Wyon proposed that based on the literature, office work performance is shown to be affected by thermal discomfort due to heat [50]. Figure 2.4(a), from Seppanen et al [38], shows the relationship between indoor air temperature and the performance decrement, based on a summary of the published literature in this field. Figure 2.4(b) from Wargocki and Wyon (reproduced from Lan et al [39]) shows the relationship between worker performance and mean thermal sensation vote. Experiencing indoor temperatures above 27°C can result in a 5% reduction in productivity while temperatures approaching 30°C can result in a 10% loss in productivity. Further, according to Cui et al [51], based on a climate chamber study with 36 subjects exposed to temperature between 22°C and 32°C while undertaking memory typing, the thermal environment can effect peoples motivation which, when conditions are slightly cool, motivation increases in turn improving productivity. In light of this, caution must be exercised with office building retrofit projects that incorporate natural ventilation strategies as they will invariably be exposed to higher risk of elevated temperatures owing to the free running nature of the indoor conditions. Given that salaries can be orders of magnitude greater than the operational energy costs associated with buildings any planned retrofit scope for free running office buildings should recognise the importance of ensuring the indoor environment remains within defined upper and lower temperature ranges, most likely based on the adaptive model [20].

In addressing this, consequently, the heat removal potential of natural ventilation systems and their effect on internal environment is increasingly becoming a critical metric in selection of the final design and operation strategy, particularly for free running buildings [52–56].

2.2.3 Method for Defining Long Term Overheating

Really there are a number of key published standards that form the main pillars of evaluation of long term thermal comfort. ISO7730 largely based on work by Fanger [49], more recently the European Standard EN 15251 on adaptive comfort criteria [20], ASHRAE 55 [57] and CIBSE TM52 [21]. Many of these documents propose differing ranges of acceptable thermal environment, summarised in Table 2 of [48]. Depending on the building function or activity a broader spread of acceptable operative temperatures is accommodated and there is some consistency/synergy across the different standards. However for indices such as PMV more input parameters are needed as this focuses on direct estimating of the physiological response of the building occupants to their surrounding thermal environment. Percentage indices such as those from CIBSE and BRE, equations 2.1 and 2.2, rely on the calculation of the number of hours exceedence and need only a reference temperature value, the number of hours of occupancy in a given time interval, usually taken as 1 year, and either simulated or measured values of operative temperature.

2.2.3.1 Predicting Thermal Discomfort in Free Running Buildings

While the development of the PMV model of thermal comfort has been for many years the standard model for assessing performance of a building, it is largely based on climate chamber studies with closely controlled conditions, more akin to mechanically air conditioned spaces. It has been shown to struggle to produce accurate predictions regarding the levels of satisfaction with internal thermal environment in real, free-running buildings, where conditions drift in response to external perturbations in ambient weather patterns amongst others. Instead methods that use a variable range of comfort limits based on outdoor mean conditions are seen as more suited to assessing performance in naturally ventilated buildings.

CIBSE traditionally recommended a single reference criteria for determining overheating. This stated that a buildings indoor operative temperature should not exceed $25^{\circ}C$ for greater than 5% of annual occupied hours. In recent times this was updated to $28^{\circ}C$ for greater than 1% of annual occupied hours. This is attractive for its simplicity and ease of use. It also provides a tangible result that can be easily communicated to building owners, architects and non experts generally. It has gained widespread use in industry as a benchmark index for assessment of overheating and is cited in the Irish Part L Building Regulations as one of the approaches that can be used to assess compliance with limiting solar overheating [58]. It calculates the number of occupancy hours above $28^{\circ}C$ in a given calendar year:

$$h^* = \frac{\sum_{i=1}^{h_{occ}} [w f_i^{h^*} h_i]}{\sum_{i=1}^{h_{occ}} h_i} \quad (2.1)$$

$$\text{where, } w f_i^{h^*} = \begin{cases} 1 & \text{if } T_i > 28^{\circ}C \\ 0 & \text{otherwise} \end{cases} \quad (2.2)$$

However, because the thermal comfort limits in free running buildings generally vary with the outdoor conditions, as shown by Nicol and Humphreys [21], this static index value does not adequately capture the full range of acceptable conditions and may incorrectly estimate whether a building is deemed as being excessively uncomfortable. Further it does not assess the duration of exposure to specific temperatures exceeding $28^{\circ}C$ and as such it is not possible to ascertain whether the overheating is from $1K$ or $4K$ temperature difference above the reference value. ISEN 15251 addresses much of this. The standard suggests a comfort temperature calculated using an exponentially weighted running mean as:

$$T_c = 0.33 \cdot T_{rm} + 18.8 \pm K \quad (2.3)$$

The temperature constant K will vary according to the thermal comfort category. This facilitates a variable reference temperature for estimating unacceptable levels of discomfort. Nicol and Humphreys define discomfort as a function of the deviation from the comfort temperature, not the temperature itself [59]. EN 15251 includes both upper and lower limits creating a comfort range and sets different categories for this comfort range using increasing deviations from the comfort temperature. CIBSE recently published TM52, 'The Limits of thermal comfort: avoiding overheating in European buildings' [21]. This publication was largely the result of the CIBSE overheating risk taskforce and contains a proposal for a new set of criteria for defining whether or not a building is overheating or at risk of overheating, differentiating between mechanically cooled and naturally ventilated buildings.

2.2.3.2 CIBSE adaptive Criteria for identifying overheating

CIBSE propose three separate criteria for the identification of excessive overheating each one addressing a different facet of the phenomena. These are outlined as follows:

- Criterion 1: The number of hours that the operative temperature can exceed the threshold comfort temperature (upper limit of the range of comfort temperature) by $1K$ or more during the occupied hours of a typical non heating season (1^{st} May to 30^{th} September) shall not be more than 3% of occupied hours.
- Criterion 2: To allow for the severity of overheating in a given day the weighted exceedence, W_e shall be less than or equal to 6 for that day. W_e can be defined as:

$$W_e = \sum_{i=1}^{3K} h_i w f_i, \quad \text{with } i = T_{op} - T_{cu} \quad (2.4)$$

The weighting factor, $w f_i$ is equal to i for each iteration giving more importance/weighting to higher ΔT values.

- Criterion 3: To set an absolute maximum value for the indoor operative temperature the value of ΔT shall not exceed $4K$

2.3 VC as a Mitigation Strategy

Ambient air is supplied to the interior of a building to satisfy one of two objectives; firstly, to ensure a minimum indoor air quality is achieved by removing pollutants, odours and other unwanted air borne elements. Secondly, to remove heat build up from sources of heat gain to the space. As a minimum, IAQ must be maintained at or above a certain level, determined by national regulations and international standards. Historically the quantity of air deemed necessary for basic air quality has changed depending on source and new research findings. ASHRAE 62.1 has been amongst the most important documents for guidance on ventilation for IAQ since its first publication in 1978 [60]. It states the minimum ventilation rates in the breathing zone to satisfy occupant air quality needs. Until more recently cooling from natural air intakes was perceived as a convenient and satisfactory by product of the ventilation provision during summer and a hindrance during winter. Ventilation flowrates required for IAQ are generally well below those necessary for cooling. Utilising enhanced ventilation flowrates for cooling purposes is at the discretion of the building designers. However, increasingly it is becoming more difficult to comply with national energy standards and still utilise active mechanical cooling solutions rather than solutions such as enhanced passive ventilation. Utilising an active mechanical cooling solution to control the internal thermal environment affords good control over the range of temperatures within the building and does ensure increased certainty regarding delivered performance. However this approach comes at a substantial energy cost. Further there is a measurable initial investment required for equipment and controls along with annual maintenance costs. In northern European climates active mechanical cooling is more commonly being perceived as an unnecessary luxury that is prohibitively carbon intensive and in many instances does not result in more satisfied occupants given the semi-autonomous nature it places on the control of the internal environment when compared with, for example, passive/local systems that rely on openable windows, desk fans and adaptive clothing policies. Passive cooling through the integration of natural ventilation principles with the building morphology and materials has long been championed as a viable alternative to mechanical cooling. However, the basic premises under which both approaches operate are fundamentally different and this has led to a scepticism from building owners regarding the ability of a natural ventilation system to adequately deliver acceptable internal conditions in buildings year round. The difficulty is the criteria by which natural ventilation is assessed is often one suited only to mechanically controlled environments and this is diametrically opposed to the basic principles of the concept. We will return to the idea of a maximum cooling potential for passive natural ventilation, contingent on the climate and circumstances of the application, and how knowledge of this is critical in understanding the constraints surrounding the use of natural ventilation for cooling.

2.3.1 Definition and justification for passive VC

A number of different approaches exist for passive cooling dissipation techniques to reduce or offset unwanted cooling needs and overheating of buildings. Passive cooling techniques can be organised into a three step framework: 1. prevention of heat gains, 2. modulation of heat gains and 3. heat dissipation [10]. Approaches used to achieve these range from utilising the ground

as a heat sink, employing evaporative cooling techniques or using the ambient air as a heat sink as part of a ventilation free cooling solution. For ventilation free cooling, or more commonly referred to as VC, this is generally accepted as an effective, energy efficient, mitigation strategy to building overheating. The foremost characteristic of VC that makes it an attractive solution is the reduced cooling energy loads. Extended monitoring has shown that naturally ventilated buildings typically use less than 50% of the corresponding energy consumption of air conditioned buildings and assessment of VC techniques in Europe have shown they may contribute highly to reducing the cooling needs of buildings and be an effective tool for tackling climate change adaptation in existing buildings [61, 62]. Blondeau et al showed that depending on the set point temperature in a space up to 54% of the cooling needs can be met using a VC system and night time operation [63]. The study was based on data from La Rochelle. Florides et al used TRNSYS [64] to investigate measures to reduce the thermal load in a four zone house [65]. They reported that using natural ventilation in summer can reduce the annual cooling load by 7.7%. However this was in a southern Mediterranean location so the cooling potential of a natural ventilation system would be somewhat restricted. Yang and Li analytically investigated how differing levels of thermal mass combined with night cooling affect the total cooling load for a daytime air conditioning system in a single zone space [66]. They demonstrated that up to 60% of total cooling load can be offset using this VC approach when the thermal time constant of the thermal mass was 400h. More recently, Rackesa and Waring used Monte Carlo simulation with EnergyPlus to investigate the energy saving potential of alternative ventilation strategies [67]. They found savings up to 84% of HVAC primary energy (Natural Gas and Electricity) from implementing free cooling in the mechanical ventilation system using an economizing approach that increases external ambient air when the temperature difference is favourable. Combining economizing with a supply air temperature reset that effectively increases the supply air temperature setpoint when ambient conditions are favourable to save mechanical cooling energy. In a different study Oropeza-Perez and Alberg Ostergaard [68] considered the amount of cooling energy that can be offset from the use of natural ventilation in both hot-humid and hot-dry climates. They found that, based on numerical simulations up to 54.4% of the energy consumed for air conditioning in Mexico could be saved if natural ventilation based on both wind and stack effects as adopted. Implemented correctly, VC can produce large cooling energy savings. When there are no momentum inducing components in the system such as fans or mechanical cooling devices, the approach is regarded as providing passive free cooling by relying on buoyancy and wind generated forces to produce a pressure driven flow through the building.

2.3.2 Extending the performance of VC

A key approach for improving the suitability of passive VC strategies is to extend the cooling range of the system, i.e. widen the ranges of boundary conditions where the system can deliver sufficient cooling to the indoor space. This can be achieved through elevated ventilation airflow rates, particularly when there exists a low temperature differential across the envelope yet is still sufficient, with adequate cooling potential, when combined with elevated airflow rates. Where there is a low ΔT_{ie} available, for example during occupied hours in periods of extended warming, then it is sometimes still beneficial to increase the airflow rate and velocities in the space. An

example of designing for enhanced ventilation airflow rates is the use of the venturi effect to generate lower pressures at ventilation outlets which in turn produces higher pressure differential to drive increased ventilation through the building. van Hooff et al investigated the performance of a venturi shape roof designed to increase airflow rates within a building [69]. They used wind tunnel measurement and computational fluid dynamics (CFD) to study how the wind pressure coefficient, C_p and the wind speed ratio U/U_{ref} changed for four different arrangements; venturi shaped roof without guiding vanes, with 90° vanes, with 10° vanes and a reference configuration with no vanes. They found that the venturi shaped roof with no guiding vanes was the most effective with C_p coefficients of up to -1.30 at the ventilation outlet and a U/U_{ref} ratio of about 1.4 giving enhanced ventilation performance. They expressed caution with the future design of such solutions given the negligible effect of introducing guide vanes. Kim et al [70] experimentally investigated the ventilation rate using a venturi roof ventilator which relies on a similar principle to the venturi shaped roof in that it generates a negative pressure region thereby increasing the pressure differential to the ventilated space, increasing the ventilation airflow rate. They found that the ventilation rate increased linearly with the wind speed and the area of the air intake opening in the room was also an important factor with larger intake areas resulting in larger ventilation rates. Various other solutions to increase wind driven ventilation have been investigated in the recent past. A summary of these is provided by Khan et al [71]. They identify static wind catcher, a rotating wind cowl and a rotating turbine ventilator as airflow enhancing devices with various levels of performance. These all rely on wind momentum to drive ventilation and can be effective solutions to increase VC capacity for wind driven systems. In some of these applications the increase in airflow rate can lead to an increase in the velocity of air in the occupied space. An increased velocity has been shown to extend the thermal comfort range (see Fig 2.27, section 2.8.2 [20]). This extended comfort range increases the cooling potential for a particular climate and buildings.

In some instances where it is difficult to obtain large ventilation airflow rates, consequently resulting in lower velocities within the space, depending on the local climate, a systems capacity for heat dissipation can also be extended based on achieving a high envelope ΔT_{ie} . This can be a particularly effective approach at times when, although ambient temperatures are quite low, there still exists a heat removal requirement in the building. The primary occurrence of this would be in low energy buildings with an unbalance between incident solar/internal heat gains and fabric heat loss during shoulder seasons in warmer climates and during the summer in temperate northern climates. Oropeza-Perez et al [68] recently investigated the free cooling potential of natural ventilation in a real passive house in Denmark, a temperate climate with mean/max daily ambient temperatures in June, July and August of $13.3^\circ C/16.0^\circ C$, $14.4^\circ C/16.1^\circ C$ and $17.1^\circ C/22.0^\circ C$ respectively. They found that the number of hours of thermal discomfort during June, July and August can be reduced through the use of the natural ventilation by 90.8%. This is based on a target indoor air temperature of $25.5^\circ C$. The study didn't state what the simulated airflow rates were to achieve this reduction. There are good opportunities for high cooling potential under these circumstances although over-cooling and draughts can be an issue with this type of system, which was not addressed in the study. In a study completed at the zero2020 building at CIT, Cork, Ireland, O'Donovan et al [72] investigated the effect on thermal comfort and the cooling potential of the MCSL system in a simulated overheating scenario in

the real building. The tests were executed with a high ΔT across the opening, the external ambient being 12°C . The study found that in a 30 minute period, beginning with an internal operative temperature of 27.3°C the full height opening configuration (see Table 3.5, Chapter 3, pg 73), the space was cooled to an operative temperature 22.4°C . The high ΔT was highly effective in removing built up heat gains. Depending on the opening area used the cooling rate, represented by the temperature ramp rate, K/h , varied from $0.5K/h$ to $-9.6K/h$. In fact, using the maximum available opening area for cooling resulted in a negative mean thermal sensation vote (MTSV) outside all comfort category ranges defined by ISO 7730 [49]. Figure 2.5 below shows the cooling effect for each opening configuration (each was tested 4 times).

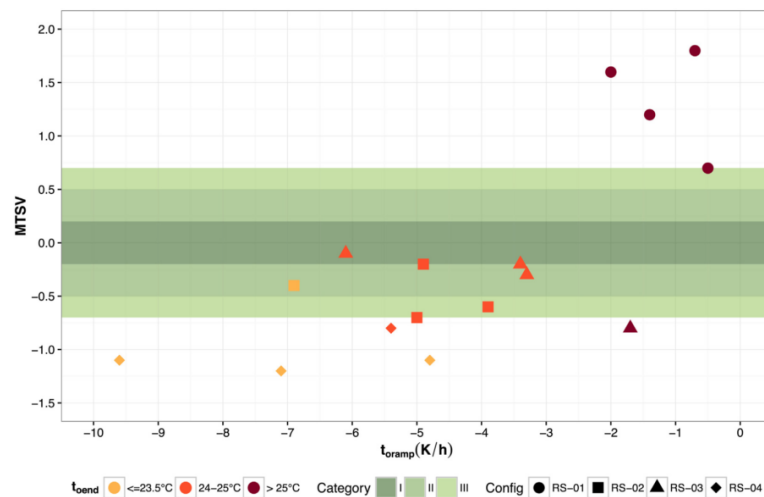


FIGURE 2.5: Scatter plot of relationship between MTSV and operative temperature ramp from the start to the finish of a test. Colour indicates the operative temperature at the end of the test using an arithmetic mean of the last two minutes. [72]

2.3.3 Estimating cooling potential

Some work has also been done attempting to quantify the cooling potential for systems that rely on natural or mechanical ventilation. The aim of the research was to develop techniques that could be used to identify the suitability of a particular climate and building combination to use ventilation for cooling purposes. This is of particular importance given the increased sensitivity of low energy, well insulated, air tight spaces to variations in the heat balance of the indoor environment. Ensuring there is sufficient potential for free cooling in the climate will assist in determining the most suitable cooling strategies during the early stage design and selection of VC systems. Ghiaus and Allard proposed a free running temperature to characterise buildings that rely on natural or mechanical ventilation for cooling [73, 74]. The free running temperature is defined as representing the indoor temperature of a free running building in thermal balance with the outdoor environment when neither heating or cooling is used. The free running temperature will need to be adjusted by heating, cooling by ventilation, or mechanical cooling depending on the outdoor air temperature and the upper and lower limits of the thermal comfort range. The extent to which ventilation can satisfy cooling is based on the available ventilation rate above the nominal value and the available ΔT_{ie} . They demonstrated that using

upper and lower thermal comfort limits that it was possible to achieve free cooling by ventilation when the outdoor temperature was below the upper limit thermal comfort temperature and the building free running temperature was above the upper limit value. The extent to which the free running temperature could be brought to the value of the outdoor temperature was a function of the increased ventilation rate with higher ventilation rates resulting in more cooling. Once the outdoor temperature exceeded the upper limit thermal comfort value free cooling was no longer available. Inard et al used this approach to investigate the free cooling potential of a natural ventilation system in a real building [75]. He showed that the method was quite accurate in predicting the cooling potential when compared with the actual cooling delivered by the ventilation system using measurement data from the building. In fact the system could provide 8% more cooling than was actually being supplied. This method highlights the importance of the thermal comfort range and systems that can extend that range, by, for example, increasing air velocities in the space.

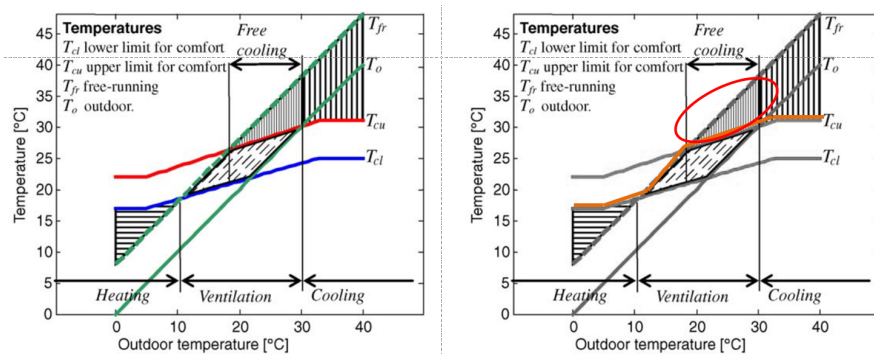


FIGURE 2.6: Ranges for heating, free-cooling and mechanical cooling when the free running temperature is higher than the outdoor temperature. The left side shows how the indoor temperature will track along the comfort ranges. [74]

While natural ventilation cooling potential is limited by the dynamic and stochastic nature of ambient conditions in and around buildings its potential can be enhanced through the use of various principles and strategies, the most effective of these being night time cooling. In an alternative approach to above Artmann and Heiselberg [9] assessed a climates potential to provide free cooling during the night time, making use of the diurnal temperature swing. They showed using this daily temperature difference that much of Northern and Central Europe has good climatic cooling potential and this should be further exploited using night time cooling. They also proposed the use of a climatic cooling potential indicator based on cooling degree hours. They show that the UK and Ireland have a strong CCP, between 120-180 Kh even during the hottest month of the year. Northern parts of Europe have greater cooling potential than Southern parts. However, they don't consider the ability of given systems or building configurations to achieve the required ventilation rates for cooling when operating in these various climates.

Axley and Emmerich proposed to use a heating balance point temperature approach to estimating VC potential [76]. However, rather than use an adaptive upper and lower thermal comfort limit it uses a single cooling set point temperature as a set upper limit above which no cooling can take place and a lower limit based on guidance from ASHRAE. They use a steady state heat energy balance model to estimate the balance point temperature for each time step. The method has been incorporated to the recent VC potential analysis tool developed within IEA-EBC Annex 62

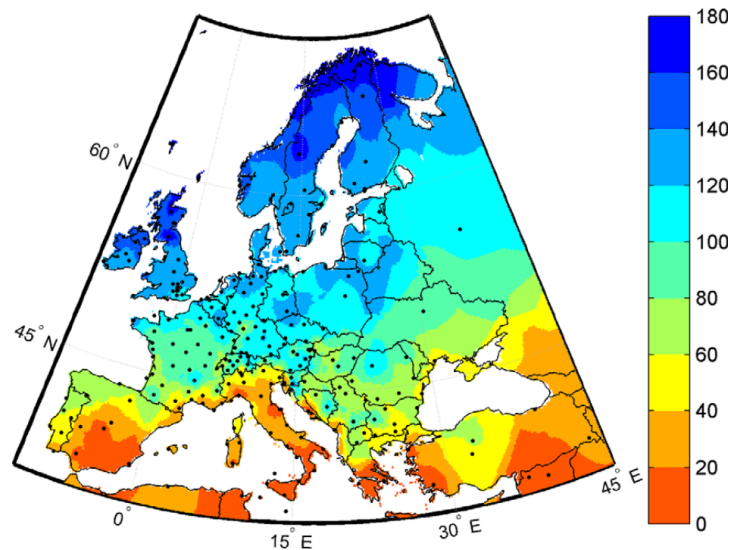


FIGURE 2.7: Map of mean climatic cooling potential (Kh/night) in July based on Meteonorm data

on VC. However, the Annex 62 approach uses the adaptive comfort model to estimate relative upper and lower comfort limits similar to Ghaius, as opposed to the fixed cooling set-point. The approach by Axley and Emmerich is discussed further in Appendix B. These various approaches have been shown to be useful tools for predicting the extent to which VC is available using the external ambient air. However, they assume that the required airflow rate can be delivered to the space without any consideration to the prediction of this using the same boundary conditions as for the estimation of cooling potential. This ventilation rate may be unachievable or may require unrealistic system dimensioning. When using a natural ventilation system for cooling in low energy retrofits, the extended period where cooling is likely needed as a result of the retention of internal and solar heat gains beyond the traditional warm summer season, there can be an issue with over cooling and thermal discomfort due to draughts. This is largely due to the requirement to provide cooling at a magnitude much reduced to that available from the low ambient temperatures. Bourgeois et al suggested that a lower limit of 12°C external ambient should be used when setting a VC suitability range [77]. O'Donovan et al also reported occupant dissatisfaction with the thermal environment when cooling with 12°C and an opening area to floor area ratio of 3.8%, well below the recommended 5.0% for natural ventilation in the Irish Building Regulations [72]. Draughts are not the only barrier to the adoption of natural ventilation for cooling. There are other obstacles that need to be overcome and in some instances there exist constraints which limit the application of VC.

2.3.4 Barriers to the adoption of passive VC

Lomas and Ji [78] demonstrated using results from a study in London of simple ventilation strategies (i.e. single sided ventilation) and advanced ventilation strategies (i.e. various stack riser configurations) in hospital wards that using advanced ventilation solutions was required to maintain hours of overheating above 28°C below 100 hours in all future scenarios except 2080.

In this instance, 2080, even though it was not possible to meet the overheating criterion there was 290% more hours of overheating using simple ventilation strategies as opposed to advanced stack driven strategies.

Maximising ventilation airflow rates are going to be increasingly important to overcome the capacity barriers imposed by the boundary conditions anticipated with the effects of the already irreversible or overshoot part of climate change. DeWilde and Coley have suggested that climate change will cause a shift in thermal operational conditions in buildings to the extent that passive systems will ultimately go out of range of options available for designers [79]. For Europe, Santamouris showed that, cooling degree days, a metric for the extent of the cooling season and elevated external ambient temperatures, could increase by 300% for an external temperature increase of 4-5K, requiring passive cooling systems to incorporate even wider ranges of application at reduced cooling potential. Santamouris suggests that passive cooling techniques may not be able to satisfy the future cooling requirements due to the climatic dependence of their capacity. [80].

daGraca and Linden identify both positive and negative effects for passive cooling from climate change. The extended period of annual weather suitable for opening windows from elevated temperatures in spring and autumn will mean natural ventilation will experience increased usability outside the core summer period with issues such as draughts less common. However in some instances, particularly cities with mild climates such as those in Ireland and the UK (San Francisco was used in the study), the number of hours where conditions favour direct natural ventilation actually increased ($10^{\circ}C \geq T_e \leq 25^{\circ}C$).

Tejero-Gonzalez et al also reviewed climate factors that are important when assessing the applicability of free cooling with ventilation [81]. They identified that a high day-time and low night-time dry bulb temperature is optimal for night time cooling. Further, an external ambient dry bulb temperature below the comfort range was also desirable for direct daytime VC. IPCC AR5 assessment report proposes that the global mean surface temperature change for the period 2016-2035 relative to 1986-2005 is likely to be in the range $0.3^{\circ}C$ to $0.7^{\circ}C$. By the end of the 21st Century, depending on the representative concentration pathway chosen this temperature change could be anywhere from $1.5^{\circ}C$ to exceeding $2.0^{\circ}C$. The recent COP21 in Paris committed to an upper limit of $1.5^{\circ}C$. This increase in mean surface temperature will come with changes in the diurnal variability of temperatures as well as an increase in high temperature extremes. According to the AR5 assessment report: *"It is virtually certain that there will be more frequent hot and fewer cold temperature extremes over most land areas on daily and seasonal time scales, as global mean surface temperature increases"*. Using the probabilistic weather generator from UKCP09, The UK Climate Projections datasets and models, Kershaw et al [82] showed that, with a 10% probability, the change in mean annual external temperature in Plymouth could be as high as $1.0^{\circ}C$. As part of a study comparing new building simulation weather file formats and approaches to characterising overheating and thermal discomfort under future climate change scenarios Lui et al, using a probabilistic future design summer year, demonstrated that overheating will increase substantially in 2050 [83]. They show that across the 14 CIBSE UK weather sites, the number of hours greater than $28^{\circ}C$ ranges from 25 hrs to 500 hrs. For London, depending on the percentile hot summer year file chosen (i.e. 10th to 90th

percentile of 100 ranked weather files generated from UKCP09), overheating hours above 28°C is anywhere from 100 to 300 hours, representing up to 12% of hours for an occupancy profile giving 2500 annual hours. Other studies have demonstrated similar warming trends for buildings [84]. These high temperatures limit the potential for VC, both by direct ventilation during the day time and also overnight with temperatures remaining above the comfort range throughout the diurnal temperature swing. However, they also show that the difference between daily maximum and night time bedroom temperatures remains fairly constant giving comparable stack driven forces for ventilation rates, albeit outside the comfort ranges. They also show heat waves are due to increase by up to 40% across the three future time periods investigated compared with a baseline. This also demonstrates the constraints a barrier such as climate change will impose on VC strategies that rely on the diurnal temperature swing for heat dissipation. Other limitations to the adoption of VC applications include effects from the surrounding built up urban profile. Urban constructs can lead to complicated interactions creating many barriers to maximising VC system capacities. Fig 2.8 shows the associations between the many localised factors.

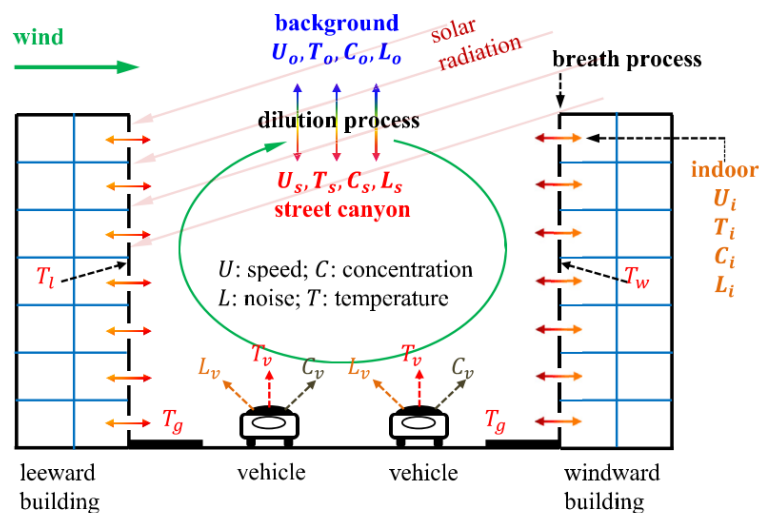


FIGURE 2.8: Various interactions between urban climate and canyons [85]

The available wind speed (and subsequent airflow rates) at a ventilation opening is substantially modified by the effects of the urban canopy layer and in particular in urban canyons [85, 86]. Georgakis and Santamouris published a detailed study of canyon conditions in Athens in the summer along with ACR measurements for single sided and cross flow ventilation using the tracer gas decay method [87]. They showed that ACR values were 82% lower for the single sided system and 68% lower for the cross flow system when compared with calculation for an undistributed building with no surrounding obstacles. VanHooff and Blocken showed using CFD and a large semi enclosed stadium that when surrounding obstacles are not included in calculations of ACR there can be an overestimation of 96% [88].

Separately to the negative effects on wind forces from the urban environment, there are also consequences for the available cooling potential due to air temperature effects. Urban Heat Island is a consequence of heat build up in densely populated cities although canyon layout can also lead to some positive effects on local temperatures. Air temperatures low down in street canyons have been shown to be somewhat below the background regional air temperature

positively extending the cooling potential of a passive cooling system [85]. Understandably this can help counteract any reductions in local wind speeds. Urban heat island effects in London have been shown to increase cooling loads and overheating in offices, both now and in the future, compared to a rural reference location [47]. The differences between locations were quite significant compared with differences into the future. In another study it was shown that while there were no substantial differences in the maximum daily temperatures between the rural and urban locations, both in and around London, there were significant differences in the minimum daily temperatures with the urban location having up to 6°C higher minimum external ambient temperatures [89]. This suggests there are additional limitations of the heat removal potential of VC systems in built up urban locations. Other important barriers that will only become more prevalent in an increasingly urbanised world in the future include air pollution and noise pollution [74]. A final barrier to the uptake of passive VC strategies which is relevant when using solutions such as night cooling is the security risks from opening windows or air intakes during the night time period of cooling.

In reviewing the suitability of passive VC as a climate change mitigation strategy we have identified evidence for its energy saving potential, demonstrated how the range of cooling provision can be extended through better exploitation of boundary conditions, presented current knowledge regarding the quantification of cooling potential for free running buildings and considered the key barriers to its adoption as a solution for indoor cooling both into the future and in light of the increasing urbanization of our lives. It is clear that using passive cooling techniques should be promoted as viable energy efficient solutions that can form part of a wider building retrofit scope. There are many different approaches to the aeration of an interior space. The work presented in this thesis empirically investigated the aeration performance of a particular purpose provided single sided ventilation solution. Single sided ventilation is an easily retrofitted, physically non-invasive approach that sits comfortably with externally applied deep retrofit envelope strategies. The next section provides a summary of the development of single sided ventilation techniques and its suitability as a VC strategy for commercial building retrofit applications.

2.4 Single Sided Ventilation

The need for energy efficient alternatives for the provision of cooling in indoor spaces is now recognised as a central motivation for the adoption of natural ventilation as the primary solution to indoor climate control. Airflow rates for cooling purposes are in almost all situations of a higher magnitude than those required for IAQ. For this reason and those listed in previous sections successful selection of the ventilation strategy and subsequent design of the envelope to deliver cooling performance is at best challenging. When developing such strategies there are various factors requiring careful consideration including, amongst others, building morphology, local micro climate, immediate surroundings & automatic controls. To augment heat removal potential the preferable solution is cross flow ventilation with airflow openings on opposing external walls. This ensures the best possible mean pressure differential across the opening. An important feature will be the aerodynamic characteristics of these openings as they are a

critical component of the overall system performance and their dynamic operation is sensitive to fluctuating local boundary conditions.

Amongst the various strategies available as alternatives to cross flow ventilation, when it is not viable, is single sided ventilation. This has the lowest capacity for aeration although it is probably the simplest configuration that is possible in order to ventilate a space. In theory it relies on an opening(s) in an exposed wall in an otherwise sealed room, providing aeration for the dilution of heat. Owing to its perceived simplicity in installation and operation its use is near ubiquitous in the built environment. However, there is still much uncertainty around its performance and predicting single sided airflow rates remains a central objective for the research community. Depending on boundary conditions, mass transfer is generated across the opening either by thermal effects, generating a buoyant momentum, or by wind effects, generating a mechanical momentum. Buoyancy forces create a difference in pressure across the opening brought about from a variation in density of the two acquiescent air masses resulting from changes in temperature. Wind forces generate more complicated air exchange mechanisms depending on the angle of incidence at the opening. At low wind incidence angles the primary exchange is from a turbulent shear mixing layer along the opening. This is driven primarily by a local parallel wind velocity at the building envelope. When this shear driven flow is combined with buoyancy driven exchanges in the opening a complicated relationship develops between various influential parameters. At higher incidence angles the difference in pressure at the opening can play a more significant role. The total pressure can be decomposed into a fluctuating component and a mean component, with the fluctuating pressure component important to the overall airflow rate achievable. When the dynamic nature of the local wind is taken into consideration this creates a complicated fluctuating ventilation rate and depending on the boundary conditions the ventilation rate can be either wind dominant or buoyancy dominant. Figure 2.9 shows the basic concept of single sided ventilation for cooling purposes [90]. The effective penetration depth of the airflow from single sided ventilation is a primary limitation on its applicability. However, in many existing buildings where there are single cell perimeter office spaces and shallow open plan offices, where there is a lower ventilation requirement than other more open plan, deeper spaces, the approach has merit. For deep retrofit projects enhanced single sided ventilation can be a viable option as it does not require substantial internal reconfiguration and is physically non invasive. In such strategies both inlet and exhaust must be positioned at the same facade with openings often positioned at high and low levels maximising buoyancy driven aeration. Achieving this maximum available height may not be possible in refurbishment situations where ventilation pathways are physically constrained by the existing fenestration apertures [33]. Further to this, the physical size of ventilation openings is often limited by practical issues such as draughts and manual opening mechanisms.

2.5 Driving Forces in Single Sided Ventilation

The mechanisms that produce airflow in single sided ventilation are generated through varying combinations of wind and buoyancy forces acting at the opening. To successfully predict the airflow rate performance of a single sided ventilation system the approach must attempt to deal

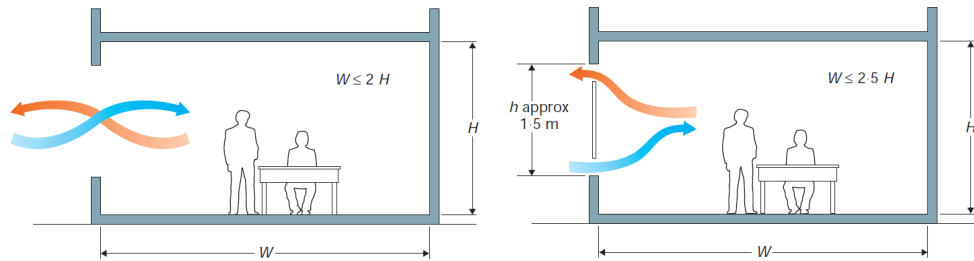


FIGURE 2.9: Various single sided strategies for cooling purposes. Reproduced from CIBSE AM 10 [90]

reasonably well with the complicated flows that arise from this situation. We are concerned here with the investigation of time averaged ventilation airflow rates through building envelopes. In this regard, we can generally apply the theory of steady flow characteristics through openings. Conventional envelope flow models that use the Bernoulli equation, which relies on the assumption of steady, inviscid and incompressible flow, are generally adopted as an acceptable theoretical basis when concerned with predicting airflow through small, sharp edged openings. The openings should be small enough so as not to influence the external wind pressure distribution and the internal air velocities should be small enough that the internal pressure can be derived using the hydrostatic equation. Mean pressure differences generated across the opening from kinetic energy in the wind and/or variations in hydrostatic pressure from the different thermal environments either side of the ventilation opening, will result in a mean volumetric flow. These pressure differences across the envelope opening can be summarised using equation 2.5:

$$\Delta p = P_e - P_i - \Delta \rho g H + p_w \quad (2.5)$$

Introducing C_d and the area of the opening, A_o , we obtain a general theoretical model for steady envelope volumetric flow rate, equation 2.6:

$$Q = C_d A_o \cdot \left(\left| \frac{\Delta \rho g H_o}{2} + \frac{p_w}{2} \right| \right)^{0.5} \quad (2.6)$$

This equation must be modified depending on whether buoyancy alone is present, wind alone is present or both forces are acting and give rise to mechanisms that due to their complicated nature, have been traditionally dealt with using empirical or semi empirical models.

2.5.1 Single sided ventilation from buoyancy alone

In the absence of wind, flow through a single sided opening is generated from a pressure gradient that arises due to differences in density between the air mass on either side of the opening. This density difference is due to variations in air temperature between the two sides of the opening, generally referred to as buoyancy driven flow. When due to buoyancy forces alone, the flow will be bi-directional with a neutral pressure at the opening mid height point. The temperature difference at the opening results in a buoyancy effect that produces a stable airflow exchange.

Semi empirical buoyancy alone envelope flow models rely on the principle of the still air discharge coefficient, C_d , with the assumption of independence from Reynolds number, Re , when dealing with envelope flows.

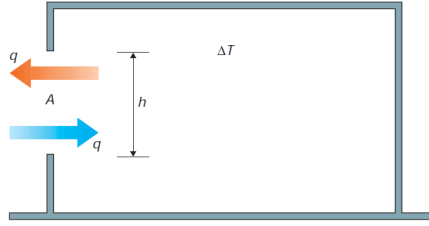


FIGURE 2.10: Single Sided ventilation with one opening driven by buoyancy alone

When working with steady envelope flow models an empirical power law, equation 2.7 below, has been used to describe flow in situations where the geometry is complex and flow is assumed as being independent of Re .

$$Q = \alpha \Delta p^\beta \quad (2.7)$$

When flow is best predicted using $\beta = 1.0$ we have a linear relationship with the constant b in equation 2.8 derived empirically although according to Etheridge and Sandberg [91] it can have a physical meaning.

$$Q = b \Delta p \quad (2.8)$$

When envelope flow models are based on orifice flow theory, we have $\beta = 0.5$. Within these two extremes β can have an influence on the ability of a given model to correctly predict ventilation rates obtained experimentally as shown for example by Sharples et al [92]. For the flow through a single opening due to buoyancy alone case a bi-directional flows establishes based on the difference in densities between the air on both sides of the opening. A neutral pressure level develops at $H_o/2$ where the pressure difference between both sides, $\Delta p = 0$. We can say that:

$$Q_b = W_o \int_{z=0}^{z=H_o/2} \left(\frac{2\Delta p(z)}{\rho} \right)^{0.5} dz \quad (2.9)$$

With z representing the vertical height at some distance $z(H)$. Solving this equation, employing a still air discharge co-efficient C_d , using the ideal gas law to substitute temperature for pressure and density, we have the well known relationship for flow due to buoyancy alone:

$$Q_b = \frac{1}{3} C_d A_o \left(\frac{\Delta T_{ie} g H_o}{T} \right)^{0.5} \quad (2.10)$$

Solvason and Brown experimentally investigated natural convection through a large single opening in a laboratory wall and found that there was good experimental agreement with the theory

[93]. More recently, researchers have investigated the suitability of this relationship in various different situations and developed empirical correlations to account for additional effects observed in reality. In addition to buoyant flows a number of semi empirical models have been developed to attempt to account for contributions from wind effects.

2.5.2 Single sided ventilation from wind alone

The presence of external wind will produce a pressure driven airflow across an opening. A pressure difference will establish between the internal and external air masses resulting from a difference in the external pressure, from the momentum due to kinetic energy present in the wind, and the internal pressure, usually assumed to be hydrostatic. The time mean pressure difference due to wind flow on to or away from a surface is given by:

$$\Delta p_w = P_i - C_p \frac{\rho U_w^2}{2} \quad (2.11)$$

C_p is the static wind pressure coefficient for a particular location on a wind exposed surface, values vary in magnitude and can be either positive or negative depending on the building shape and location. The static pressure at the surface will usually be positive when the surface is windward and negative when the surface is leeward to the upstream wind. Values are usually obtained by CFD or wind tunnel experiments and organisations such as AIVC publish tables for simple shapes. However, the wind direction and speed vary in time due to wind turbulence, wind gustiness and the effects of obstacles making the estimation of C_p values difficult in the urban environment. Further, while this approach is fine where mean pressure difference is the main driving force it does not work well where the airflow mechanism generating flow is not related to the mean pressure difference. In cases with only a single unobstructed opening in an otherwise near sealed room, studies have shown that when the wind is present there exists a shear mixing layer, promoting turbulent eddy penetration. The existence of this acts as the primary airflow exchange mechanism at the opening, rather than the mean pressure difference normal to the opening driving flow [94]. Other studies have shown that wind gustiness can also lead to the presence of a pulsating flow [95]. There can be a number of different mechanisms generating flow across an opening:

- Fluctuating pressure difference
- Turbulent diffusion from a shear mixing layer
- Mean pressure difference
- Aerodynamic interaction with the opening geometry

Malinowski was amongst the first to describe a number of different mechanisms that generate flow across a single opening when due to the wind, a pulsation flow and an eddy penetration due to the shear layer [96]. Cockroft and Robertson proposed that ventilation through a single sided opening in a building envelope could be characterised primarily by a pulsation flow. Later

Warren [97] proposed a mixing layer theory based on a shear jet developing across the opening as the dominant air exchange mechanism.

2.5.2.1 Pulsating Flow, Fluctuating Pressure Difference & power spectrum approach

Cockroft and Robertson developed a model based on the principle of a pulsating flow in and out of an opening related to the external wind pressure fluctuation and the compressibility of the internal air mass. They proposed the following equation:

$$Q = \frac{d\omega}{dt} = \pm C_d A_o \left(U_w^2 - \left(\frac{2\gamma P_i}{\rho V} \right) \omega \right)^{0.5} \quad (2.12)$$

The principle suggests a pumping effect across the opening similar to a second order spring damper configuration. The limitation of this approach however, is that it does not take into account the effect of incident angle on the airflow mechanism. It assumes the flow is normal to the opening surface, i.e. $\theta = 0^\circ$, and this situation rarely occurs in practice. Narasaki et al investigated the relationship between turbulence generated pressure fluctuation and airflow rate in a single circular opening using an enclosed laboratory model [98]. They found that the pulsation flow model proposed by Cockroft and Robertson was adequate at predicting airflow rates at zero wind incidence angle with various different turbulent boundary conditions but at other incidence angles the model over predicted the airflow rate. They also showed how there was a better correlation with measured airflow data when using velocities with certain fluctuating frequencies. They suggested a new model was needed that took account of the eddy penetration mechanism at higher wind incidence angles [98]. Crommelin and Vrins used wind tunnel measurements to experimentally investigate airflow rate through an opening driven by unsteady conditions [99]. They proposed an empirical relationship between the upstream wind velocity, the standard deviation of the fluctuating pressure difference at the external envelope and the airflow rate. They also investigated the influence of wind direction on the airflow but omitted this from their final correlation. However, these correlations have not gained much momentum in the literature. More recently Yamanaka et al tested the pulsating flow theory in a laboratory experiment [94]. They found good agreement between measured and calculated airflow rates for $\theta = 0^\circ$ although this was using a velocity sampling frequency of 100Hz which they suggest was arbitrary. Cockroft and Robertson suggested that 37% of the airflow rate across the opening due to pulsation will contribute to an air change rate [95] as some of the entering air will leave again.

Haghighat et al proposed a power spectrum analysis approach to account for airflow from the fluctuating pressures at the opening due to turbulent and unsteady wind [100]. They showed using the model that the fluctuating airflow rate was proportional to the opening size and opening depth. The parameters were important as they influence how much of the unsteady inflow air cleared the depth of the opening and came into contact with internal air. However, due to the slow mixing process between both air streams some of this inflow exited the opening without proper mixing thus not contributing to an air exchange. They suggested this was a complex

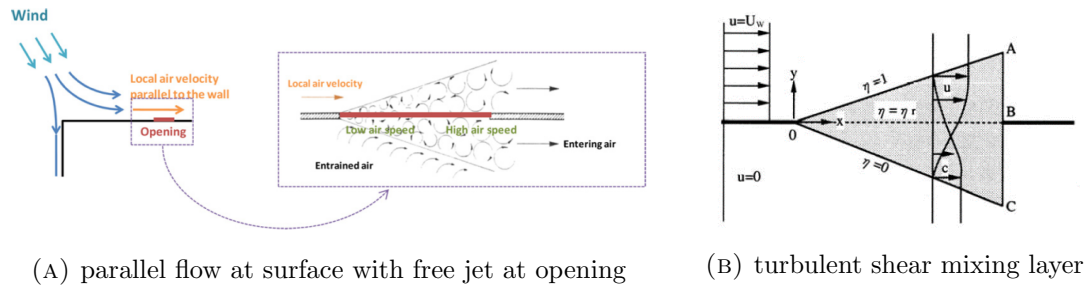


FIGURE 2.11: Two way symmetrical exchange of entrained air in a turbulent shear mixing layer.

phenomenon to understand and required additional research. Some of this work was extended later by the authors [101]. Recently Wang and Chen [102] proposed a method that uses power spectral analysis that decomposes the mean and fluctuating velocity components and calculates separate contributions to the fluctuating component based on both pulsation flow and eddy penetration.

IEA-EBC annex 20 - Airflow through large openings, completed in 1992, brought together much of the existing knowledge surrounding airflow through single sided openings [103]. It addressed ventilation due to pulsation flows and fluctuating pressure differences and in discussing the Haghghat and Cockroft models identified that the main challenge in understanding airflow exchanges due to fluctuating pressure differences at the opening is quantifying how much of the penetrating air actually mixes with the internal air and contributes to an air change rate. It seems that while some progress has been made in modelling single sided airflow much opportunity remains regarding the effects of a fluctuating pressure difference on the mean flow.

2.5.2.2 Turbulent Shear Mixing Layer

For most wind directions the localised flow along the face of a building envelope will be parallel to the surface. In this instance a turbulent free jet develops along the plane of the opening. Warren and Perkins [97] were amongst the first researchers to investigate turbulent shear mixing layer theory for building envelope flow. They proposed a two way symmetrical exchange between the high velocity external air and the acquiescent internal air, an application of the Morton-Taylor-Turner entrainment hypothesis, Figure 2.11. Their work sought to establish theoretical estimates of a dimensionless flow, denoted F_l , that incorporated how the shear mixing layer spreads along the opening. They proposed the relationship equation 2.13 with α suggested as having values of somewhere between 1.60 – 1.71 for a highly turbulent three dimensional mixing layer. Based on field studies and subsequent wind tunnel tests they established a more suitable value for F_l of 0.1.

$$F_l = 0.056 \cdot \alpha \quad (2.13)$$

Depending on the wind incidence angle at an opening, the mechanisms that produce a flow rate across the opening change. According to Chu et al [104] the flow through the opening in

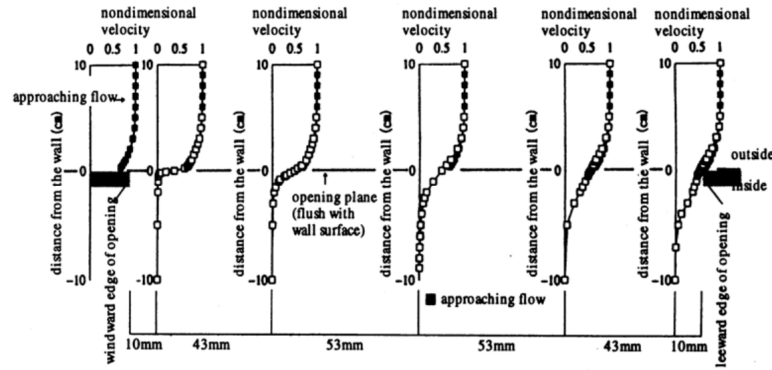


FIGURE 2.12: Velocity distributions inside a single opening; aspect ratio of opening is 2, external free stream velocity is $6m/s$, [94]

single sided ventilation is either dominated by the mean pressure difference or, when the mean pressure difference is close to zero as is the case for certain wind directions, the root mean square of the fluctuating pressure difference dominates the airflow exchange. when the angle is $\pm 47^\circ$ the airflow through the opening is dominated by a pressure difference between the external air and internal acquiescent air. when incidence angle is $47^\circ - 90^\circ$ the flow is parallel to the opening and a shear mixing layer develops across the opening. The turbulent jet exchanges air through shearing along its external edge. When the air exchange mechanism across a single sided opening is a shear mixing layer and not driven by a mean pressure differential, the Bernoulli orifice equation is unable to correctly predict the airflow and is unsuitable for this type of situation. For this reason Warren proposed using an empirical equation based on the local dimensionless flow number F_l :

$$Q_w = F_l A_o U_l \quad (2.14)$$

Other published studies showed that there in fact exists an asymmetric entrainment rate with the shear layer spreading towards the low velocity region, with mixing predominantly in one direction only. This is based on work published by Champagne et al [105]. Dimotakis [106] more recently proposed that 70% of the outside air is entrained and Yamanaka [94] using wind tunnel studies subsequently suggested new values for the relationship between the local wind velocity U_l and Q_w with F_l as low as 0.03 when the flow is parallel and 0.063 when different wind directions are taken into account. Figure 2.12 shows the velocity distributions along a single sided opening measured in a wind tunnel by Yamanaka et al [94]. The evolution of the mixing layer on the inside can be clearly observed. Adams et al [107] updated Warrens approach by adjusting the spread rate of a non symmetric turbulent jet that generates a shear mixing layer spreading along the horizontal length of the opening normal to the envelope. They suggested an alternative α value to deal with the jet spread rate resulting in a value of $F_l = 0.075$. An important component contributing to the airflow rate for single sided ventilation is the turbulent exchange, characterised by the fluctuating pressure at the opening which will be larger where the flow is not parallel, i.e. for other wind directions. This seems to increase the air exchange.

Due to the difficulty in estimating the local wind velocity at an opening, U_l , an important feature for existing wind driven models is to use the reference wind velocity, U_r , normally available from

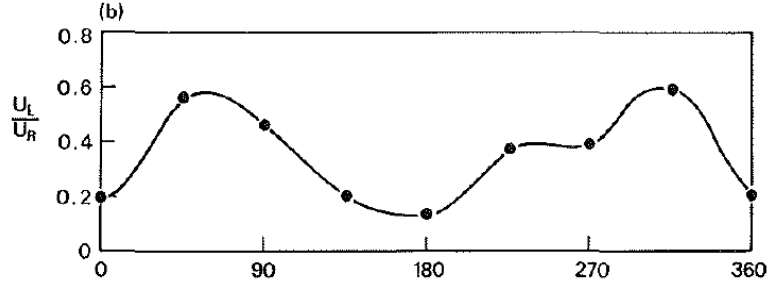


FIGURE 2.13: Ratio of local wind velocity to reference wind velocity from measurements by Warren [97]

a nearby weather or met station, directly for calculation of ACR. Alternatively the model should be capable of predicting the local velocity at the opening given some knowledge regarding U_r . Warren experimentally investigated this. They used a wind tunnel experiment to establish the relationship U_l/U_r as a function of wind incidence angle, θ , shown in Figure 2.13. Using these values they then transformed measured values of U_r taken during full scale ACR tests. They then calculated the airflow rate using equation 2.15:

$$Q_w = F_l A_o \left(\frac{U_l}{U_r} \right)_{\theta_r} U_r \quad (2.15)$$

They suggested based on the U_l/U_r results that this ratio will unlikely go below 0.25 and designers can adjust accordingly for Q_w in equation 2.15. Adams et al compared the velocity ratio of Warren to their own wind tunnel studies. Their results agreed well with Warren. They considered nine different cases in total and from this they proposed equation 2.16 to predict U_l from θ given U_r .

$$U_l/U_r = 0.527 \cdot \exp(-0.000638(\theta_r - 62)^2) + 0.25 - 0.00028\theta \quad (2.16)$$

As an alternative approach Larsen and Heiselberg [108] suggested using an empirically derived 4th order polynomial, $f(\beta)$, describing the ratio between the wind pressure coefficient data for the opening of interest and the velocity ratio $(U_l/U_r)/\sqrt{|C_p|}$. This fitted model can then be used to predict U_l once the C_p data and U_r are both available. Using the C_p value to estimate the velocity ratio is useful as there are a number of existing sources for these values, often based on simplified geometries. Recently it was shown that there is up to only 15% difference on predicted VC performance for natural ventilation models using C_p depending on the source [109]. Their results show favourable predictions for the opening studied in the wind tunnel. The fitted model was based on Warren and Parkins data.

$$U_l = f(\beta) \cdot \sqrt{|C_p|} \cdot U_r \quad (2.17)$$

Using the reference wind velocity, U_r produces a modified equation for ventilation airflow rate and introduces a reference dimensionless exchange rate parameter, F_r , equation 2.18 below.

TABLE 2.1: Dimensionless exchange rate F_r of a building with a single opening

Reference	ϕ	F_r
Warren [97]	0°	0.023 – 0.026
British Standard	0°	0.025
Chu et al [104]	0°	0.0265
Kato et al	90°	0.015 – 0.020
Larsen and Heiselberg [108]	90°	0.025
Chu et al [110]	90°	0.018
Chu et al [104]	90°	0.020

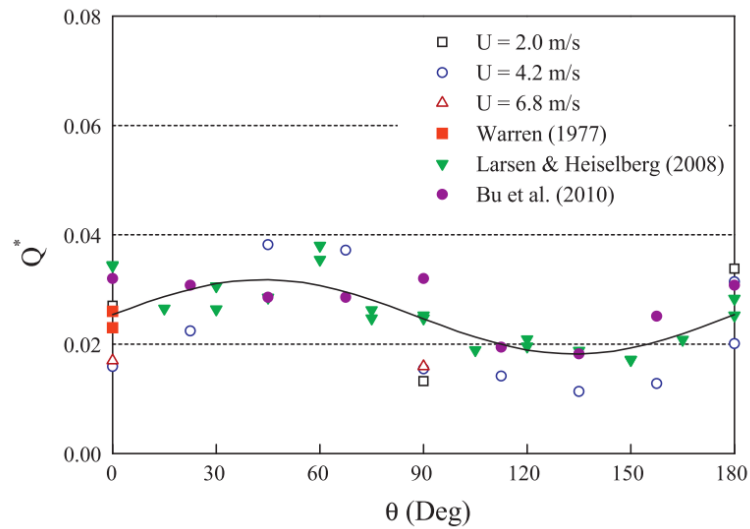


FIGURE 2.14: Ratio of local wind velocity to reference wind velocity from measurements by Warren [97]

Combining $F_l = 0.1$ with the velocity ratio (U_l/U_r) Warren gives a reference F_r value of 0.025 for smooth flow and 0.035 for a turbulent flow field. Chu recently found from a laboratory experiment that F_r could be as low as 0.018 [110]. A number of different researchers have investigated values for F_r using various techniques. Table 2.1 and Figure 2.14, reproduced from Chu et al [104, 110] shows the typical values obtained from these studies. Many of these studies are either wind tunnel or CFD based and few have real experimental data from field studies. Further, they seem to use flow with a low turbulence characteristic and often do not represent the levels of turbulence in a atmospheric sub boundary layer with obstacles upstream of the opening.

$$Q_w = F_r A_o U_r \quad (2.18)$$

In a real building both wind and buoyancy forces are simultaneously present and our understanding of this situation is important for making accurate performance predictions about the

ventilation strategy as well as designing effective ventilation openings.

2.5.3 Combined Wind and Buoyancy

In reality both wind and buoyancy forces will be present in varying magnitudes depending on the local boundary conditions and building characteristics. Maximum ventilation rates are required for cooling during periods of elevated external temperatures and this usually coincides with low wind speed conditions. Buoyancy forces will be dominant in this situation and it is common practice to design ventilation openings considering only buoyant flow. The prevailing principle is that if ventilation rates are achievable with buoyancy force alone then the presence of wind will further enhance this and improve performance further. However, there is a risk that wind forces will oppose the buoyancy driven flow pattern across the opening, reducing the ventilation rate. Further, some openings are specifically design to operate using the wind and their performance can be affected by the presence of buoyancy. To date, efforts to characterise this combination of forces have been largely empirical. For example, as early as 1962, Solvason and Brown investigated the effect of a wind speed also present parallel to an opening during a buoyant flow exchange and found that depending on the Grashof number for the test it either enhanced flow or limited flow when compared to natural convection alone [93]. One of the main motivations for natural ventilation research is the development of accurate prediction techniques to account for the additional installation effects from the presence of turbulent wind. A number of different approaches and models exist to account for this local flow condition, when wind and buoyancy are simultaneously present. These models attempt to account for both wind and buoyancy forces while incorporating the effects of wind direction also. While it is possible to isolate both buoyancy and wind forces independently in a laboratory environment when undertaking measurements of single sided ventilation this is not possible in field studies. Owing to the inability to control boundary conditions in field measurements, both forces will generally be present. Annex 20 brought together various research around dealing with buoyancy and wind forces simultaneously in single sided ventilation [103]. When dealing with estimating boundary conditions work completed by de Gids and Pfaff, presented in Annex 20, relating to the transfer of met data using the ratio of the reference wind speed to the local wind speed and a similar ratio for temperature difference was discussed. They showed that met temperature differences were systemically lower than local equivalents with a good correlation possible. The wind data was shown to be less reliable and a function of the incidence angle. They employed the non-dimensional analysis using the Warren plot to analyse airflow rate measurement data.

2.5.3.1 Dimensional Analysis

In dimensional analysis there are a range of quantities known as dimensionless numbers or non-dimensional groups. These are numbers, to which no physical quantity is attributable, that generally characterise various ratios of forces and phenomena present in fluid mechanics and heat transfer problems. They are useful for determining relationships between several variables and can parameterise problems to find general solutions. When investigating permutations of

contributing forces for ventilation rate tests Warren [97] used the relationship between the ventilation parameter, the dimensionless reference Flow Number F_r , and an adjusted dimensionless Archimedes Number, $Ar^{0.5}$. The Archimedes Number is used as a measure of the relative magnitudes of the buoyancy (gravity) forces and the momentum (inertial) forces acting on elements of fluid. The general form of the Archimedes number is given as:

$$Ar = \frac{gL^3\rho_0(\rho - \rho_0)}{\mu^2} \quad (2.19)$$

with ρ_0 taken as a reference density. He proposed the use of an xy scatter plot of both of these dimensionless numbers, each calculated using data from ventilation rate measurements. The purpose of what is now commonly referred to as the Warren plot, is to separate out the data dominated by buoyancy effect. This is effective in isolating when different forces were dominant and can greatly assist in understanding underlying relationships between measured ventilation rates and either wind or buoyancy forces in field measurements. Warren plots have been previously used by a number of researchers to analyse air change rate data and investigate the nature of the driving forces, for example see [97, 103, 111]. We are interested in characterising the relative strength of buoyancy driven flow, due to density differences across the opening, with momentum flow, due to inertia in the wind at the opening. The ratio of these forces can be expressed as equation 2.20 where L is a characteristic height.

$$\frac{\Delta\rho gL}{p_w} \quad (2.20)$$

For dynamically similar flows substituting ρv^2 for total wind pressure, P_w , in equation 2.20, one obtains a dimensionless parameter which is physically equivalent to that known as Ar [112]:

$$Ar = \frac{\Delta\rho gL}{\rho U_w^2} \quad (2.21)$$

When the density difference of air is due to heat transfer at constant pressure we can adopt the boussinesq approximation that allows for a linearly varying density field proportional to the temperature field, giving a simplification of the relationship between temperature and density based on the perfect gas law, figure 2.15.

This shows, for temperatures differences less than about $30^\circ C$ that we can substitute temperature differences directly for densities, equation 2.22:

$$\frac{\Delta\rho}{\bar{\rho}} = \frac{\Delta T}{\bar{T}} \quad (2.22)$$

Substituting for equation 2.22 above using internal and external temperature, adopting H instead of L to define the opening height and taking the velocity to be the reference wind speed we can rewrite equation 2.21, taking the square root, as:

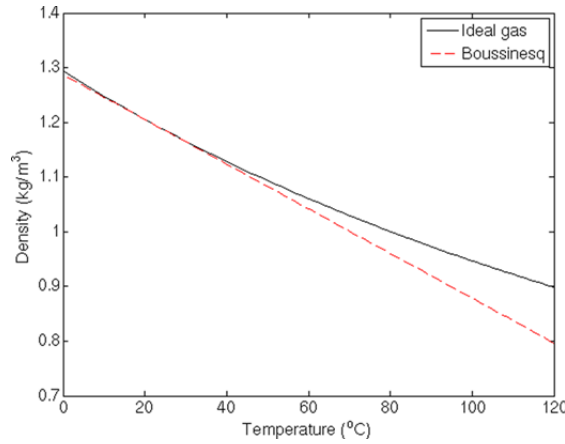


FIGURE 2.15: Variation of density with temperature according to the ideal gas law and the boussinesq approximation

$$Ar^{0.5} = \left(\frac{\Delta T_{ie} g H_o}{\bar{T} U_r^2} \right)^{0.5} \quad (2.23)$$

As discussed, the ventilation parameter, F_r , is a practical dimensionless flow number based on a reference wind velocity to characterise the quantity of wind induced ventilation for a given situation, usually based on results from an ACR measurement. Based on equation 2.18 above but using a measured ACR value, Q_m , F_r can be defined as:

$$F_r = \frac{Q_m}{A_o U_r} \quad (2.24)$$

When the measured flow is due to buoyancy alone we can also define a dimensionless Flow Number, F_b , for this condition as:

$$F_b = \frac{Q_b}{A_o U_r} \quad (2.25)$$

We can define Q_b as equation 2.26 below using a velocity due to buoyancy forces alone. Substituting for Q_b in equation 2.25 and for the velocity U_b based on equation 2.10 we can rewrite for F_b :

$$Q_b = \frac{1}{3} C_d A_o U_b \quad (2.26)$$

$$F_b = \frac{\frac{1}{3} C_d A_o U_b}{A_o U_r} \quad (2.27)$$

$$F_b = \frac{\frac{1}{3} C_d A_o \left(\frac{\Delta T_{ie} g H_o}{\bar{T}} \right)^{0.5}}{A_o U_r} \quad (2.28)$$

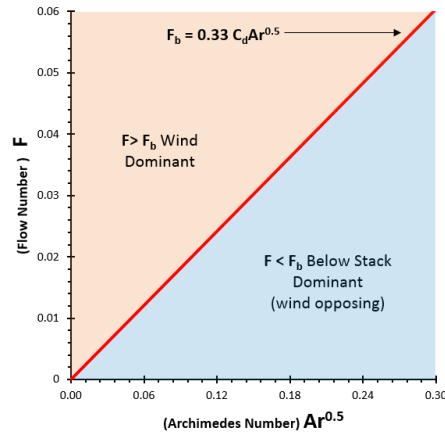


FIGURE 2.16: Warren Plot of F_r versus $Ar^{0.5}$ used for differentiating ventilation rate measurements depending on the dominate force generating airflow. Buoyancy asymptote shown in red. data close to this are generally driven by buoyancy forces alone. [97]

Rearranging equation 2.28 gives F_b in terms of $Ar^{0.5}$ in equation 2.23:

$$F_b = \frac{1}{3} C_d Ar^{0.5} \quad (2.29)$$

F_b is included in the plot representing buoyancy driven flow alone. A Warren plot is shown in Figure 2.16 below:

Generally, where flow is buoyancy dominated, there will be large Ar values and F_r data should approach the asymptote defined by F_b in equation 2.29. When wind dominates $Ar^{0.5}$ tends to zero and F_r becomes independent of $Ar^{0.5}$. For parallel flows, with no additional turbulent contribution from a pulsating pressure difference, according to work by Warren [97] and by Yamanaka et al [94], F_r should be approximately constant at 0.03. Chu et al suggested this value could in fact be as low as 0.0175 [110]. Plotting data using this tool provides knowledge on the dominant forces for an ACR test in a particular opening, room and building. Where patterns emerge under a wide variety of boundary conditions this can give insight into how to better predict ventilation rates for a given situation or whether or not the wind is having any beneficial contribution to ventilation rates for a given location. It also assists in the process of selecting suitable values for F_r , a dimensionless ventilation flow parameter that is currently used in the British Standard for single sided ventilation and by designers and design tools. There has been some work on developing single sided correlations that can account for the combined effects of wind and buoyancy.

2.6 Existing Single Sided Empirical Correlations

Often working from a semi-empirical basis, for example using equation 2.10, different researchers have attempted to include additional experimentally derived factors to account for the complicated installation effects from turbulent wind, gustiness, opening geometries and wind incidence angle. Much of the work is based on the inclusion of empirical coefficients that deal with wind

effects or the development of techniques for predicting wind driven ventilation rates that contribute to buoyancy driven flow. The main parameters of interest in almost all correlations are the envelope temperature difference, wind speed, wind direction, opening height and opening area. The approaches vary somewhat depending on the underlying assumptions of the research or the methods used to develop the correlation. We have marked those that were compared to measurement data as part of this research with an asterisk. It follows a summary of some of the key existing empirical correlation based prediction models for single sided ventilation.

2.6.1 de Gids & Pfaff

de Gids and Pfaff were amongst the first researchers to investigate correlations for single sided ventilation that take account of both mean and fluctuating wind pressures alongside buoyancy. They carried out 33 ACR measurements across three different buildings measuring the local external velocity, the window and room air velocities as well as temperatures. From the work they suggested the use of an effective velocity in the calculation of the volume flow rate through the opening:

$$Q = \frac{1}{2}A_o U_r = \frac{1}{2}A_o (C_1 U_r^2 + C_2 H_o \Delta T_{ie} + C_3)^{0.5} \quad (2.30)$$

The three terms, C_1 , C_2 & C_3 were derived experimentally with values of 0.001, 0.0035 and 0.01 respectively. C_1 is a dimensionless coefficient depending on the wind, C_2 is a buoyancy constant and C_3 is a turbulence constant. The turbulent term C_3 is equivalent to an effective turbulence pressure that provides ventilation in the absence of stack effect or steady wind.

2.6.2 Warren

We have already discussed the work of Warren and his proposed dimensionless Flow Numbers, F_r and F_l . To deal with the combined effects of buoyancy and wind Warren suggested calculating the ventilation rate for both separately and taking the larger of the two. His approach to predicting single sided ventilation is to calculate both the buoyancy airflow rate and wind airflow rate separately and take the larger of the two values.

$$Q = \max[Q_w, Q_b] \quad (2.31)$$

Where;

$$Q_w = 0.1A_o \left(\frac{U_l}{U_r} \right)_\theta U_r \quad (2.32)$$

$$Q_b = \frac{1}{3}C_d A_o \left(\frac{\Delta T_{ie} g H_o}{\bar{T}} \right)^{0.5} \quad (2.33)$$

2.6.3 Dascalaki & Argiriou

Dascalaki [113] investigated airflow network models and how they calculated single sided ventilation showing that only buoyancy effects were considered with no accommodation of wind driven airflow. Their work was based on 53 full scale ACR measurements in two different locations using a real building and an outdoor test cell facility. Comparing predicted ventilation rates from airflow network models such as COMIS and PASSPORT-Air with measured values from measurements they proposed a correction factor, CF , that replaced the discharge coefficient (by setting this to 1). The correction factor was based on the relative strength of the inertia forces from the wind to the buoyancy forces. Using the Archimedes number as the dependent variable to predict airflow rates they found a clear trend between this and both measured and predicted airflow rates.

$$Q = (CF) Q_n = (0.08Ar^{-0.38}) Q_n \quad (2.34)$$

Q_n is the volume flow rate calculated from the airflow network model. This means a program capable of doing this is first required before estimating the corrected volume flow rate. The Dascalaki correlation is currently implemented in TRNSYS for single sided ventilation. More recently Argiriou [114] investigated alternative values for the linear scaling constant and exponent in CF in equation 2.34 above for various external shading devices. He investigated external louvres, or tilted external slats, and found a modified set of values:

$$CF = aAr^b, \text{ with } a = 0.16 \pm 0.09 \text{ and } b = -0.25 \pm 0.07 \quad (2.35)$$

While the horizontal slats were separated from the opening and have a straight profile, these may still have some similarities to the external slotted louvre system at zero2020.

2.6.4 Larsen

Some models such as Pfaff & DeGids [115] and Larsen & Heiselberg [108] incorporated mean wind pressure, buoyancy and a turbulent component to their correlation using regression coefficients from wind tunnel and full scale measurements. They proposed a more complex correlation that takes account of the thermal effects, wind speed & direction. They also found that the dominating force differs between wind speed and T_{ie} depending on the ratio between these forces and the wind direction. The local wind speed at the opening is very much dependant on wind direction due to changes in flow patterns along the envelope given different wind directions. Larsen shows how ACR depends on wind direction with effect more pronounced at low wind speeds and the dominating force differs between wind speed and ΔT_{ie} depending on the ratio between these forces and the wind direction [108]. They proposed the following correlation:

$$Q = A_o \sqrt{C_1 f(\beta) \sqrt{|C_p| U_r^2 + C_2 \Delta T_{ie} H_o + C_3 \left(\frac{\Delta C_{p,ope} \Delta T_{ie}}{U_r^2} \right)}} \quad (2.36)$$

2.6.5 Caciolo

Caciolo et al recently compared some of these correlations with experimental results [111] concluding that in the case of windward opening the best results were obtained with the Warrens correlation. Warrens correlation also captured both positive (increased mixing layer) and negative (opening effective temperature difference decrease) effects due to wind quite well for windward conditions. In the case of leeward openings all correlations overestimated the air change rate. Caciolo et al [116] proposed improvements for leeward conditions, predicting effective envelope temperature differences that allow for localised interactions with the wind depending on speed, incidence angle and magnitude of temperature difference respectively. However, at low wind speeds and a leeward direction the effective envelope temperature has been shown to be reduced due to a recirculation zone counteracting buoyancy effects resulting in ACR lower than in the absence of wind [116]. Caciolo proposed the following adjusted correlation for leeward conditions:

$$Q_b = \frac{1}{3}C_dA_o \left(\frac{\Delta T_{ie}\Delta T^*gH_o}{\bar{T}} \right)^{0.5} \quad (2.37)$$

$$\Delta T^* = 1.355 - 0.179U_w \quad (2.38)$$

For windward conditions Caciolo suggests using Warrens correlation. Although based on CFD results they published the following equation for windward, using a Q_{tot} value, stating that the difference in results between their correlation and Warrens did not merit reconsideration of Warrens:

$$Q_b = \frac{1}{3}C_dA_o \left(\frac{\Delta T_{eff}gH}{\bar{T}} \right)^{0.5} \quad (2.39)$$

$$\Delta T_{eff} = \Delta T_{ie} T^* = \Delta T_{ie} (1.234 - 0.490U_w + 0.048U_w^2) \quad (2.40)$$

$$Q_w = 0.0357A_o (U_w - U_{w,lim}) \quad (2.41)$$

$$U_{w,lim} = 1.23ms^{-1} \quad (2.42)$$

$$Q = Q_b + Q_w \quad (2.43)$$

2.6.6 Tang

More recently Tang et al [117] completed an empirical study investigating ACR values when $U_l \leq 0.75 \text{ m s}^{-1}$ and $\Delta T \leq 1 \text{ K}$. They found that all the existing correlations under predicted the airflow rate at very low ΔT conditions. They proposed that normal air exchange mechanisms that the existing correlations are developed from are not present under these conditions and instead an un-organized flow exists. They fit a new correlation using their data that worked at very low ΔT and at higher values also:

$$Q = \frac{1}{3} C_d A_o \left(\frac{\Delta T_{ie} g H_o}{\bar{T}} + \frac{C}{\Delta T_{ie}} \right)^{0.5} \quad (2.44)$$

2.6.7 FprEN 16798-7

In the proposed revision to EN standard 15242:2007, referred to as FprEN 16798-7, a new simplified correlation for single sided ventilation is proposed. This correlation was recently outlined by Larsen et al [118]. The authors identified a consistent over prediction of ventilation rates at low wind speeds and low temperature differences when using the deGids and Pfaff correlation, which was adopted originally for EN15242:2007. This was related to the turbulence component, C_3 in equation 2.30. They proposed to remove this and further, to separate the calculation of wind and buoyancy driven airflow, taking the larger of the two, effectively adopting Warrens approach. The new correlation is:

$$Q = 3600 \frac{\rho_{ref}}{\rho_e} \frac{A_o}{2} \max(C_w U_r; C_b H \Delta T_{ie})^{0.5} \quad (2.45)$$

2.7 Slotted Architectural Ventilation Openings

The geometry of the opening is also significant, but sometimes secondary to, or limited by, practical constraints. Its design and operation can influence the ventilation rate performance and can lead to installation effects that further complicate the flow at the opening. Traditionally, for single cell, isolated spaces, windows systems have been designed and selected to allow both natural daylight and air into the occupied interior. In the more recent past the benefits of passive solar heat gains have been also recognised as a desirable constituent of low energy design, especially so for Northern climates, and window designs have evolved with this in mind. Window designs have been developed with various opening arrangements either to assist with ventilation or in response to aesthetic aspirations, user functionality or safety requirements. Access to sufficient natural daylight is a basic requirement for an occupied indoor space. Windows are necessary to satisfy this requirement and it is convenient to also use them for ventilation purposes, although this can come at a cost owing to the additional scope required for opening mechanisms and framing needs. In many scenarios windows as ventilators has proved effective and in single sided situations windows have overwhelmingly been the ventilator of choice for commercial, and residential, buildings. However, when we take into account some of the barriers to passive VC

there can be limitations to the use of windows as the primary air supply mechanism. With night cooling strategies for example, security poses a major problem for the use of open windows as the air inlet, irrespective of size, due to the compromised security barrier of the building envelope during night hours. During winter months, if any ventilation is required above that provided by trickle ventilators, rain ingress can be an issue when this coincides with a need for ventilation. As mentioned earlier, in urban areas, ingress of external noise and air pollution are negative consequences of direct ventilation strategies that rely on windows. There are also less evident consequences of employing windows as ventilators. For instance situations can arise when considering building retrofits that there is already an excess of glazing in the existing building or a need to address the current extent of glazing. This is particularly so with buildings constructed during the brutalist movement in architecture and from the 1960's onwards. The existing glazing design is often associated with glare and visual discomfort and a need to address this as part of a retrofit scope can question the existing extent of glazing. Concluding that there is excessive glazing in an existing building may also relate to energy performance standards. Windows possess substantially reduced resistance to heat flow compared with opaque composite walls. With these various constraints in mind, when dealing with deep retrofit of existing buildings using an external envelope driven approach, an alternative to windows for ventilation that facilitates solutions that create a reduction in glazed area and can go some way to dealing with the other main barriers to natural ventilation, is to consider the use of purpose provided openings (PPO). PPO are an increasingly popular solution to overcome various barriers to VC and they facilitate strategies with demonstrated high potential for VC in climates similar to Ireland, such as night cooling [9, 119]. These are designed with the specific intent of providing air for ventilation. As a consequence, windows are no longer openable and provide exclusively for daylight, an external view and passive solar gains in winter. PPO can come in various forms, passive or active, mechanised or architectural in their underlying features. Fixed external horizontal slotted architectural louvres have been used for air intakes in many applications. When used as air intakes to mechanical HVAC systems there are generally no real design and performance issues. When used in natural ventilation systems they are directly connected to the ventilated space. Owing to this there needs to be some mechanism used in conjunction with the louvred opening that can maintain the airtight envelope barrier when no ventilation is required. Some strategies propose the use of automated, multi leaf dampers integrated with the louvres to provide flow control and on/off activation of the air supply. An example of this approach is the Passivent Aircool, shown in figure 2.17 below. These require an internal grille to conceal the damper components for aesthetic purposes.

A difficulty that has been reported in the literature with the use of multi-leaf dampers with architectural louvres for natural ventilation purposes has been the leakiness of dampers with degradation of the seals over time. An alternative approach to dealing with the provision of an airtight barrier in the envelope inside of the external architectural louvre is to use insulated, openable doors that can be operated either manually or automatically. These provide excellent thermal and airtightness performance when closed and when used in lieu of windows sections for ventilation can further improve the overall thermal transmittance of the envelope. Some examples of these are shown below.

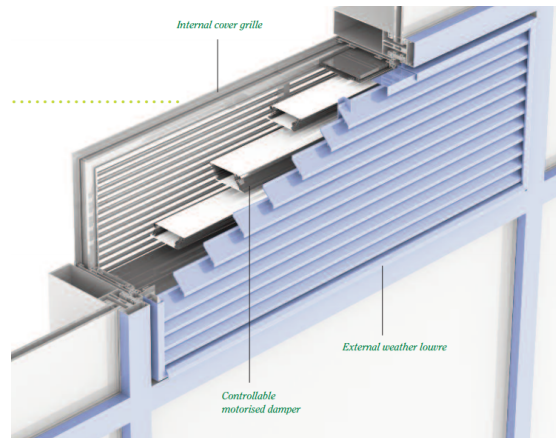


FIGURE 2.17: Passivent Purpose Provided Aircool Ventilator using external louvre, multileaf damper and internal grille

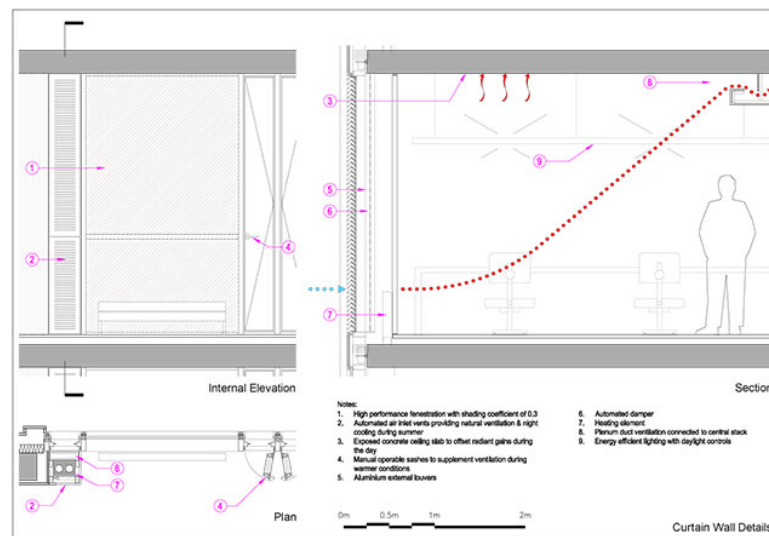


FIGURE 2.18: Purpose provided louvre solution at St Patricks Place, Cork City, Ireland

The use of an internal insulated door for activation of the ventilation supply reduces the number of components interacting with the airflow in the opening. It also reduces the flow resistance with the external louvre acting as the primary airflow guiding component. The internal doors can have variable opening angles if necessary and there is some interaction with the airflow depending on the opening angles much like inward opening windows. An advantage to the use of louvred systems is the new possibilities for opening heights. Large opening heights generally present issues during operation related to draughts, for occupants and, in office environments, stationery etc. Using a slotted louvre in the opening, allows a much larger overall opening height dimension while retaining the equivalent geometric area as a window opening overall. The use of these larger heights has positive benefits for buoyancy driven airflow. Similar heights can be achieved using high and low level openings of smaller cross sectional area although these then may not be best positioned for instances where wind driven airflow is more efficient.

When using PPO solutions that incorporate architectural slotted louvres, it is clear that there will very likely be some modification of the ventilation rate, partly due to the geometry of the

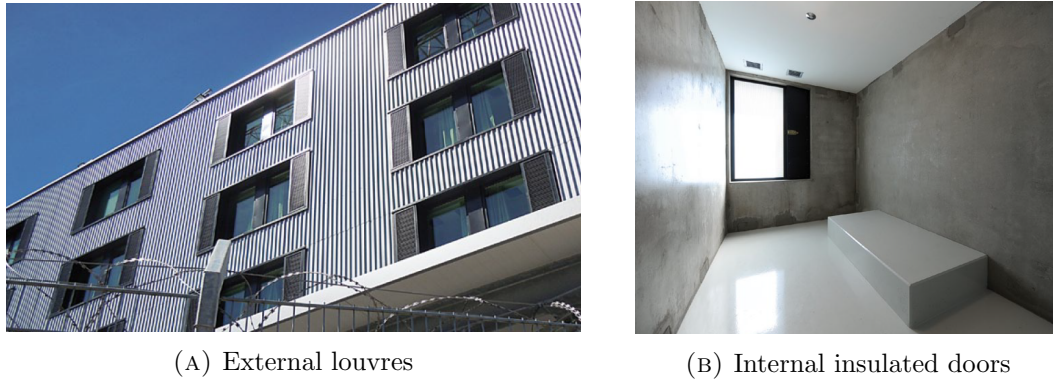


FIGURE 2.19: Swiss prison Champ-Dollon incorporating slat type slotted louvres and internal insulated doors for single sided ventilation

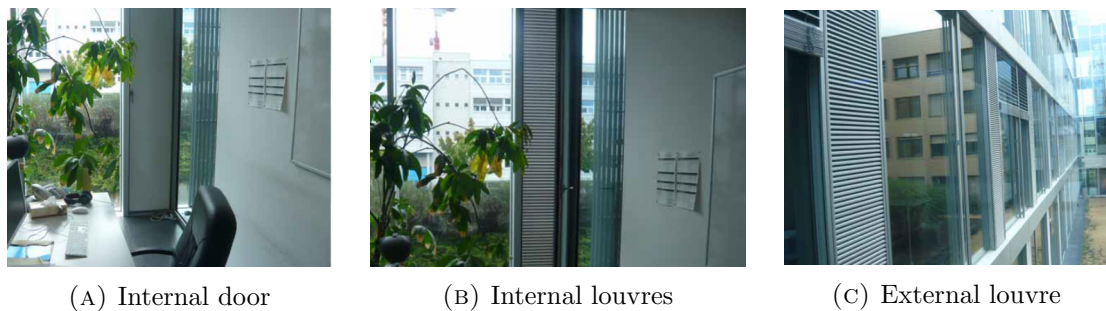


FIGURE 2.20: EPFL GC Building in Switzerland utilising PPO design for natural ventilation purposes.

louvre and in part due to the reconfigured opening shape and operation with the insulated doors. However, while louvred vents are common in many engineering applications there exists little experimental data demonstrating their performance when subject to the interactions present in single sided ventilation of internal spaces. A significant body of research has been published investigating the mechanics of single sided ventilation in both plain openings and for typical window types though according to the findings from a literature review there are few published experimental studies investigating the airing performance of architectural style slotted louvres when this shear flow is present.

2.7.1 Recent Investigations of airflow through slotted openings

Due to the importance of opening geometry, the introduction of a slotted louvre component would suggest a modification in how buoyancy and momentum forces will interact at the aerating opening. Published experimental work measuring macroscopic ACR across louvre/slot like systems appears limited. A literature review has revealed little reported work of full scale experiments characterising how slot louvre systems with low hydraulic diameters perform within ventilation strategies where mechanisms such as turbulent eddy diffusion play an important function. For example Kang investigated how different louvre ventilator angles installed in the windward face of a factory wall changed indoor velocity field and turbulence. They showed that louvre ventilator angle can increase the internal mean velocity and turbulence further away from

the ventilation inlet. However it did not consider shear induced flow and also used a double sided ventilator to direct the internal flow and the study included a roof mounted exhaust point [120]. Nakanishi et al showed that the pressure loss characteristic varies significantly relative to louvre angle and the differential pressure was close to a quadratic function of impinging wind velocity at normal incidence [19]. However different impinging wind incidence angles were not investigated, buoyancy was not included and the louvre angle at air entry was flipped compared to the louvre system presented in this paper. Hughes et al have also looked at the effect of external louvre angle on the ventilation performance of the windcatcher system and have demonstrated that the louvres follow aerodynamic stall theory [121]. Argiriou et al [114] investigated the impact of external tilted venetian blinds on the airflow across large openings using full scale testing and proposed a correction coefficient based on Archimedes number, Ar [113]. Koffi et al [122] considered the effect on aeration performance using an acoustic shutter, effectively creating staggered pathways through a double skin opening. They found the shutter reduced ventilation rates by 72% but did not consider how the forces generating flow were modified. Recently Lee et al [123] measured the pressure loss rate through exterior venetian blinds and found the blinds can alter the velocity by about 50%. However, these measurements were based on cross ventilation, had a separation space between the blind and opening and did not consider low wind incidence angles. Hughes et al discuss the importance of louvre design in commercial wind towers with louvre angle and length important factors in directing airflow into the internal space while reducing resistance to flow [18] though they did not investigate a system where the flow is often parallel to the louvered opening and within the building envelope rather than at roof level. In a different application concerned with obstruction spacing patterns affecting airflow Mara [124] considered whether a solidity ratio alone, similar to the principle of net free area ratio in envelope openings, was sufficient for estimating drag coefficients for lattice type structures, finding that the spacing pattern was also an important parameter requiring consideration. There appears to be a lack of full scale experimental data for ventilation rates through integrated louvre systems. Other studies concerning flow interactions along perforated plates, arguably an idealised representation of the slot louvre, considered either a flow normal to the main perforated face or, where it does consider flow parallel to slotted or perforated cavities, the slotted openings were either; oriented normal to the direction of shear flow rather than with or parallel like a typical architectural louvre in a building envelope (similar to that considered here) [16], or were sive like [17].

2.8 Characterising unsteady air movement

Atmospheric motions are produced from the irregular surface heating of the earths surface from the absorption of solar radiation. A thermal energy exchange takes place between the heated surface and adjacent air giving rise to temperature gradients in the atmosphere. These thermal gradients produce corresponding pressure differences which give rise to air motion, effectively the wind that drives airflow through buildings discussed earlier. This process takes place in the Planetary Boundary Layer, which is made of different sub layers [125]. Flow in and around buildings is generally known as the Urban Canopy Layer, see Figure 2.21. Here the flow is almost always turbulent and when undertaking experimental research investigating the quantity

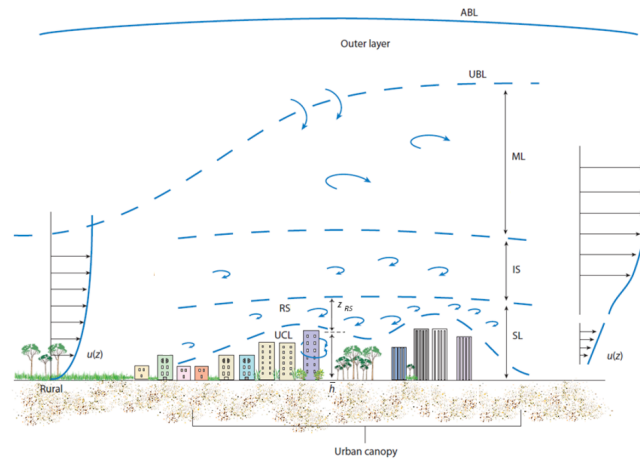


FIGURE 2.21: Schematic illustration of the different layers of the planetary boundary layer above an urban area. The urban boundary layer (UBL) is divided into a mixed layer (ML), inertial sublayer (IS) and surface layer (SL), which in turn is divided into a roughness sublayer (RS) and an urban canopy layer (UCL). [125]

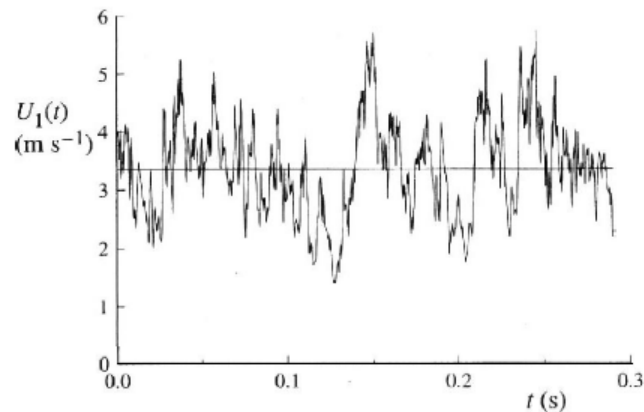


FIGURE 2.22: The time history of the axial component of velocity on the centreline of a turbulent jet. [126]

and nature of airflow through an external opening in a building into an internal space, the flow will be turbulent throughout.

According to Etheridge and Sandberg a turbulent flow is simply that of a flow accompanied by disordered fluctuations in all the fluid mechanical variables, i.e. velocity, pressure, temperature, etc. When observing flows in everyday scenarios we can see that the flow is unsteady, irregular, appearing random and chaotic with every individual 'eddy' seemingly unpredictable [91]. An essential feature of turbulent flows is that the fluid velocity field varies significantly and irregularly in both position and time. Turbulent flows are often imagined to be flows with numerous 'eddies' (i.e. length scales) of various sizes. An example of the velocity fluctuations in a turbulent flow can be seen in Figure 2.22.

Bradshaw defined Turbulence as:

Turbulence is a three dimensional time-dependent motion in which vortex stretching causes velocity fluctuations to spread to all wavelengths between a minimum determined by the viscous

forces and a maximum determined by the boundary conditions of the flow. It is the usual state of fluid motion except at small Reynolds Numbers. [127]

The length scales of different eddies are an important feature in characterising the flow. Eddy sizes are bounded at the large end of the scale by the dimension of the flow field and at the small end of the scale by the diffusive action of molecular viscosity. As the motion of a turbulent fluid evolves, large scale eddies in the motion will breakdown into smaller and smaller eddy sizes until at the smallest eddies viscous forces in the fluid dominate and the energy is dissipated as heat. Richardson first qualitatively discussed this energy cascade, and subsequently Kolmogorov proposed a quantitative model to describe this process. Richardson penned a short poem, now famous amongst turbulence researchers, to describe this process:

Big Whorls have little whorls,
That feed on their velocity.
And little whorls have lesser whorls,
And so on to viscosity.
(In a molecular sense).
Richardson, 1922

The range of scales present can be very large. In a typical single office application the upper bound can be set at $V^{1/3}$, about 3-5 metres, while the end of the Kolmogorov scale in this application is about $1mm$. There can be various forms of distribution of scales within these bounds. How the scales are distributed is often used for identifying how the flow changes when interacting with phenomena such as solid surfaces or other fluids.

We are not concerned with a detailed treatment of turbulence in this work. Nonetheless as the airflow that was measured in the experimental building is turbulent, we will use some established parameters and techniques available to statistically characterise the flow to investigate whether the slot louvre system has modified in any way the nature of the flow. This approach has been used by researchers previously concerned with air movement within ventilation openings as well as within internal spaces when interacting with occupants. Power spectral analysis is a technique used to visually represent turbulence using the shape of the power spectrum as well as some descriptive statistics based on the spectrum.

2.8.1 Spectral Analysis

To characterise velocity in a turbulent flow field Taylor [128] proposed spectral analysis as a technique for studying the distribution of energy at different eddy scales.

Often it can be useful to transform a mathematical function describing some physical phenomena from the variable in the time domain into a different variable from another domain. Integral transformations are most often used to solve differential equations. Laplace transforms are the most popular and important of these, the second of which is the Fourier transform. The Discrete Fourier transform, (DFT), can be used to produce a frequency spectrum of a given signal in

the time domain, for example a sampled wind speed measurement. The DFT is based on the Fourier Integral which in turn is based on the Fourier series. Fourier series are mathematical tools designed to represent general periodic functions in terms of simple trigonometric ones such as cosines and sines [129]. It involves the superposition of multiple sine and cosine functions with different properties (amplitude, frequency, phase) to produce an approximation of the original functions. They are a powerful tool in solving differential equations. To extend the principles of Fourier series to non periodic functions we can employ the Fourier transform which is an extension of the Fourier integral. The Fourier transform can be stated as:

$$\hat{f}(\omega) = \frac{1}{\sqrt{2\pi}} \int_{-\infty}^{\infty} f(x)e^{-i\omega x} dx \quad (2.46)$$

The fourier transform is used to transform times series data in into the frequency domain. Doing this we can obtain a spectral representation of the data decomposed into its constituent frequencies. In non-technical terms, any stationary time series may be thought of, approximately, as the random superposition of sines and cosines oscillating at various frequencies. If we consider the times series data x_t as a color (waveform) made up of primary colors x_{t1} ; x_{t2} ; x_{t3} at various strengths (amplitudes), then we might consider the power spectrum as a prism that decomposes the color x_t into its primary colors (spectrum). Hence the term spectral analysis. Details of the derivation of $\hat{f}(\omega)$ can be found in [129] and its use as a spectral density in time series analysis in [130]. We can also use this approach as a way of discovering the periodic components of a time series. The use of the Fourier transform applies where a function is given on some defined interval. Where a times series function is defined only at equally spaced points on some defined time interval and we want to transform the data into the frequency domain, this time we would use the Discrete Fourier transform instead of the Fourier transform. To arrive at the DFT we first Take, x_k to refer to each sampled data point:

$$x_k = \frac{2\pi k}{N}, \quad \text{for } k = 0, 1, \dots, N - 1 \quad (2.47)$$

We want to determine the complex trigonometric polynomial that interpolates at the sampled data points, x_k . This allows us to reconstruct the original signal:

$$f(x_k) = \sum_{n=0}^{N-1} c_n e^{inx_k}, \quad \text{for } k = 0, 1, \dots, N - 1 \quad (2.48)$$

We determine the fourier co-efficients c_0, \dots, c_{N-1} by using trigonometric orthogonality [129]. This is achieved by multiplying both sides of equation 2.48 by e^{-inx_k} and summing over k from 0 to $N - 1$:

$$\sum_{k=0}^{N-1} f(x_k) e^{-inx_k} = \sum_{n=0}^{N-1} c_n \sum_{k=0}^{N-1} e^{i(n-m)2\pi k/N}, \quad \text{for } k = 0, 1, \dots, N - 1 \quad (2.49)$$

For $n = m$ on the right hand side we have $e^0 = 1$. For $n \neq m$ on the right hand side, using the equation for a geometric and rearranging equation 2.49 by setting $e^{i(n-m)\frac{2\pi}{N}} = r$ giving us r^k we can show that the right hand side also equals 1 in this instance [129]. Applying this results in the formula for the DFT:

$$\hat{f}_n = Nc_n = \sum_{k=0}^{N-1} f_k e^{-inx_k}, \quad \text{for } n = 0, 1, \dots, N-1 \quad (2.50)$$

This is the frequency spectrum of the original signal, x_k . In vector notation, $\hat{\mathbf{f}} = \mathbf{F}_N \mathbf{f}$ where the $N \times N$ Fourier matrix, $\mathbf{F}_N = [e_{nk}]$ has the entries:

$$e_{nk} = e^{-inx_k} = e^{-2\pi ink/N} = \omega^{nk} \quad (2.51)$$

For each entry e_{nk} in the Fourier matrix, \mathbf{F}_N , ω is first calculated depending on the value of N , with ω^{nk} then established. The matrix is populated and multiplied by \mathbf{f} to obtain $\hat{\mathbf{f}}$. A fuller treatment of this is available in [129]. $\hat{\mathbf{f}}$ is the frequency or power spectrum of the original time series signal and the DFT is used to obtain this spectrum. Computationally, the DFT can be an expensive algorithm give nthe number of operations required for large values of N which is common in experimental data for times series applications. However, the fast Fourier transform, (FFT), is a computational method developed to reduce the number of operations necessary for the DFT from $\mathcal{O}(N^2)$ operations to $\mathcal{O}(N) \log 2N$ operations. It makes the DFT a practical tool for large N . For the research presented here the Cooley - Tukey Fast Fourier Transform [131] was implemented in R (citation) available in the base stats package to transform time series data of velocities in the opening and at the occupant location (see chapter 5) into the frequency domain.

In terms of air movement and turbulence, the power spectrum of data such as that in Figure 2.22 gives the distribution of energy in the air at various frequencies, showing the underlying structure, with small eddy scales having higher frequencies than larger eddy scales. In the context of the composition of airflow through ventilation openings in buildings Malinowski [96] demonstrated that only an eddy with a scale smaller than the opening size can penetrate into the room. Recently, researchers have used power spectra to investigate whether the characteristics of the airflow as it undergoes some change owing to the surrounding environment is "mechanical" or "natural" showing that this characteristic is a function of mean wind speed [108, 132, 133]. The discrete power spectrum, $\hat{\mathbf{f}}$, can provide this information giving the energy distribution by decomposing the sampled time series wind data into various component frequencies. Figure 2.23 shows three different sampled time series data for air velocity with their corresponding power spectrum. Axes are log scaled. The power spectrum can be used to investigate how different types of air movement has different underlying structures and characteristics.

The total energy distribution in the power spectrum scales as a function of the frequency power exponent, β . Different values for β are shown in Figure 2.23. Figure 2.24 shows the typical range of values and the relationship to the frequency fluctuations. Equation 2.52 defines this relationship. Kolmogorov proposed $\beta = -5/3$ in equation 2.52, for a theoretical isotropically distributed turbulent fluid [135].

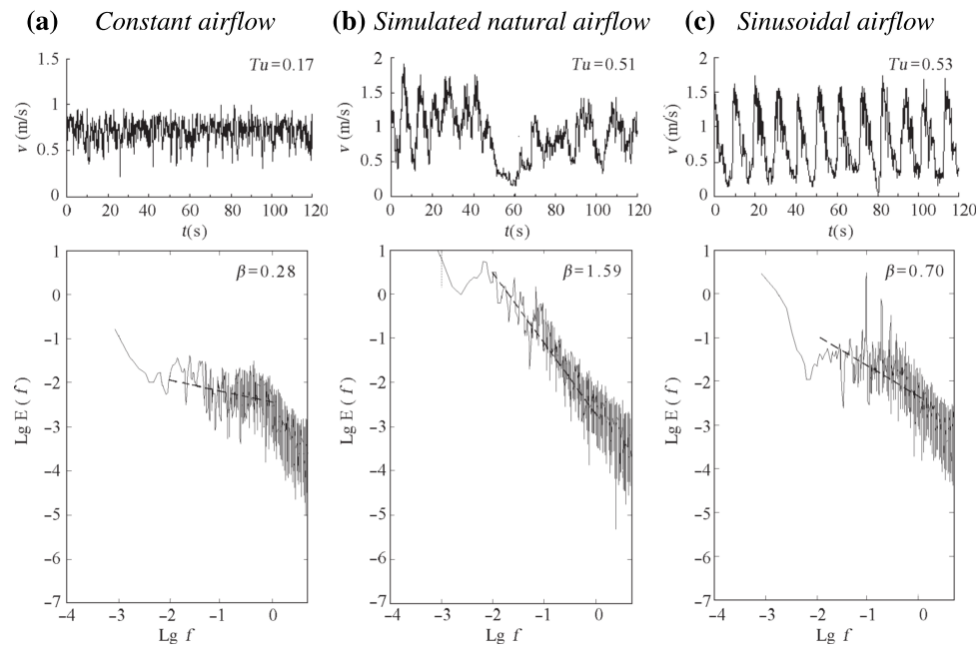


FIGURE 2.23: Time series of air velocity and power spectrum for the different samples. [134]

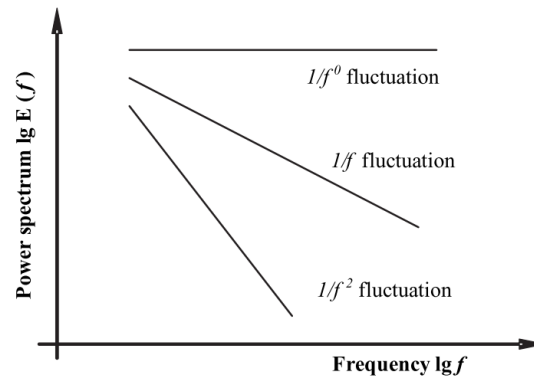


FIGURE 2.24: Relationship between power spectrum fluctuations and the frequency exponent β [134]

$$\hat{f} \propto \omega^{-\beta} \tag{2.52}$$

The frequency exponent has been used by previous researchers as a statistic that can be useful to characterise whether air movement is similar to natural wind, close to $\beta = -5/3$ or mechanical fan driven wind, close to a range $\beta = 0.2 - 1.0$. Figure 2.25 shows an example where different β values are compared for different airflow generating devices. β is usually calculated as the slope coefficient of a linear regression on the power spectrum between certain frequency ranges, depending on the sampling rate and type of air movement.

This approach can be an effective way of investigating whether the geometry of different opening types has modified the nature of the air that is passing through and how is the energy distributed across the turbulent eddy scales.

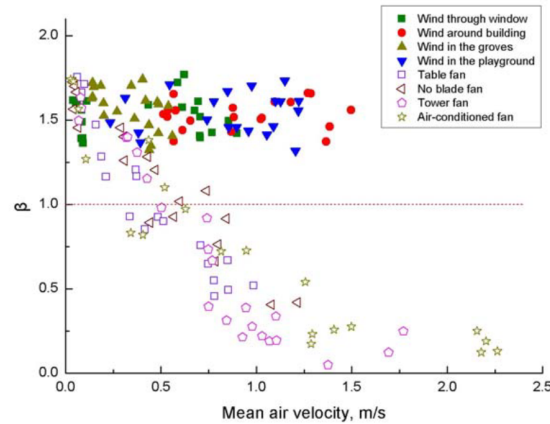


FIGURE 2.25: Variation of β with velocity for different sources of natural and mechanical wind [133]

2.8.2 Air movement and Thermal Comfort

With this in mind, it is widely reported that there are a range of different parameters that influence a person's indoor thermal comfort, not solely air temperature, as mentioned previously. Besides air and surface temperatures, the dynamic characteristics of air is an important criteria for determining interactions between an occupant and their thermal surroundings. These characteristics can include air speed, turbulence intensity, fluctuation frequency and spectral characteristic. An enhancement of the positive characteristics of these parameters can be an effective way of increasing cooling potential where there is limited additional opportunity for heat removal. Traditionally, particularly in controlled, mechanically conditioned internal spaces, perceptible air movement was, historically, seen as a source of thermal discomfort. This opinion was supported by controlled, climate chamber tests by Fanger et al as well as a number of field studies [136, 137]. An upper limit of 0.2 m/s was proposed in the ISO 7730 standard to prevent discomfort due to draughts [49]. This limiting value was subsequently adopted by both ASHRAE-55 [57] and IS:EN 15251 [20] although both standards recognise the added benefit from elevated air speeds following various results in the literature. Figure 2.26, reproduced from CIBSE TM52 [21], based on IS:EN 15251 and ISO 7730 shows the extended acceptable thermal comfort temperature range, shown as the net temperature increase in K above the upper limit.

It had been shown that depending on how a person perceived different thermal environments affected how they responded to the same velocity of air movement. Work done by Hoyt et al considered whether there was any benefit to comfort from increased air velocities under certain conditions following analysis of a set of ASHRAE case study buildings which occupant survey information [138]. They concluded that even when limiting the responses analysed to those from environments with 22.5°C to 23.5°C and ± 1 on the ASHRAE sensation scale there was a clear problem with too little air movement. This finding was further supported by Toftum with evidence of insufficient air movement across survey respondents [139]. With the recognition that under certain circumstances increasing air movement has a positive effect on occupant satisfaction with their thermal environment a number of studies sought to investigate this further. Fountain et al reported using a percentage of satisfied people model, the PS model, that people were

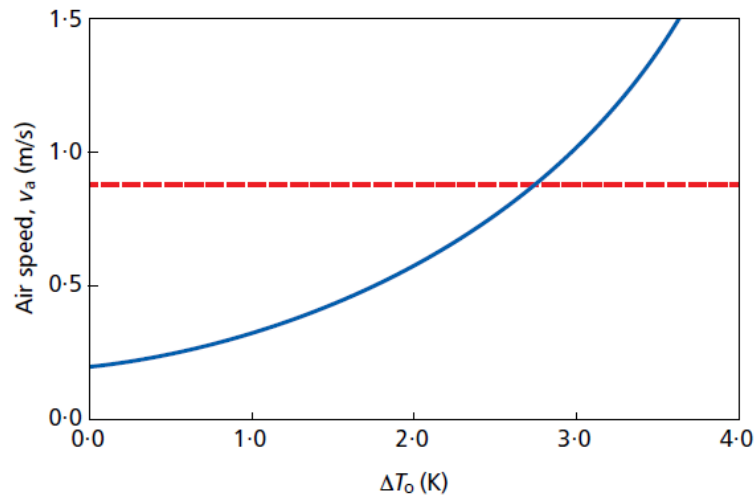


FIGURE 2.26: Reproduced from CIBSE TM52. EN15251 allowance for elevated air speed effects on thermal comfort [21]

positively satisfied with increased air movement when in the range of 25.5°C to 28.5°C [140]. The Standard Effective Temperature model was used to extend the still-air comfort zone in ASHRAE 55 under elevated air speeds. Increased mean air velocities above those recommended by ASHRAE were shown to be acceptable in another study that considered participants responses to elevated temperatures and air velocities (0.8 m/s).

Turbulence intensity, another key parameter, can be a difficult parameter to reproduce at specific intensities in a controlled environment and its direct effects on thermal comfort are less well known. It is not even directly mentioned in the IS EN 15251 standard or ASHRAE 55. A draft risk model that included the fluctuation characteristics of air movement in the form of Turbulence Intensity was published in the late 1980s and showed that turbulence intensity can have a significant effect on draught sensation [137]. However, it was shown using the SET model and a longitudinal study that adjusting TI from the 19% value assumed in the SET model to 30% had about a 0.1 unit effect on the TSV scale [141]. Recent work was also done demonstrating how for a given mean air speed, increased turbulence intensity can increase the heat transfer by convection from the body with the rate of increase also being more pronounced with higher air speeds [142]. A bivariate empirical relationship as a function of mean air speed and turbulence was proposed to deal with this:

$$h_c = 9.08\dot{v}^{0.5} + 22.16\dot{T}I\dot{v} \quad (2.53)$$

This correlation can be used in the SET model to account for increased air speeds. An increase in heat transfer with increasing TI when TI is above 40% was shown by [143]. As well as turbulence intensity and mean air speed parameters such as fluctuation frequency and the similarity of the underlying spectral characteristic of the air movement to the natural wind spectrum have been shown in the literature to be important factors that can contribute to extending the comfort range beyond recommended upper limits when excluding their effects. A number of studies have reported various fluctuation frequency ranges deemed as optimal for thermal comfort when

exposed to air movement. An air speed of 0.6ms^{-1} , a TI of 30-40% and fluctuation frequency of between 0.3 and 1.0 can give rise to improved cooling effects offsetting the negative effects of temperatures greater than 28°C [141, 144].

2.9 Conclusions of the Literature Review

There is mounting evidence that a building overheating endemic is likely given the intersecting consequences of high thermal performance building strategies, increasing urban densification and a warming world. This is compounded by narrowly defined ranges of what is acceptable as an appropriate internal thermal environment for working and habitation. VC is recognised in the literature as a viable alternative for cooling and, designed and managed correctly, can minimise or in some cases eliminate building cooling loads. Therefore, the heat removal potential of VC systems is becoming critical when evaluating their suitability as strategies for cooling in low energy buildings. Often solutions that extend the capacity of these systems are necessary given the increased internal gains present in modern offices and the limited ability for heat dissipation through the high performance envelope. Nonetheless, cooling potential remains a constraint to the wider uptake of VC, in particular passive VC solutions. Based on the literature review the following conclusions can be made:

- An increase in the cooling capacity of passive VC strategies can be achieved through lowering incoming air temperature, increasing the velocity of the air supply or guiding the airflow more effectively.
- There exists barriers to the adoption of VC, including external air pollution, building security, rain ingress, acoustic integrity and modified boundary conditions from increasingly urban environments. Solutions are needed that can address these barriers and demonstrated performance of these under real conditions is valuable to the research and professional communities.
- The driving forces present in single sided ventilation were identified and dimensional analysis as a technique to analyse the interactions of these forces was discussed. When both wind and buoyancy forces are present this complicates the nature of the airflow exchange mechanism. A Warren plot has been used by many researchers as a method of categorising whether flow is buoyancy or wind dominant in experimental measurements where both forces are present.
- Due to the complicated role wind direction has in determining whether airflow is pressure driven, or turbulent mixing is dominant in the air exchange across the single sided ventilation opening, empirical correlations have traditionally been proposed to deal with airflow predictions. A full chronological review of empirical correlations for predicting single sided ventilation rates was completed and the performance of each was discussed along with the application to which they were relevant.
- A lack of experimental data exists for non standard openings, such as slotted louvre systems, when operating in single sided ventilation strategies. There has been some research

on systems with similar geometries but none of these considered how slotted architectural louvres, which are widespread in building applications, function when exposed to a combination of wind and buoyancy forces. Further, none of the existing data includes how internal air movement, and in turn, thermal comfort, might be affected by the use of such openings. Some research in this area was identified as a key contribution to the existing body of knowledge.

- To date, the accuracy of existing empirical correlations for predicting airflow in single sided ventilation has not been investigated for slotted louvre systems, particularly for wind driven applications. This was identified as another gap in the current knowledge. A new empirical correlation may be required for slotted louvre ventilation components depending on the forces acting at the opening.

In summary, the literature review has shown that, airflow guiding components, such as the MCSL system of the zero2020 building, have the ability to increase the cooling capacity of passive VC systems. At a time when performance is becoming increasingly critical, knowledge about their performance and improved techniques for prediction, can strengthen their uptake in the built environment to deal with the mitigation of building overheating while minimising cooling loads, either as part of a retrofit strategy or in a new building application.

Chapter 3

Experimental Field Studies

This chapter has two purposes. Firstly, an outline of the design, manufacture and installation of the externally applied envelope retrofit solution at the zero2020 building used for all experimental measurements herein is presented. The objective is to provide information about the experimental building prior to description of the experimental field studies. A summary is also provided of the thermophysical characteristics of the building structure along with the externally applied deep retrofit solution and an outline of the ventilative cooling solution adopted including the ventilation components used for cooling.

The second purpose is to provide details about each of the experimental field studies. Information is presented about the experimental methodology adopted, the equipment and testing setup along with the scope of the measurements undertaken. Finally, some details about processing of raw experimental data prior to analysis of results is presented.

3.1 Description of the Building Retrofit Solution

In 2012 Cork Institute of Technology in Ireland (CIT) completed the construction phase of zero2020, a pilot project/research testbed for the low energy retrofit of their existing 29,000m² teaching building originally constructed in 1974 (<http://www.zero2020energy.com>). The retrofit pilot project covered approximately 1.0% of the total building floor area and is shown in Figure 3.1. The primary aim of the envelope upgrade is to extend the lifetime of the building and ensure low thermal energy demand and improved occupant comfort. The zero2020 project was undertaken to investigate in use performance of a solution that was developed locally by researchers within CIT and partner organisations including Arup Engineers, HJL Architects, Kingspan Insulated Panels and AMS Ltd. The retrofit space has been developed as a research testbed with facilities in place for data logging and performance monitoring allowing researchers to undertake monitoring campaigns and experimental studies.

Table 3.1 summarises key information regarding the completed low energy building retrofit. This table includes various information describing the overall characteristics of the building and



FIGURE 3.1: External view of the zero2020 testbed envelope upgrade

TABLE 3.1: Key Building Information

Location	Cork, Ireland
Building Type	Office
Retrofit (Y/N)	Y
Surroundings (Urban / Rural)	Rural
Ventilative Cooling Strategy	Natural
Year of Completion	2012
Floor Area (m ²)	222.5
Openable Area to Floor Area Ratio (%)	2.3
Window to Wall Ratio (%)	56
Sensible Internal Load (W/m ²)	29
Climate Zone (K-G Class)	(Cfb)
No. of Days with Te max >25° C	0
Cooling Season Humidity	Low
Heating Degree days (Kd)	639

is largely based on work completed for an IEA-EBC Annex 62 case study brochure (<http://venticool.eu/annex-62-home/>).

3.1.1 Design criteria

The environmental design criteria set out at the beginning of the design process in 2011 was based on guidelines recommended by CIBSE Guide A [145] with a winter indoor operative temperature in the range 21-23 °C, a summer operative temperature of 25 °C, with an hours exceedence overheating criterion of not more than 1% of annual occupied hours above a static threshold value summer peak temperature of 28 °C. The required ventilation rate was $10 \text{ l s}^{-1} \text{ p}^{-1}$, maintained luminance of 300-500 lux and a noise level rating NR30. Current standards for fabric performance are set out in TGDL 2008 Conservation of Fuel and Energy (Buildings other

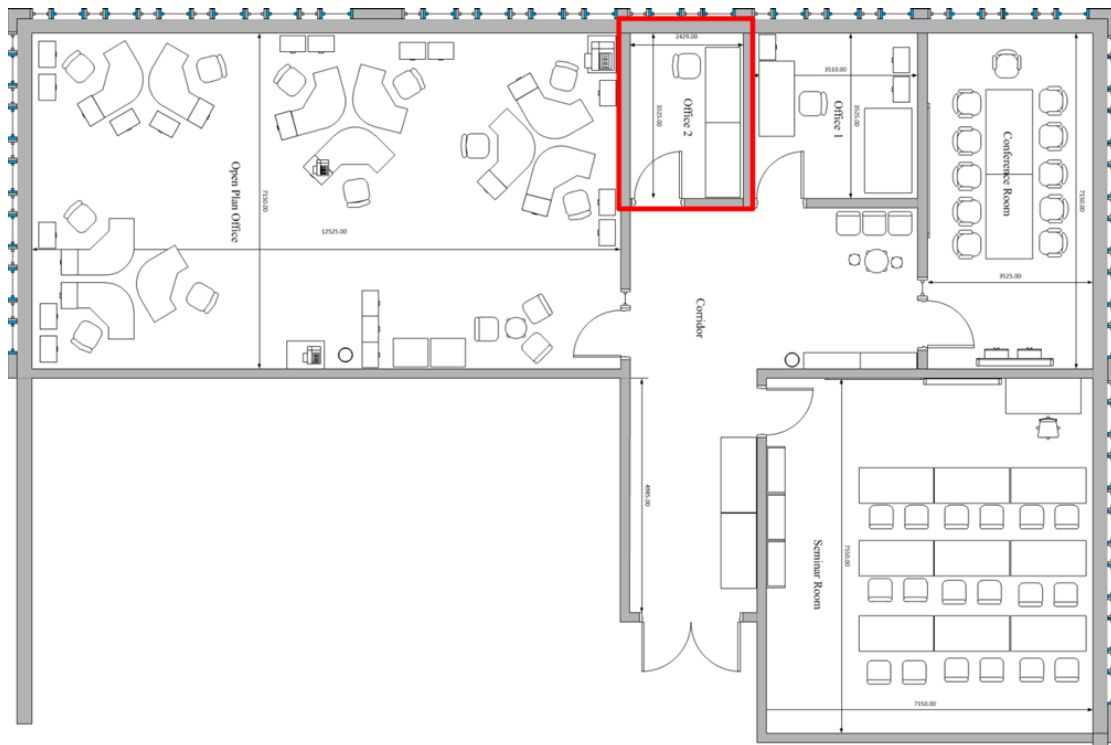


FIGURE 3.2: Plan layout for the zero2020 testbed space at CIT. First floor only. Room used for experimental work shown in red border. Further details of experimental setup for different measurement campaigns in Chapters 4 & 5

than dwellings) [58]. It lists U-values for opaque elements in the range 0.16 to $0.27 \text{ W/m}^2\text{K}$ with glazing at $2.2 \text{ W/m}^2\text{K}$ depending on glazing area. Energy performance standards are set at a maximum permitted energy performance coefficient (MPEPC) of 1 and a maximum permitted carbon performance coefficient (MPCPC) of 1. These are calculated when comparing the actual building to a reference building in SBEM. No standard is set for renewable energy contribution or structural air tightness. At both concept and design stage there were no guidelines within the Irish context upon which to base performance targets to achieve a nearly zero energy building (NZEB) through retrofit. The design proceeded along a simple strategy of firstly, ensuring compliance with the environmental specification for occupant comfort and secondly to achieve the best fabric and energy performance subject to constraints imposed by budgets and retrofit/structural limitations. This resulted in U-values, calculated according to ISO6946:2007 [146], for opaque elements over 6 times better than current regulations ($0.09 \text{ W/m}^2 \text{ K}$ vs. $0.6 \text{ W/m}^2 \text{ K}$ for material alterations and existing building refurbishment) and glazing U-values twice as good ($1.1 \text{ W/m}^2 \text{ K}$ vs. $2.2 \text{ W/m}^2 \text{ K}$ for material alterations and existing building refurbishment). The occupancy nature of the internal use also informed the design brief as this limited the retrofit methodology to the external envelope and an installation period of 6-8 weeks.

3.1.2 zero2020 Architectural Concept

The common basic modular structure of the nine Regional Technical Colleges (RTCs) in Ireland was designed in 1967 using a modular two storey reinforced concrete precast structural frame

with externally hung concrete aggregate panels and single glazed aluminium windows as its facade. The original tabular structure, shown in figure 3.3, designed to take a third floor, was originated by Michael Scott and Jock Harbinson (IRIS 1974). Over time the 1200mm repetitive glazing module was used as the principle dimension for internal subdivision.

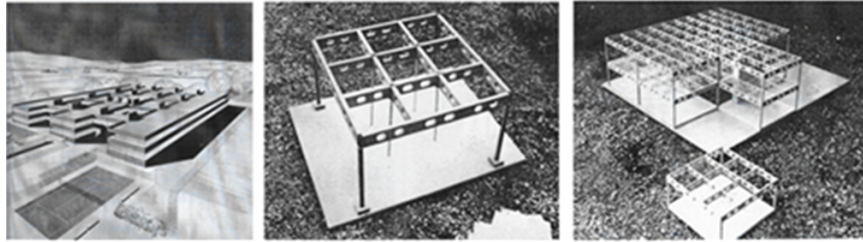


FIGURE 3.3: Left: Waterford campus 1969, Middle: existing structure table concept, Right: existing structure grid concept

The existing internal subdivision and existing structural grid pointed the design toward a grid optimized solution, reducing internal change. Existing internal servicing resulted in the retention of aggregate panels. The design requirement to replicate the structural modularization limited aesthetic improvements to materiality and massing variation. A plan to deliver natural ventilation via envelope louvres and the need to reduce the glazing fraction allowed for the introduction of verticality into the envelope design. Cost informed the choice for interstitial shading. The use of a high polished black granite like composite panel created a low maintenance improved cosmetic envelope finish.

3.1.3 Envelope Components

The existing, pre retrofit, wall structure in CIT comprised of a 100mm internal block, an un-insulated air gap and an external concrete aggregate panel approximately 125mm thick. See Figure 3.4 components 1-3. The existing roof comprised of 150mm concrete slab, 25mm cork insulation and a poured asphalt covering, see Figure 3.5 components 5-7. The external envelope retrofit solution involved the installation of a new external facade, independently supported at the base and tied into the structure at certain locations. The solution can be sub-divided into three broad modular categories; Roof module, opaque wall module and the fenestration module comprising both the glazing and ventilation openings.

3.1.3.1 Opaque External Wall and Roof modules

For the external wall modules vertical support mullions, designed and supplied by AMS Ltd, were installed externally to the existing aggregate panels. These support the new Kingspan Benchmark system which comprises a 125mm insulated panel, carrier rails and a 12mm ceramic granite panel as shown in Figure 3.4. It should be noted that the entire existing structure has remained in place as part of the solution. The main thermophysical properties for the final opaque wall build up including the retained existing building components and the retrofit components are summarised in Table 3.2.

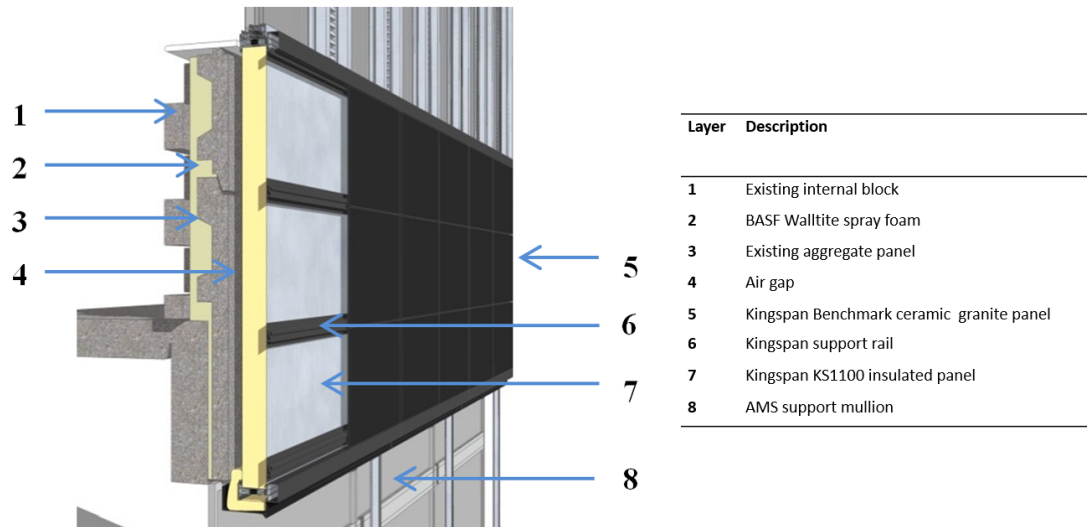


FIGURE 3.4: External retrofit opaque wall construction build up. (reproduced courtesy of Henry J Lyons Architects)

TABLE 3.2: Retrofit External Wall Components and Thickness's

No	Description	Dim (mm)
1	Existing Internal Block	100
2	BASF Wall-tite Spray Foam	86
3	Existing aggregate panel	125
4	Air gap	30
5	Kingspan benchmark ceramic granite panel	12
6	Kingspan support rail	37
7	Kingspan KS 1100 insulated panel	125
8	AMS support mullion	125

For the roof solution the external insulation was upgraded to 200mm thick Kingspan Kooltherm rigid insulation. The existing roof structure was retained in place. Figure 3.5 highlights the final opaque roof build up and Table 3.3 summarises respective components.

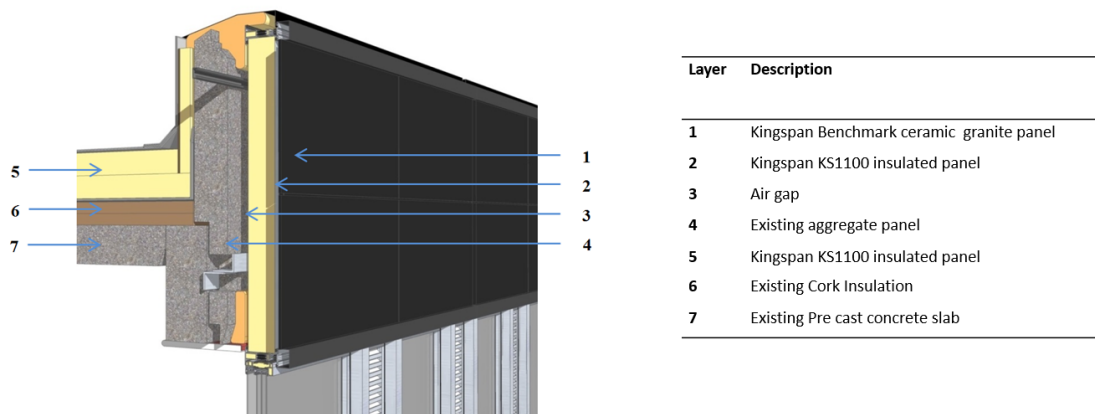


FIGURE 3.5: External retrofit opaque roof construction build up. (reproduced courtesy of Henry J Lyons Architects)

TABLE 3.3: Retrofit External Roof Components and Thickness's

No	Description	Dim (mm)
1	Kingspan benchmark ceramic granite panel	12
2	Kingspan KS 1100 insulated panel	125
3	Air gap	30
4	Existing aggregate panel	125
5	Kingspan KS 1100 insulated panel	250
6	Existing Cork Insulation	75
7	Existing Precast Concrete slab	250

TABLE 3.4: Thermal characteristics of retrofit external envelope opaque elements

Property	Roof Pre	Roof Post	Wall Pre	Wall Post
$\varphi, (Wm^{-2}K^{-1})$	7.210	7.220	5.490	5.920
Time shift for $\varphi, (h)$	1.452	1.424	1.017	0.963
$S, (Wm^{-2}K^{-1})$	0.463	0.008	2.209	0.000
Time shift for S (h)	-6.137	-15.320	-4.84	-15.830
$U, (Wm^{-2}K^{-1})$	1.156	0.092	3.633	0.090
f , Decrement Factor	0.401	0.087	0.608	0.004

The calculation of dynamic properties of the structural elements was done in accordance to EN 13786:2007 [15]. For a composite building component, consisting of homogeneous layers, the heat transfer matrix is calculated by multiplying the matrices of the individual components, $Z = Z_n Z_{(n-1)} \cdots Z_1$. The effect of surface resistances can be taken into account to allow the calculation of temperature and heat flow from external to internal environments as follows:

$$Z_{ei} = \begin{bmatrix} 1 & -R_{se} \\ 0 & 1 \end{bmatrix} \begin{bmatrix} Z_{11} & Z_{12} \\ Z_{21} & Z_{22} \end{bmatrix} \begin{bmatrix} 1 & -R_{si} \\ 0 & 1 \end{bmatrix} \quad (3.1)$$

Assuming the heat transfer matrix is calculated allowing for the surfaces resistances, the dynamic properties of the composite structure can then be calculated from the matrix Z_{ei} using relationships as defined in EN ISO 13786:1999 [147]. These properties have been calculated for the existing structure and the completed retrofit and are outlined in Table 3.4 above. Thermal transmittance is calculated in accordance with EN ISO 6946:2007 [148], ignoring thermal bridging.

Of primary concern was limiting thermal bridging throughout, particularly at critical junctions between the new and old interfaces. A thermal break was manufactured into the mullion support systems to reduce the effects of thermal bridging across the new facade. Extensive thermal bridging modelling was carried out by AMS Ltd at all junctions within the new facade using BISCO V9 simulation software which is compliant with EN ISO 10077-2:2012 [149]. This highlighted areas where extra insulation was required and resulted in a number of details that substantially reduced the risk of thermal bridging and proved to be a necessary and valuable process for retrofit detailing. Linear thermal transmittance values, ψ Values (W/mk), typically ranged from 0.191 to 0.328 W/mk .

3.1.3.2 Integrated Fenestration system

As part of the envelope solution an integrated fenestration module was developed to satisfy requirements for acceptable indoor air quality (IAQ) and occupant thermal comfort in line with Irish Building Regulations Part F and current best practice (e.g. see IS EN 13779:2007 [150]; ISO 7730:2006 [49]; CIBSE Guide A 2006 [145]). The unit comprised of high performance glazing and purpose provided ventilation openings. The glazing components are completely sealed - with interstitial blinds for glare and solar shading control. Ventilation is supplied using dedicated insulated doors controlled either manually or automated based on conditions in the enclosed spaces, described in more detail in Section 3.2 below. The overall thermal transmittance performance of this unit including doors and linear transmittance is $0.84W/m^2k$ (calculated by AMS Ltd using BISCO V9 software), according to IS EN 10077-2:2012 [149]. The new fenestration module resulted in an overall opaque/transparent surface area ratio reduction of 20%. This alteration in the envelope configuration was achieved without interference with the existing structural profile. This reduction was feasible following results from a day-lighting study of the proposed solution by the project engineers, Arup, that indicated acceptable light levels throughout. The day lighting study was completed in response to occupant feedback from the existing building during the design development phase of the project. Excessive glare was identified as the primary source of discomfort throughout the year and it was agreed a reduction in glazing would be feasible. The glazing unit, integrated into the new AMSTS125 fenestration system, consists of a Saint Gobain sealed, argon filled, low-e coated, triple glazed external component, interstitial venetian blinds and a fourth pane of clear float inner glass completing the glazing transparent component. Details of the system are outlined in Figure 3.6 & Figure 3.7. The blinds are adjustable by running a control mechanism through the window system and fitted to the mullion on the inside. This gives occupancy control of glare avoidance and solar shading during periods of high solar irradiation which, as mentioned, was a problem for occupancy comfort in the existing space. Each glazing unit is 1800mm x 800mm. There are 2 glazing units for every module. The overall fenestration system, including shading layers, was modelled using LBNL Window 7.1 [151].

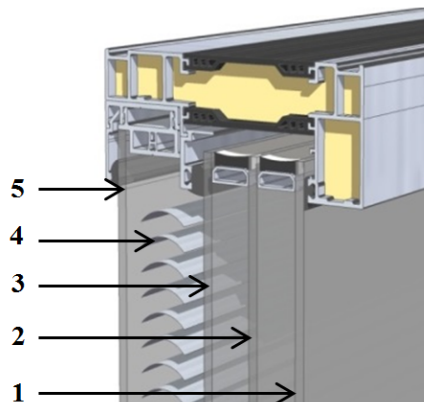


FIGURE 3.6: External retrofit glazing module build up. (reproduced courtesy of Henry J Lyons Architects)

There are alternative fenestration specifications depending on facade orientation. The south and west facades had a solar control coating. The U-value of these glazing/interstitial blind

components is $1.1W/m^2k$, with a centre of glass value of $0.82W/m^2k$. These values include for the linear transmittance values at the sash and cill. The total Solar Heating Gain Coefficient is 0.296 and the VT is 0.150. For the North facade the glazing is triple glazed only and incorporates internal roller blinds as opposed to an interstitial solution and no solar control coatings.

3.1.4 Installation

The design brief stipulated that the envelope solution should be an indigenous product. The solution also had to be scalable in nature and be an off-site build to ensure physical retrofit installation times were greatly reduced at the building and for any future roll out of the solution. The Architectural Metal Systems (AMS) 7-5 high performance renovate facade system was installed at zero2020 incorporating all the various components outlined in 3.1.2 and 3.1.3 above. The new high performance curtain wall solution was easily constructed and assembled so as to minimise disruption on site, and also allowed ease of integration with the Kingspan Benchmark system.



FIGURE 3.7: External retrofit glazing module build up. (reproduced courtesy of Henry J Lyons Architects)

The envelope retrofit has proven to be both modular and scalable as a retrofit system the ground floor upgrade was completed at a later stage than the first floor and was completed in a short number of weeks with a seamless execution. The modularity of the solution means any part of the structure can now be easily upgraded which lends itself to phased retrofit planning. The solution demonstrated a high potential for very good thermal comfort levels.

3.1.5 Energy Performance

In order to demonstrate that the building is in fact low energy following the retrofit, Figure 3.8 presents energy consumption data for three years, 2014 to 2016. Energy is divided into electrical energy from the heat pump, the heating system circulating pump, lighting and general services (pcs, etc). The heating energy performance in 2016 can be classified as complying with new build Passive Haus standards which require a maximum of 15 kWh/m^2 of annual energy demand for space heating. The space is low energy on account of its high performance thermal envelope. In 2013 there was a 3D laser printer in use in the space and this is the reason for higher general services that year. In 2014 and 2015 there were long periods of time when the heat pump was unavailable due to issues associated with the pressurisation of the system. Some electric heater were employed during this time and this is the reason for low heat pump loads in these years.

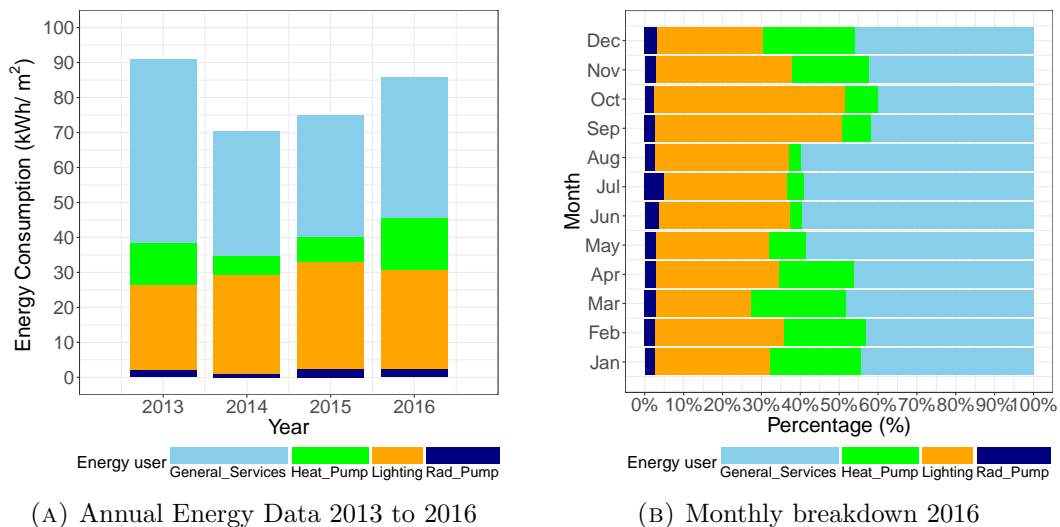


FIGURE 3.8: Energy consumption data for 2013 to 2016 categorised according to user type.

The general services loads have increased in 2016 due to increased occupancy and the heating loads are based on normal operation, similar to 2013. The lighting loads have remained relatively constant throughout. There is a small heating load shown even in summer when we consider the monthly breakdown. This is due to a minimum flow circulating requirement where the heat energy meter is picking up the flowrate even when no heating energy is actually required. In 2013 and 2016 the measured delivered energy for heating was 13-14 kWh/m².

3.2 Description of the MCSL System

In the existing pre retrofit spaces single sided natural ventilation is the dominant principle used for passive cooling. There are no mechanical ventilation systems except for specific server rooms, IT labs etc and these system types are outside the scope of the work presented here. In most cellular, enclosed office spaces in the existing building the ventilation system is based on top hung pivoting window sections located in a single external faade. There is generally one opening window per structural grid. These are the original 1974 windows. See Table 3.5 for further details relating to the existing window. In the retrofit space, single sided natural ventilation is the over-arching principle adopted due to the cellular nature of the existing internal layouts. Single sided strategies used with airflow guiding and/or enhancing components, can be attractive as they can easily integrate into an externally applied envelope retrofit system. There were also practicality constraints regarding the continued operation of the existing building and minimal invasive rework of the structure internally. This limited the opportunity for using cross flow ventilation strategies or passive centralised stack ventilation. Large opening heights are employed to promote buoyancy forces in hot, still summer periods. Some instances of cross flow exist in the open plan office space when openings are activated on both south and west faades. Cooling is available during occupied hours through the activation of the openings. In the retrofit space the ventilation module uses a flush faced external louvre system, (Figure 3.9). Each slot louvre section comprises 17 air inlet slots with a facade porosity of 0.057% and a net

free opening area, A_o , for each section of $0.107m^2$. The building has an average POF of 3%. The anodized aluminium slot louvre has a 47% net free open area for airflow and each vertical louvre bank, comprised of two sections, has overall structural opening dimensions of 0.30m (w) x 1.60m (h) (the overall height includes intermediate cross mullion and framing). Each louvre slot also incorporates a unique concave shape which acts as a guiding component to incoming air, (see Figure 3.9 and also Figure 5.9 page 128). Under normal operation there are two louvre banks in the cellular space utilised for experimental measuring campaigns in 2013 and 2014 (see Figure 3.2 page 65). Inside this louvre, ventilation is supplied using dedicated insulated doors controlled either manually or automated based on conditions in the enclosed spaces (see Table 3.5 for different operating configurations and effective opening areas). Unwanted ventilation through adventitious openings has also been greatly reduced. The retrofit envelope air permeability was tested as part of the building commissioning in accordance with BS EN 13829:2001. The envelope achieved an air permeability of $1.76(m^3/hr)/m^2$ at 50Pa building pressure. The existing structure was measured as $14.77(m^3/hr)/m^2$.

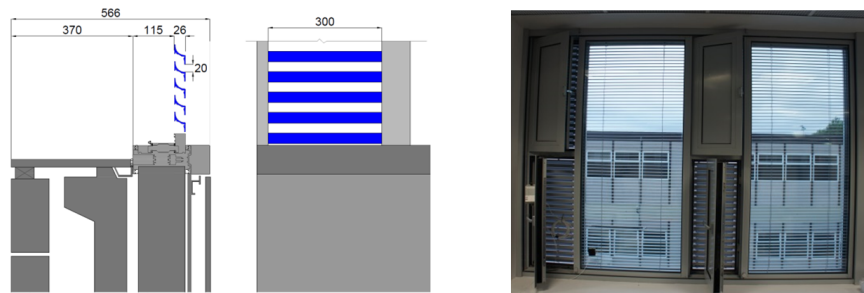



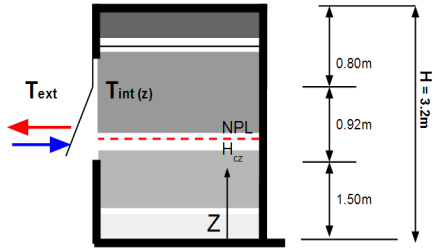

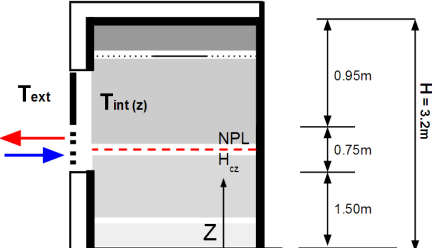

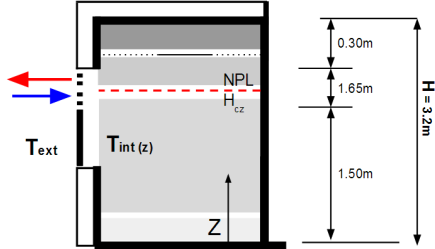

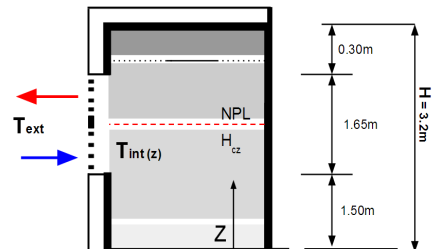
FIGURE 3.9: Purpose Provided Narrow Slotted Architectural Louvres and Insulated Ventilation Doors. Left: Detail section of openings, Right: Installed Combined glazing and ventilation modules.

The following sections describe the physical set up of experimental work completed and the execution of measurements for the different measuring campaigns stated in Table 1.1 page 6 which outlined the research objectives and technique applied for each. Three of the four studies from Table 1.1 are summarised here; Full scale OH performance, Full scale ACR performance and Airflow effects of the slotted louvre. These were all field studies undertaken in a full scale building.

3.3 Description of Experimental Field Studies

In order to complete an accurate comparison of how two different ventilation openings perform under similar boundary conditions there are a number of approaches possible. Firstly a physical model can be developed in a controlled laboratory or wind tunnel environment. This model can be full size or, depending on any constraints that may exist, a scaled model can also be used. When working in a laboratory environment measurements of specific phenomena and boundary conditions can be obtained with a high level of certainty and accuracy. This is largely due to the reproduction of boundary conditions in a way that isolates their effect and removes additional interference from sources of noise. As wind forces are of particular interest in this

TABLE 3.5: Ventilation Opening Configurations for Control space and Retrofit Space. Note: CS=Control Space; RS= Retrofit Space; M = Manual; A=Automated with manual override (flow schematics not to scale)

Configuration	Ventilation Opening	Envelope Flow Schematic
CS.01/M $0.32m^2$		
RS.02/M $0.21m^2$		
RS.03/A $0.21m^2$		
RS.04/M/A $0.42m^2$		

research, the magnitude of the force, the incidence angle of attack and the additional effects of the interactions with the opening geometry, this can make laboratory studies less attractive due to the scale of equipment needed for full scale laboratory experiments. As the combined effects of wind and buoyancy forces are often present in real environments both their effects would need to be accommodated in varying magnitudes within the laboratory study. An alternative experimental approach is to use full scale, field study data for the analysis. The benefit of field study measurements is in using the real physical nature of the boundary conditions, giving

the opportunity to capture, as close as is reasonably possible, the response of the ventilation system to real environments. The difficulty with field studies when comparing two different external ventilation openings in actual buildings can be the experimental set up, reproducible test conditions and obtaining near identical installation configurations for the two openings to undertake the study without additional uncertainty from dissimilar installation effects. Due to the availability of a test room within the experimental building it was decided to use a full scale field study methodology for the research. Data from field studies are valuable and often lacking in published research. The louvre has an airflow guiding profile and little knowledge exists on how this will affect the net air exchange across the opening when the airflow is driven by a combination of natural wind and buoyancy forces. As mentioned three separate measuring campaigns in the experimental building were carried out supplemented by demonstration of the potential for cooling using the MCSL system using a modelling approach. These methods are summarised below.

3.3.1 Full Scale OH Performance: Experimental Setup

The objective of this part of the study is to present results from long term monitoring of the indoor thermal environment at zero2020 and assess, using measured data, whether or not the solution employed for cooling during summer periods has successfully removed the need for additional mechanical cooling.

While thermal discomfort is attributable to many factors including the effects of air velocity, humidity, air temperature, surface temperatures, radiation asymmetry, vertical temperature asymmetry, clothing levels and localised draughts, when assessing long term cooling performance of a free running building it is often impractical to attempt to continuously measure all such parameters. A traditionally accepted approach is to use the indoor operative temperature as an indicator of thermal environment. This allows a simplified approach to quantifying the extent of unacceptable levels of thermal discomfort during cooling seasons in ventilative cooling spaces. As mentioned in Chapter 2, a number of different standards exist for determining upper threshold values when calculating overheating indices using operative temperature alone, though the differences tend not to be substantial. In order to assess the long term performance of the installed ventilative cooling solution at zero2020 calculation of overheating using various criteria based on indoor air temperature alone was chosen as an acceptable and effective indicator. A separate study at the experimental building showed very close correlation between indoor air temperature and operative temperature [72]. This allowed to present overheating performance in a format that was in line with standards [20, 49] and allowed for ease of comparison of the data with other similar systems and buildings by other researchers.

There are seven spaces within the experimental building. May to September 2013 was chosen as the measurement period. Air temperature was measured at a single location in each room within the building using Hanwell Radio-logger RL4000 wireless data loggers with precision thermistors (± 0.1 °C between -25 °C to 50 °C) at a sampling rate of 10 minutes. This data was then averaged to a 1 hour interval for the purposes of this study. Figure 1.3 (page 8) shows a

photo of the thermistor and data logger in situ as well as an example of the interior space used for analysis of overheating.

Both the static thresholds traditionally proposed by CIBSE and BRE (see section 2.2.3, page 22) were calculated from the measurement data. The adaptive thermal comfort approach, outlined in CIBSE TM52 [21], (see section 2.2.3, page 22) was also used to investigate whether the spaces in the experimental building were subject to overheating. These indices were calculated for each space and used to assess the performance of the system in maintaining an acceptable indoor environment without the need for supplementary cooling.

3.3.2 Full Scale ACR performance: Experiment Setup

This section brings together the description of the spaces utilised for testing in this field study as well as the experimental set up of each space where both internal environment and ACR measurement were completed. In the study two separate existing rooms were identified to undertake measurements, one in the existing building, used as the control space, and one in the retrofitted space, containing the slot louvre ventilation opening of interest to the research. The following section describes specific experiment setup information for the two spaces used for the comparison of macroscopic ACR performance.

3.3.2.1 Location study of control and retrofit test spaces

Figure 3.10 is a part site map for Cork Institute of Technology. The control and retrofit spaces are identified for the field study as red and orange squares respectively. The elevation location of each test space is shown in Figure 3.11, both facades are west facing, one pre retrofit and the other post retrofit.



FIGURE 3.10: Part site map of cork institute of technology. Location of control and retrofit spaces shown in red and orange respectively.

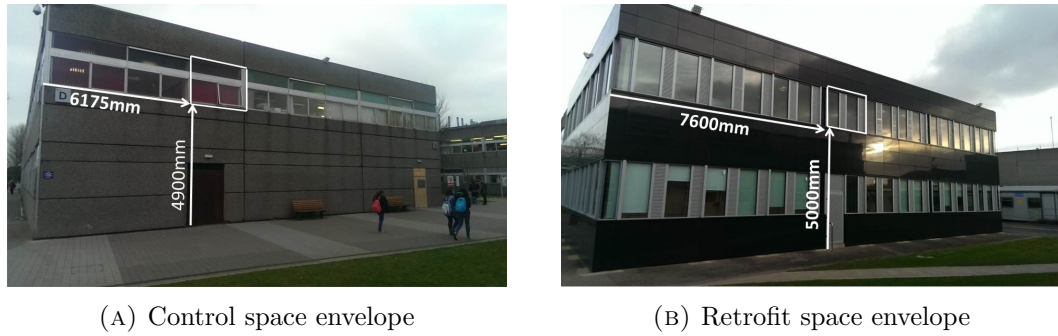


FIGURE 3.11: Dimensioned locations for control space and retrofit space chosen for field study. Overall facade width approximately 22m

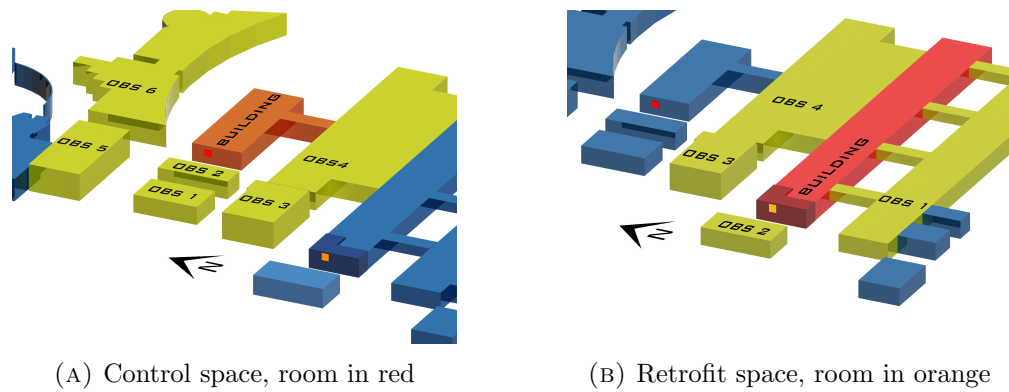


FIGURE 3.12: 3D obstacle study of control and retrofit space. Surrounding obstacles included in calculation of C_p values shown in yellow

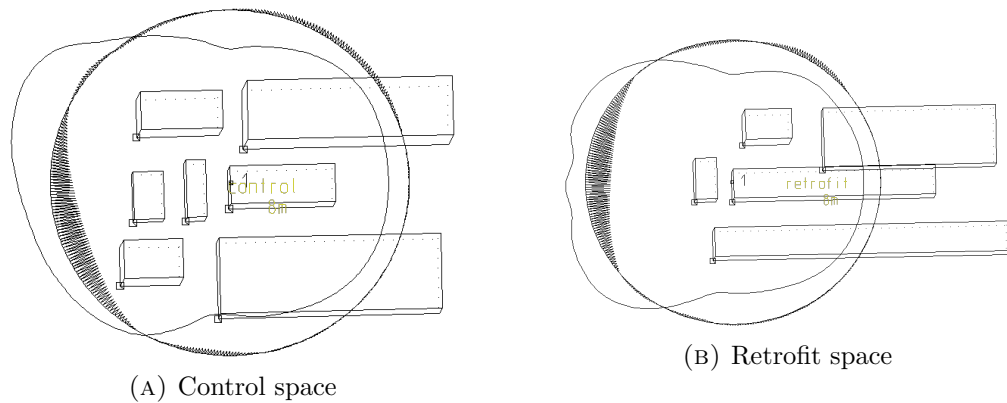


FIGURE 3.13: C_p generator polar plots of obstacle correction factors

Figure 3.12 presents a 3D image of the various obstacles surrounding each location. Static wind pressure coefficients were used as an indicator of the similarity of both locations to the conversion of free stream wind velocity and corresponding forces. C_p Generator (www.cpgen.bouw.tno.nl), [152], was utilised to calculate the C_p values for each ventilation opening.

Figure 3.13 highlights the correction factors applied to base C_p values for obstacles within a distance 5 times the obstacle height from the ventilation opening. Finally Figure 3.14 compares both calculated C_p characteristics as a function of wind attack angle relative to the envelope orientation (west facing in both spaces). It can be seen from Figure 3.14 that for leeward wind

directions the C_p values are near identical. Where the wind direction is normal to the envelope there is a difference between C_p values of 0.053 with 0.087 between maximum values. Overall it can be said that both retrofit and control spaces experience comparable effects from obstacles. This suggests that while the site has urban canopy layer obstacles, the control space is still an acceptable match for the retrofit space for the purposes of investigating differences in time averaged ventilation rates under similar climate conditions.

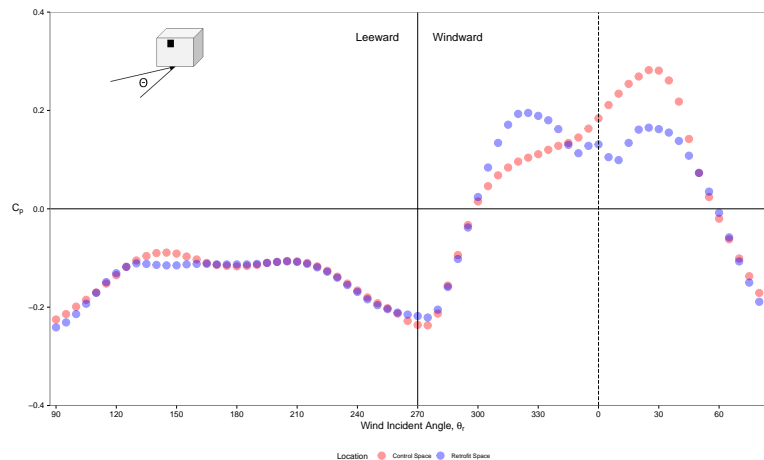


FIGURE 3.14: C_p characteristics for control and retrofit spaces as a function of wind incidence angle

3.3.2.2 ACR Measurement

The single sided ventilation ACR for both the control and retrofit spaces was measured using the single zone regression based Tracer Gas Concentration Decay (TGCD) method. TGCD techniques are among the most efficient to assess airflow patterns within buildings. A theoretical description of the different measurement techniques available is presented in Appendix A: Single Sided Ventilation Measurement Techniques including optimum decay time and estimation of measurement error. The technique consists of marking the air with a tracer gas and observing the rate of dilution of gas concentration that can be attributed to the aeration from the ventilation opening [153]. Carbon Dioxide (CO_2) was chosen as the tracer gas for this work due to the ease of use, availability of analysis equipment, its density being similar to air and cost. CO_2 qualities as a tracer are summarised in Table A.1, Appendix A (See also Table 7.2 of Roulet [153]). One main concern when using CO_2 as a tracer gas can be the presence of a large background concentration and, if constant, account must be taken for this in analysis of data by substituting the difference between indoor and outdoor concentration for indoor concentration in the analysis [154]. For each of the tests presented in this work outdoor CO_2 concentrations and indoor zone CO_2 concentrations prior to and during the test were monitored and test concentration levels adjusted accordingly. Table 3.6 provides summary information about tracer gas concentration measurements during testing for the different opening types/configurations (See Table 3.5 page 88 for information on configurations). Tracer gas characteristics were similar for testing of each opening type/configuration. Average outdoor CO_2 concentration during testing for each opening

TABLE 3.6: Tracer gas test characteristics for TGCD tests, categorised according to opening location or configuration

Config.	No of Tests	Test Durations	Conc Uniformity	Start ppm Range	End ppm Range	Average B.G. ppm
CS-1.0	13	24 - 90 min	2.57%	3181 - 6203	175 - 1214	10.3%
RS-2.0	6	26 - 60 min	1.51%	3538 - 5431	364 - 1481	12.3%
RS-3.0	6	31 - 60 min	4.46%	3511 - 5051	703 - 1327	13.4%
RS-4.0	13	30 - 161 min	2.37%	3647 - 4746	212 - 1067	13.0%

type/configuration (as a percentage of the indoor concentration) is also summarised in Table 3.6. Good consistency was observed across all tests.

TGCD tests were completed in accordance with the procedures set out in Section 8 of ASTM E741-11: '*Standard Test Method for Determining Air Change in a Single Zone by Means of a Tracer Gas Dilution*'. Two tracer gas sampling locations and a single gas injection location were used within the zone being tested. This was a standard CO₂ cylinder and heated flow regulator. Direct automated sampling of CO₂ gas was done using AlphaSense IRC-A1 Non Dispersive Infra-Red (NDIR) Sensors ($\pm 1\%$ of full scale at -20°C to 50°C), shown in Figure 3.15 below. CO₂ sampling frequency was 1Hz, with data averaged to 10 second values for estimation of ACR values. Refer to Figure 3.16 for equipment layout for both the control space and retrofit space. As CO₂ is denser than air (its relative density, to air, σ , is 1.53) the gas was actively mixed as it entered the space, aided with a portable desk fan, located at the nozzle outlet of the heated flow regulator for the CO₂ bottle.

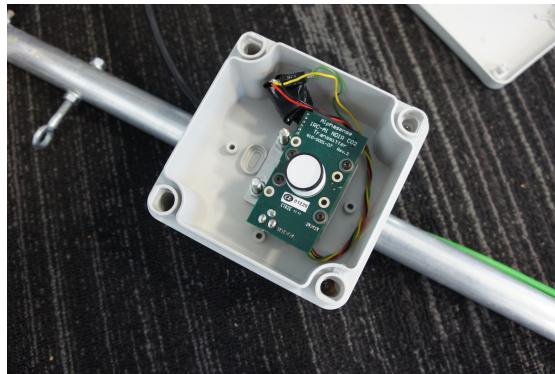


FIGURE 3.15: NDIR sensor being installed into protective housing for external mounting

A maximum 10% deviation between a particular location and the average zone concentration in accordance with section 12.4.1 of ASTM E741-11 was used to determine when there had been sufficient gas mixing prior to commencement of each test. After monitoring CO₂ levels for a period of time to ensure mixing was stable the ventilation opening was activated and the test started. CO₂ levels were visually monitored during the test using the Alphasense data logging software. When the decay rate of CO₂ concentration had stabilised and levels were close to the initial pre test condition the test was stopped. The average test time was around 42 minutes. The lowest ACR measurement was 1.4 h^{-1} (test 38 - RS.03) with a test duration of 60 minutes. The longest test duration was 90 minutes for test 34 which was in the control space, CS.01, and resulted in an ACR value of 2.0 h^{-1} . Test durations for the measurement of full scale ACR were

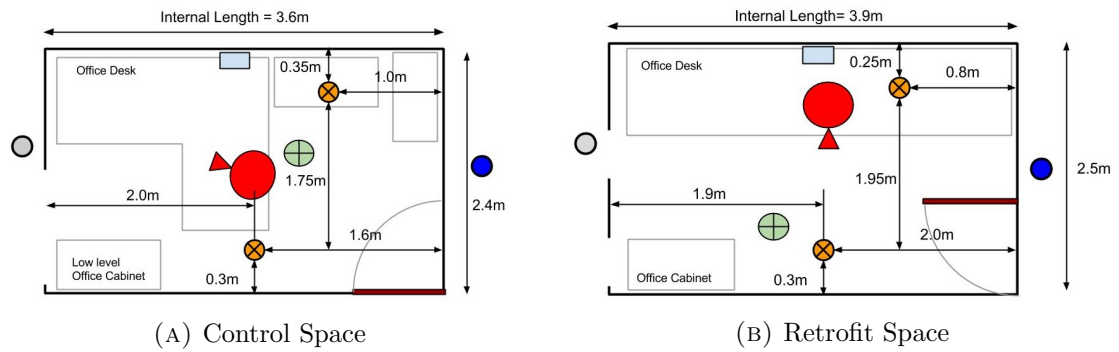


FIGURE 3.16: Instrument and equipment positioning for July-August 2013 measurement campaign. (Legend: Orange - CO_2 NDIR; Green - Vertical precision thermistors; Grey - External CO_2 NDIR; Blue - Corridor CO_2 NDIR; Red - CO_2 Cylinder and Injection point)

in all instances greater than the minimum recommended values in Table 2 of ASTM741-11. ACR were subsequently calculated using the linear regression decay technique [155], equation A.14 on page 187, with the normalised concentration, equation A.13 on page 187, from [156]. Thirty eight TGCD tests were completed in total for the full scale field study of ACR performance of the VC system. All measurements were completed over fifteen days during 1st July 2013 to 11th September 2013, an average of 3 tests conducted on each day of testing. Twenty five separate tests of the ACR in the retrofit office space were completed. These were made up of a number of tests for each of the three possible configurations of the retrofit VC system, (13 tests for RS.04, 6 for RS.02 and 6 for RS.03). Thirteen separate tests of the control space, CS.01, were completed. Where possible, different configurations were generally tested on the same day. This was to ensure measurements of ACR were recorded with similar boundary conditions for different opening configurations. Test durations varied depending on the dilution rate or corresponding ACR. This involved testing in the morning in one location and then relocating the CO_2 injection rig to the other location in the afternoon. Given that 75% of configurations were in the retrofit space there were some days where only configurations in the retrofit space were tested.

When we consider the findings from the literature review on measurement uncertainty for the TGCD technique in Appendix A section A.4.2, the measurement accuracy of the in-situ CO_2 sensors and the very good levels of mixing demonstrated in Table 3.6 we can reasonably estimate that the measurement error is less than 10%. We discuss uncertainty due to an unsteady ACR during tests in Appendix A and presents results for ACR measurements in chapter four and chapter five.

3.3.2.3 Internal Environment Measurement

Indoor air temperature and its distribution within a single zone depending on the zone dimensions, is an important parameters effecting ventilation airflow rates and its role in this regard as well as human thermal comfort has been discussed in Chapter two. The vertical temperature profiles were investigated as part of the measuring campaign described here. In order to investigate what level of thermal stratification was present in the existing building and how this has been modified by the retrofit strategy the vertical temperature profile was measured at eight

vertical locations during each of the TGCD tests. As well as this vertical temperature profiles were recorded for an extended period covering 9th June 2013 to 23rd July 2013, with 24 hour data obtained for each day. Hanwell Radio-logger RL4000 wireless data loggers with precision thermistors ($\pm 0.1\text{ }^{\circ}\text{C}$ between $-25\text{ }^{\circ}\text{C}$ to $50\text{ }^{\circ}\text{C}$) were used for vertical temperature distributions. Measurements were recorded every 10 minutes in the retrofit space and every 5 minutes in the control space. Measurements were taken at eight equally spaced vertical positions from floor to underside of the false ceiling level throughout the 3.2m height. Surface and air temperatures were also continuously logged using Gemini Tiny-tag data loggers. The mid point measurements was taken for the calculation of envelope temperature differences.

3.3.2.4 Boundary Conditions Measurement

A roof mounted Campbell Scientific weather station was recommissioned as part of the research work. This was an existing station that was out of service. A number of instruments were reconditioned and fully recalibrated by Campbell Scientific. They were then reinstalled at the weather station. The station is located on a metal platform 8.0m above the finished roof level of the building. Figure 3.17 below shows the completed weather station. Table 3.7 provides information about the various instruments and parameters recorded during all field studies. The weather station continuously logs data at the building and was used for recording reference weather data that could be used for defining boundary conditions at the building. The building is located in a valley with the local meteorological weather station positioned at the nearby airport with an altitude difference of 160m. For this reason the weather station at the building was chosen as preferable when representing reference boundary conditions.



FIGURE 3.17: Roof mounted weather station with recommissioned Campbell Scientific instrumentation. See Table 3.7 for instrument specifications

TABLE 3.7: Roof mounted weather station instrumentation specifications.

Parameter	Model	Operating Range	Accuracy	Interval
Temperature	HC2S3 Rotronic Hygroclip 2 probe	-40 to 100° C	0.1° C at 23° C	5 min
Humidity	HC2S3 Rotronic Hygroclip 2 probe	0–100%	0.8%RH at 23° C	5 min
Air Pressure	Vaisala PTB101B	600–1060 mbar	0.5 mbar at 20 ° C	5 min
Solar Radiation	Campbell Sci SP1110 Pyranometer	-35° C to 75° C	5% for 350–1100 nm/lin 1% dev	5 min
Wind Speed	Campbell Sci 05103 Vane Wind Monitor	0–100m/s	0.3 ms ⁻¹ or 1% of reading (0100 ms ⁻¹)	5 min
Wind Direction	Campbell Sci 05103 Vane Wind Monitor	0–360°	5.0°	5 min

3.3.3 Mapping and Prediction of Airflow with the Slotted Louvre: Experiment Setup

There are two objectives of this field study, the first being to investigate the performance and prediction of single sided ACR for the slotted louvre component and the second to identify any modifications to air movement at the local occupant environment from the use of the slotted louvre.

An empirical model that adequately predicts single sided ACR from an opening that utilises a slotted architectural louvre arrangement such as that installed at zero2020 is an important tool for ventilation system designers. Making use of existing single sided correlations for predicting ACR through plain aperture openings may not be sufficient. To date the suitability of existing correlations to slotted louvres has not been investigated in any of the published literature in the field, particularly those with airflow guiding features. The first objective of the study presented in this section is to measure ACR for a single, isolated, slot louvre section directly and compare this to a plain open aperture with comparable geometric dimensioning under similar full scale boundary conditions. To aim is to infer any modifications to local airflow exchange mechanisms at the opening and investigate, using the experimental data, the ability of existing semi empirical correlations in adequately predicting the measured single sided ACR. This differs to the previous field study in that a direct comparison is made with and without the slotted louvre using the same opening in the same space, isolating additional variables influencing performance, allowing a direct investigation of phenomena. The second objective is to investigate whether there is any effect on the local air movement at the occupant location from the use of the slotted louvre in lieu of a plain opening. Enhanced local air movement in the form of increased air speeds,

increased turbulence or modified spectral characteristics can be an important aspect of extending the bandwidth of conditions where passive ventilative cooling applications are suitable. The study investigated the characteristics of airflow at a typical occupant location during testing and compares measurements with and without the use of the slotted louvre at the opening.

3.3.3.1 Study Outline: Louvre vs Plain Opening

To achieve the research objectives outlined in chapter 1 regarding the effects of using a slotted louvre in single sided ventilation, the existing west facing, first floor, isolated single cell retrofit office space, described in section 3.1 generally, more specifically in 3.3.2.1 above and also shown in Figure 3.2, was utilised for experimental testing and data collection. In order to quantify performance the main parameters requiring measurement were identified as the ventilation airflow rate, represented as an ACR, wind speed and direction information for quantifying momentum forces and temperature differences across the opening to quantify buoyancy forces. To characterise air movement and the local thermal environment at the occupant location air speed information and air temperature data needed to be measured. The experimental setup for measuring all parameters is described in the following sections. A number of different opening test cases were defined to allow a comparison between the slotted louvre and plain opening. A single structural opening was used for all tests with overall dimensions, 0.76m x 0.30m, Figure 3.18 below (A single section of the openings shown in Figure 1.1(B)). The standard single opening louvre module used during testing is shown in Figure 3.19.



FIGURE 3.18: Plain Opening in retrofit space used for comparing with slotted louvre. The existing individual louvre sections normally screwed into the facade frame (see figure 3.9) were removed and replaced with a single mock up louvre shown in Figure 3.19

As mentioned above two opening types were tested, a slot louvre, denoted L , and a plain aperture, denoted P , with 5 cases in total, two for the slot louvre openings and three for the plain opening, each with varying overall dimensions. Table 3.8 presents information relating to each opening case for the purposes of comparison of opening geometry. POF represents the opening area to floor area ratio as a percentage. Figure 3.20 presents the two slot louvre cases and three plain opening cases tested. A blanking plate was inserted to facilitate the reduced opening dimensions

TABLE 3.8: Geometric dimensioning information for each of the opening cases measured in the field study. Aspect Ratio, AR, based on individual louvre slots for L cases with 17 slots in total within the louvre for airflow passage making up the available free opening area. subscript 's' denotes slot

Case	Tests	H_o	H_s	W_o	AR	A_o	POF
(-)	(-)	(m)	(m)	(m)	(H/W)	(m ²)	(%)
L1	11	0.76	0.021	0.30	0.07	0.107	1.10
L2	9	0.76	0.021	0.15	0.14	0.051	0.53
P1	8	0.76	-	0.30	2.53	0.228	2.34
P2	7	0.76	-	0.15	5.06	0.114	1.17
P3	9	0.38	-	0.30	1.27	0.114	1.17

for some of the cases. In total 44 independent ACR tests were completed from 27th August 2014 to the 20th September 2014 with varying amounts of tests completed each day (3 on average) and no testing on some days. Figure 3.21 presents CO₂ decay profiles for a typical ACR test, including external and internal adjacent CO₂ profiles. During each ACR test all parameters required to investigate ACR performance, changes in air flow through the opening and at the occupant location were monitored and recorded. In total over 80 hours of measurement data was collected. However not all 80 hours of data was used in the analysis, only those that align with the specific test durations used for calculation of ACR. The parameters measured are outlined in the respective sections below. Figure 3.22 provides information relating to instrument setup and positioning in the retrofit test space and Figures 3.23 - 3.26 show some of the installed instrumentation during testing including location of instruments, cylinder injection location, opening blanking plate and opening in-situ anemometers.



FIGURE 3.19: Left: Louvre module used for testing. Middle: louvre opening. Right: External facade of the testbed building showing the pre and post retrofit (see www.zero2020energy.com for more details). Integrated vertical slotted louvre banks also visible

3.3.3.2 ACR Measurement

Again, for this set of experimental tests, ACR during test periods were measured using the TGCD technique [153], outlined in Appendix A. In the study presented here tests were also completed in accordance with the procedures set out in ASTM E741-11 [156]. All CO₂ concentrations were measured using AlphaSense IRC-A1 Non Dispersive Infra-Red (NDIR) Sensors connected to a

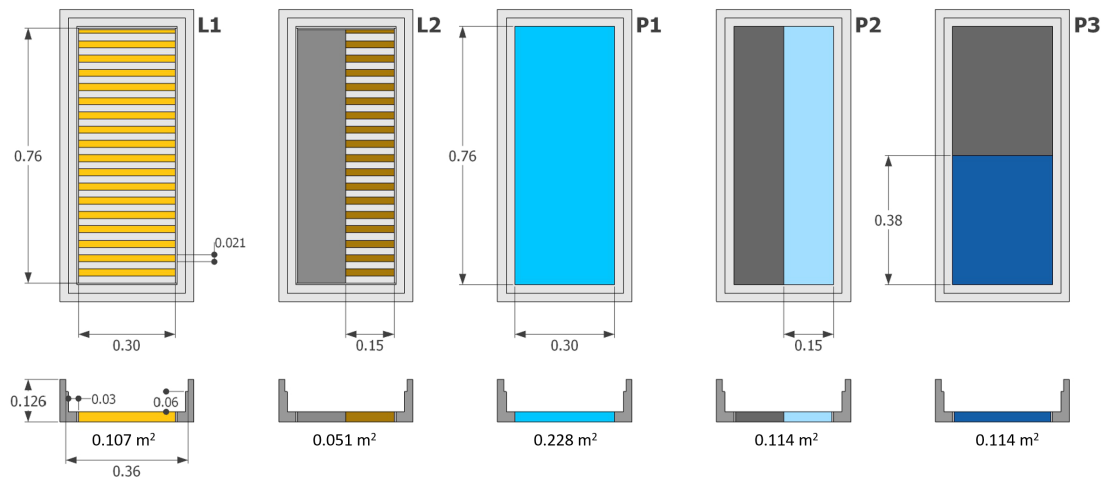


FIGURE 3.20: Plan and elevation drawings of various opening types measured including main dimensioning. Net free opening area for each case, A_o , shown coloured, with the m^2 value below each plan drawing. Slot louvre, L, with 2 cases, L1 & L2. Plain opening, P, with 3 cases, P1, P2 & P3. Blanking plates used to create reduced H_o , W_o dimensions shown in dark grey

National Instruments DAQ card and data logged using Labview software. One external ambient, one adjacent corridor (the door was closed during testing) and four in-situ, internal zone CO_2 concentration measurement locations were used for these tests with a spatially averaged zone concentration value calculated for estimating mean ACR. Cui et al [157] recently showed that using the TGCD method with 6 in situ zone sensors provides ACR measurements with an uncertainty of between 6.8 and 15.6% when compared to a reference measurement using duct mounted airflow measuring blades (cases 3,4 and 5 in Cui et al [157]). The procedure used for injecting and mixing CO_2 , starting and stopping the test was same as that described in section 3.3.2.2 above. Table 3.9 presents the mean, standard deviations and maximum values for the percentage difference between the measured concentration from a particular CO_2 sensor and the spatially averaged concentration for the zone at the beginning of each test, based on data from all 44 tests completed. The values shows good levels of mixing for all tests minimising measurement uncertainty due to imperfect mixing. Figure 3.21 presents decay profiles for a typical ACR test.

To further reduce measurement errors influencing ACR the optimum concentration decay period for each test, t_m , was obtained based on the lumped parameter term, Nt_m , suggested by Okuyama & Onishi [158] and described Appendix A, page 184. Here N is taken as the measured ACR value calculated from the concentration decay. For the number of measurement points, n , greater than 60, Nt_m tends monotonically to 1.25. An algorithm was developed using R-language to search iteratively and solve for Nt_m in each test. The corresponding time period satisfying this criteria was subsequently selected, taken to be the optimum decay period and used for the calculation of ACR. The resulting mean n was 165 points with only 3 tests having values below 60. Once the raw data had been collected the data was processed and analysed to obtain the ACR values. More information on these steps is available in section 3.4 and the Results chapter 5.

Again, when we consider the findings from the literature review on measurement uncertainty for

TABLE 3.9: Summary statistics for CO₂ uniformity of concentration across all 44 tests in accordance with ASTM E741-11. (% difference between individual location and spatially averaged concentration). Also shown for windward and leeward tests separately. See Figure 3.22 for sensor positioning

Parameter	NW	NE	SW	SE
Mean (All)	1.0%	1.7%	1.6%	1.1%
σ (All)	2.6%	2.3%	1.6%	2.4%
Max (All)	5.4%	8.6%	6.9%	5.7%
Mean (Windward)	0.3%	1.0%	1.2%	0.5%
σ (Windward)	2.3%	1.8%	1.9%	1.8%
Mean (Leeward)	1.5%	1.9%	1.7%	1.6%
σ (Leeward)	2.6%	2.3%	1.6%	2.5%

the TGCD technique in Appendix A section A.4.2, the measurement accuracy of the in-situ CO₂ sensors and the very good levels of mixing demonstrated in Table 3.9 we can reasonably estimate that the average measurement error is less than 10%. As mentioned, we discuss uncertainty due to an unsteady ACR during tests in Appendix A and present results for ACR measurements in chapter 4 and chapter 5.

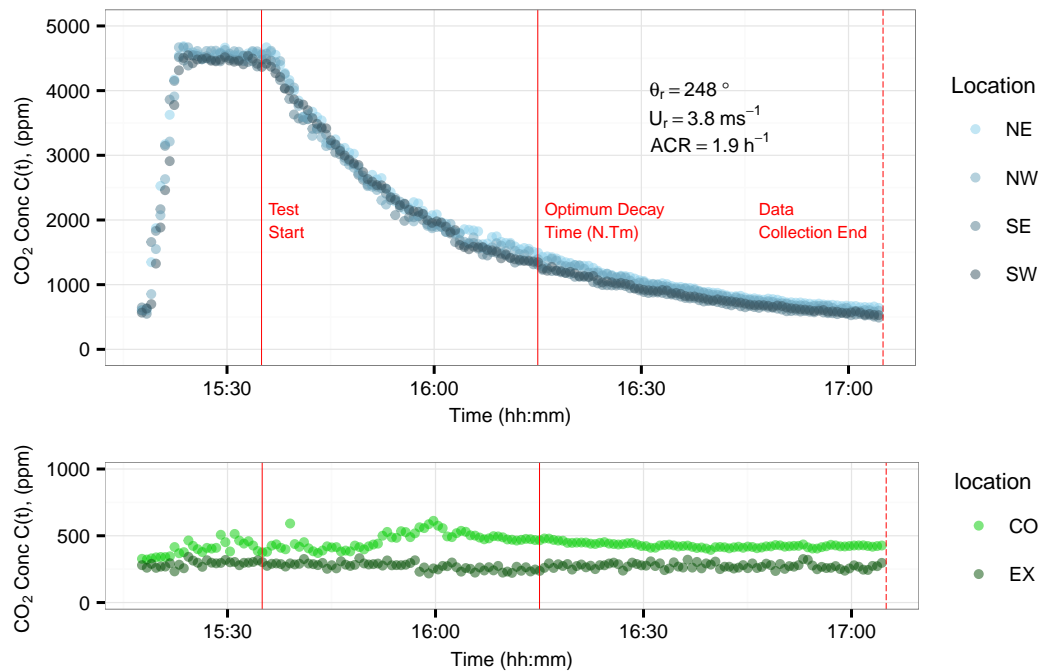


FIGURE 3.21: Typical CO₂ decay profiles (Test 35, 11th Sept 2014, case P2). Test start time, Optimum decay Time and data collection end time shown as vertical red lines. CO is adjacent corridor CO₂ sensor and EX is external CO₂ sensor. Figure 3.22 shows sensor locations

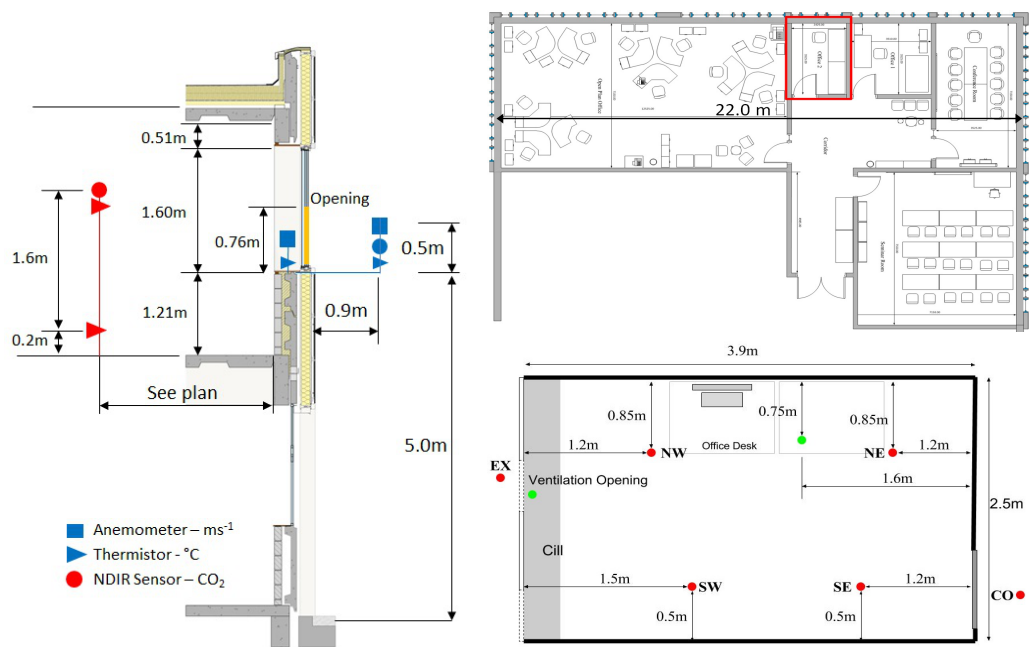


FIGURE 3.22: Experiment setup details. Left: Building section showing heights and depths of instrument positions. Right top: Overall testbed first floor plan with test room marked in red. Right bottom: Dimensions of CO_2 and Temperature measuring locations

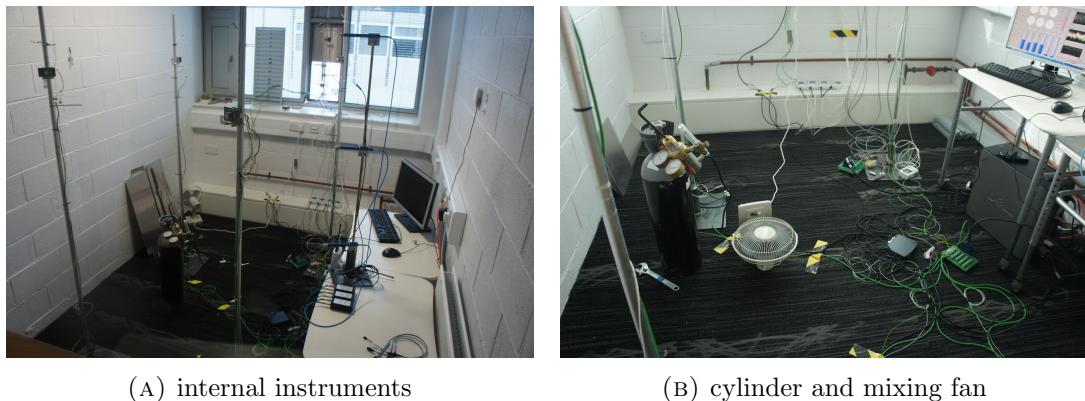


FIGURE 3.23: experimental room setup showing internal instrument layout and cylinder injection location with mixing fan used for CO_2 dispersion

3.3.3.3 Boundary Conditions and Opening Measurements

Boundary conditions during testing were measured at two locations. The first location, the weather station at roof level, recorded reference building conditions. Any reference boundary conditions required for the analysis of results were obtained using instrumentation listed in Table 3.7 above, mainly external ambient temperature, reference wind speed and direction. The Campbell Scientific 05103 wind vane anemometer sampling every 5 minutes was used to calculate the reference wind speed, U_r , for each ACR test. Wind data was also collected from the nearby local met station, Cork Airport. This data was used for comparative purposes in the analysis of results. At 1.0m from the building envelope directly outside the ventilation opening a RM Young 81000 3D ultrasonic anemometer was installed and operated in 3-Dimensional wind

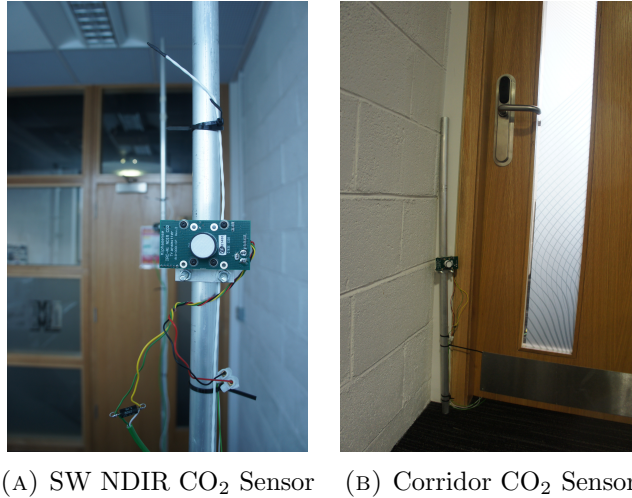


FIGURE 3.24: Alphasense CO₂ NDIR sensors used for measurement of concentration levels during TGCD ACR testing.

speed vector uvw mode, giving vector values for each xyz component of the wind, to allow for calculation of turbulence characteristics and local wind speed, U_l sufficiently near to the opening to adequately represent local boundary conditions, with a sampling rate of $10Hz$. Equation 3.2 is used to calculate the mean resultant vector, \bar{r} , in the 2D dimensional plane from the measured u, v components (the z -component is excluded as the velocity of the turbulent jet spreads linearly as a strongly dominant 2-Dimensional flow when the flow direction is shown to be parallel to the facade):

$$\bar{r} = \frac{1}{n} \sum_{i=0}^n r_i \quad (3.2)$$

where the individual unit vectors, r_i can be defined as equation 3.3 with $\cos \phi_i$ taken as measured u and $\sin \phi_i$ taken as measured v . The mean local orthogonal wind direction $\bar{\phi}$, is then calculated using the arctangent, from equation 3.4, and converted from radians to degrees.

$$r_i = \begin{pmatrix} \cos \phi_i \\ \sin \phi_i \end{pmatrix} \quad (3.3)$$

$$\bar{\phi} = \frac{\pi}{2} - \tan^{-1}(\bar{r}) \times \frac{180}{\pi} \quad (3.4)$$

To correct for the $atan2$ function used for the arctangent we transform as follows:

$$\bar{\phi} = \begin{cases} \bar{\phi} + 360 & \text{if } \bar{\phi} < 0, \\ \bar{\phi} & \text{Otherwise} \end{cases} \quad (3.5)$$

This data, together with U_r is used to investigate the ratio U_l/U_r , a ratio used by various researchers in single sided correlations.

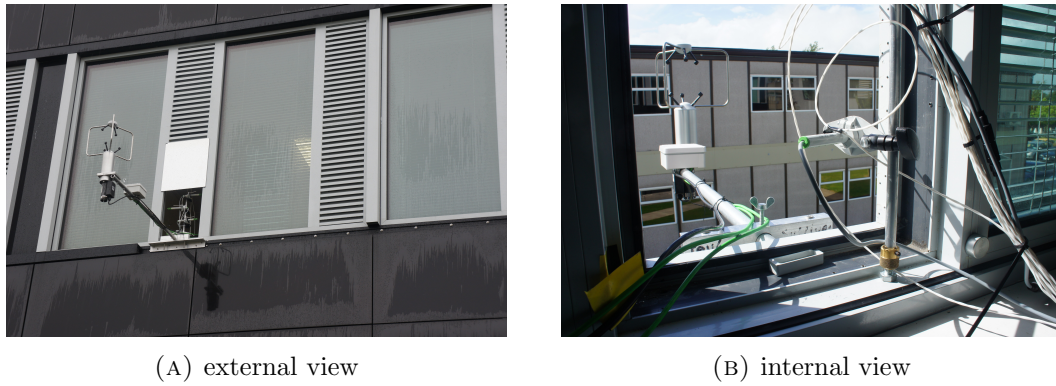


FIGURE 3.25: 3D Ultrasonic anemometer measuring boundary conditions.

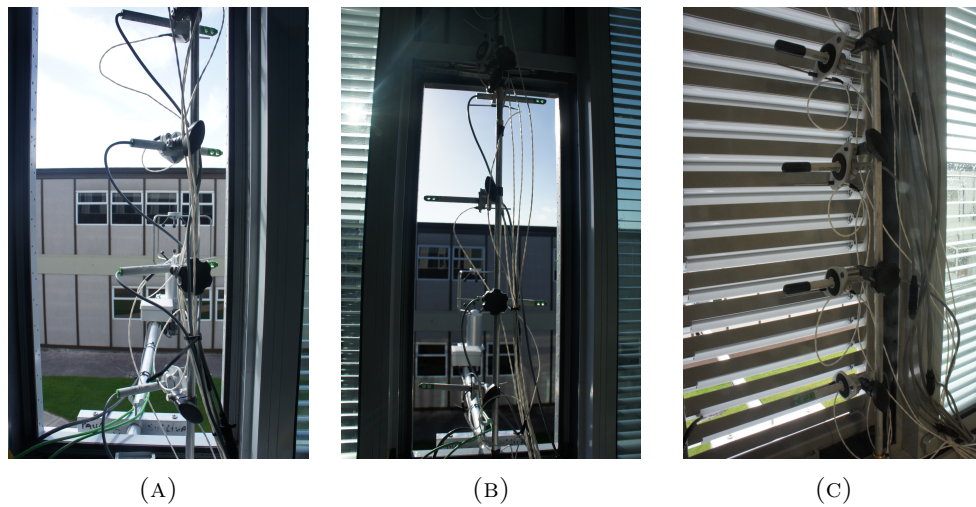


FIGURE 3.26: Opening Anemometers shown for a Plain opening test in differing positions for differing wind directions. Slot Louvre configuration also shown

During each ACR test air speed in the ventilation opening was measured in 4 locations using E+E Elektronik EE576 miniature thin film anemometers ($\pm 0.08 \text{ m s}^{-1} + 4\%$ measuring velocity) at a sampling rate of 1 Hz . Measuring locations varied horizontally and vertically to accommodate different opening heights and widths according to the test case but remained consistent for each test case subset and wind direction. Anemometer positions remained consistent for different test cases having the same dimensions (i.e. see for example *L1* and *P1* Figure 3.20). Air temperature at the opening was also measured at 4 locations similar to the air velocity measurement locations using Hanwell Radio-logger RL4000 wireless data loggers with precision thermistors ($\pm 0.1 \text{ }^\circ\text{C}$ between $-25 \text{ }^\circ\text{C}$ to $50 \text{ }^\circ\text{C}$) at a sampling rate of 1 minute. Air temperature was measured in 8 locations within the zone using the same precision thermistors. Table 3.10 below provides summary statistics for wind and temperature conditions categorised according to opening case.

The information obtained from the ACR measurements and the boundary condition data was used to test the predictive power of existing semi-empirical single sided ventilation rate correlations. A multiple linear regression (MLR) model was also used to complete a sensitivity study of influential boundary conditions when directly predicting ventilation rates. Results and analysis are included in chapter 5.

TABLE 3.10: Summary of external weather conditions during testing categorised according to each opening case. Conditions during testing for each case were comparatively equal for all boundary conditions.

Case	Tests	\bar{U}_r	σ_{U_r}	$\bar{\phi}_r$	\bar{T}_e	σ_{T_e}	$\Delta\bar{T}_{i-e}$
(-)	(-)	(ms^{-1})	(ms^{-1})	($^{\circ}$)	($^{\circ}C$)	($^{\circ}C$)	($^{\circ}C$)
L1	11	3.7	1.9	178	17.2	0.9	5.6
L2	9	3.1	1.7	179	17.3	1.5	5.9
P1	8	3.3	2.1	194	16.9	2.0	5.9
P2	7	2.7	0.8	137	18.0	1.8	5.4
P3	9	2.8	1.1	130	18.0	1.5	5.8

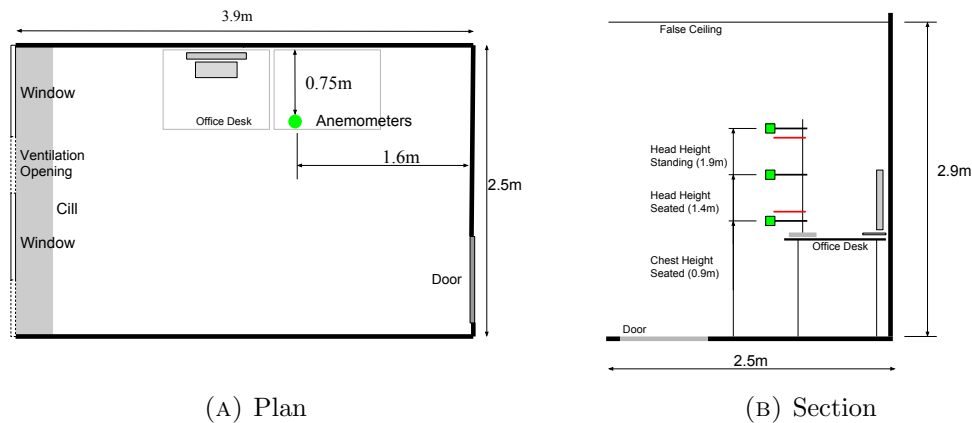


FIGURE 3.27: Experimental setup details for occupant location measurements. Temperature and RH measurement locations shown as red in section. Anemometers shown in green.

3.3.3.4 Internal Occupant Location Measurements

As well as investigating the air exchange mechanisms at the opening during testing in summer 2014, local air speed, temperature and relative humidity was recorded at the occupant location. The purpose of this was to identify whether the slotted louvre arrangement might have a direct effect on the air movement experienced by an occupant. In other words, is there an appreciable change in air movement or conditions experienced by an occupant a depth of approximately 2.0m from the opening. During each ACR test environmental parameters were measured at an occupant location, shown in figure 3.27.

To measure air speed three Schiltknecht Thermo Air 64 omni directional hot wire anemometers (range; $0 - 5ms^{-1}$, accuracy; $\pm 1.5\%$ of reading + 0.5% of full scale) with a measuring frequency of 10Hz were used at heights 0.9m, 1.4m and 1.9m. These heights were at seated chest height, seated head height and head height standing. Air temperature was measured in 2 locations within the zone using Hanwell Radio-logger RL4000 wireless data loggers with precision thermistors ($\pm 0.1^{\circ}C$ between $-25^{\circ}C$ to $50^{\circ}C$) at a sampling rate of 10 minutes. Relative humidity was measured in 2 locations with Hanwell Radio-logger RL4000 wireless data loggers and capacitive polymers ($\pm 2.0\%$ between $0\%RH$ and $90\%RH$ and $\pm 3.0\%$ otherwise). The raw data was used for analysis of the air speed, turbulence characteristic and spectral frequency in investigating

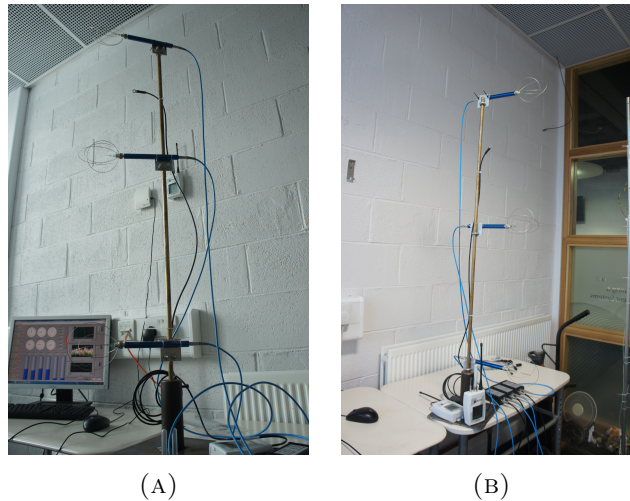


FIGURE 3.28: Schiltknecht Omni Directional Anemometers used to capture high speed air velocity data at a typical occupant location within the single zone office.

whether the opening modifies the nature of the internal air. Results and analysis are presented in Chapter 5.

3.4 Processing of raw experimental data

Data is rarely recorded in a neat, convenient way ready for use in analysis by data logging equipment. Often there are multiple data recorders, all sampling at different intervals with marginally different time stamps. This generally results in multiple unstructured data files in a raw state that need to be 'wrangled' into a format that is suitable for completing the analysis of the data. The analysis may involve plotting multiple variables together, calculating new parameters using the recorded data and combining different facets of each set for various intermediate steps. All the data sets that were collected as part of experimental measurements are times series.

The following sections is intended to give an overview of some of the work done preparing data for analysis. Its merit for inclusion lies in the fact this step can take up most of the time required in doing experimental research, and when combined with the experimental setup, it represents arguably over 80% of the research work.

3.4.1 General Data Storage structure

Figure 3.29 Presents the data management framework for filing and accessing data at different stages of processing. The raw data stage is post testing when files are still unprocessed. The formatted output is the final publication quality plots and results contain within the thesis. The typical file structure used for each experimental field study is shown also. R-programming language was used for the field studies in 2014 while excel was primarily used for much of the initial data processing in 2013. For each ACR measuring campaign a test-log spreadsheet in

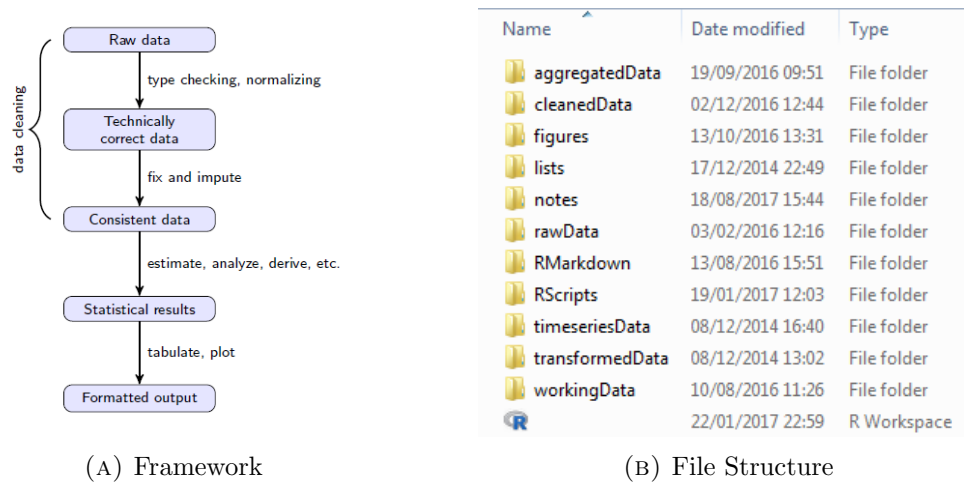


FIGURE 3.29: The framework concept which was broadly followed for filing, accessing and processing data. The folder structure for each experimental field study is also shown

excel was maintained to log all key information about each test. The test-log included manually logged info such as location, pre-start time, injection start time, start time, end time, adjusted end time, duration, injection end time, injection rate, notes, etc. Notes and information about any point of interest during a test was logged here for follow post testing.

3.4.2 2013 testing

In 2013 the Full scale OH performance study and the comparison of pre and post retrofit ACR measurements were completed. All the data processing here was done using Microsoft Excel with VBA Macros.

Weather data was continuously logged 24 hours a day as this was not operated solely for the ACR testing periods. Both 5 minute sampling and 1 hour sampling was stored in the same file with every twelfth row providing the 1 hour average value. The time stamp was split across multiple columns, used integers for year, day, hour, minute etc in an unprocessed format which was not a standard timestamp. A VBA code was written to process this data into separate 1 hour and 5 minutes weather files and produce a formatted timestamp that could be used with the test-log to extract specific periods that coincided with the ACR testing. A separate VBA code was prepared to search and extract all 38 test periods and format these into separate files. Data within these could then be called using code loops along with data logged on different systems. The wind data from the roof station had to be adjusted by an offset of 180° due to the configuration of the installation.

The CO_2 data was logged to 38 separate csv files from the alphasense software. These files then had to be processed to find and extract the test start and end data that would be specifically used to calculate ACR values. A VBA code loop was written for this purpose. These had a sampling rate of 1 Hz which was subsequently averaged to 0.1 Hz. All files were combined into a global excel file. the LINEST function in excel was used to calculate ACR value using the

regression method. As each test had a different duration they had to be treated separately which was time consuming and had to be completed methodically to avoid errors.

All temperature and internal environmental parameters were logged using the hanwell radiolog environmental monitoring system. Again these needed to be processed in a similar way to the CO₂ data sets.

All the finalised, averaged data for each test including ACR values, boundary conditions and so on was then combined into a single excel file for calculation of all analysis parameters and to facilitate plotting and comparative studies.

3.4.3 2014 testing

For the 2014 testing R-Language was adopted for all processing and analysis work. This gave greater power and flexibility to the analysis. It also reduced the amount of manual processing work and facilitated the development of reproducible research codes for each processing task.

The third field study, airflow effects of the slot louvre, was undertaken in 2014. In terms of data topology this involved 44 individual tests covering 5 different geometry configurations with 37 different parameters recorded at various sampling rates during each test. These were output in 3 main raw data files as follows:

- NI Labview DAQ (17 parameters at 10Hz sampling in .csv format)
- Roof weather station (4 parameters at 5 min sampling in .dat format)
- Hanwell Radiolog (16 parameters at 1 min or 10 min sampling in .csv format)

Figure 3.30 shows the parameter x configuration matrix. This shows the possible different dataset types. There were more than one of each of these depending on the number of tests for the particular configuration.

	UVW	T.Occ	WStn	T.Rm	CO2	V.Ope	T.Ope	V.Rm
	UVW.L1	T.Occ.L1	WStn .L1	T.Rm .L1	CO2.L1	V.Ope .L1	T.Ope.L1	Par.L1
	UVW.L2	V.Rm.Cfg

	V.Rm.O2
	UVW.Cfg	Par.O3	Par.O3	Par.O3	Par.O3	Par.O3	Par.O3	Par.Cfg

FIGURE 3.30: Matrix showing the different sub sets of data depending on parameter and testing configuration

It was initially planned to group the 37 parameters into eight main phenomena largely based on their sampling rates and parameter type. This would have resulted in 352 files requiring processing for analysis. However, all temperature data logged in the Hanwell file was kept in a single file that included all 44 tests. The weather station data was also initially kept in a single file with 44 tests. These two file types were then processed with individual test data extracted using R loops by matching timestamps from the test-log. This reduced the restructured file types to 4 for each test; a UVW local wind data file, a ventilation opening anemometer file, a room omni-directional anemometer file and a CO₂ concentration file. This resulted in 176 files in total that needed to be imported to the R project environment and subsequently used for processing. There was different categorical ways how data might need to be grouped and called within loops and processing codes. For example, all cleaned L1 configuration data may need to be imported or all L1 cleaned CO₂ data only would be needed. Structured filenames were developed to deal with this making it possible to call certain files from a project folder using the file string.

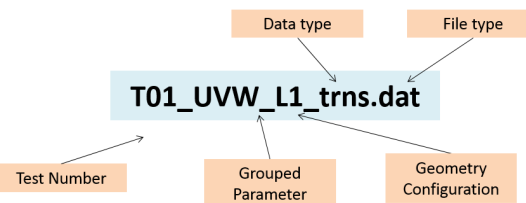


FIGURE 3.31: Structured filenames used for all .csv data to allow an efficient callign system within the analysis environment

```

1 # Test log, filepath directories and filename vectors for different subfolder
2 # note tests_2014 must be set as working directory
3 path_let = "./lists/"
4 path_raw = "./rawData/"
5 path_wkg = "./workingData/"
6 path_cln = "./cleanedData/"
7 path_agp = "./aggregateData/"
8 path_ts = "./timeseriesData/"
9 out.file=""
10 #subset rawData data based on injstart and finish times from the test log. loop through all tests and save
11 #the workingData directory must be empty before this code is run
12 setwd(path_2014)
13 filenames_raw <- dir(path_raw, pattern = ".csv")
14 for(i in 1:length(filenames_raw)){
15   x<-read.csv(paste(path_raw, filenames_raw[i], sep=""), stringsAsFactors = F, header=T)
16   x$time<-paste(x$Date,x$Time, sep=" ")
17   x$time<-as.POSIXct(x$time,format=" %d/%m/%Y %H:%M:%S", origin="1970-01-01 00:00:00", tz="GMT")
18   y<-subset(x, time >= testlog[1,5] & time <= testlog[1,8])
19   padded<-pad_int(2,10)
20   myfile<-file.path(path_wkg, paste("T",padded, "_wkg", ".csv", sep=""))
21   write.table(y, file=myfile, sep=" ",row.names=FALSE, append=FALSE)
22 }
23 filenames_wkg <- dir(path_wkg, pattern = ".csv")
24 for(i in 1:length(filenames_wkg)){
25   x<-read.table(paste(path_wkg, filenames_wkg[i], sep=""), stringsAsFactors = F, header=T, sep=",")
26   b<-x[,c(21,3:5)] #Omni
27   c<-x[,c(21,6:11)] #CO2
28   d<-x[,c(21,12:14)] #UVW
29   e<-x[,c(21,16:19)] #V.Opens
30   padded<-pad_int(2,10)
31   myfile_b<-file.path(path_cln, paste("T",padded, "Omni ", testlog[i,2]," cln", ".csv", sep=""))
32   write.table(b, file=myfile_b, sep=" ",row.names=FALSE, append=FALSE)
33   myfile_c<-file.path(path_cln, paste("T",padded, " CO2 ", testlog[i,2]," cln", ".csv", sep=""))
34   write.table(c, file=myfile_c, sep=" ",row.names=FALSE, append=FALSE)
35   myfile_d<-file.path(path_cln, paste("T",padded, " UVW ", testlog[i,2]," cln", ".csv", sep=""))
36   write.table(d, file=myfile_d, sep=" ",row.names=FALSE, append=FALSE)
37   myfile_e<-file.path(path_cln, paste("T",padded, " Vops ", testlog[i,2]," cln", ".csv", sep=""))
38   write.table(e, file=myfile_e, sep=" ",row.names=FALSE, append=FALSE)
39 }
40 # steps of main code
41 # 1 - read in the testlog file to obtain test times for each test
42 # 2 - convert from factor to character for the data frame (.csv)
43 # 3 - set the path for the rawData directory and create the filenames vector
44 # 4 - create the function mycsvfactor
45 # 5 - loop through each file and extract data based on time from log file, create a new file and save into
46 # 6 - end
47
48
49
50
51
52
53
54
55
56
57
58
59
60
61
62
63
64
65
66
67
68
69
70
71
72
73
74
75
76
77
78
79
80
81
82
83
84
85
86
87
88
89
90
91
92
93
94
95
96
97
98
99
401 | (Top Level) | R Script 1
  
```

FIGURE 3.32: R code used to process raw data files into working data files and eventually cleaned data for use in analysis

A sample of the R script written to process raw data is outlined below. The script takes raw files, imports them to R, separates data according to the grouping discussed above, corrects anomalies with timestamps, assigns them as cleaned data and then saves them into the cleanedData folder.

Once data had been successfully added to the cleanedData folder it could then be re-imported as part of any analysis and used.

```

1  ### BASE ANALYSIS OF CO2 DATA (each calculations using regression method)
2  ##setup
3  library(circular);library(aster); library(chron);library(xts);library(ggplot2)
4  library(fpp)
5  options(digits.secs=6)
6  options(digits=2)
7  setwd(path_2014)
8  co2filenames<-dir(path_cln, pattern="CO2")
9  ## import datasets
10 for(i in 1:length(co2filenames)){
11   padded<-pad_int(i,10)
12   name<-as.character(paste("Co2", padded, sep=""))
13   co2<-read.table(paste(path_cln, co2filenames[i], sep=""), stringsAsFactors=FALSE, header=T, sep=",")
14   co2$time<-as.POSIXct(co2$time, format = "%Y-%m-%d %H:%M:%S", origin="1970-01-01", tz="GMT")
15   co2$time<-make.time.unique(co2$time, eps=1e-1, drop=FALSE)
16   #co2<-co2[,3]
17   assign(name, co2)
18 }
19 ## create a list and put all dataframes into same for looping using apply family
20 co2list <- lapply(paste("Co2", sprintf("%02d",seq(1:44)), sep=""), get)
21 rm(list=ls(pattern="Co2"))
22
23 modae<-lapply(1:44, function(i) co2list[[i]][,3]+232)
24 for ( i in 1:length(co2list)) {
25   co2list[[i]][,3] <- modae[i]
26 }
27
28 ### loop through all tests and calculate natural log of normalised conc for each test location
29 for(i in 1:44){
30   name<-paste("lnCo2", sprintf("%02d",i), sep="")
31   cn<-sapply(2:5, function(n) lncn(co2list[[i]][,n],co2list[[i]][,7]))
32   cndf <- data.frame(time=(co2list[[i]][,1]),
33                     ne=as.numeric(cn[,1]),
34                     se=as.numeric(cn[,2]),
35                     nw=as.numeric(cn[,3]),
36                     sw=as.numeric(cn[,4]),
37                     stringsAsFactors=FALSE)
38   assign(name, cndf)
39 }
40 ## compile a list of data frames of lncn values from loop above
41 lnco2list <- lapply(paste("lnCo2", sprintf("%02d",seq(1:44)), sep=""), get)
42 rm(list=ls(pattern="lnCo2"))
43
44 ## calculate the linear regression for each vector in each data frame in the list above
45 for(i in 1:44){
46   name<-paste("achCo2", sprintf("%02d",i), sep="")
47   #lnc<-sapply(2:5, function(n) lm(lnco2list[[i]][,n]~lnco2list[[i]][,1]))
48 }

```

FIGURE 3.33: R code used to import cleaned data, assign to a dataframe, add to a list and begin applying analysis functions

Managing data during analysis meant being able to access all 44 data sets for various parameters simultaneously. To do this use was made of the dataframe and list data types in R. An R dataframe is an $n \times m$ matrix that can contain strings as well as numbers. Files were individually re imported and allocated as dataframes meaning they were be permanently available within the project environment without the need to work with external files, making code more efficient. R is a vectorised environment and many of the looping and data mining techniques rely on a vector referencing approach. An R-list is a vector containing multiple $n \times m$ dataframes allowing a single piece of code to loop through all dataframes and access specific locations and apply functions, actions etc. A sample of the R script written to import and assign data frames to R-lists is shown below.

Different processing scripts were written for the Hanwell Radiolog file and Weather station file given their unique structures. These had individual issues around subsetting and timestamps.

In general there is a lot of work required in processing data, preparing it for analysis, undertaking the analysis and formatting results outputs for publication. While there are more systems and equipment now available to completed data logging and monitoring of systems working with multiple systems in an experimental study requires a large amount of processing and post processing.

In total about 3000 lines of R code was written and over 30 different R packages used (each containing various functions and capabilities)to complete all processing, analysis and plotting for the 2014 study. In reality this could have been closer to 1500 lines of code when redundant

script and the in-efficient style having not used the language/software previously is factored in. Nonetheless this is an important part of the execution of the research work and should not be underestimated when deciding on the amount of work and duration of a research study.

Chapter 4

Pre and Post Retrofit Ventilation Performance

In this chapter results and analysis are presented from two field studies completed during 2013; Full scale overheating performance and Full scale ACR performance. A retrofit space in the experimental building and a control space in the existing building have been identified and utilised for comparative purposes. Details of both spaces are summarised in chapter 3.

Section 4.1 presents results from the overheating performance monitoring during May to September 2013. Section 4.2 presents results from the field study investigating full scale ACR performance of the MCSL. This includes information about the test boundary conditions during macroscopic ACR testing and measurement of environmental parameters. Section 4.2.2 presents results from measuring internal environmental parameters in retrofit and control spaces. Section 4.2.3 presents results from ACR measurements in both spaces. Results are categorised according to the four configurations detailed in Table 3.5. Subsequently, in section 4.2.4 an analysis of the mechanisms contributing to time averaged macroscopic ACR from test results is completed using Dimensional Analysis. It considers two key aspects of the macroscopic ACR; the combined effect of momentum and buoyancy forces on mean ventilation rates and analysis of the nature of the ventilation rate during tracer decay tests using a fluctuation parameter, σ_c . The objective is to investigate the conditions contributing to macroscopic ACR for a slot louvre system used in single sided ventilation. A comparison with the pre retrofit environment and window opening is included throughout.

4.1 Full Scale Performance: Long term overheating

Table 4.1 presents climate data for summer 2013 at the site location. It includes measured data using the zero2020 weather station as well as data from the TMY3 weather file for Cork Airport met station. Figure 4.1 presents indoor air temperature data for the cooling period May 1st to September 30th for an open plan office, B294, in zero2020. External ambient temperature

TABLE 4.1: Climate data for summer period May to September 2013

Month	Cork Airport TMY3 95th Percentile				Summer 2013 95th Percentile			
	Gh (Wh/m^2)	Ta ($^{\circ}C$)	WS (m/s)	WD ($^{\circ}$)	Gh (Wh/m^2)	Ta ($^{\circ}C$)	WS (m/s)	WD ($^{\circ}$)
May	742	17.2	10.0	345	730	16.0	6.3	304
June	815	19.5	9.3	344	826	20.6	5.0	343
July	707	20.7	9.0	352	795	25.0	4.3	344
August	662	20.0	9.3	342	592	20.1	4.7	306
September	574	19.4	9.0	341	511	18.5	4.6	326
October	385	17.3	10.3	338	340	18.1	4.4	336

is also shown. There appears to be a reasonably good relationship between external ambient temperature and indoor air temperature. There was a period of extended warm weather during the month of July resulting in increased indoor temperatures. It is evident from the heatmap that much of the elevated indoor air temperatures are occurring outside of the occupied period, this suggesting some ability of the building structure to shift the effects of incident heat gain to later in the day. Further, by 02:00am temperatures greater than $28^{\circ}C$ have been removed although by 09:00am the following day temperatures are still somewhat higher than the mean daily external ambient temperature. Night cooling was in place during the month of July, the strategy resulted in all manual openings (RS.02) remaining open throughout July and the high level automated openings (RS.03) were also fully open for almost 100% of the time.

4.1.1 Percentage Hours above static threshold

To isolate specifically the percentage of hours above certain reference temperatures Figure 4.2 presents periods of time when the internal space experienced air temperatures above two of CIBSE recently recommended reference temperatures, $25^{\circ}C$ and $28^{\circ}C$. There were a number of days during July 2013 when temperatures didn't fall below $25^{\circ}C$. Temperatures greater than $25^{\circ}C$ were almost never experienced on arrival at the beginning of the day by occupants with values typically between $20^{\circ}C$ and $24^{\circ}C$. There is evident of a measurable amount of heat dissipation during the diurnal cycles. Much of this can be attributed to the effect of ventilation given the extremely high performance thermal barrier resulting from the retrofitted envelope. In specific terms Figure 4.2 shows that 5.5% of the occupied hours between May and September were above $25^{\circ}C$ and 0.75% were above $28^{\circ}C$. Given the targets are normally based on total annual occupied hours these values are well within CIBSE recommendations.

4.1.2 Assessment using CIBSE adaptive Criteria

As suggested earlier a single value reference temperature oversimplifies the process of assessment of thermal comfort and an overheating index based on this alone will not adequately capture how occupants might respond in a free running building. For this reason CIBSE three criteria have also been calculated. Figure 4.3 presents indoor air temperature as a function of the exponentially weighted outdoor running mean temperature and also includes the variable upper



FIGURE 4.1: Heat-map of indoor air temperature in open plan office B294 (taken as operative temperature as discussed earlier)

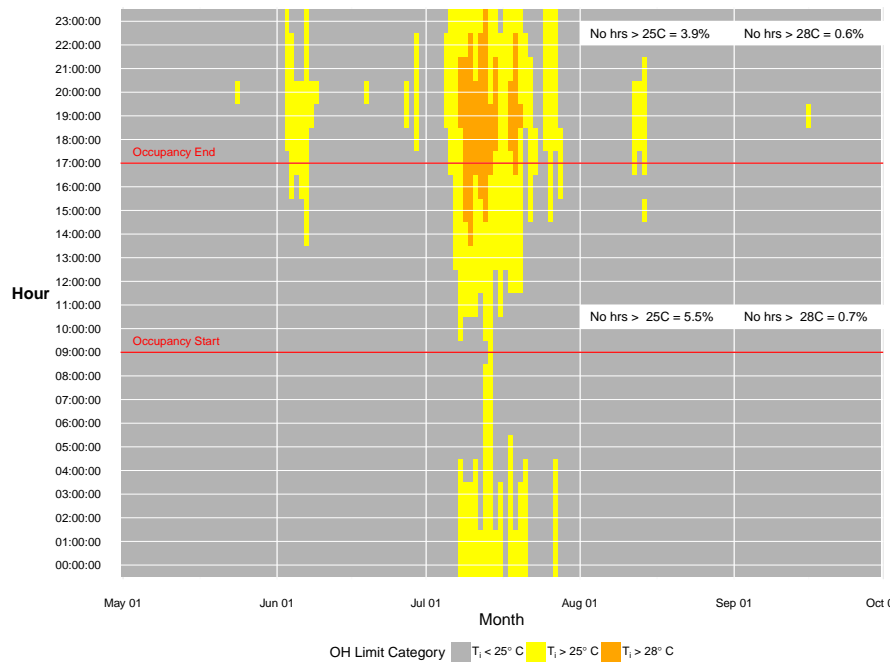


FIGURE 4.2: Exceedance of overheating limits in open plan office B294 (taken as operative temperature as discussed earlier.)

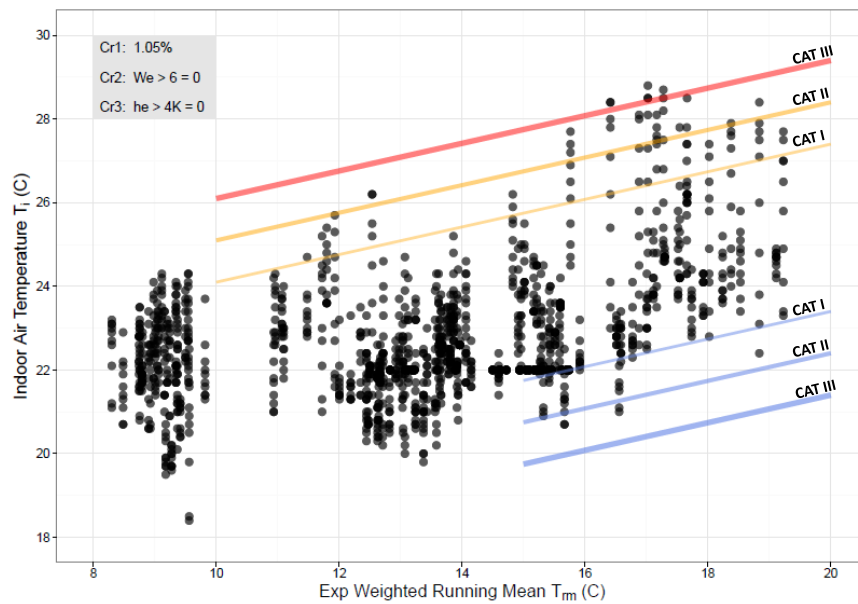


FIGURE 4.3: Indoor Air Temperature as function of exponentially weighted running mean for B294)

and lower temperature limits for three thermal comfort categories as defined in Table 1 of IS EN 15251:2007 [20]. These categories define different levels of expectation regarding the thermal environment with CAT I having the highest level of expectation and therefore the narrowest allowable temperature range for indoor operative temperature. Existing buildings should use comfort category CAT III. Figure 4.3 exposes a number of instances outside the outermost limits ($T_z - T_{cu} > 3K$) for temperatures in excess of the comfort temperature, here taken as equation 2.3, page 23. However, the upper limit "reference temperature" is now variable and a function of the outdoor running mean. This takes proper account of the thermal history of occupants allowing higher (or lower) values for the reference temperature accordingly. In summarising the results for each criteria:

- Criteria 1, (CR1): There are only 1.06% occupied hours that exceed the upper threshold limit by 1K or more. In fact there were no instances of exceedence above 1K. This is comfortably within the 3% allowance for criteria 1
- Criteria 2, (CR2): Owing to there being no temperatures greater than 1K above the upper threshold comfort limit the weighted exceedence was calculated based on the number of 1K instances in each day. With no day having more than a W_e of 4 the space complied with this criteria.
- Criteria 3, (CR3): There were no occurrences of ΔT above 1K.

Using the CIBSE approach in TM52 the open plan office space is shown to meet the requirements for limiting overheating. Additionally a number of other internal spaces within the zero2020 were investigated according to the CIBSE criteria. These are highlighted in Table 4.2 below. B291 is the experimental test space for the field studies presented in subsequent chapters.

TABLE 4.2: Summary of CIBSE overheating criteria for all internal spaces in zero2020

Room	Name	CR1	CR2	CR3	h^*
B287	CAMMS Seminar Room	0	0	0	0.0000
B289	Conference Room	0.6	0	0	0.0050
B290	CAMMS Secretary Office	0.2	1	2	0.0020
B291	CAMMS Managers Office	0	0	0	0.0006
B294	MeSSO Open Plan Office	1.05	0	0	0.9800

4.1.3 Discussion

This section presented the long term indoor thermal environmental performance at zero2020 for summer 2013. Overall the system was shown to maintain an acceptable indoor thermal environment when evaluated using long term indices based on the adaptive approach to thermal comfort. However, given the usage profile of the space is for academic staff and occupancy density is quite low during summer months there is a risk of increased overheating if the space were to be used as a full occupancy office year round. Night cooling was also in place and this clearly assisted with heat removal during non occupied hours. The ventilation openings remained open throughout the day and closing this for periods of high ambient temperatures during the occupancy hours may have further contributed to lower indoor temperatures. It is intended that this and other long term monitoring results will influence future decision making in relation to the extension of the solution to other parts of the existing 29,000m² building.

4.2 Full Scale Performance: ACR

4.2.1 Wind Boundary Conditions

Figure 4.4 presents polar frequency plots of wind speeds distributed according to wind direction for each test configuration summarised in Table 3.5. An analysis of wind data for each test using directional statistics [159] shows that the mean resultant length of direction vectors, a measure of concentration for circular data such as wind direction, were in many instances close to 1.0 with low dispersion of wind orientation during individual tests. This suggests that wind direction was consistent during a given test and the resulting analysis can assume to represent the effects from flow phenomena present for this type of orientation relative to the ventilation opening. There was a good mix of wind directions overall. The ventilation opening faces west, 270°. We have taken parallel flow to occur between wind directions of 347.5° – 22.5° & 157.5° – 202.5°. 270° wind direction is normal to the ventilation opening.

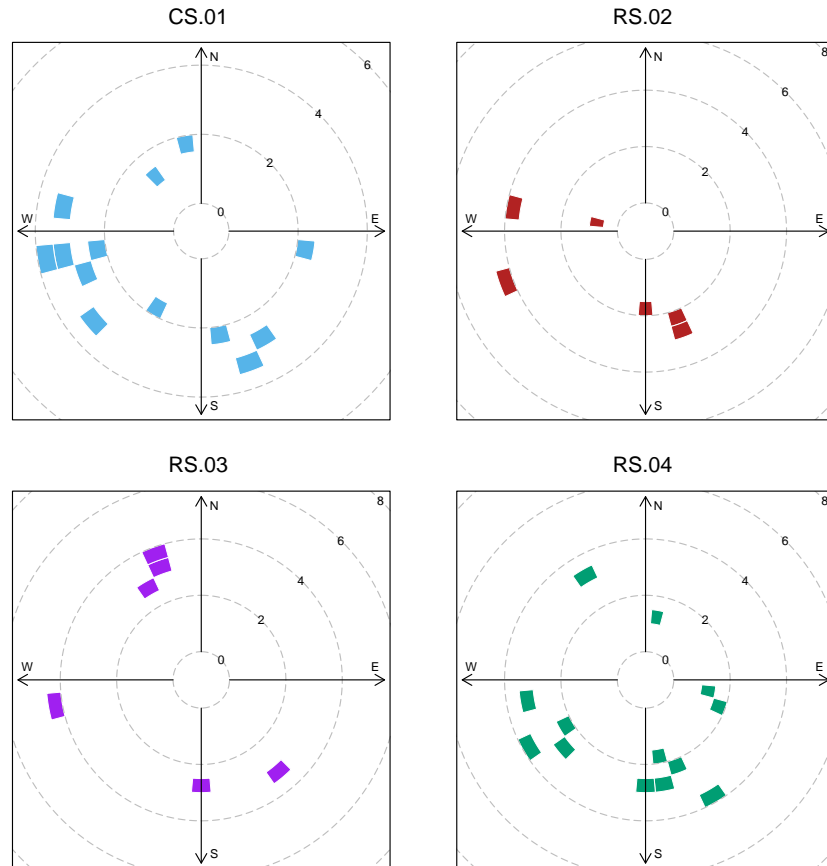


FIGURE 4.4: Polar frequency plots of mean wind speed and direction for all 38 tests categorised according to configuration. Wind speed is plotted on the polar axis. For each data point shown, data is averaged over the test period using 5 minute recordings of wind speed and wind direction.

4.2.2 Internal Environment Measurements

4.2.2.1 Zonal Vertical Temperature Distribution

The use of an empirically derived dimensionless parameter, Stratification Factor (STR), to characterise the relative strength of zone vertical temperature distribution compared to zone envelope temperature difference is used for analysis purposes [112]:

$$\frac{\Delta T_s}{\Delta T_{ie}} = \frac{T_H - T_0}{T_{H/2} - T_E} \quad (4.1)$$

This STR is used in the presentation and analysis of results as it is a good indicator of whether or not the vertical temperature distribution is having an appreciable effect on ventilation performance and also whether or not it is contributing to sub zone airflow phenomena that might be important when assessing cooling potential of a given ventilation system in cooling mode.

Comparison of a number of vertical temperature distribution profiles, measured at the end of different ACR test periods, are presented for tests recording high ACR values (top row Figure 4.5)

and with high STR values (bottom row Figure 4.5). All data was obtained during a particularly warm period with external temperatures reaching 10 year highs. Table 4.3 summarises STR, σ_c and ACR values for a number of selected tests highlighting the spread of STR values across the different configurations. CS.01 has an average STR of 0.69, RS.02 an average STR of 0.52, RS.03 an average STR 0.50 and RS.04 has an average STR of 0.88. Even though the highest vertical temperature differences were measured in the control space, CS.01, the full height ventilation opening in the retrofit space had a stronger stratification relative to the envelope temperature difference. Five of the highest STR values recorded were with RS.04, one of these being greater than 2.0 showing the vertical temperature difference was twice that of the average envelope temperature difference. The large opening height plays a significant role in the internal temperature distribution. This is something that should be considered further in buoyancy flow models that use an average room temperature to calculate airflow rates.

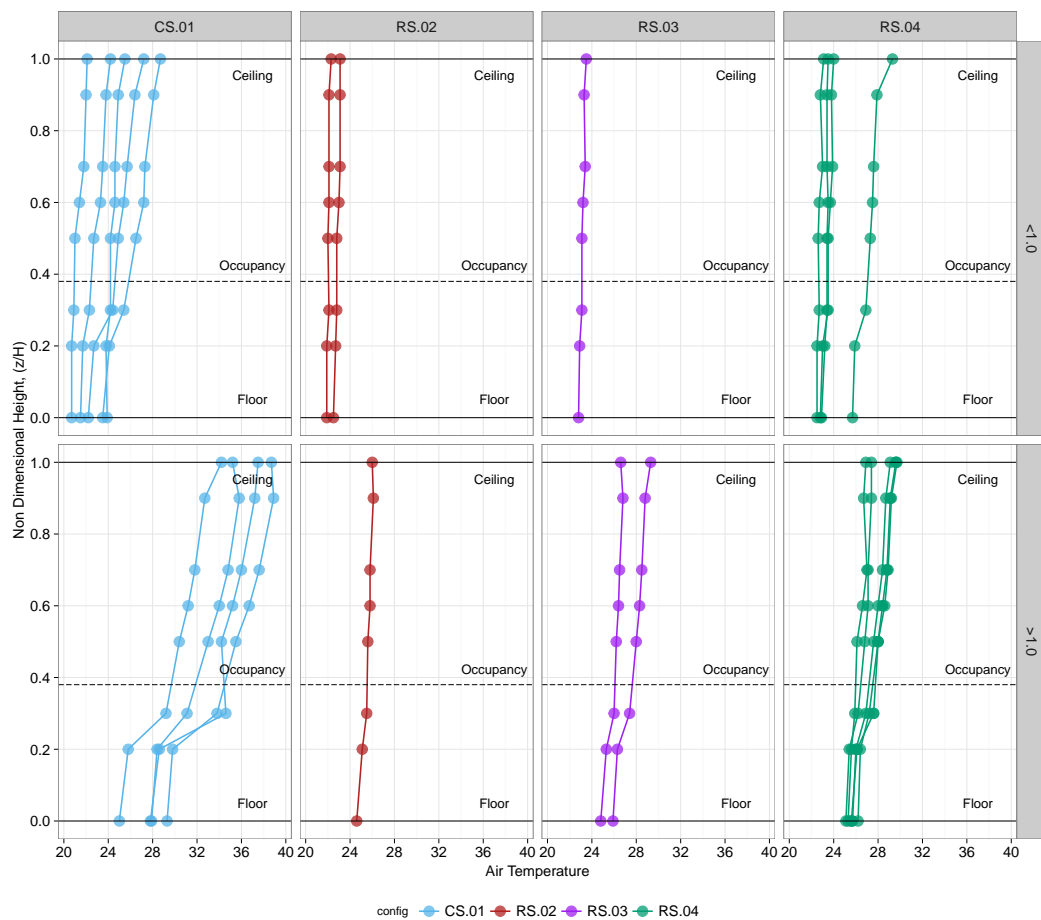


FIGURE 4.5: Mean vertical temperature profiles during different ACR tests for different configuration categorised according to whether STR was greater than 1.0 (bottom) or ACR was greater than 4.0 (Top)

With STR values ≥ 1.0 there is some variation in vertical temperature distribution for 5 of the tests under configuration RS.04 though the control space, CS.01, generally exhibits higher stratification than all configurations in the retrofit space. RS.04, the full ventilation opening height, demonstrates that some stratification potential exists in the low energy retrofit space under certain conditions. Vertical temperature distribution under free cooling from outdoor air

TABLE 4.3: Sample of Stratification Factors with a range of low and high values and corresponding test conditions

Config	Test	STR	σ_c	ACR
CS-1.0	2	0.06	0.104	5.3
RS-3.0	37	0.09	0.015	2.9
RS-4.0	8	0.11	0.063	5.8
RS-3.0	38	0.28	0.029	1.4
CS-1.0	22	0.47	0.077	3.9
CS-1.0	14	1.05	0.093	4.1
CS-1.0	33	1.05	0.061	3.6
RS-4.0	17	1.33	0.056	4.5
RS-4.0	24	1.81	0.030	3.3

has been substantially modified following the retrofit works. Configuration RS.04 still displays some vertical temperature difference however, RS.02 & RS.03 have little or no vertical temperature variations except for 1 or 2 tests when $STR \geq 1.0$. Figure 4.6 presents the frequency distributions for STR values for both occupied and unoccupied hours for the control and retrofit spaces for the period 9th June 2013 to 23rd July 2013. During this period temperature data was continuously recorded.

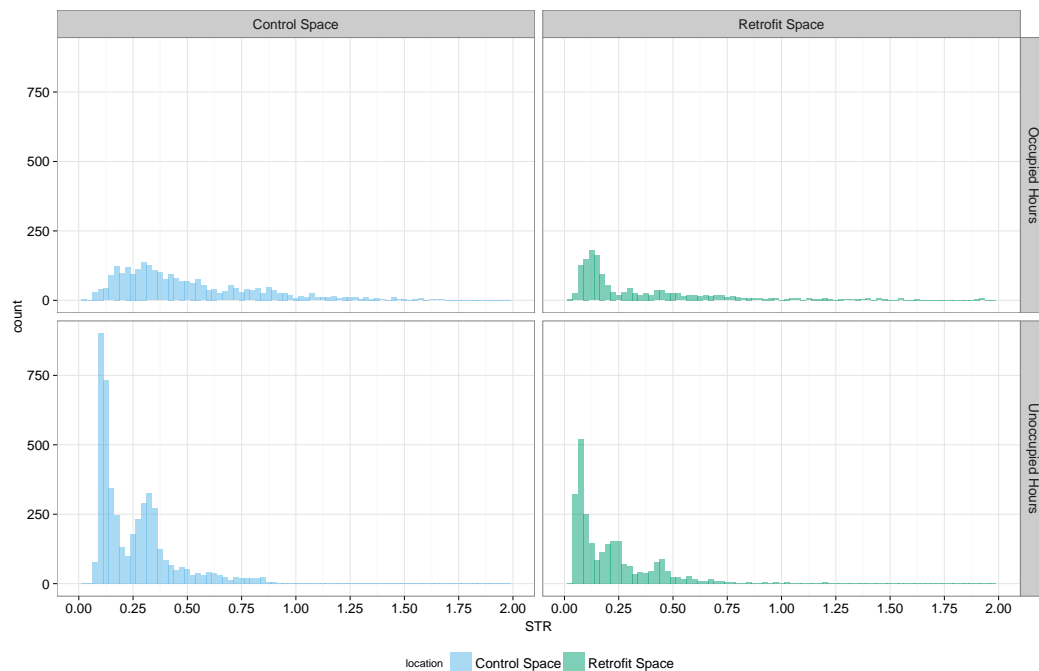


FIGURE 4.6: Histogram for STR values for control and retrofit spaces categorised according to occupied and unoccupied hours

Figure 4.6 shows how stratification is substantially reduced during overnight periods. The 95th percentile value for unoccupied hours of 0.611 is largely based on conditions up to around 21:00 each evening where there is still significant stratification. Both spaces monitored are west facing and this suggests an association with incident solar irradiation and the occurrence of peak conditions later in the evenings. Most of the peak conditions take place at this time even though

TABLE 4.4: Measured Peak $T_{\frac{H}{2}}$, Time Lag during week 8th-14th July 2013. (*Denotes night cooling present the previous night. †, denotes using RS-4.0; ‡, denotes using RS-3.0)

Day	Ext T_{ext}		RS T_{int}				CS T_{int}			
	Max	Occ.	Max	Occ.	Min	Occ.	Max	Occ.	Min	Occ.
8th	25.4	16:35	29	18:50	24.4	06:00	36.8	19:35	25	05:40
9th	27.1	14:40	28.6	18:40	25.5	23:40	36.1	19:00	26.8	07:05
10th	26.4	13:00	29.1*†	19:50	22.8	07:10	36.5	19:25	28	06:10
11th	23.9	11:45	30.0*†	18:40	22.8	06:50	-*	-	25	07:40
12th	26.4	15:15	28.0*†	19:00	22	06:30	35.6*	17:35	-	-
13th	27.8	14:20	28.4*‡	18:40	25.1	06:20	36.1*	17:45	24.3	07:45
14th	25.8	16:55	27.9*‡	20:00	25.8	07:20	33.9*	17:20	25.7	23:40

peak day time air temperatures occur as early as 11:45am. The retrofit occupied hours 95th percentile value of 2.59 does highlight that there is stratification still present in the space and it has a significant relative strength compared to ΔT_{ie} . Temperatures at the surface of the exposed roof slab are often 2 – 3°C higher than would be reported based on a mid-level zone thermostat which can be significant when designing systems for ventilate cooling of a low energy space.

4.2.2.2 Zonal ambient/indoor air temperature time lag

Tables 4.4 presents time of occurrence for maximum and minimum mid height air temperature values for a single week in July 2013. We see a substantial reduction in peak indoor air temperatures in the retrofit space. We have a mean temperature difference across the envelope of 2.7K for the retrofit space with a mean deviation in time of occurrence between external and internal peak temperatures of 4 hours and 10 minutes. Conversely, in the control space we had a mean temperature difference of 9.4K and a mean deviation of occurrence of 3 hours and 18 minutes. There are substantial reductions in peak indoor air temperatures, reducing the extent of heat removal required by a night cooling strategy. There is also an increase in the mean time lag of almost an hour. In the first three days there are similar time lags in both spaces with a clear change in pattern for the last three days of the week. There was ventilation throughout the day for all measurements. It seems that the control space exhibits similar ability to shift the time of peak indoor temperatures earlier in the week when no night cooling was used.

4.2.3 ACR Measurements

Figure 4.7 summarises variability in recorded mean ventilation rates for each test configuration with mean values stated for each and median shown as horizontal bars. The time period of each test varied based on the configuration and according to the guidelines in Table 2 of ASTM E-741-11 [156]. Figure 4.8 presents results from all TGCD tests under different operating configurations. Data is presented using $\ln C_N$ for each test. As mentioned in Chapter 3 ACR values have been calculated using the decay regression technique outlined in Appendix A, section A.4.2. Table 4.5 contains summary data regarding the 38 tests. Magnitudes were estimated based on the slope coefficient resulting from the best linear fit equation. This method assumes the airflow

TABLE 4.5: Descriptive Statistics for ACR tests

Config ¹	Max ²	Min	SD	Ave	Max σ_c ³	Min σ_c	Ave σ_c	WS ⁵	W/L	ΔT_{ie}
CS-1.0	6.4	1.9	1.5	4.2	0.1219	0.0381	0.0744	1.4-5.2	9/4	4.2-8.9
RS-4.0	5.8	2.3	1	3.8	0.1201	0.0114	0.0487	1.4-5.2	7/6	0.5-5.5
RS-2.0	5.1	1.5	1.3	3.1	0.0577	0.0101	0.0316	3.3-4.2	4/2	1.1-5.3
RS-3.0	3.8	1.4	0.9	2.3	0.0286	0.0073	0.0175	1.5-4.5	4/2	0.4-7.1

1. Opening configuration,

2. Column 2 to 5 relates to ACR values,

3. Columns 6 to 8 relate to the unsteadiness parameter

4. Remaining columns relate to boundary conditions during testing

5. WS = wind speed (ms^{-1}), W/L = No of Windward/Leeward tests, ΔT_{ie} is envelope temperature difference

rate was steady during the decay period. The uncertainty in the results associated with this assumption has been estimated using the approach in Appendix A, section A.4.2. The average measurement uncertainty for the control space CS.01 tests was 7.9% although when test 11 is removed from the data set (which had a high leverage on the average) this reduces to 5.8%. For the retrofit MCSL system the average uncertainty in 4.1% with RS.02, RS.03 and RS.04 having uncertainties of 4.1%, 3.4% and 4.8% respectively. This error, when added to those discussed in chapter 3 for mixing and instrument specification gives measurement uncertainty in the region 5% to 15% depending on test. The control space has consistently higher ACR values with an average value of $4.2 h^{-1}$ and standard deviation of $1.5 h^{-1}$. In the retrofit space RS.04 had the best performance profile with average value of $3.8 h^{-1}$ and standard deviation of $1.0 h^{-1}$ indicating a slightly more concentrated spread of results. Based on the guideline values for indoor air quality classification in BS EN 13779:2007 [150] both the control space and retrofit space time averaged ventilation rates can be classified as IDA-1 (High). ACR values were on average lower for the RS.02 & RS.03 configurations although there were individual instances of high ACR values above $5.0 h^{-1}$. Where there is steady ventilation rate conditions during tests the lines representing the concentration decay should display a smooth linear profile. σ_c is the standard error of estimate in prediction of Y_i , Y'_i , from the regression model and is used as a measure of the magnitude of concentration fluctuation during decay for each test and can be used as an indicator of the potential unsteadiness in ventilation rates. It is defined as:

$$\sigma_c = \sqrt{\frac{\sum_{i=1}^N (Y_i - Y'_i)^2}{N - 2}} \quad (4.2)$$

Regarding the type of ventilation flow conditions in control and retrofit spaces there were consistently higher σ_c values and visibly more unstable decay profiles in the control space. This would suggest there were higher unsteady flow effects during testing in the control space. The retrofit space configuration RS.04 also displayed some tests with unsteady flow effects likely present with the same maximum σ_c values although the average RS.04 σ_c was 35% lower. The profiles of the decay are consistently more stable for RS.02 & RS.03 with average σ_c values 57.5% and 76.5% lower respectively.

Having measured mean single sided ventilation rates using the TGCD regression technique the next step of the analysis was to investigate whether the dominant driving forces were different for each operating configuration. The two main forces that can give rise to ventilation rates

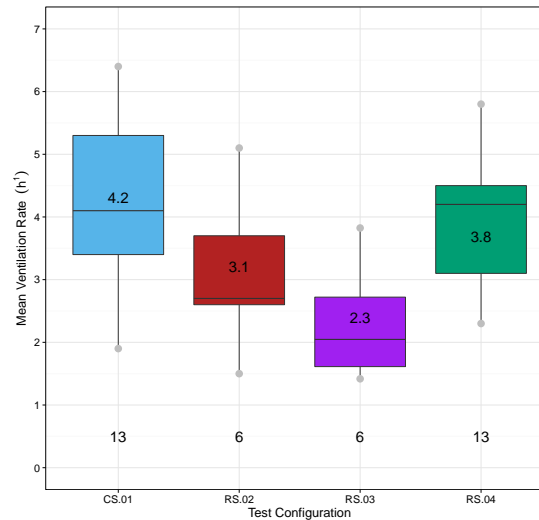


FIGURE 4.7: Boxplot of mean ACR, (h^{-1}), for each configuration

are stack effect, generated by temperature difference across the building envelope in single sided ventilation flow models, and pressure at the building surface due to wind effect (effected both by the magnitude and direction of the wind). The following section investigates the existence of these forces in the ACR measurement data presented above.

4.2.4 Analysis

Single sided ventilation strategies rely on a number of low and high frequency unsteady flow phenomena relating to wind pressure, gustiness and turbulence. Tracer decay rates were measured at a frequency of 0.1 Hz during each test and Figure 4.9 presents recorded mean ventilation rates as a function of mean wind direction and Figure 4.10 as a function of wind speed, grouped according to test configuration. The colour scale for data points indicates magnitude of envelope temperature difference for each test while the data point size indicates the amplitude of concentration fluctuation, σ_c , again based on the estimate of error in prediction from the regression model fitted to the normalised concentration decay, C_N , to determine the mean ventilation rates. This is taken as an indicator of the level of unsteadiness present during each test.

4.2.4.1 Influence of buoyancy and momentum forces

Considering Figure 4.9 in all configurations the highest recorded mean ventilation rates generally occurred with $\Delta T_{ie} > 4^\circ C$ and a windward wind direction. Lower mean ventilation rates generally occurred with low ΔT_{ie} which also coincided with leeward conditions. Parallel wind directions show less defined patterns. This suggests an important relationship exists between the magnitude of ΔT_{ie} and the wind direction. Low ΔT_{ie} generally resulted in lower ventilation rates for low opening height RS.02 & RS.03 while some CS.01 & RS.04 tests have mean ventilation rates higher than $4.0h^{-1}$ even at $\Delta T_{ie} < 4^\circ C$. Figure 4.9 suggests that where the wind direction is not approximately normal to the surface then it is more likely to have lower ventilation

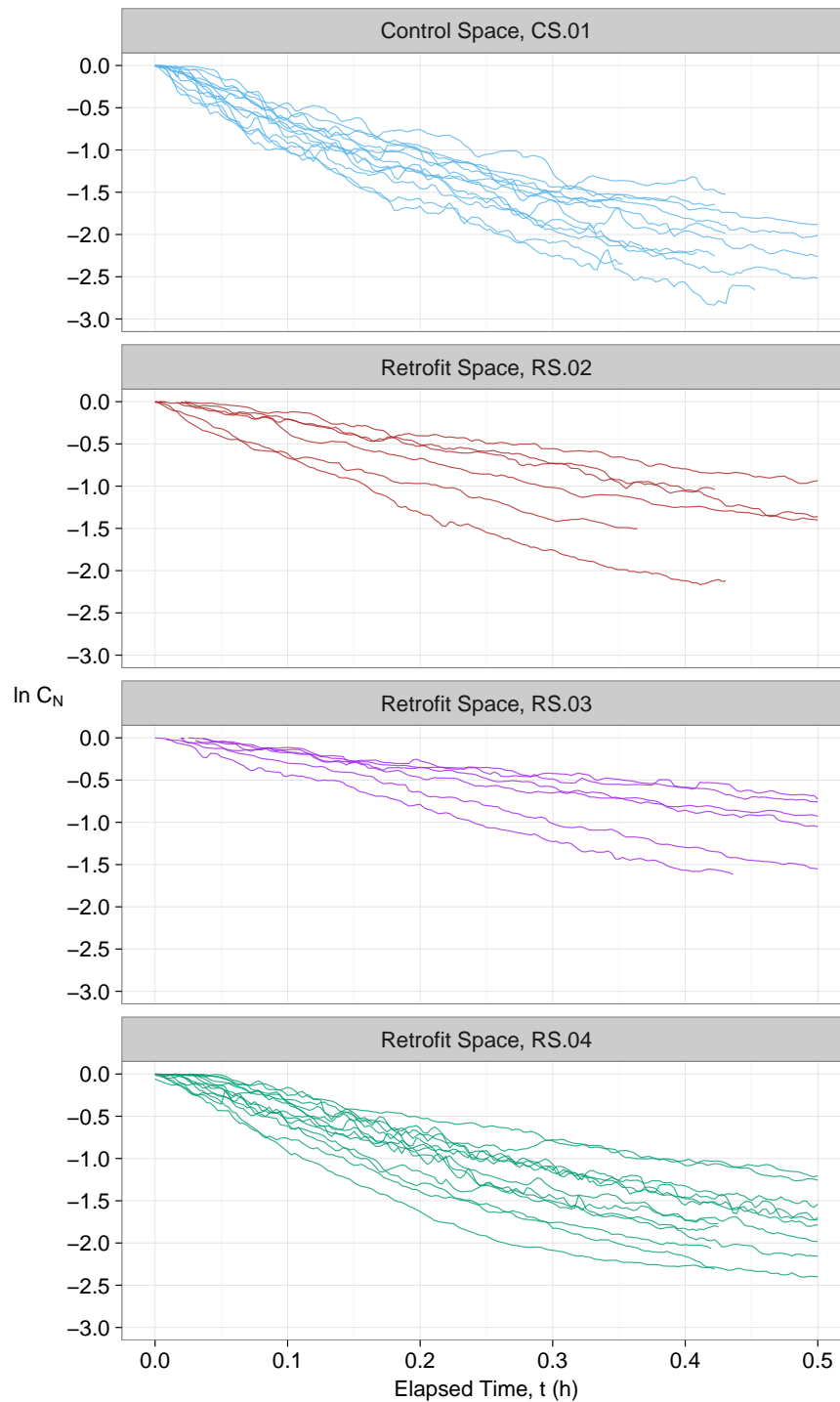


FIGURE 4.8: Natural logarithm of CN as a function of elapsed time for each test

rates even at relatively high ΔT_{ie} values. Results suggest that leeward and parallel flows at the opening are more likely to generate phenomena that will oppose buoyancy forces, for example turbulent diffusion reducing the effective temperature difference through mixing [111]. RS.04, the largest opening height, shows a more pronounced trend between mean ventilation rate and wind direction while CS.01 also shows some agreement in this regard. Furthermore σ_c is consistently larger under windward wind direction potentially showing a correlation with pulsating

flow from wind gustiness and resulting air compressibility rather than turbulence mixing. This underlying trend for slot louvred systems is something that has not been hugely investigated in the literature.

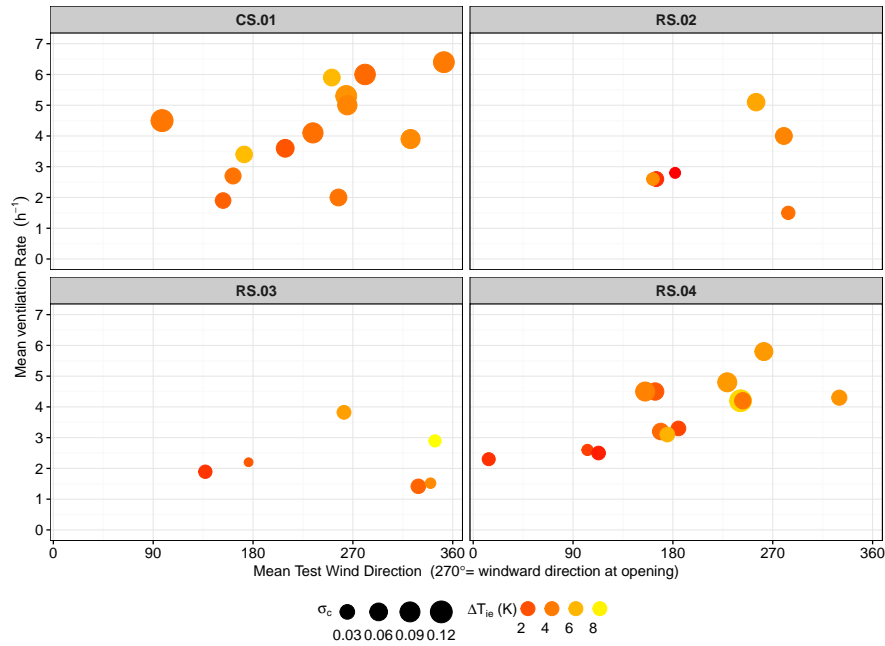


FIGURE 4.9: Scatterplot of mean ventilation rates (h^{-1}) vs wind direction, (classified with ΔT_{ie} & σ_c)

Furthermore when considering Figure 4.10 the data suggests a co-dependency exists between mean ventilation rates, ΔT_{ie} and wind speed for the RS configurations but this same trend is not present in the CS.01 dataset. In fact it suggests that wind speed contribution is less important for the outward opening window type and ΔT_{ie} and wind direction are more important to predicting the resulting ventilation characteristics. Compared to the CS.01 configuration the reduced aspect ratio of the slot louvre system seems to reduce the effects of phenomena such as eddy penetration, particularly during windward conditions permitting buoyancy forces to better establish.

While it is difficult to draw any clear quantitative conclusions regarding high frequency fluctuating phenomena when examining time averaged test data, the concentration fluctuation parameter, σ_c (based on 0.1hz arithmetic averages of readings taken at 1hz), can still give a measurable indication of the overall unsteadiness present in a ventilated space during a tracer decay test. The cause of this unsteadiness however, can be due to several factors: pulsation flow, penetration of eddies (depending on sensor location), and static or molecular diffusion. 10 of the 13 CS.01 window opening tests exhibited unsteadiness at the upper end of all recorded σ_c values. These appeared to happen primarily under windward wind directions and across all wind speeds. There was no visible correlation with wind speed and most of these high σ_c instances had $\Delta T_{ie} > 5.0^\circ C$ although these appeared wind dominant according to the non-dimensional analysis in section 4.2.4.2 below. This would suggest that the fluctuating component of the ventilation rates is more amplified when wind is normal to the outward opening window case. This may be due to the nature of flow impingement with the window obstructing entry resulting in

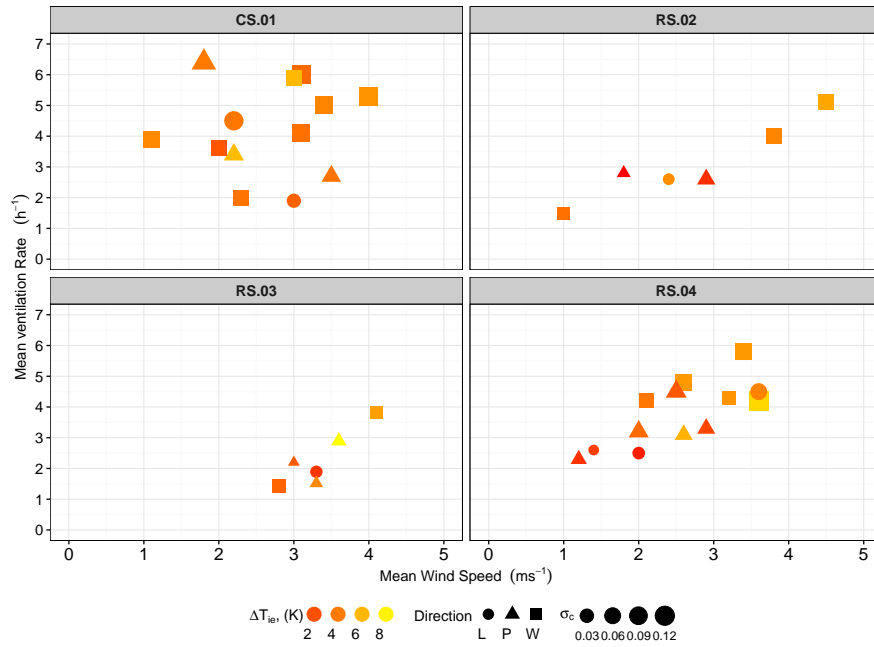


FIGURE 4.10: Scatterplot of mean ventilation rates (h^{-1}) vs wind speed, (classified with ΔT_{ie} & σ_c)

increased localised turbulence. The highest fluctuation value for parallel flow in CS.01 happened with one of the lowest average test wind speeds ($1.8ms^{-1}$) while the two other parallel flow tests showed lower unsteadiness profiles with lower non-dimensional F_r values suggesting that with parallel flow and an outward opening window fluctuating components of ventilation rate are less pronounced and buoyancy driven flow is able to better establish. This may be due to the fact the opening section of the window does not obstruct parallel flow at the boundary layer of the structural opening. More parallel flow tests are needed however before this is conclusive. In the slot louvre system only RS.04 exhibits tests with significant unsteadiness and all these tests occurred at a windward wind direction and higher wind speeds with a more noticeable trend visible in Figure 4.9 and Figure 4.10. Higher σ_c values are associated with higher ventilation rates in RS.04 suggesting the importance of dynamic phenomena such as wind gustiness to single sided ventilation rates even for slot louvre systems. These also generally occurred at windward wind directions. Ai and Mak [160] have shown that for plain openings velocity and pressure fields are relatively stable for windward wind directions and the resulting unsteadiness is mainly associated with a large impinging mean flow rather than turbulent exchange. This would suggest a more likely correlation of σ_c with the pulsating flow of the wind than turbulent exchanges at the opening for results presented here. For RS.03 & RS.02, irrespective of wind direction fluctuation parameters were always low as were ventilation rates although a trend existed with increasing wind speeds.

4.2.4.2 Non-Dimensional Analysis

Sensitivity study of Non-Dimensional Analysis Approach

Dimensional analysis using the Warren plot is predicated on the correct selection of the asymptote through the origin defining flow number due to buoyancy alone, F_b , described in equation 4.3.

$$F_b = \frac{Q_m}{A_o U_r^{2\beta}} = \frac{1}{3} C_d A r^\beta \quad (4.3)$$

The gradient of this asymptote is sensitive to correct selection of both the still air discharge coefficient, C_d and the exponent used in the power law relationship for pressure and flow (i.e. $\beta = 0.5$ for orifice flow). C_d is an important parameter for a ventilation opening as it depends on the geometry of the opening and the Reynolds number, R_e of the flow, and is normally taken as 0.61 for a flush faced sharp edged orifice. Various research studies have considered the effect on C_d of different opening types and their geometry, shape and porosity under wind driven flow [161, 162], while other studies have concentrated on the effects of wind in terms of direction and the effects of dynamic pressure [163]. Caciolo et al [111] used a C_d value of 0.6 to describe the flow characteristic when calculating F_b for various open window geometries while a C_d of 1.0 is used in [113]. The work by Grabe, described below, proposed an equation to estimate the C_d value for a window opening [164, 165]. Both Pinnock [166] and Sharples et al [92] have carried out experimental work considering the use of alternative exponent values in the power law equation when dealing with the buoyancy alone case and slot louvres respectively. Pinnock proposed $\beta = 0.6348$ and Sharples suggested $\beta = 0.9301$. As indicated in Figure 2.16 page 45, a comparison of the value of F_r with F_b using the warren plot indicates whether the non-dimensional ventilation rate is buoyancy dominant or otherwise. F_b can be said to be a function of three primary parameters based on equation 4.13 summarised in equation 4.4 as:

$$F_b = f(Ar, C_d, \beta) \quad (4.4)$$

The sensitivity of these parameters on the buoyancy asymptote was tested, F_b , and the resulting modal shift from wind dominant to buoyancy dominant F_r . While the physical relationship between Ar and β is not clearly defined in the literature for values other than $\beta = 0.5$ (with Ar for the cases of interest defined based on Bernoulli flow) it was still worthwhile to include Ar^β as a linear coefficient in testing the sensitivity of F_b to the results. Using a sample size $N = 38$ based on experimental test data we divided the measured distribution of all F_r into q equally sized quantiles with the k_{th} quantile equal to k/q . For this study we set $q = 2$, took the smallest F_r observation to correspond to a probability of 0 ($0/2 = 0$), the largest observation to a probability of 1 ($2/2 = 1$), giving us the 0, 50th & 100th percentiles from the measured data. We then selected matching Ar values for each F_r based on the measured data. This resulted in a manageable parameter space and gave realistic ranges for combinations of F_r and Ar . The range of values chosen for parameter x_i in equation 4.4 is the set defined using the cardinality and interval in equations 4.5 through equation 4.7. $i = 1$ for C_d , 2 for β and 3 for Ar .

$$|x_1| = 8, \{x_{1,j} \in \mathbb{R} \mid 0.4 \leq x_{1,j} \leq 0.9\} \quad (4.5)$$

$$|x_2| = 6, \{x_{2,j} \in \mathbb{R} \mid 0.5 \leq x_{2,j} \leq 1.0\} \quad (4.6)$$

$$|x_3| = 6, \{x_{3,j} \in \mathbb{R} \mid 0.005 \leq x_{3,j} \leq 0.12\} \quad (4.7)$$

Each combination c , equates to a value of F_b with all possible combinations of parameters calculated from the cardinality of the Cartesian product of all sets, in this case $n = 3$

$$\mathbb{X} = |x_1| \cdot |x_2| \cdot \dots \cdot |x_{n-1}| \cdot |x_n| \quad (4.8)$$

This configuration of parameters resulted in 192 different possible combinations. Each F_r value was compared with only those $F_{b,c}$ values that had the same Ar (i.e. 48 $F_{b,c}$ values for each of the 4 Ar values selected), as would be on the Warren plot. An error value for each combination, e_c , shown in equation 4.9 was calculated giving the difference between F_r and a baseline, standard asymptote, denoted $F_{b,0}$, (based on $C_d = 0.61$ and $\beta = 0.5$), ΔF_b , and F_r and the particular $F_{b,c}$ for the combination under consideration, ΔF_c .

$$e_c = \Delta F_b - \Delta F_c \quad (4.9)$$

For example lowering C_d reduces the apparent slope of the asymptote, reducing β actually reduces Ar^β values shifting F_r values towards the ordinate linearly resulting in an apparent reduction of the asymptote, both changes manifest as a modified ΔF_c . Figure 4.11 presents values for e_c for each of the various different combinations of Ar , C_d and β at particular F_r values. Each sub grid represents a particular F_r/Ar combination on the warren plot and the tiles within each sub grid are the e_c values. For $F_{b,c}$ where $C_d = 0.61$ and $\beta = 0.5$, e_c is always shown as zero. On the warren plot, as $F_{b,c}$ passes through $F_{b,0}$, with both asymptotes co-located, e_c reduces to zero, increasing again as $F_{b,c}$ moves away from $F_{b,0}$ towards F_r . e_c continues to increase without a modal shift until it passes through F_r a critical point where there is then a modal shift and is represented with a sign change in Figure 4.11.

In considering Figure 4.11, at low Ar there is little sensitivity to a modal shift from wind dominant to buoyancy dominant conditions. At low Ar test conditions are usually wind dominant with high F_r values. At $F_r = 0.015$ there is a modal shift at $C_d > 0.61$ showing high sensitivity. At $0.01 < Ar < 0.04$ no modal shifts appear for almost all C_d at $\beta = 0.5$. Only as β increases do we see results with high sensitivity to input parameters. At $\beta = 0.5$ sensitivity is present at $F_r = 0.036$ for $C_d < 0.61$ with modal shifts taking place for these parameters, in this instance shifting from buoyancy to wind dominant conditions. A number of test results presented in this chapter are in this range. At $F_r = 0.085$ and $Ar = 0.12$ there is modal shifts at $C_d > 0.75$ but only at $\beta = 0.5$ and very few test results had these conditions. In summary there appears to

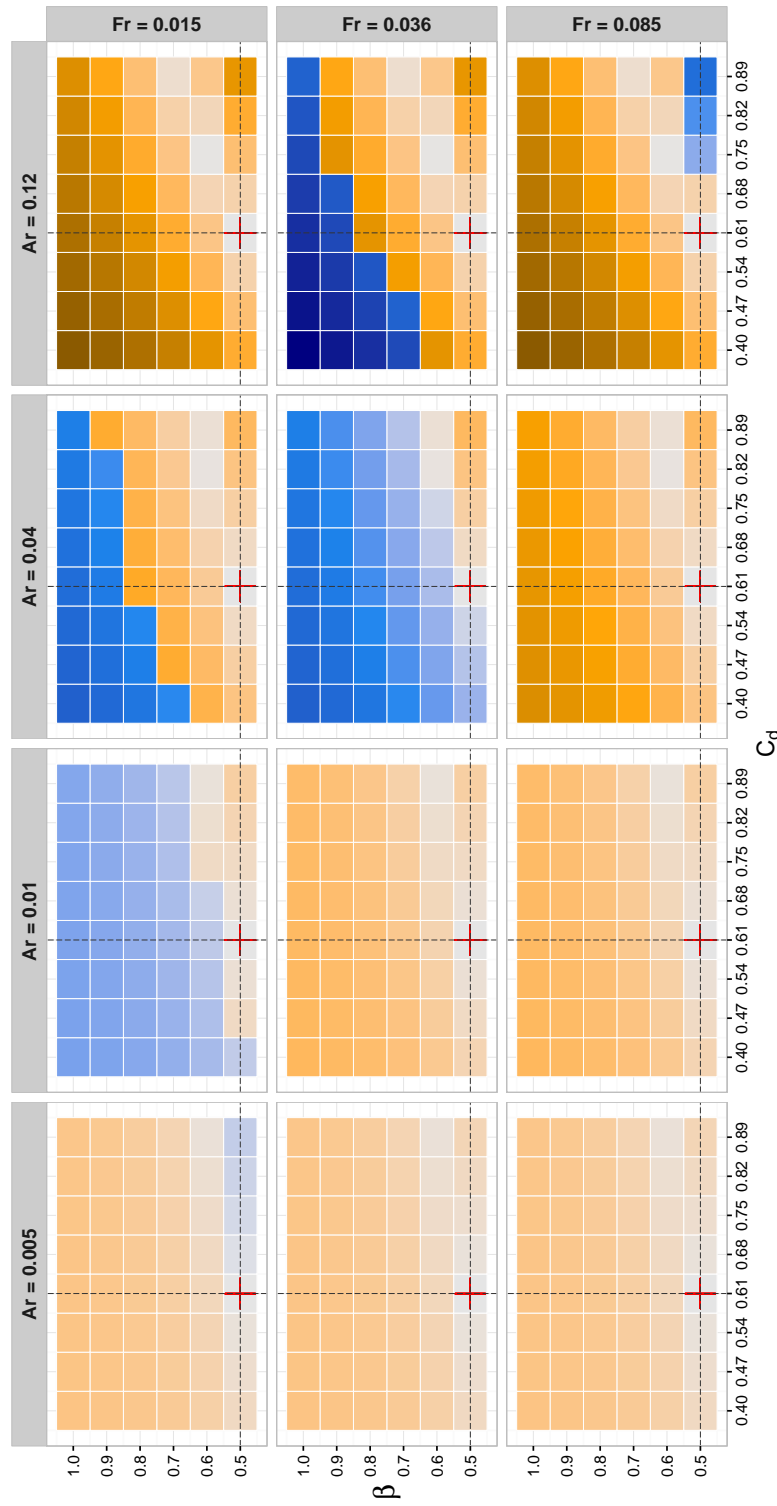


FIGURE 4.11: e_c for all X combinations grouped according to F_r (vertical axis) and Ar (horizontal axis). Negative e_c values represent a modal shift with $F_{th,c}$ passing through F_r giving the critical C_D/β combination causing change in contribution from wind forces. Magnitude of e_c represents scale of modal shift.

be some sensitivity to C_d for the tested F_r/Ar ranges but this is neither systematic throughout and generally low at $\beta = 0.5$. At $Ar < 0.04$ values, where a lot of the measured data is situated, there is little evidence of modal shifts, irrespective of the magnitude of F_r . At mid-range Ar and with F_r values reported by Warren (0.025 – 0.035), it appears sensitivity to the physical geometry of the opening exists when interpreting the contribution from wind forces.

Selection of C_d for analysis

Notwithstanding the analysis above the value selected for C_d for the control space window opening to facilitate analysis is 0.422 and is largely based on Von Grabe [164]. There appears to be limited data available on full scale performance of this type of window in the literature. Recently Grabe presented work characterising flow resistances for different window types [164]. Based on laboratory tests of buoyant flow through the openings he proposed different resistances for inlet and outlet areas where openings were asymmetrical (i.e. a combination of triangular and rectangular). He proposed an empirical law between flow resistance and total opening area for awning windows similar to the one used in the control space.

A C_d value of 0.55 is assumed for RS.03. The slot louvre system used here is a flush faced sharp edged orifice at the inlet and flow is likely unidirectional through the individual slot openings. There is a length component of the louvre in a circular shape (see Figure 5.8, page 127) that might promote some flow reattachment allowing viscous forces and a boundary layer to develop, reducing the flow separation that normally results in C_d being independent of Re. However, for the purposes of establishing a C_d value under buoyancy alone conditions 0.61 may be a little low but acceptable for RS.04 and RS.02 for the purposes of initial analysis here. The RS.03 configuration has the combined effect of slot louvre and inward opening ventilation door due to its restricted opening angle and a C_d probably lower than 0.61 as a result.

Non-Dimensional analysis of ACR data

Figure 4.12 presents Warren Plots for CS & all RS configurations. Figure 4.13 presents individual Warren Plots for each cardinal wind direction. The purpose of the different plots is to investigate trends that relate to opening geometry, test environment and associated combinations of buoyancy and momentum driving forces. Considering Figure 4.12 we see a comparable spread of F_r values for both spaces with the retrofit $Ar^{0.5}$ range extending further towards zero ordinate. F_r values seem to display slightly higher dependency on $Ar^{0.5}$ in CS.01 and RS.04. When the data is split according to RS opening configuration as shown, three different patterns emerge. RS.04, ($H_{ope} = 1.60m$), shows a pattern of buoyancy dominant ventilation irrespective of the wind direction, which seems to agree with data in figure 4.9 where the highest RS.04 ventilation rates had high ΔT_{ie} values. Alternatively RS.03 has $H_{ope} = 0.76m$ ($H_{int} = 2.43m$ (above floor level)) and also has a potentially lower C_d value than RS.02. It exhibits increased contributions from wind forces with similar F_r values but consistently lower $Ar^{0.5}$ values compared to RS.04. It appears that with a lower opening height buoyancy forces have less ability to establish irrespective of ΔT_{ie} resulting in lower $Ar^{0.5}$ values and as a result F_r values appear more independent of $Ar^{0.5}$ in lower ranges suggesting the nature of the wind contribution is more important than its ratio to buoyancy forces.

RS.02 ($H_{ope} = 0.76m$) ($H_{int} = 1.59m$) has a greater internal door opening angle than RS.03 and a higher C_d value. It exhibits the least dependency on buoyancy forces with nearly all tests showing wind dominant F_r values. In general results suggest that for slot louvre systems the opening height, H, is an important factor modifying the nature of the contribution from momentum forces (i.e. wind direction and magnitude) in determining whether or not they assist buoyancy forces. Considering figure 4.13 for RS configurations only, both parallel and windward

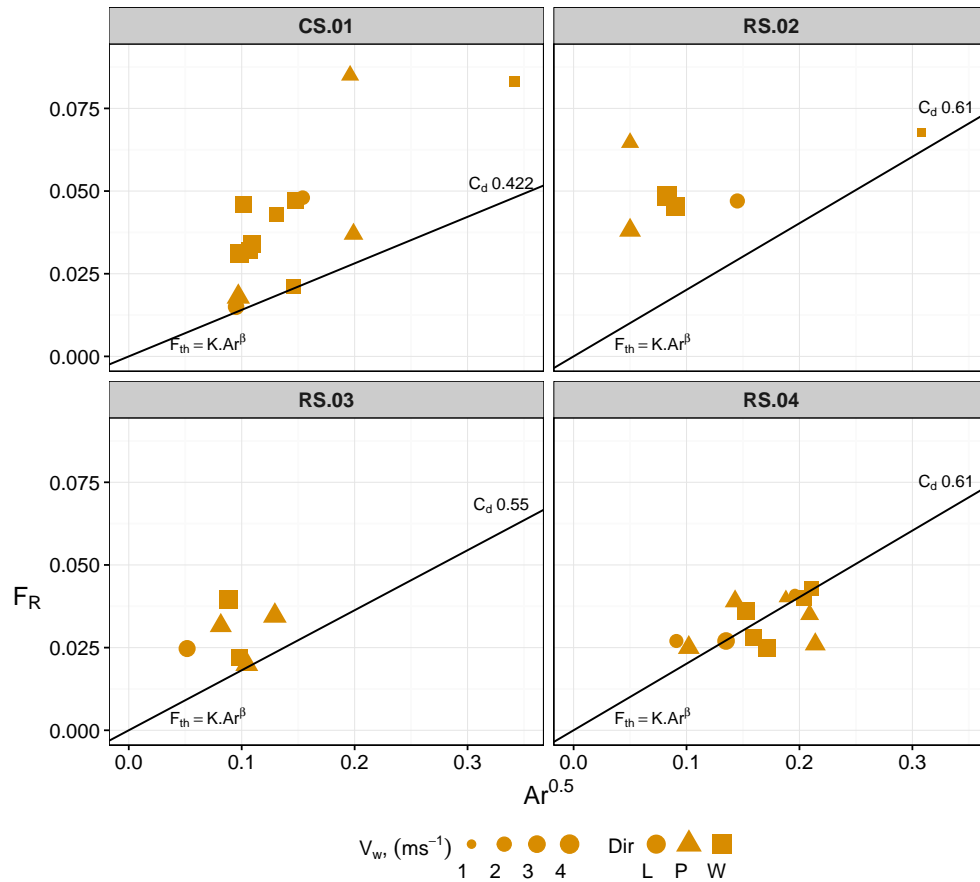


FIGURE 4.12: Warren Plot for all CS and RS configurations varying F_{th} asymptotes included as dashed lines

wind directions show a pattern of reducing dependency of F_r on $Ar^{0.5}$ as its value tends to zero, a trend less pronounced with leeward tests. At low $Ar^{0.5}$ F_r is a function of wind direction. At higher $Ar^{0.5}$ values windward and parallel wind directions show a tendency of F_r towards the F_{th} asymptote and the contribution from momentum forces are either diminished or generate conditions that favour buoyancy effects. In general the non-dimensional analysis indicates the contribution from momentum forces is a function of the overall structural opening height and location with this effect dependant on the ratio of momentum and buoyancy forces.

Overall these results suggest that at low $Ar^{0.5}$ wind incidence angle becomes important in determining whether or not wind becomes dominant. Warren plot analyses suggest these are generally wind dominant with low $Ar^{0.5}$ but they consistently exhibited low σ_c values appearing counter intuitive. When comparing fluctuation rates for parallel wind directions in the RS configuration they are generally lower than windward wind directions. What is apparent from the data presented is the characteristic of ventilation rate is a function of the combination of opening geometry and wind direction. Furthermore the characteristics of the momentum forces (magnitude and direction) in turn influence the nature of ventilation and the resulting effect buoyancy forces will have. We have shown how mean ventilation rates depend on wind direction even for complex geometries such as slot louvres agreeing with findings from Larsen and Heiselberg [108]

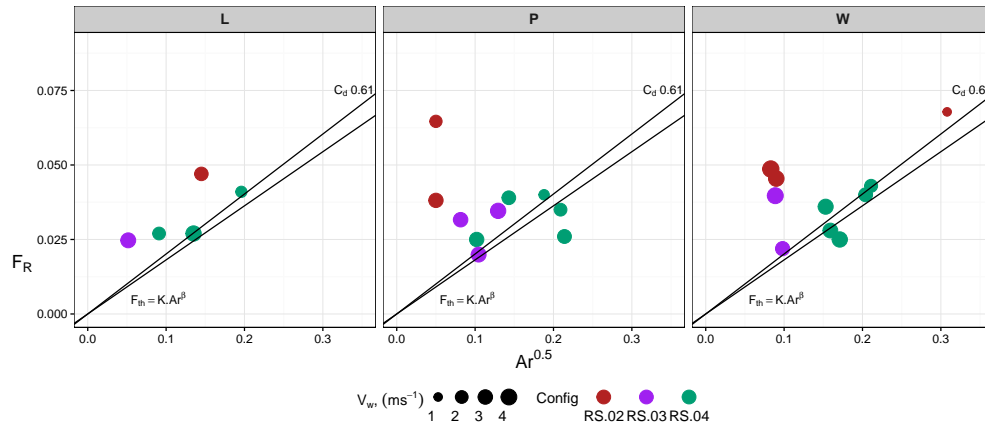


FIGURE 4.13: Warren Plots for wind directions

and furthermore the relative importance of this is also function of opening geometry and $Ar^{0.5}$. It may not be sufficient to only consider ΔT_{ie} when investigating this effect.

4.3 Conclusion

Experimental findings presented in this chapter suggest that the retrofit works have modified both the internal thermal environment and mean ventilation rates during the cooling season for isolated spaces with single sided ventilation. The largest recorded ventilation rates in the retrofit space were, on average, still lower than the existing building under similar driving forces. Results indicate increased time varying ventilation rate fluctuations in the control space during testing compared with the retrofit space, suggesting an increased presence of unsteady air flow effects. The new louvred ventilation opening design in the refurbished building may be contributing to more stable instantaneous ventilation rates. Regarding Internal thermal environment, results suggest some properties have been modified with the mean zone air temperature substantially reduced. Diurnal internal air temperature amplitude has also been reduced. The retrofit space generally complied with category A of ISO7730 under vertical temperature difference criteria. ΔT_s had a lower magnitude in the retrofit space but had instances of higher STR values suggesting it had a higher relative strength compared to the existing building.

Research presented in this chapter investigated the combined effect of buoyancy and momentum forces for slot louvre systems and has shown the magnitude and range of $Ar^{0.5}$ to be dependent on overall opening geometry. In physical terms this interdependence highlights the challenges in correctly predicting the airflow phenomena driving single sided ventilation for different types of ventilation components. An allowance for wind direction, opening height, characteristic aspect ratio and opening elevation is required as these will all affect ventilation rates. In conclusion the following points can be made:

- In single sided ventilation for low wind patterns ($v_w < 4.0ms^{-1}$) wind direction plays an important role in determining whether buoyancy forces can properly establish.

- The opening geometry is important in determining whether this low wind pattern dependency emerges at all and the opening height, aspect ratio and opening elevation are key parameters in determining subsequent effects of wind.
- Slot louvre systems act as flow stabilizers dampening the unsteadiness characteristics of ventilation and enhance the assistive contribution to buoyancy from windward momentum forces potentially dampening the mixing effects from turbulent diffusion in the opening.

If σ_c is taken as an indicator of internal airflow environment this suggests for single sided slot louvre ventilation the interdependence of opening geometry, wind speed and wind direction has a large influence on the effects of wind-generated air exchange mechanisms. Current semi empirical models for plain openings might not take proper account of this geometry dependent situation. Modification of thermophysical properties due to the retrofit have not necessarily reduced the magnitude of $Ar^{0.5}$ for similar F_r values although wind driving forces can have an increased contribution in low energy spaces even though the slot louvre system is generally perceived as restricting flow. Additional measurements in the retrofit space comparing a plain opening with that where a louvre is installed should give further insight into how wind shear interactions with buoyant flow are modified with the slotted geometry generating differing ventilation rates for similar opening areas. These measurements would include local velocity measurements at the opening and at the boundary allowing analysis of the spectra of turbulence for alternative geometries amongst other phenomena; such measurements are presented in chapter five.

Chapter 5

Mapping and Prediction of Airflow Rate with the Slot Louvre System

Here we present results from the field measurements completed in 2014. Measurement of the local and reference velocity ratio is summarised. A comparison of results from the measurement of ACR values in the retrofit space using a single slot louvre section and a plain opening section is presented. A non-dimensional analysis is employed to categorize tests according to driving forces; a spectral analysis of velocities at the opening is then used to investigate any changes in the wind characteristic in the opening and energy distribution with the addition of a slot louvre. A number of existing semi-empirical correlations are compared with measurement results and, following a discussion about potential causes for the pattern of measured ventilation rates, a new dimensionless exchange rate parameter is suggested for improved modelling of wind dominant macroscopic flow through the louvre components. Finally, results from an investigation of local air movement at a typical occupant location is also presented.

5.1 U_l/U_r measurements

Figure 5.1 shows polar plots for U_r and incidence angle θ_r (converted from ϕ_r), during each test at three locations; the local met station Cork Airport, the building roof level, and at the test opening, U_l . It is apparent that for almost all wind incidence angles the local direction of flow was almost always parallel. Figure 5.1 also compares measured U_l/U_r ratios as a function of θ_r for each test plotted using a polar axis. U_l/U_r values recorded by Warren in a wind tunnel study are included for comparison [97] as is the results from Adams equation 2.16, page 40. Similar magnitudes to Warren at 315° is observed while greater magnitudes were consistently found at 0° compared with Warren and Adams; the results between 180° and 270° present no clear trend other than the fact they are all at or below the values measured by Warren and closer to those

proposed by Adams. Some good agreement was also seen at 90° . Large U_l/U_r values were well correlated with large reference wind speeds (shown by the size of the data point) for windward incidence angles but for leeward incidence angles even with large U_r values low U_l/U_r ratios are regularly observed. The measurements suggest that simplified wind tunnel studies cannot easily predict the local velocity when there are additional effects from surrounding obstacles and terrain and confirm the strong dependency on wind incidence angle.

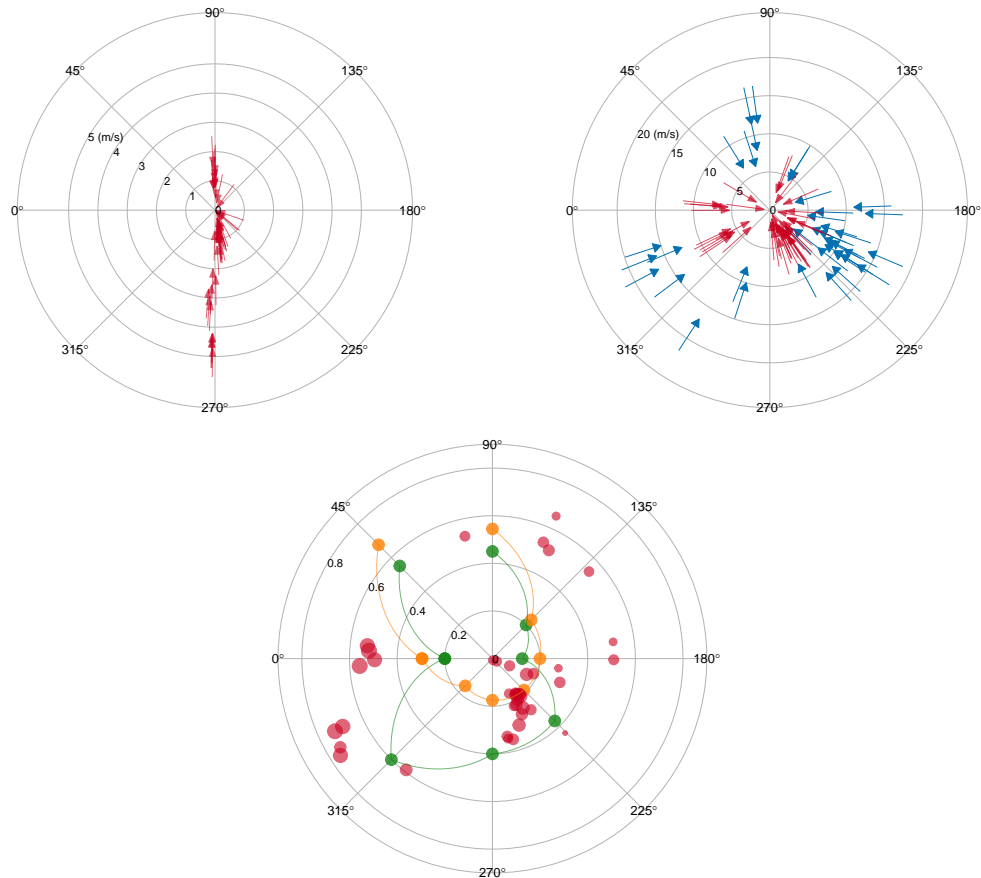


FIGURE 5.1: Wind data for individual tests. Top Left: Mean wind speed, U_l and incidence angle, θ_l , measured local to the opening taken as local conditions at the opening. Top Right: U_r and θ_r measured at 6.0 metres above roof level (shown in red) and data taken from the nearby met station, Cork Airport (shown in blue), for the same 44 test periods. Bottom: Ratio of U_l/U_r for each test according to θ_r , with size of point proportional to U_r . Warren wind tunnel measurements shown in green, Adams equation for estimating U_l/U_r shown in orange.

5.2 ACR Measurements

Figure 5.2 presents measured macroscopic ACR, Q_m , associated with each test case (described in Table 3.8, Figure 3.20). Values are binned at $0.25h^{-1}$. Again, ACR values have been calculated using the decay regression technique outlined in Appendix A, section A.4.2. Magnitudes were estimated based on the slope coefficient resulting from the best linear fit equation and as stated previously, this method assumes the airflow rate was steady during the decay period. The

uncertainty in the results associated with this assumption has been estimated using the approach in Appendix A, section A.4.2. The average measurement uncertainty for the plain opening tests was 5.41%. For the slot louvre system the average uncertainty in 4.9%. This error, when added to those discussed in chapter 3 for mixing and instrument specification gives measurement uncertainty in the region 5% to 15% depending on test. Wider distributions with higher mean values for L1 & P1, with low σ values for L2, P2 & P3 can be observed. The L type openings have a combined mean ACR of $2.13h^{-1}$ whereas the P type openings have a mean value of $2.0h^{-1}$ an average increase of 6.5% for L type openings. However, a more direct comparison, considering openings with the same overall facade opening dimensions, L1 has mean ACR of $2.5h^{-1}$, with P1 having $3.4h^{-1}$ giving an average reduction of 29%. L2 has mean ACR of $1.67h^{-1}$ with P2 having a value of $1.44h^{-1}$. However, the 3rd Quartile value for P2 is $1.5h^{-1}$ while for L2 it is $1.3h^{-1}$. P3 had a mean value of $1.24h^{-1}$. For the same opening height and reduced opening width, W_o , giving the same available free opening area, A_o , (effectively comparing L1 with P2) a 78% improvement in ACR with the slot louvre is measured. Retaining the same opening length but reducing the available height to provide the equivalent net free area (effectively comparing L1 with P3), results in an 100% improvement using the slot louvre. For this study only 1 section of the 4 ventilation opening sections that make up the 2 multi-configuration bank arrangement in the room were used.

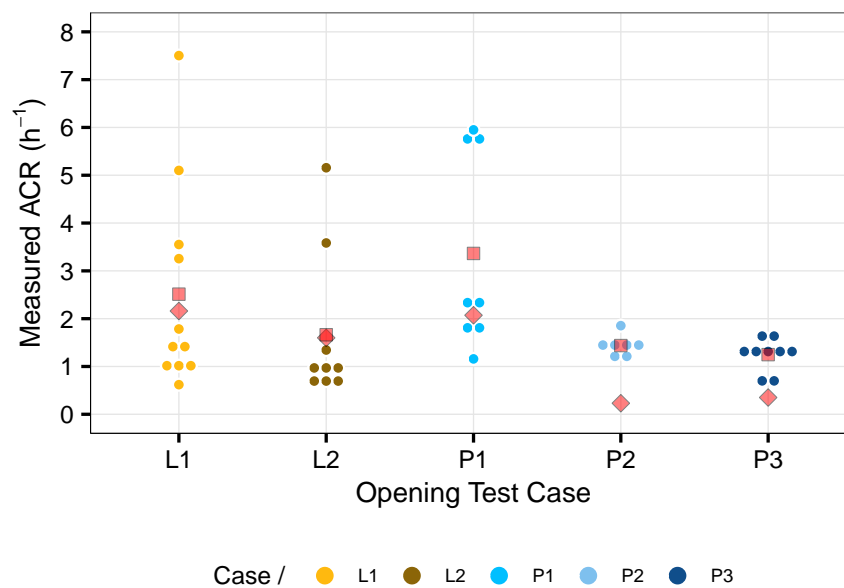


FIGURE 5.2: Measured mean ACR values presented using discrete categories according to opening type and case (see Figure 3.20). Also shown is the sample mean (red square), standard deviation (red diamond).

Therefore, ACR would have been higher for normal operation. It is not possible to correct for differences in boundary test conditions for each measured ACR value as presented in Figure 5.2 leaving a certain ambiguity as to the causality behind the distributions. Therefore, a Warren plot is used to separate individual test results that are buoyancy dominant from those that are wind dominant. Figure 5.3 presents a Warren Plot of all tests for the two different opening

types. Warren plots have previously been used by researchers to analyse ACR data in this way, for example see [97, 103, 111].

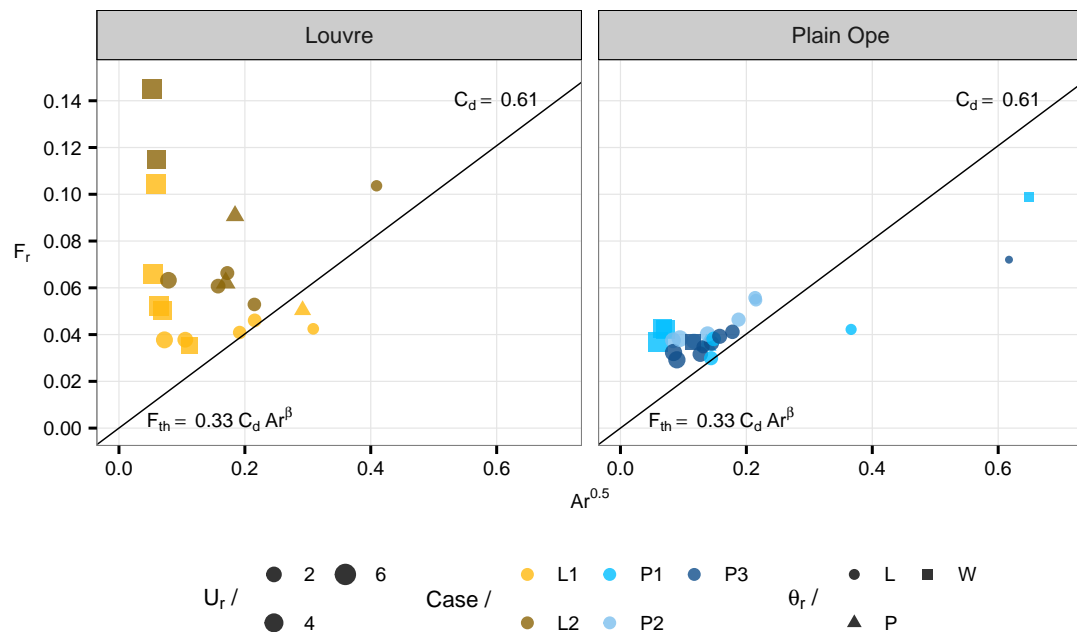


FIGURE 5.3: Non-Dimensional Flow Number, F_r Vs adjusted Archimedes Number, $Ar^{0.5}$. Data categorised according to opening type and case (Figure 3.20)

5.3 Analysis

5.3.1 Non-Dimensional Analysis

We can note the following observations from the Warren Plot, Figure 5.3:

- The plot suggests a higher F_r range for the L opening cases for a given U_r and $Ar^{0.5}$, somewhere between 0.03 - 0.15 depending on opening dimensions and θ_r , versus 0.025 - 0.1 for P opening cases.
- The slot louvre displays increased independence from $Ar^{0.5}$ suggesting the louvre cases at the opening height tested rely more on momentum than buoyancy forces.
- Increasing reference wind speed generally results in lower $Ar^{0.5}$ values and higher F_r irrespective of opening case.
- Similar distributions of $Ar^{0.5}$ values are present in all opening cases suggesting similar boundary conditions across all test cases with varying performance.
- There is a much wider spread of values for the slot louvre cases with the plain opening cases displaying consistency about values between 0.035-0.04. These values are similar to those published by Warren for a turbulent flow field.

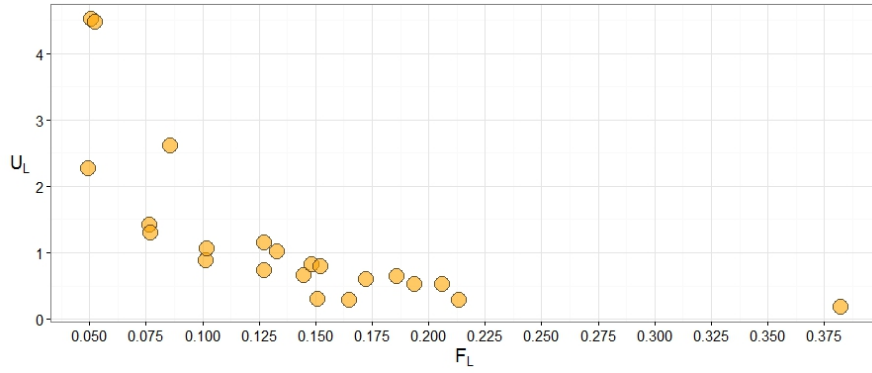


FIGURE 5.4: Non-Dimensional Local Flow Number, F_L Vs Local wind speed, U_L for all plain opening cases only.

Measurements of local flow numbers in Figure 5.4 for the plain opening tests only (please note color may be misleading here) show a large range as a function of local wind speed. However at very low wind speeds, less than 1.0 ms^{-1} , these are likely buoyancy dominant tests. The wind dominant tests, above 2.0 ms^{-1} have F_L in line with more recent research suggesting values lower than 0.1 for plain openings [94, 107].

5.3.2 Sensitivity Study of Influential Boundary Parameters

The non-dimensional analysis suggests that there exists a value of F_r for the slot louvre different to that recommended by previous researchers [97, 107, 110]. Some dependency on temperature might also exist for leeward test conditions with the slot louvre, even for the low opening height (Figure 5.3). To investigate the most suitable candidate set of boundary parameters for predicting ventilation rates with the slot louvre system we employ a sensitivity analysis using multiple linear regression (MLR) with bi-directional stepwise selection. This was completed using an efficient branch and bound algorithm from the leaps package in R [167]. As a measure of fit we use the adjusted R-squared value, \hat{R}^2 , correcting for undesirable effects from increasing the number of variables in the MLR model. We used equation 5.1 as the basis for the model:

$$y = a + \sum_{i=0}^n b_i x_i + \epsilon, \quad \text{for } i = 0, 1, \dots, n - 1. \quad (5.1)$$

For the predictor variables, x_i , We used the empirical parameters $U_l \cdot A_o$ & $U_r \cdot A_o$, the wind incidence angle $\bar{\theta}$ and the envelope temperature difference ΔT_{ie} . Table 5.1 summarises the results from the stepwise selection search process for the full slot louvre data set (all directions), Windward tests only and Leeward tests only. Only the best three candidate combinations for each variable are presented giving ten models in total for each (some combinations are amongst the best three for more than one variable). For the all wind directions combined we obtain $\hat{R}^2 = 0.871$ for the combination $[U_l A_o, \theta_r]$ with a marginal reduction when $U_r A_o$ is added to the model. When we omit both θ and ΔT_{ie} we have $\hat{R}^2 = 0.829$ for $U_l A_o$ and $\hat{R}^2 = 0.836$ for $U_r A_o$ arguably an acceptable decrease for a simplified candidate set. The windward data set shows strong correlations with better predictive ability when using $U_r A_o$ compared with all wind

directions. $U_l A_o$ combined with various parameters still gives the best prediction ability with $\hat{R}^2 = 0.914$ when θ and ΔT are included. The leeward study displays the strongest correlations in general with ΔT featuring in 5 of the models compared with the previous data sets and $U_r A_o$ giving the best predictions as opposed to $U_l A_o$ suggesting a more disturbed local velocity pattern when the wind is leeward. In terms of prediction ability, $U_l A_o$ and $U_r A_o$ have strong correlations even when considered in isolation from other parameters.

5.3.3 Airflow Characteristics at the Opening

Chu et al [110] recently demonstrated that the dimensionless exchange rate parameter can have different values depending on the wind incidence angle. This is due to differing air exchange mechanisms generated. How these different airflow exchanges interact with any buoyancy forces present depends to some extent on the magnitude of the buoyancy force which itself is influenced by the geometry of the opening. The spectral characteristic of the velocity, and by extension the airflow, in the opening can reflect whether or not the interaction is affected by a particular change in opening geometry and design. As windward and leeward conditions exhibit different local airflow exchange schemes, results from windward/leeward tests with similar boundary conditions for L1 & P1 were identified and compared, Table 5.2, to investigate how the slot louvre influences the local $U_l - \Delta T$ relationship. To identify these we used the local 1D turbulence intensity I_l , equation 5.2, mean local wind speed \bar{U}_l , mean wind incidence angle $\bar{\theta}_r$ and Archimedes number, $Ar^{0.5}$. Turbulence Intensity, I , is defined as the standard deviation of longitudinal wind speed, σ_U , normalised with the mean wind speed, \bar{U} .

$$I = \frac{\sigma_U}{\bar{U}} \quad (5.2)$$

Using velocity data at locations shown in Figure 5.5, The Cooley - Tukey Fast Fourier Transform [131] was implemented in R to transform time series data of velocities in the opening into the frequency domain. This transformation results in a power spectrum representing all frequencies over which the data is distributed. This is useful as a means of characterising the different scales of the data, with lower frequencies being larger eddies and higher frequencies smaller eddies. Figure 5.5 shows log transformed power spectra for the boundary velocity and the opening locations for tests in Table 5.2 (different locations for windward and leeward were chosen in part due to the varying nature of air exchange at the opening).

For location V6 and V8 the plain opening displays similar distributions of energy for both leeward and windward tests, both showing quite flat profiles, with the energy spread more evenly across all scales. No noticeable difference exists in the nature of the wind between all 4 locations in the opening. The steep distribution of energy at the higher frequencies in the boundary wind for both windward and leeward is redistributed to the lower frequencies as it passes through the opening. No energy above $1.0m^2s^{-1}$ was seen in the opening while the boundary wind contained values upwards of $50.0m^2s^{-1}$. For the slot louvre a different wind characteristic is clearly visible depending on $\bar{\theta}_r$ as well as measurement location. A steeper distribution is visible near the trailing edge of the opening where the turbulent jet is likely deflected inwards. At location V8

TABLE 5.1: Results from stepwise selection process for four boundary parameters U_l , U_r , θ and δT with three different sets of experimental test results, All wind directions, windward only & leeward only

No	All θ subset	Windward θ			Leeward θ		
		\hat{R}^2	No	subset	\hat{R}^2	No	subset
A1	$U_l A_o, \theta$	0.871	W1	$U_l A_o, \theta, \Delta T$	0.914	L1	$U_r A_o, \Delta T$
A2	$U_l A_o, U_r A_o, \theta$	0.866	W2	$U_l A_o, U_r A_o, \theta, \Delta T$	0.909	L2	$U_r A_o, \theta, \Delta T$
A3	$U_l A_o, \theta, \Delta T$	0.866	W3	$U_l A_o, \theta$	0.856	L3	$U_r, \Delta T$
A4	$U_l A_o, U_r A_o, \theta, \Delta T$	0.864	W4	$U_r A_o, \theta, \Delta T$	0.850	L4	$U_l A_o, U_r A_o, \Delta T$
A5	$U_l A_o, U_r A_o$	0.857	W5	$U_r A_o$	0.841	L5	$U_r A_o, \theta$
A6	$U_l A_o, U_r A_o, \Delta T$	0.849	W6	$U_r A_o, \theta$	0.840	L6	$U_l A_o, U_r A_o, \theta, \Delta T$
A7	$U_l A_o, \Delta T$	0.839	W7	$\theta,$	0.835	L7	$U_r A_o$
A8	$U_r A_o$	0.836	W8	$U_l A_o$	0.827	L8	$U_l A_o, U_r A_o$
A9	$U_l A_o$	0.829	W9	$U_l A_o, U_r A_o, \theta$	0.826	L9	θ
A10	θ	0.697	W10	$U_l A_o, U_r A_o$	0.812	L10	$U_l A_o$

TABLE 5.2: Test summary data for L1 & P1 tests with similar high and medium/low turbulence boundary conditions

Case	I_o	Test	A_o	\bar{U}_l	I_l	θ_r	$Ar^{0.5}$	\bar{I}_o	\bar{U}_o	ACR
(-)	(-)	(-)	(m^2)	(ms^{-1})	(%)	(deg)	(-)	(%)	(ms^{-1})	(h^{-1})
P1	High	10	0.228	2.62	49	359	0.067	7.7	0.42	5.7
L1	High	07	0.107	3.35	69	4	0.054	20.8	0.81	5.1
P1	Low	14	0.228	0.30	11	188	0.367	8.7	0.10	1.2
L1	Low	15	0.107	0.04	15	213	0.192	10.9	0.07	0.9

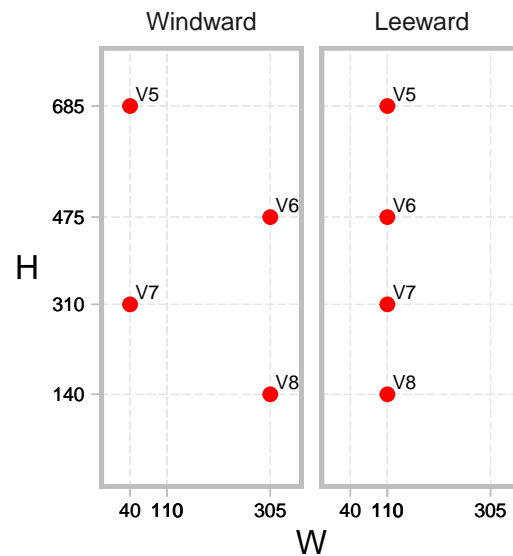


FIGURE 5.5: Elevations of openings selected in Table 5.2 showing dimensions of anemometer locations during windward and leeward tests. Dimensions were taken from inside of room facing outwards. Note: the origin (0,0) represents the south corner of the opening when considered in plan, i.e. the bottom right corners in Figure 3.20

we see energy at scales comparable to those in the boundary wind spectrum though at lower frequencies. The windward and leeward tests have different spectrum for the slot louvre with a more natural characteristic for the windward test. Both P1 and L1 cases have similar power spectra for leeward conditions with a slight variation in the slope, β , of the distribution. Figure 5.6 shows β values as a function of the local mean velocity in the opening, \bar{U}_o , at all 4 measuring locations during each test (176 values in total for 44 tests). β is calculated as the negative slope of the OLS model fit $lg(S(\omega_j)) = \beta \cdot lg(\omega_j)$ within the frequency range $0.01Hz < \omega_j < 1.0Hz$. The points representing the 4 positions in the 4 different tests in Table 5.2 are specifically highlighted. The Louvre measurements show slightly higher values for both high turbulence tests (windward) and low turbulence tests (leeward) compared with the plain opening. In general a similar pattern exists between the two different opening types, L and P, although the plain opening shows slightly flatter distributions of energy across the various opening velocities, particularly for low velocity leeward tests. The mean β for L cases is 0.534 while for P cases it is 0.481. For windward tests only these values are 0.532 and 0.473 respectively. These results are lower than published by previous researchers. However, the narrow, deep nature of the opening may also contribute to this marked change in the opening wind characteristics. The slot louvre may attenuate these

effects somewhat by deflecting the incoming air using its concave profile. While the nature of the wind seems relatively similar there is more energy in the slot louvre cases suggested by Figure 5.10. Kernel Density estimates are also shown in Figure 5.6 showing the different distributions of β depending on opening case.

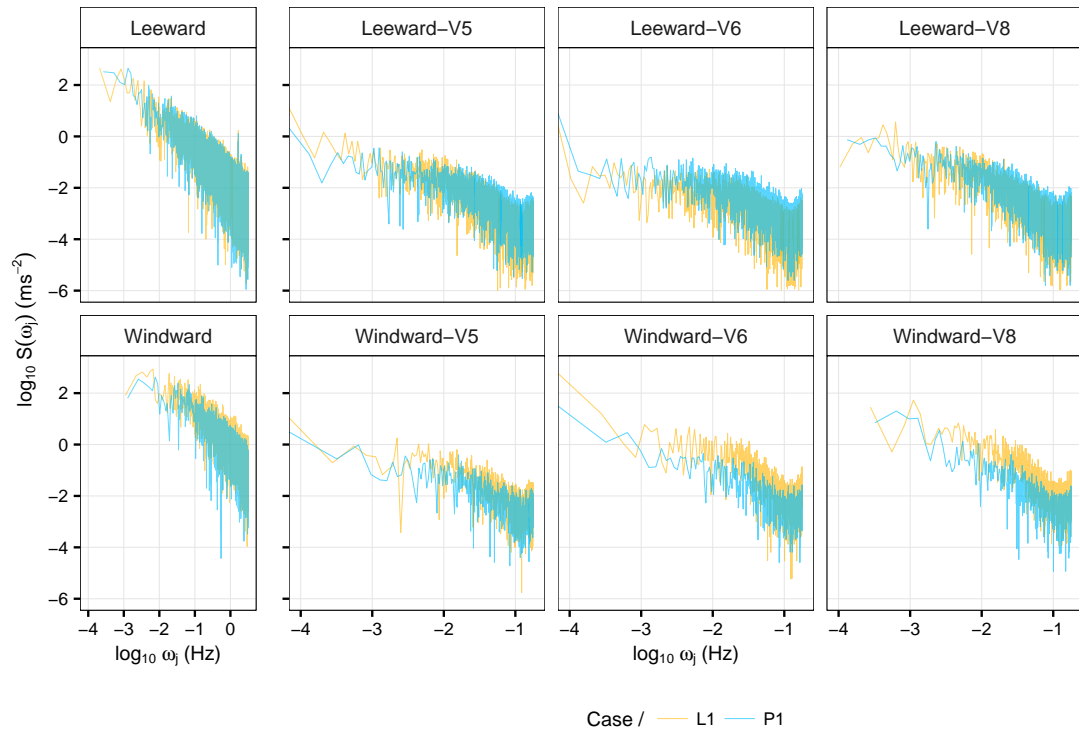


FIGURE 5.6: Power spectra for wind velocity measured at the opening for high turbulence (windward) and low turbulence (leeward) tests. Opening boundary spectra (U_l) shown to the left. Top: Comparison of spectra for leeward tests & cases L1 and P1. Bottom: Windward tests. Axes are log transformed.

5.3.4 Performance of Existing Correlations

Experimental results have shown that, with comparable overall facade opening dimensions, the slot louvre system performs comparably well to the plain opening. Existing single sided correlations have been developed from studies using either a plain opening or some form of conventional window geometry. To investigate the suitability of these correlations a comparison of some of those outlined in section 2.6, page 45, with experimental data was completed, presented in Figure 5.8. Axes are log transformed to accommodate the wide range of predictions from various correlations and 25% error range is also shown. Table 5.3 presents correlation error metrics using root mean square error (rmse), mean absolute percentage error (mape) and the standard R^2 goodness of fit value (R-sq). The Caciolo correlation uses the simplified single coefficient of $F_r = 0.025$, from Warren for windward tests and their own correlation for leeward tests. The Warren correlation, based on $F_l = 0.1$ and includes the U_l/U_r ratio as a function of $\bar{\theta}$.

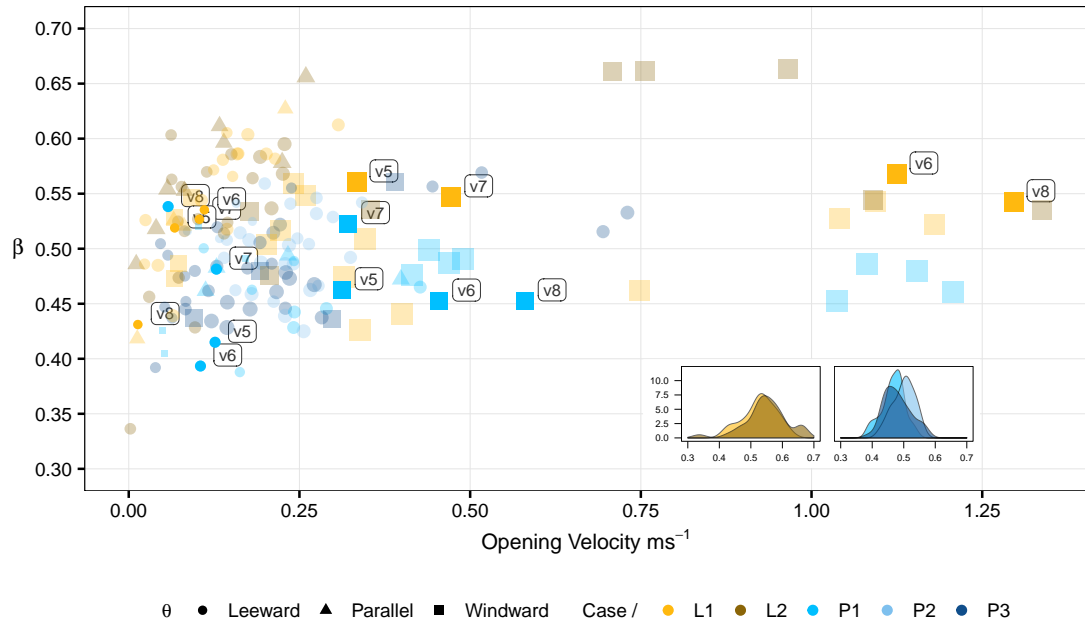


FIGURE 5.7: β for all velocity measuring positions within the opening according to mean test opening velocity categorised according to opening case tested. Size of each data point relative to mean boundary wind speed, U_i . Values used to calculate mean opening conditions in Table 5.2 coloured darker. Kernel density estimates for each case also shown

TABLE 5.3: Model metrics for existing correlations fit to measured ACR data.

Model	Louvre Cases			Plain Ope Cases		
	rmse (h^{-1})	mape (%)	R^2	rmse (h^{-1})	mape (%)	R^2
Warren	1.6	36	0.49	0.9	22	0.78
Argiriou	2.0	39	0.30	0.8	21	0.81
Larsen	1.9	39	0.33	0.9	28	0.70
Caciolo	2.0	48	0.51	1.0	43	0.81

We first consider Plain opening cases. For case P1 all correlations except Argiriou generally predicted low velocity, leeward tests within to within 25% error and provided predictions of high velocity windward tests for this case also within this range (These tests had $U_i > 4.3ms^{-1}$). All correlations under predicted P2 tests even though the level of under prediction varied. Argiriou had the lowest mape at 21% with Warren having an mape of 22% when considering all P cases combined.

We now consider Louvre opening cases. All correlations under predicted almost all the case L2 tests particularly for the high wind speed windward tests. In some cases these under predictions were substantial. For the low wind speed case L1 tests (which were predominantly leeward), except for Caciolo, correlations either predicted close to 25% or over predicted ACR. All correlations except Warren systemically under predicted windward tests. Warren had the lowest mape at 36% when considering all L cases combined and appeared to predict the L1 pattern adequately.

In general most correlations predicted the correct pattern for the P cases and for the L cases had gave large under predictions for nearly all measured ACR. Figure 5.3 suggests most tests for cases L1 & L2 are wind dominant with shear mixing the most likely mechanism driving flow attenuating pressure driven flow due to temperature differences at the opening. For Q Warren’s correlation selects the maximum value, $Q = \max [Q_w, Q_{th}]$, and therefore may not always necessarily use a correlation based on the appropriate theory. A better but less direct approach might be to consider an upper limit Ar, F_r range, beyond which a buoyancy correlation is selected. The sensitivity study in section 5.3.2 demonstrates a strong correlation with wind speed for the slot louvre for windward conditions and also for leeward conditions.

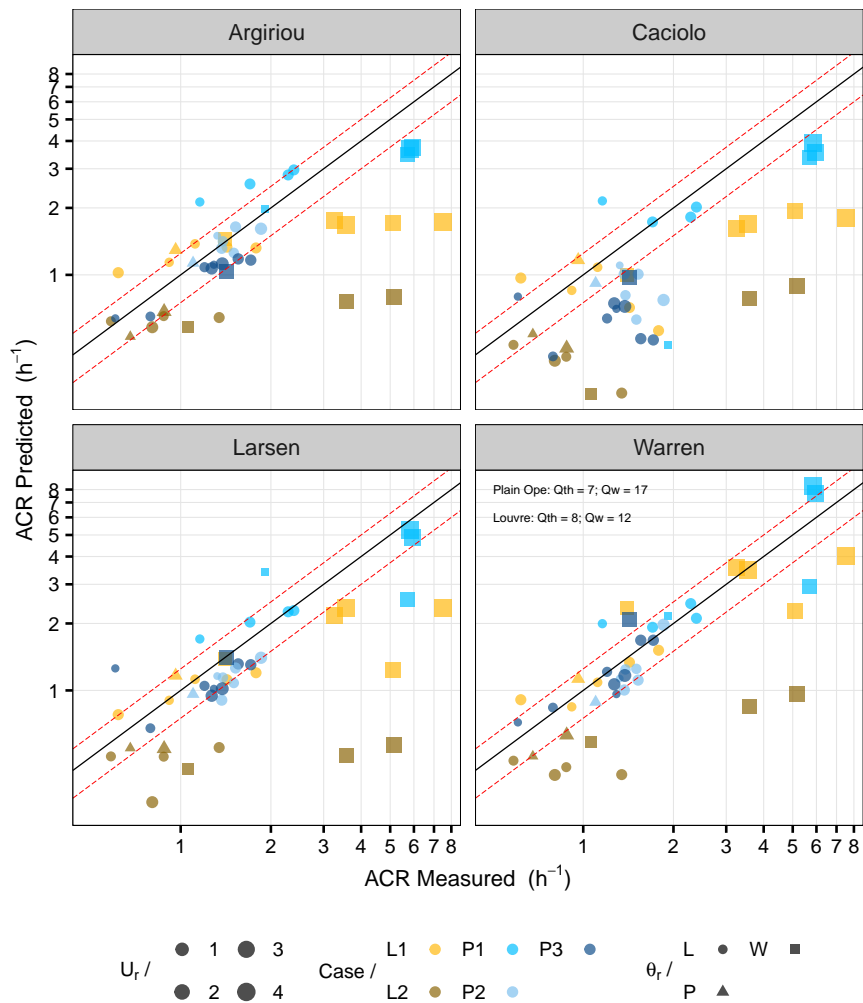


FIGURE 5.8: Comparison of existing correlations with measured ACR values for all tests. Axes are log transformed to accommodate large spread of predictions in some correlations. 25% error ranges shown as red dashed lines.

5.3.5 Discussion

The slot louvre has comparable performance to a plain opening using the same overall faade opening dimensions and has substantially improved ACR performance for comparable net free

opening area. The existing models generally predict ACR within 25% error for plain openings. With such a narrow, deep opening (see dimensions in Figure 3.20) it is reasonable to suspect the existence of a strong jet deflection into the space with the resulting effects potentially not accounted for in existing models. Hasama et al [168] showed the depth of an opening is critical in determining the extent of the jet deflection and changes to the mixing layer characteristic in shear driven flow across an opening. Using a square opening of dimension D and an opening depth ratio $0.2D$ they show the existence of a large jet deflection (case-T). Taking $D \equiv l$ for the cases presented here we have a ratio of $0.44l$ which is substantially greater than their case T. This jet deflection may produce an aeration mechanism at the opening that wasn't predicted by existing correlations. Further, as most P2 and P3 tests were leeward where an additional 3 dimensional complicated flow can develop, the models under predicted these tests. However, In general the average prediction accuracy for the P cases is similar to that demonstrated in previous studies. The concave redirecting profile of the slot louvre suggests that the jet would be guided through an angle of approximately 90° as it enters the opening. This change in the entry angle of the jet could change the relationship between inflow and outflow as well as mixing in the shear layer. To confirm this further work investigating the spatial evolution of the jet across the slot louvre is needed. Further to this there has been some research investigating the impingement of a slot jet on a curved surface, often normal to the axis of curvature. For example it has been shown by Thomann [169] that for flow over a concave surface centripetal forces can cause Taylor - Gortler vortices to develop and these can significantly increase the momentum and energy exchange near the wall. Gau [170] also demonstrated the development of Taylor-Gortler when an air jet is flowing across a concave surface. Choi et al [171] measured jet flow characteristics for impinging and wall jet for semi circular concave surfaces. When we consider the concave shape of the slot louvre and the resulting guiding of the deflected jet this may promote a more efficient mixing with the acquiescent indoor air than with the plain opening. The investigation of these phenomena is required to further verify their existence as the source of more efficient airflow exchanges at the opening with the slot louvre. Alternatively, there could also be a venturi effect contributing to increased air exchange at low incidence angles when a pressure differential is the dominant force causing an air exchange.

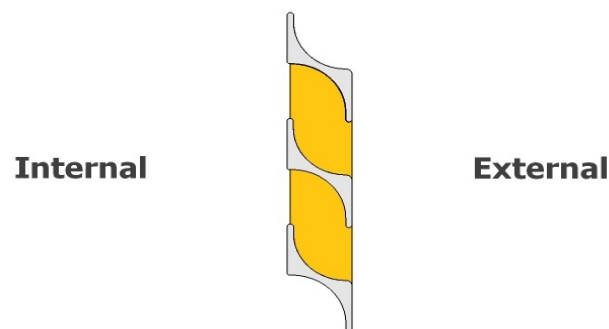


FIGURE 5.9: Section of slot louvre showing concave profile, with flow travelling normal to this profile when parallel along envelope. Airflow path shown coloured.

For the opening height considered it has been shown that the slot louvre was wind dominant under all windward conditions and some leeward conditions. The results from the sensitivity study show that, with the same candidate set of boundary parameters, equally strong correlations

TABLE 5.4: Values for F_r according to different wind directions, windward and leeward (Parallel U_r taken as leeward or windward depending on θ_r). No windward tests for P2 were recorded. Values based on combining all L cases and all P cases also shown. All values rounded to two significant digits.

Case	F_r (Windward only)	F_r (Leeward only)	F_r (All Directions)
L1	0.067	0.039	0.061
L2	0.131	0.063	0.107
P1	0.041	0.035	0.040
P2	-	0.041	-
P3	0.037	0.034	0.034
L1 & L2	0.073	0.043	0.067
P1, P2 & P3	0.040	0.036	0.039

TABLE 5.5: Change in F_r between different opening cases with comparable geometry characteristics. Wind direction used for each comparison based on available data from field study.

Cases	Comparable Geometry	% change in F_r	Wind Direction
L1 ~ P2	$A_o, (H_{o,L1} = H_{o,P2})$	-5%	Leeward
L1 ~ P3	$A_o (W_{o,L1} = W_{o,P3})$	+79%	All
L1 ~ P1	H_o, W_o	+53%	All
L2 ~ P2	H_o, W_o	+54%	Leeward

exist for both windward and leeward tests depending on whether U_l or U_r was included with ΔT . When all tests are included, U_l , U_r & θ were shown to have the strongest correlation with ACR values with a marginal decrease when ΔT was included. When using U_l or U_r alone with A_o strong correlations were still present. Consequently, to predict macroscopic wind driven ACR through these types of openings, we suggest a simplified correlation similar to Warren. Table 5.4 presents values for the dimensionless parameter F_r . These were calculated using the regression variable b_i in equation 5.1 from section 5.3.2 above to estimate F_r values setting x equal to the empirical parameter $U_r A_o$. Values are included for the plain opening cases (P1, P2 & P3) for comparison purposes (and are themselves generally in line with the findings of Warren [97] and recently discussed by Chu et al [104]). From Table 5.4 the lower limit value of 0.25 for the ratio U_l/U_r suggested by Warren may be too low for the louvre profile studied and appears highly dependant on the local surroundings.

In fact even setting this value to 0.35 for a turbulent flow field will still under predict ACR. When using U_r directly to predict ventilation rates for the slot louvre an alternative F_r value should be further considered. Table 5.5 shows that for similar overall facade aperture dimensions a 53% efficiency improvement was observed and a higher F_r value, potentially dependant on wind direction should reflect this. When all L cases are combined a value of 0.067 for F_r is observed while a value of 0.039 for P cases is observed and close to that of 0.035.

TABLE 5.6: Summary of Occupancy Temperature Data for each test configuration

Case	Max/Mean T_{occ} h_1	Max/Mean T_{occ} h_2	Max/Mean RH h_1	Max/Mean RH h_2
L1	24.4° C / 22.6° C	25.1° C / 22.6° C	63.3% / 54.9%	67.4% / 55.3%
L2	24.4° C / 23.1° C	25.0° C / 23.5° C	60.3% / 55.1%	63.8% / 55.7%
P1	23.1° C / 22.5° C	23.6° C / 22.6° C	59.7% / 55.0%	63.1% / 54.6%
P2	23.8° C / 23.1° C	24.1° C / 23.5° C	61.8% / 53.5%	60.5% / 52.3%
P3	24.4° C / 23.1° C	25.1° C / 23.7° C	61.6% / 55.6%	59.6% / 54.1%
All	24.4° C / 22.9° C	25.1° C / 23.2° C	63.3% / 55.0%	67.4% / 54.4%

5.4 Airflow Characteristics at the Occupant Location

In advance of presenting the airflow characteristics measured at the occupant location within the room during individual ACR tests we present the occupant location temperature data for tests below. This is owing to the fact that air temperature is generally accepted as being of greater importance than local air movement when considering thermal comfort. For example, the need for elevated air speeds and/or increased turbulence is generally only present when temperatures have drifted outside the upper limit threshold of the accepted thermal comfort temperature range. As discussed in Chapter 2 elevated air speeds is one way of extending the comfort range in ventilative cooling systems and this approach has been shown to facilitate indoor temperatures of up 32°C and satisfactory building inhabitants. We summarise the instrument set up at the occupant location prior to continuing the discussion.

5.4.1 Occupant location temperature data

During testing in 2014 the maximum temperatures recorded at the occupant location, Figure 3.27 page 89, are present in Table 5.6. The values in Table 5.6 demonstrate that there were no instances of air temperatures greater than 26° C in the low energy space during ACR testing. Table 3.10, page 89, shows that ambient conditions were not excessive at between 16.9° C and 18° C.

Consequently, while it appears based on these measurements that there exists no need to consider the cooling potential from enhanced characteristics of the airflow at the occupant location, recalling results from Chapter 4 and 5, it is possible to experience air temperatures of 28° C or even higher depending on the ambient conditions (for example see Figure 4.1). Two further points are worth noting here. Firstly, with the likelihood of an increasingly warm to hot climate and hotter summer periods in the future the ability to provide more effective airflow to the occupant location will be an important feature of any ventilative cooling system. Airflow enhancing components that are specifically designed with this in mind, i.e. desk fans, nozzles etc have been shown to allow substantially higher comfort temperatures in occupied spaces. Secondly, certain components facilitate strategies such as night cooling but there is a risk that they will under perform when their performance is predicted with techniques based on more common type openings, an example being the slot louver systems at zero2020. In this situation there are two performance criteria of interest; the heat removal potential, manifest in ACR values

and the conditions experienced due to secondary flows at the occupant location and whether these secondary flows are effected by the primary flow at the opening in single sided ventilation applications. Airflow guiding components such as slotted louvres with profiles similar to the concave profile in Figure 5.8 can modify the path of a primary flow and consequently effect the perception of air movement of an occupant when compared with a conventional opening. Using air movement as a strategy to extend the acceptable comfort ranges could be useful for free running buildings where there was an opportunity to generate increased presence of certain airflow characteristics.

5.4.2 Airflow Characteristics at the occupant location

To investigate the presence of either a reduction or enhancement in cooling potential from the nature of air movement from employing the slot louvre type opening, we consider air speed, turbulence intensity and airflow characteristics using the three measurement points at the occupant location, described above.

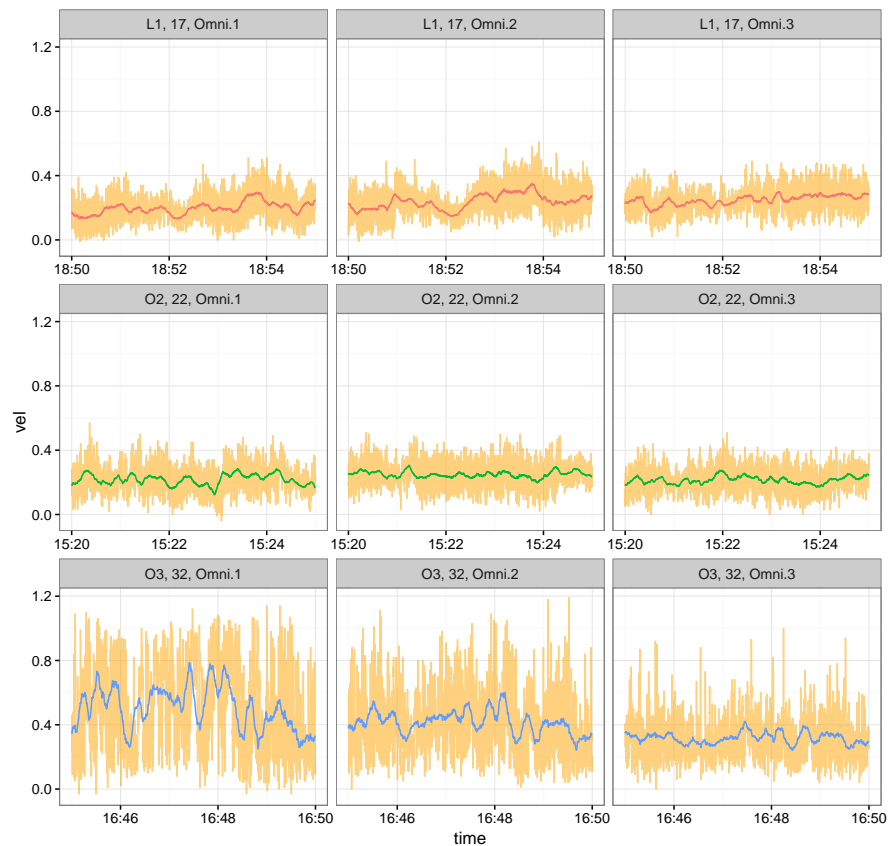


FIGURE 5.10: Time series data for velocities at the occupant location for different tests and opening cases.

Figures 5.12 and 5.13 present frequency histograms of air speed across all 44 tests categorised according to opening type, normalised depending on total number of sampled observations in each measurement data set as these varied according to test durations. The y axis presents density of values rather than counts. Using density results in a total integral of 1 for the distribution so

TABLE 5.7: Summary of Occupancy Air Speed Data for each test case

Type	Louvre (ms^{-1})			Plain (ms^{-1})		
	Mean	sd	95th	Mean	sd	95th
seated chest height	0.22	0.13	0.43	0.24	0.25	0.81
seated head height	0.23	0.12	0.42	0.23	0.21	0.65
head height standing	0.25	0.11	0.44	0.24	0.15	0.51

when using variable values much less than 1 as in our case, the y axis shows densities much higher than usual to allow for the total integral equal to 1. Table 5.7 presents descriptive statistics for air speed data across all tests according to opening type.

From Table 5.7 we can see the mean velocities for both Louvre and Plain openings are very similar in magnitude and marginally above the recommended $0.2ms^{-1}$ threshold described earlier. However there is a wider spread of data for the plain opening with much higher standard deviations demonstrating the presence of both higher and lower air speeds for the Plain opening. This is less evident for the anemometer at 1.9m, head height standing. This suggests similar conditions at this height irrespective of the opening type employed. It must be remembered that the slot louvre opening tested was only 25% of the maximum available opening area under normal operation for the system and this could lead to increased air movement for both systems. The plain opening area tested represented 50% of the opening area under normal operation with the P1 case having a POF value of 2.34%. This is a reasonable POF and while the Irish building Regulations recommend a POF of 5% Figure 5.11 from O’Sullivan et al [172] shows POF ranges from 0.5% to 8.0% with an average value of 4.0% for 12 non domestic buildings employing VC in various locations. These are case studies from IEA-EBC Annex 62. Some spaces have a POF similar to 2.34%. So while there is a 50% step back in available area due to the nature of the test procedure the resulting data is still valuable and representative of typical VC system characteristics. 95th percentile values for the Plain opening are significantly higher. This does indicate that at the height of the occupant the louvre system has narrowed the local air speed range and while the values recorded are acceptable and in line with best practice standards this is a negative consequence when attempting to use increased air velocities to extend the comfort range.

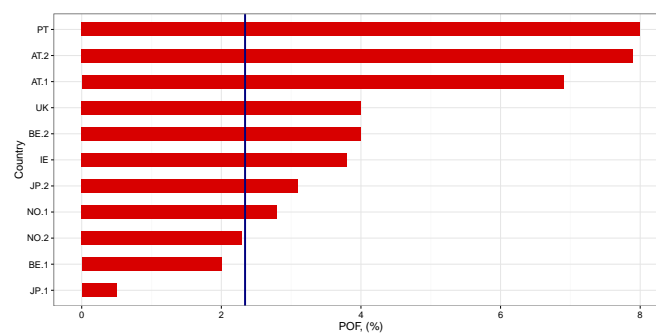


FIGURE 5.11: Percentage opening area to floor area ratio, POF, for various non domestic buildings using VC in different countries. Buildings represented are case studies from IEA-EBC Annex 62. Case P1 shown in Blue. [172]

In order to establish suitable representative distributions to reproduce air speed at the occupant location based on the empirical histograms in Figure 5.12 and 5.13 we employed the fitdist package in R [173]. More specifically a maximum likelihood estimator was used to find suitable agreement between the empirical data and the selected statistical model. In this case a Weibull distribution produced the best agreement with the data. Figure 5.14 shows empirical and theoretical density plots, Quantile-quantile plots, probability-probability plots and cumulative distribution functions for all air speed measurements from the L1 case tests. Very close agreement is observed. Similar results are visible for the L2 cases in Figure 5.15 with a pronounced skew in the right tail. This is valuable for modelling the effect air speed can have on the expected thermal comfort range in the space being served by the slot louvre ventilative cooling system and therefore can provide a probabilistic demonstration of the cooling potential for the system within the range of conditions observed during testing. Natural wind speed variation has been shown to generally fit a Weibull distribution and the results here indicate that this is also the case for internal air movement driven by natural wind.

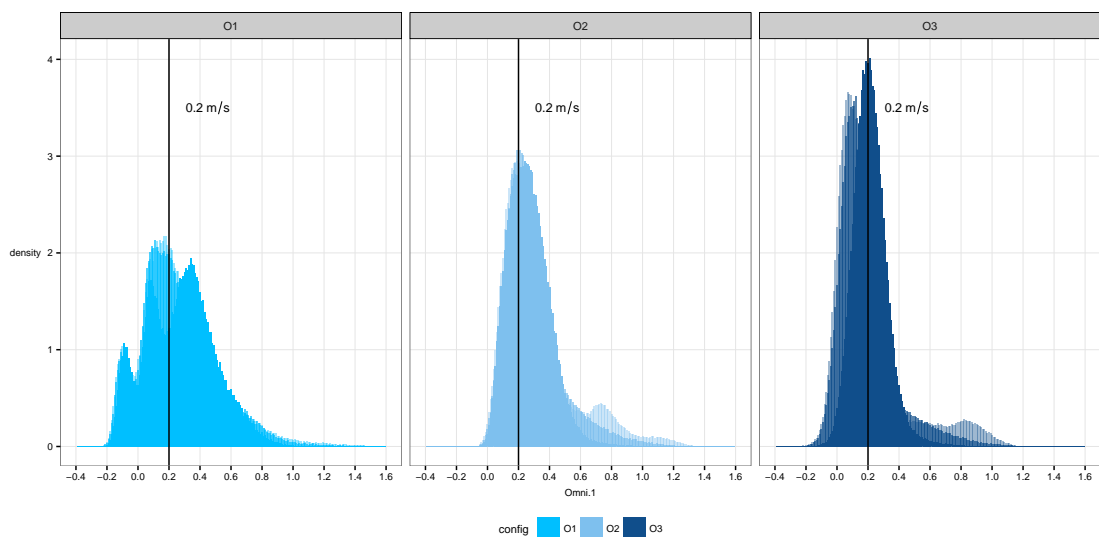


FIGURE 5.12: Histogram of all air speeds measured at all three locations for plain opening cases tested (shown as separate distributions). Each measuring location shown with gradient transparency and substantial overlapping exists for each.

Figure 5.16 presents observed turbulence intensity values for the slot louvre system and plain opening. T_i was calculated as one dimensional values using an equation similar to equation 5.2. A ten minute time interval was chosen to calculate values for two reasons; firstly to ensure stationarity in the data a sample size of 6000 (6000 samples = 10 minutes of data measurement) was chosen to ensure stability in the mean and standard deviation values for calculation purposes; secondly it was decided not to calculate an average T_i for each test based on the full data set as there were instances of slight changes in boundary conditions during some tests.

The data shows that values were generally less than 10% for all cases. Only in the Plain opening at seated chest height do we see the 3rd quartile T_i value above 10%. The SET model uses 19% in all calculations and this would be somewhat higher than the results from testing presented herein. In fact values calculated from measured data suggest the louvre system produces very low T_i in the occupied space and this may be something that needs to be taken into account given the

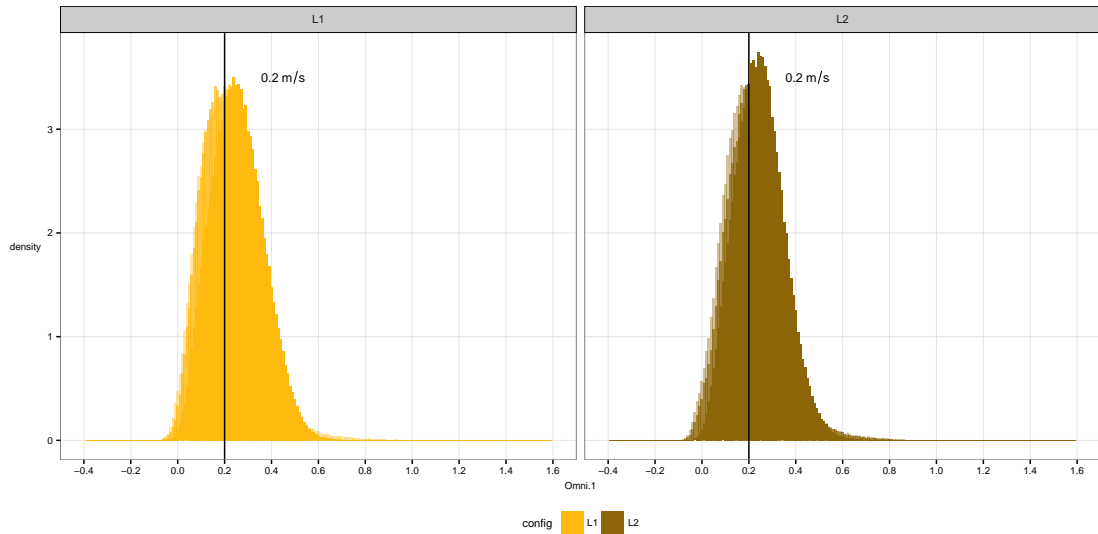


FIGURE 5.13: Histogram of all air speeds measured at all three locations for Louvre opening cases tested (shown as separate distributions). Each measuring location shown with gradient transparency and substantial overlapping exists for each.

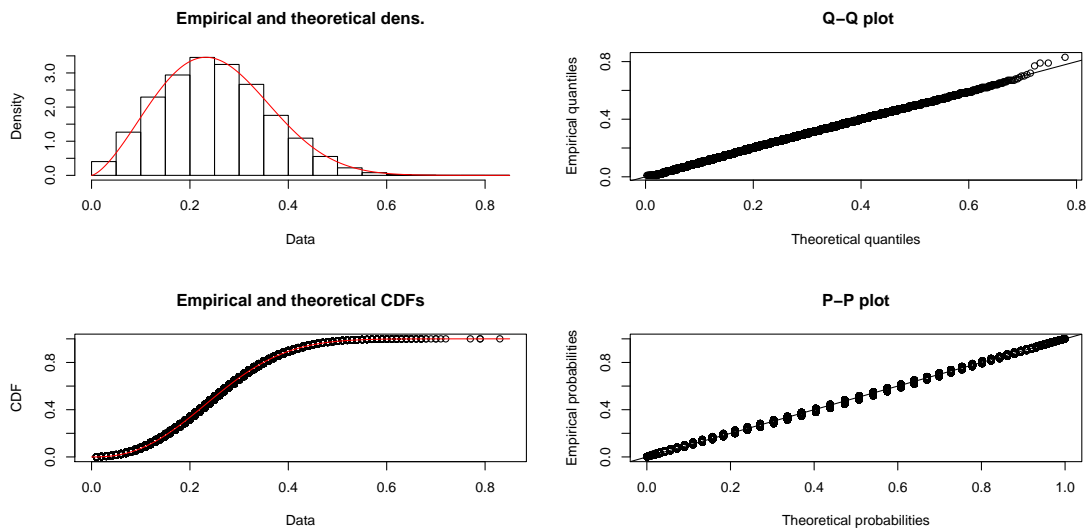


FIGURE 5.14: Empirical and theoretical density plots, Quantile-Quantile plots, probability-probability plots and cumulative distribution functions for air speed data at the occupant location during all L1 case tests.

potential implications for draught sensation when attempting to quantify the cooling perception of the system. The low values also go some way to explain anecdotal feedback from occupants in the zero2020 building that the air can feel still in the retrofit internal spaces. There is a very narrow turbulence range for the louvre type opening which suggest very stable conditions in the room. Again this may increase slightly under normal operation (tests were based on 25% available opening area). While T_i can enhance heat transfer between an occupant and their surroundings there seems to be little effect on the thermal sensation scale with an adjustment of about 0.1 [141].

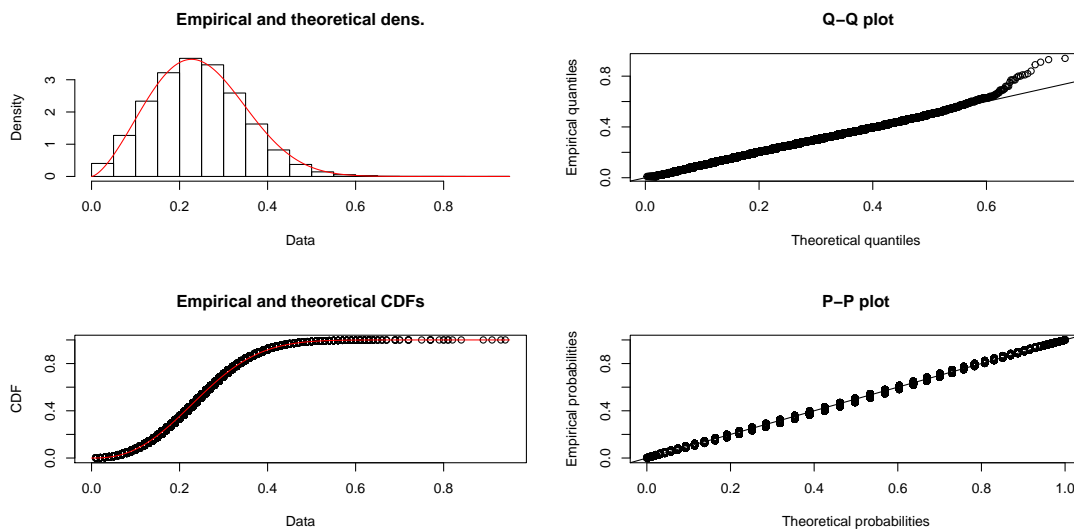


FIGURE 5.15: Empirical and theoretical density plots, Quantile-Quantile plots, probability-probability plots and cumulative distribution functions for air speed data at the occupant location during all L2 case tests.

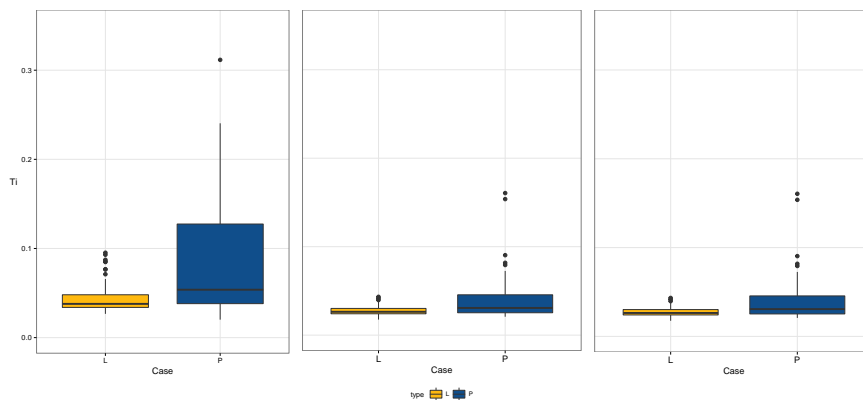


FIGURE 5.16: Box plot of 10 minute turbulence intensities calculated for all tests categorised according to case type and grouped into, from left to right; seated chest height, seated head height and standing head height.

In general it appears that it is not just the opening contributing to low turbulence levels. While a direct comparison of opening types does highlight lower turbulence levels for the slot louvre system, particularly noticeable at the seated chest and head height, there are two additional factors to consider for the low levels overall for both types. Firstly, the high thermal mass and highly decoupled interior space without any occupant or additional causal heat gains present reduces the amount of buoyancy driven air movement. Recalling Figure 4.5 page 101 we see negligible stratification in the space even at elevated ambient and internal temperatures. So this stability may prevail irrespective of opening type. Secondly single sided ventilation is a localised air exchange mechanism to a large extent and often the bulk of air in the interior space will be more or less acquiescent thus limiting the potential for enhancing local air movement through exchanges at the opening. This would be quite different with cross flow ventilation where there is a jet developed through the space transferring pressure driven momentum which may or may not pass directly through the occupant location. When considering or predicting occupancy

TABLE 5.8: Summary of Occupancy Turbulence Data for each test case

Location	Louvre (T_i)		Plain (T_i)	
	Mean	sd	Mean	sd
seated chest height	0.043	0.014	0.121	0.323
seated head height	0.037	0.008	0.197	1.090
head height standing	0.027	0.005	0.044	0.053

satisfaction with the internal environment during cooling periods consideration should be given to lower turbulence levels than those present in existing models.

Another characteristic identified in the literature as having an influence on acceptable thermal comfort ranges is the fluctuating frequency of the air and the distribution of energy across various frequencies. We can use both the power spectrum and the β ve value mentioned earlier to investigate these phenomena. However, it should be noted that the reason for considering these in the literature is primarily to extend the thermal comfort ranges to beyond what is normally deemed acceptable, namely $T_o > 28^\circ C$, and temperatures above this value were rarely seen in the retrofit testbed. Nonetheless it is worthwhile understanding whether the nature of the air movement has been modified in any way from employing the slot louvre system.

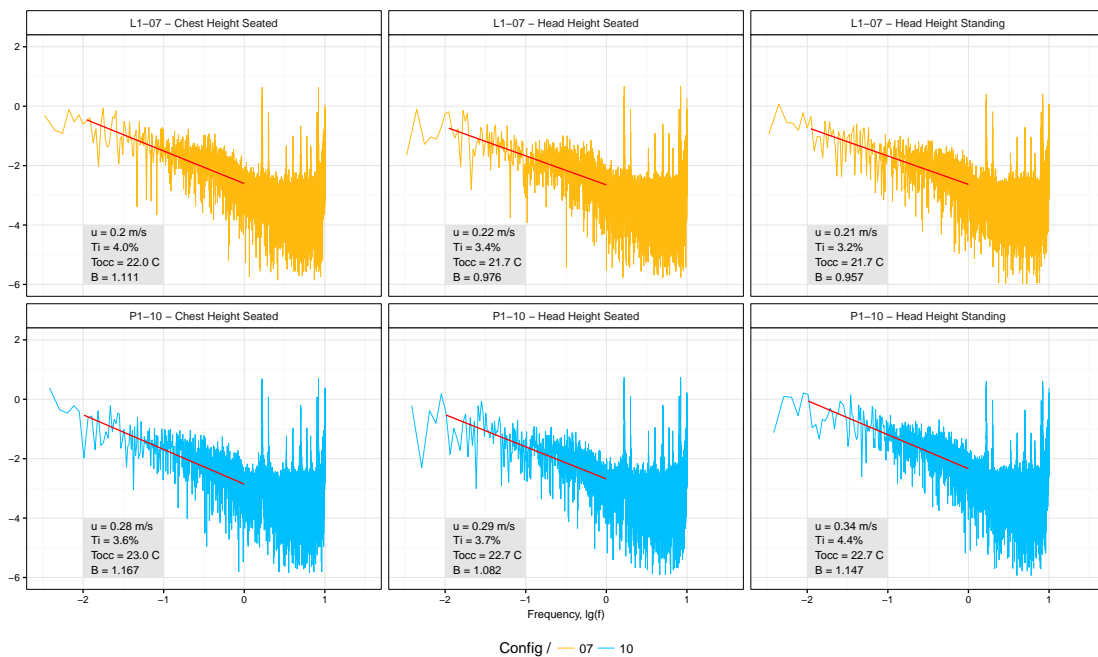


FIGURE 5.17: Power spectra for air velocity measured at the three occupancy vertical locations for **high boundary turbulence** (windward) tests (see Table 5.6). Top: Comparison of spectra for L1. Bottom: Comparison of spectra for P1. Axes are log transformed.

Figure 5.17 presents power spectra for the high boundary turbulence tests analysed earlier, (see Table 5.2 page 124). The spectra has a high concentration of power at frequencies of between 1Hz and 10Hz, though these were at low power. Human skin has been shown to be sensitive to air movement in the frequency range 0.01hz to 1hz and this range is used to investigate the wind characteristic. From investigation of the data in this range, calculating β as an indicator

(see page 138), we see that most of the values of β are between 0.8 and 1.2. These values begin to approach that of natural wind, somewhere close to the $-5/3$ scale for theoretical turbulence. There appears to be no real discernible trend between the power spectra for both opening types in Figure 5.17 and Figure 5.18. Neither have values equal to natural wind and this may or may not be associated with the opening. Given the fact that there were relatively flat spectra in the opening for the range 0.01Hz to 1.0Hz for these tests (see Figure 5.6 and 5.7), in the region of 0.45 - 0.65, the distribution of energy across all turbulence scales is spread less equally at the occupant location as the power decreases at a higher rate and more or less monotonically with increasing frequency. In the low boundary turbulence tests in Figure 5.18 the Louvre case has slightly better β values at each measuring height. Figure 5.17 shows results for high boundary turbulence tests. Similar values and distribution are present although there appears to be higher variation in power density at sequential frequencies. The standing head height (1.9m) measuring location has flatter distributions than any other in both figures. In fact these are the only power spectra that have tending towards those of the opening values (0.45 - 0.55). However, overall it seems there is little connection between the airflow at the opening and at the occupant location. The air exchanges at the opening are isolated to that part of the internal space and the flow at the occupant location should be treated as independent. This is reinforced by the minor differences in power spectra between the two dramatically different opening types. So the thermal comfort of the occupant is not directly affected by the opening type, more so by the ventilation strategy (Single Sided vs. Cross Flow) and by the heat removal potential of the ventilation system thereby reducing peak indoor temperatures. Figure 5.19 shows test data for test 17, case L1, which had one of the highest recorded mean indoor temperatures of all 44 tests completed. The literature suggests that natural wind characteristics are more favourable than mechanical characteristics when at elevated temperatures, extending the acceptability of the conditions by the occupants. Here we see values of $\beta = 1.122$ in the seated vertical height range which is approaching that of natural wind and could be perceived as favourable rather than using a mechanical device which modifies the spectrum. As stated earlier natural wind characteristics have been shown to produce higher acceptability of the internal environment at elevated temperatures and the values measured in this study. It was shown that a cooling effect was present at $28^{\circ}C$ for air movement in the frequency range 0.5 to 1.0 Hz [144]. This range is shown in Figure 5.19 with grey dashed lines. The wider "fluctuation zone" mentioned by the same researchers is shown as solid grey lines. It seems that there are power spikes at frequencies higher than these ranges in the data though the distribution is closer to natural wind than mechanical wind.

When we inspect all calculated power spectrum exponents for each height and the 44 tests (132 values) in Figure 5.20, plotted as a function of the mean air speed, \bar{u} , we see similar trends for both opening types. Mean values for each are shown with the louvre system having a slightly higher value at $\beta = 1.026$ compared with $\beta = 0.944$. There is a larger spread of \bar{u} values for the plain opening and we see a slight drop off in values of β for higher air speeds. In reality it seems there are a combination of conditions that the results could represent. At low air speeds even a weak natural wind characteristic would always have β above 1.0 and this isn't always the case here. Further testing of the louvre system in a more controlled environment is needed to investigate the relationship between air speed, β , ventilation opening geometry etc.

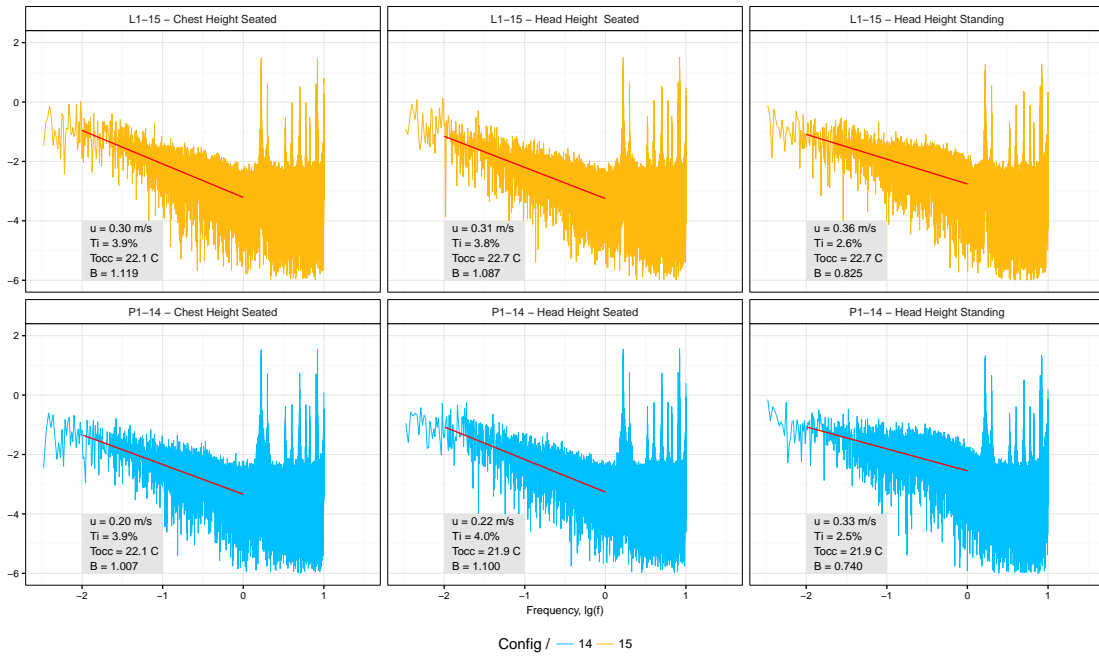


FIGURE 5.18: Power spectra for air velocity measured at the three occupancy vertical locations for **low boundary turbulence** (Leeward) tests (see Table 5.2). Top: Comparison of spectra for L1. Bottom: Comparison of spectra for P1. Axes are log transformed.

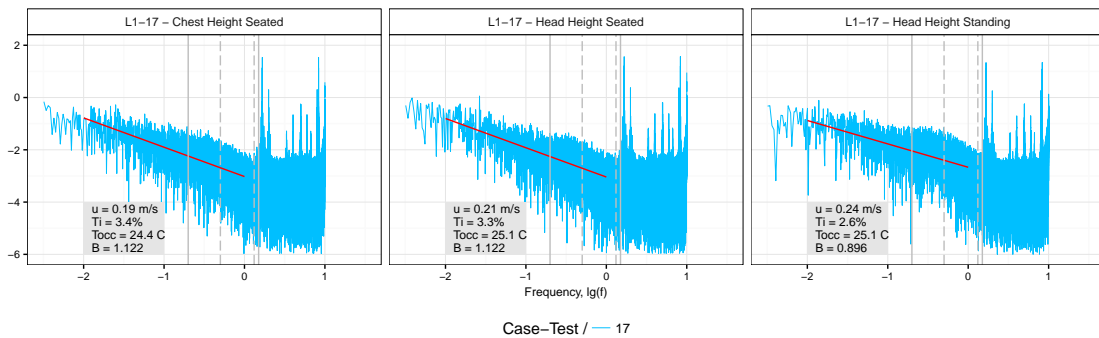


FIGURE 5.19: Power spectra for air velocity measured at the three occupancy vertical locations for **high indoor air temperature**, test No. 17 of 44. Solid grey lines show the "fluctuation zone" important to human perception while the dashed lines represent the narrow zone shown to provide cooling at elevated temperatures.

5.5 Conclusion

Predicting ACR performance is generally based on using existing semi empirical correlations developed from studies involving window devices or plain apertures. Investigating how these correlations might perform with slotted louvre devices was identified as important to determining the correct contribution to ventilative cooling from architectural louvres. As expected existing correlations better predicted ACR with the plain opening P cases compared with the slot louvre L cases. The field study has demonstrated improved dimensionless exchange rate performance for a concave profiled slot louvre when compared with a plain opening. A value in

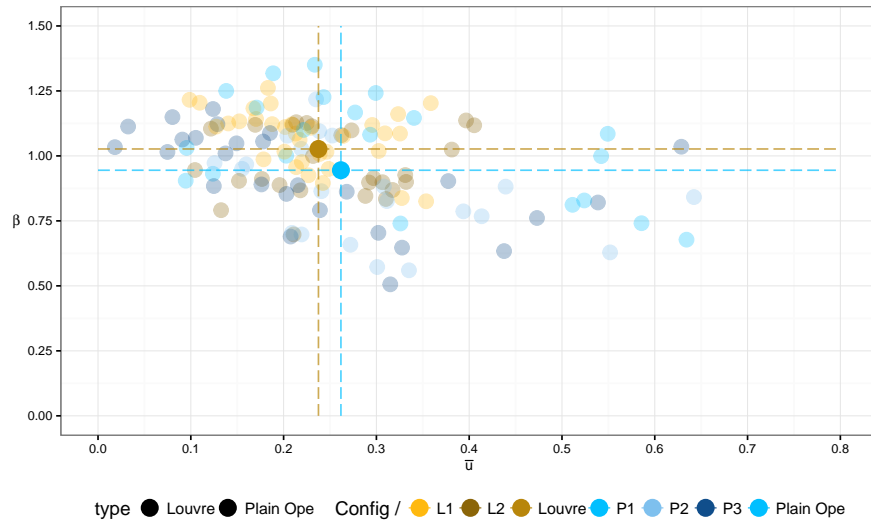


FIGURE 5.20: Beta values for room air velocities at all occupancy measuring locations. All 3 vertical heights included. Data is categorised based on test case and grouped according to opening type.

the range 0.04 - 0.07 for F_r is suggested when modelling slot louvre systems having similar characteristics though this depends on the depth and overall geometry of opening. There appears to be a clear enhancement taking place for windward tests with a modified velocity characteristic in the opening when using the slot louvre and the concave nature of the louvre profile is considered important in this regard. The improved dimensionless exchange rate performance suggests there is an increased heat removal potential with these components that should be considered when considering various purpose provided opening types for a building operating with single sided ventilation. However, they require large opening heights to achieve the desired area for adequate airflow and this should be taken into account when developing such a design. Further investigations are needed to isolate the exact phenomena contributing to the improved macroscopic ACR and F_r . Air speed data at the occupant location produced mean values broadly in line with those utilised in standards such as ASHRAE 55 and EN15251. There were instances of 95th percentile air speeds as high as 0.44 ms^{-1} , these speeds allowing a thermally acceptable environment where operative temperatures would be about 1.5K higher than the standard upper limits in EN15251 (see Figure 2.26 page 60). This demonstrates a moderate potential to extend the cooling performance of the natural ventilation system outside normal ranges. The air speed data agreed well with a Weibull distribution and this can be useful when modelling the likelihood of experiencing acceptable thermal comfort using the slot louvre system over a ranges of boundary conditions. However elevated air speeds are usually applied when operative temperatures are excessive. In a low energy retrofit such as zero2020 the observation reported herein that temperatures are unlikely to exceed 28°C suggests elevated air speeds are not as important or useful as the thermal environment is already in the acceptable comfort range at normal air speeds. Nonetheless this data can be useful for investigating how the system might perform when temperatures exceed threshold values. More data is needed for performance under 'normal operation' mode. The direct effect from specific boundary conditions on air speed at the occupant location is still unclear as correlation with measured boundary parameters and local

air speed were weak from the measurement data. Turbulence levels at the occupant location were quite low, below 5% in most instances. This can lead to reduced heat transfer between the occupant and surroundings restricting cooling effects of the ventilation system. There was no discernible difference in measurements between opening types. The low turbulence intensity values may be more related to the stable thermal environment as well as the reduced opening area used for the comparative study. Some consideration should be given to this in designing future studies as thermal comfort models such as the SET that take turbulence into account should be adjusted accordingly if turbulence is substantially lower than the 19% used. Finally, the characteristics of the air movement at the occupant location was investigated and found to be generally favourable with conditions similar, though not the same as, natural wind, a condition shown to be desirable for extending the comfort ranges. There seemed to be more opportunity for enhanced conditions for ventilative cooling at the occupant location using a plain opening with no louvre but this solution is impractical for security reasons and rain ingress during night time cooling regimes. An approach where the louvre system is automated and can be removed from the opening at times of peak cooling requirements but kept in place when high winds are present to reduce draught risk or to protect against rain and security breaches could be an interesting evolution of the current concept.

Chapter 6

Ventilative Cooling Potential of the Slot Louvre System

6.1 Introduction

In addition to the aeration performance of the slot louvre system presented in previous chapters, the heat removal potential for the system for a given climate is another important measure of a system's effectiveness in meeting the objectives of the ventilation strategy for a building. The climate cooling potential for a system requires the application of knowledge regarding the local climate, the building characteristics and, importantly, the performance of the ventilation openings. In chapter 2 it was shown how the capability of a passive ventilation system to provide cooling was linked to the limits imposed by two separate phenomena; the ambient conditions and defined internal thermal comfort range. Figure 2.6 demonstrated how the free cooling potential of a system requires the right configuration of the buildings free running temperature, the outdoor temperature and the defined upper limit temperature of the comfort range. As well as this the ventilation system must have the capacity to deliver the ventilation rate needed to remove sufficient heat from the space to ensure the threshold comfort temperature is not exceeded. Once this happens cooling is no longer possible with untreated outdoor air alone. In this chapter we assess the climate cooling potential for the slot louvre system, effectively the component cooling potential. We use an approach developed within IEA-EBC Annex 62 on Ventilative Cooling. The objective is to investigate whether or not the system can maintain acceptable internal environment throughout the full annual occupied period in the low energy retrofit space. Once the component cooling potential is known a short sensitivity analysis will be undertaken to test the limits of performance for the louvre system.

6.2 Methodology: Component Cooling Potential

For a given time interval and a defined internal finite space a net quantity of heat energy exchange with external surroundings will be observed based on the balance of various exchanges that have taken place between different energy sources and sinks. When the net quantity of heat energy is positive entering the space under observation this will result in a rise in the temperature of the air mass. Where the trend is for a continuous increase in air temperature above a certain acceptable threshold value the space is said to be in cooling mode or requiring an additional contribution to the existing energy balance to correct for this situation. When in cooling mode, internal spaces that do not employ an active mechanical cooling system to directly or indirectly bring about the reduction in air temperature instead rely on forced air movement, driven by mechanical or natural forces, from the external ambient to offset the positive heat build up in the space. Evidently the extent to which the heat energy build up can be offset depends on a number of factors:

- Ventilation strategy chosen
- Aeration potential of the ventilation component
- Boundary conditions (ambient temperature, wind speed and direction)
- Target indoor environment (indoor temperature)

The key to understanding the potential of a ventilation system to provide cooling requires knowledge about the local climate, performance characteristics of the component and its use in a given strategy as well as the target indoor conditions that are acceptable for occupants. The proposed approach to investigating the component ventilative cooling potential of the slot louvre system will be to employ information from the first three of these areas, along with any predefined constraints, and combine with knowledge of the cooling energy required to maintain the target indoor environment.

Information about the space where experimental measurements were completed will be used to quantify ventilative cooling requirements. To estimate the climate cooling potential the approach proposed by Belleri et al [174] at EURAC Research as part of IEA-EBC Annex 62 Subtask A has been adopted. This method, described in Appendix B, calculates a ventilation rate required in order to maintain acceptable indoor conditions based on an hourly time step throughout the annual occupied period. Subsequently, the predicted ventilation rate for the slot louvre system is then calculated using the empirical data generated from the work presented in previous chapters. These two ACR values are then compared to quantify the ability of the system to provide sufficient ventilative cooling potential.

Using this method allows an evaluation of the climate potential for a given building configuration. However it does not investigate whether the calculated enhanced VC mass flowrate, \dot{m}_{vc} , is actually achievable given the performance data associated with the ventilation strategy and system/components. To do this an additional step needs to be included that takes the same boundary conditions as those used to estimate the enhanced VC flowrate, \dot{m}_{vc} but calculates

the flowrate based on the ventilation system/component characteristics as opposed to the energy balance requirement to maintain the upper limit temperature in the comfort range.

To estimate the predicted ACR value for the slot louvre system at a given time step, t , for comparing with the required ACR value for ventilative cooling we employ correlations based on the experimental work presented in previous chapters. The slot louvre system has three different operating configurations and these will be treated separately below given their different characteristics. The aim is to estimate a predicted ACR value using the same boundary conditions used in the assessment of VC potential available from the chosen weather file, combining these ambient boundary conditions with the indoor temperature values determined from the criteria of the adaptive thermal comfort model, outlined in the previous section. The ventilation rates possible from each configuration will then be compared with those required from the ventilative cooling potential exercise. This will allow an adjusted climate cooling potential for the system incorporating the limits effects of the ventilation component performance. This can be said to represent the component cooling potential for a given set of climate conditions.

Once both the required ACR from the VC analysis, henceforth denoted N_{re} , and the predicted component ACR from the correlations above, referred to as N_{pr} , have been calculated for each time step these are compared to establish the potential of the ventilation system to deliver sufficient cooling to maintain acceptable indoor environment.

6.2.1 ACR for RS.02

The experimental measurements and analysis presented in chapter 5 focused on a single opening of configuration RS.02 (see Table 3.5). The results of the dimensionless analysis demonstrated a strong wind dominance (Figure 5.3) for the low level opening. A correlation based on wind forces will be adopted for this configuration. The Warren Correlation from 1985, reproduced below:

$$Q_w = F_l \cdot A_o \left(\frac{U_l}{U_r} \right)_\theta U_r \quad (6.1)$$

This is modified by adopting a value of 0.1 for F_l and applying a value for the $\frac{U_l}{U_r}$ ratio as follows:

$$\frac{U_l}{U_r} = \begin{cases} 0.39 & \text{if } 0^\circ \leq \theta_r \leq 180^\circ, \\ 0.67 & \text{if } 180^\circ \leq \theta_r \leq 360^\circ \end{cases} \quad (6.2)$$

This results in the following formulae for RS.02. For Windward boundary conditions:

$$Q_w = 0.067 \cdot A_o \cdot U_r \quad (6.3)$$

For Leeward boundary conditions:

$$Q_w = 0.039 \cdot A_o \cdot U_r \quad (6.4)$$

These empirical correlations were developed using the measurement dataset from 2014 testing in chapter 5. To test their performance in predicting measurements outside the training data set we use the 2013 test data for RS.02 (results from chapter 4 for RS.02). Using the correlations above to predict ACR along with the boundary data and opening dimensions for the six 2013 RS.02 tests we found a mape value of 26.5% when compared with the experimental measurements. While this value was not within the $\pm 20\%$ range of RS.04 (see below) it is deemed acceptable for the purposes of evaluation of the component cooling potential.

6.2.2 ACR for RS.04

Figure 4.12 shows from the dimensionless analysis that all tests with RS.04 were broadly in the asymptotic range for flow due to buoyancy alone, F_b . This suggests a strong buoyancy force is present with the large opening height for this configuration. We used equation 6.5 to investigate its suitability for predicting the measured airflow rates for RS.04 during 2013 testing. This is based on the inference that the flow is largely buoyancy driven. The equation, shown below, also includes the empirical coefficient, the discharge coefficient, C_d , to account for installation effects.

$$Q_{th} = \frac{1}{3} C_d A_o \left(\frac{gh \Delta T_{ie}}{T} \right)^{0.5} \quad (6.5)$$

Using a C_d value of 0.55 a mape of 18.7% was obtained when comparing the predicted ACR with the experimental measurements in 2013. When we used a wind driven model the mape value was substantially higher at 68.9%. This shows that the opening is very likely driven primarily by buoyancy forces and the most suitable correlation is one that uses the thermal boundary conditions to estimate the ventilation rates. Further, it appears that the louvre has little effect on the strength of the buoyancy driven ventilation rate with the existing correlation predicting reasonably well. A slightly lower C_d value compared with the commonly applied value of 0.61 is required to achieve this result. Above a certain height wind forces, while still present, appear to have a diminished effect. It would be difficult to use an opening height of 1.6m with a plain opening as this would cause undesirable effects relating to draughts, internal air movement amongst others. Further without the louvre in place, which effectively creates a collection of smaller slotted openings, the opening would be classed as a large opening and the variation in pressure across the height would make it unsuitable for analysis using a correlation based on Bernoulli theory.

6.2.3 ACR for RS.03

Based on the results in figure 4.12 for RS.03 the dominant force is not as readily apparent as was the case for RS.02 or RS.04. There is a positive contribution from the wind it seems, irrespective

of wind direction, although the opening isn't exclusively wind dominant as was the case with RS.02. The increased height of the opening location above the finished internal floor level is the most acute difference in the openings. Understandably the higher the opening the more likely there is to be a contribution from buoyancy effects. Figure 4.12 adopts a lower C_d value for RS.03. This is based on the literature review summarised in section 4.2.4.2. There appeared to be a more complicated effect taking place at the opening in part due to the lower opening height, which would suggest more opportunity for wind shear to develop across the opening, in part due to the elevated location of the opening within the room, potentially modifying the buoyancy driven effects and also the nature of the restricted opening angle of the ventilated door inside the louvre which remained in place during 2013 testing.

Considering Figure 4.5 there is around 1K difference in the vertical temperature distribution in each test for RS.03 between the occupancy height (the location for RS.02 approximately) and the full height, the location of RS.03 approximately. This would suggest a similar envelope temperature difference across RS.03 and RS.02. However, the mean STR value for RS.02 tests was 0.48 and for RS.03 the mean was 0.80, showing a variation in the stratified internal air which could suggest stronger buoyancy forces. The sample sizes were somewhat smaller than other measurements, six tests each in 2013. This may mean only limited knowledge regarding the pattern of interactions driving ventilation rates can be drawn from these tests.

We tested correlations based exclusively on wind and exclusively on buoyancy for RS.03. We used the correlations proposed for RS.02 to estimate the measured ACR values from 2013. We found a mape value of 29.7% for the buoyancy correlation in equation 6.13. This was based on a C_d value of 0.69. When we used the wind driven correlations in equations 6.3 and 6.4 we obtained a mape value of 84%. While 29.7% is not within the desirable range of $\pm 20\%$ it is a much improved estimate when compared with the wind driven correlation. In fact if we were to reproduce the Warren plot in Figure 4.10 with a C_d value of 0.7 for RS.03 this would suggest a more buoyancy dominant condition for the high level opening. For this reason we have chosen the buoyancy driven correlation for use in estimating the predicted ACR value for configuration RS.03.

6.3 Results

6.3.1 Model Inputs

We use the data from Table 6.1 and 6.2 as input data for estimating the climate cooling potential of the test space. The table formats are reproduced from the IEA-EBC Annex 62 Ventilative Cooling Potential Analysis tool. For weather data we use a TMY3 format generated from Meteonorm. For boundary conditions, hourly temperature data is taken from the 1961 - 1990 period and solar radiation data is taken from 1990 - 2009.

The occupancy profile for the office was taken as being from 09:00 to 17:00 each day with 1 hour of non occupancy from 13:00 to 14:00. Weekends have currently been included in the study. This profile was applied to lighting heat gains, equipment heat gains and occupancy heat gains. This

TABLE 6.1: Location and Building data

Parameter	Input	Units
City	Cork	-
Country	Ireland	-
Latitude	51.53077	°
Longitude	8.33	°
Time Zone (with respect to GMT)	0	hr
Building Type	Office	-
Ceiling to Floor Height	3.32	<i>m</i>
Envelope Area	18.05	<i>m</i> ²
Floor Area	10	<i>m</i> ²
fenestration Area	2.56	<i>m</i> ²
Fenestration Orientation	West	-
Comfort Requirement	Cat II	-

TABLE 6.2: Technical Specifications

Parameter	Input	Units
U-Value of the opaque envelope	0.10	<i>Wm</i> ⁻² <i>K</i> ⁻¹
U-Value of the fenestration	1.09	<i>Wm</i> ⁻² <i>K</i> ⁻¹
g value of the glazing system	0.517	-
shading control setpoint	50	<i>Wm</i> ⁻²
Min required ventilation rate	1	<i>l</i> <i>s</i> ⁻¹ <i>m</i> ⁻²
Lighting power density	11	<i>Wm</i> ⁻²
Electrical Equipment power density	10.20	<i>Wm</i> ⁻²
Occupancy Density	10	<i>m</i> ² <i>p</i> ⁻¹

meant that the ventilative cooling potential has only been assessed during these hours. Outside these hours no ventilation is in operation. This is a simplified approach and does not incorporate the contribution from night time cooling. As N_{re} for ventilative cooling is estimated based on no night time cooling availability this facilitates a demonstration of the potential performance of the system. Night time cooling can be incorporated at a later date although this requires the correct modelling of thermal mass within the space to correctly quantify its contribution to reducing indoor temperatures at the beginning of the following day.

6.3.2 Climate VC potential

The output from the IEA-EBC annex 62 VC potential analysis tool is a summary of the number of hours in each month where each of the three modes are required. A theoretical explanation of each mode is provided in Appendix B, however each mode can be approximately summarised as:

$$VC \text{ mode} = \begin{cases} 0 & \text{Heating only, no VC} \\ 1 & \text{VC with minimum IAQ airflow rate only} \\ 2 & \text{VC with enhanced airflow rate required} \\ 3 & \text{No VC possible} \end{cases} \quad (6.6)$$

Figure 6.1 below summarises the extent of hours in each month that enhanced ventilation rates above the minimum for IAQ purposes is required, calculated based on mode 2 in equation 6.8.

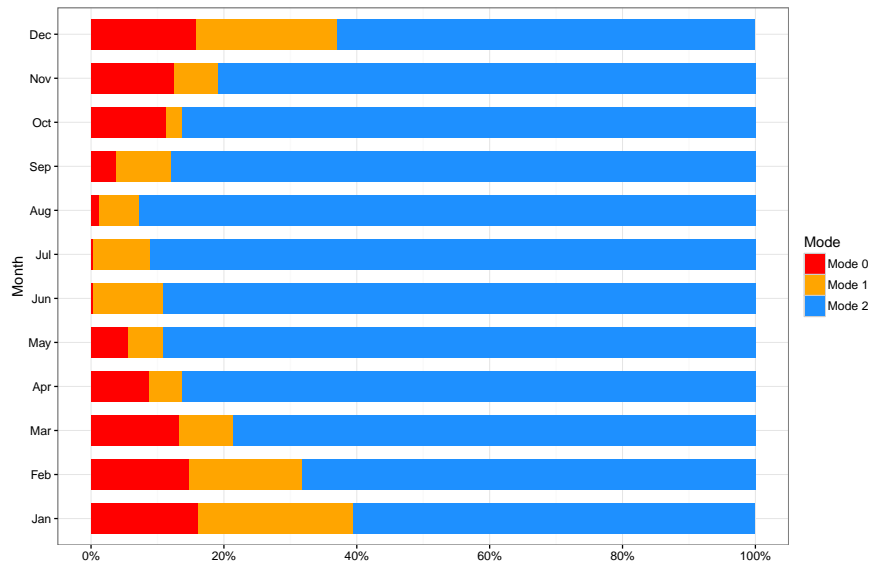


FIGURE 6.1: Percentage split for various ventilative cooling operating modes for each individual month

The monthly distribution shows that VC above that provided from the minimum ACR for IAQ purposes, mode 1, is required consistently throughout the whole year. For 60% of the occupied hours during January N_{re} values were greater than the IAQ requirement, based on 12 l s^{-1} . This percentage increases to over 90% of the occupied hours during August, which is not surprising given the minimum ACR is not intended to satisfy thermal comfort and only for addressing basic air quality requirements. Figure 6.2 shows the total annual breakdown in percentage of occupied hours. Over 82% of the annual time enhanced ACR for VC values are needed. A review of the profile of N_{re} from the VC analysis is completed in the next section. N_{re} values are compared with N_{pr} values using the same boundary conditions and building configuration, calculated from the proposed correlations for estimating ACR values in section 6.2.2 above.

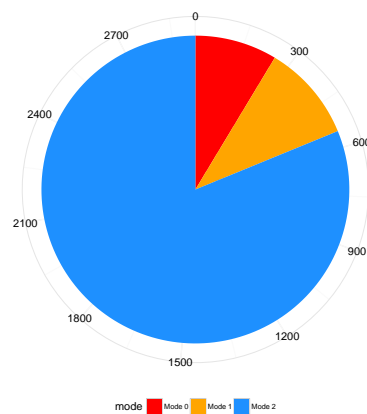


FIGURE 6.2: Percentage split for various ventilative cooling operating modes for annual occupied hours

6.3.3 ACR Profiles: Required and Predicted

The preceding section summarised the climate cooling potential for the zero2020 office space in Cork, Ireland. However, for single sided strategies, the ability of the chosen component and opening type to deliver N_{re} values to successfully provide sufficient ventilative cooling is not addressed within the existing scope of the Annex 62 VC tool. This is an important criterion ensuring the results from the analysis are within the practical limits of the chosen ventilation strategy, system and constituent components. Separate semi-empirical correlations are adopted for each configuration in the slot louvre system, summarised in sections 6.2.1 to 6.2.3. These correlations were used to calculate N_{pr} using each configuration at each of the 2920 hourly time steps in the boundary conditions weather file. These were then individually compared to N_{re} to establish whether or not the configuration can deliver the required ACR value. A discrete binary state system of $[0, 1]$ was adopted when testing whether N_{pr} satisfied N_{re} , 1 when the condition was met, 0 when it wasn't. This allowed a mapping of component cooling potential across the full interval range of 2920 hours for each configuration effectively allowing a matching process to take place, selecting the most suitable opening type. Evidently in some cases more than one configuration satisfied the value of N_{re} .

Recently, a thermal comfort study completed at the zero2020 testbed was published. It investigated both objectively and subjectively the mean thermal sensation vote for study participants for all three of the configurations listed in Table 3.5 and sections 6.2.1 to 6.2.3. It found that there was a risk of over-cooling and occupant dissatisfaction with the internal thermal environment when RS.04, full height opening, was employed with ambient temperatures of $12^{\circ}C$ [72]. For this reason we have limited the availability of RS.04 to time periods when the external ambient temperature is above $12^{\circ}C$. This reduces its availability during winter and shoulder seasons though the ACR values during some of these periods were unrealistically high given the high ΔT across the envelope. In many of these instances N_{pr} was excessively high and didn't match N_{re} in a practical way.

6.3.3.1 Required ACR values, N_{re}

Distributions for N_{re} are presented for each month in Figure 6.3. These values represent what capacity is required to maintain an acceptable indoor thermal environment year round through the use of ventilative cooling principles alone. There is a clear trend in the changing shape of the distribution from January into July. This morphological change then reverses itself again from August to December. Based on the shape of the distribution the traditional winter heating range of October to April has probably reduced further here given the increasing requirement for ventilation to offset cooling. It is plausible to suggest that the appearance of more than 20% of ACR values greater than 4 ACH during occupied periods in April highlights the presence of a substantial cooling requirement. October has N_{re} values of 3.5 for more than 20% of the occupied time. This 20% upper range drops to 3 ACH in March and November. June, July and August have noticeably flatter distribution, more closely approximating a Gaussian distribution with a left skew. Conversely, May and September have similar distributions with lower mean and standard deviations. Table 6.3 presents descriptive statistics for each month. Each of the

distributions in figure 6.3 display increasingly narrow profiles diametrically from July with the largest standard deviation in July at 1.65. Figure 6.4 plots the 12 monthly mean values for N_{re} , as a function of time, with monthly intervals. The plot also includes a normal distribution with the same mean and standard deviation, effectively the probability distribution of annual N_{re} values. The mean and standard deviation for the whole year are shown in Table 6.3. A mean N_{re} value of 2.7 ACH is required along with a standard deviation of 1.50. These values in themselves are useful for profiling different configurations of building and climate. However, they do not help in determining whether a particular system configuration, (principles, strategy, components etc) will be capable of providing the required airflow rates to offset heat gain contributions while maintaining conditions within the thermal comfort range. It is insufficient to only ensure the mean and spread of airflow rates are satisfied. The provision of a given airflow rate at the required time is understandably what will establish whether the conditions remain within the thermal comfort range at all times. To do this a comparison of hourly values better ascertains whether a ventilation solution meets the requirements of the analysis above.

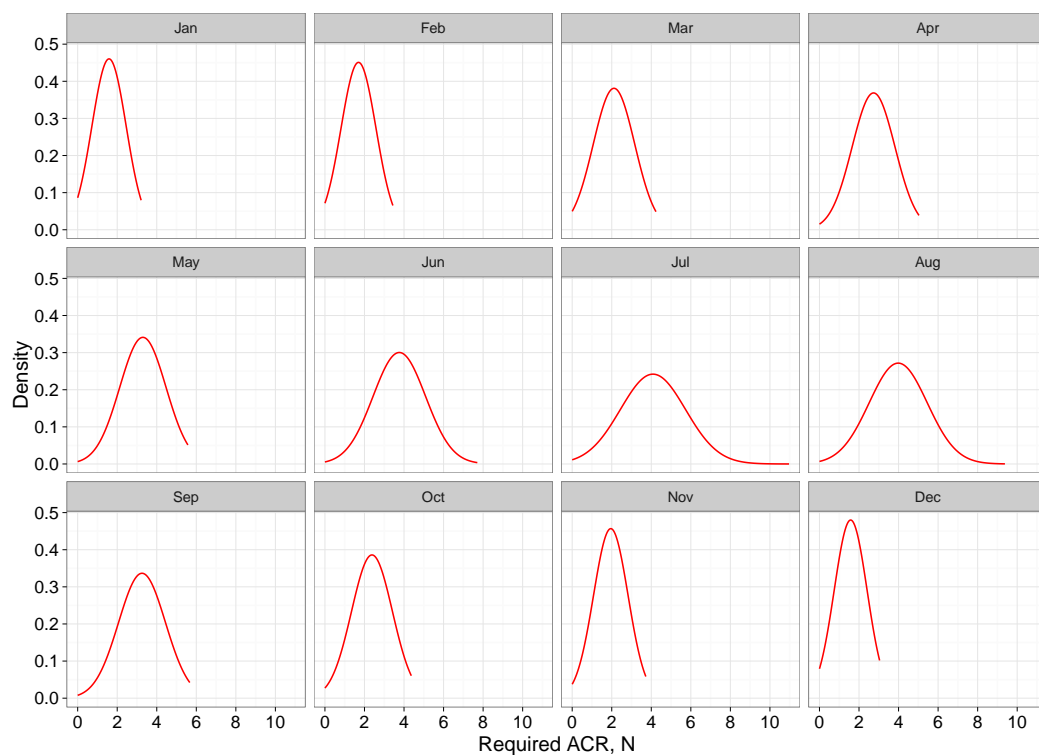


FIGURE 6.3: N_{re} probability distributions for 12 months based on results from equation 6.7 in VC Potential analysis tool. (converted from mass flowrate to ACR)

The next section addresses this comparison by investigating at each time step which slot louvre configuration meets the required ACR and can therefore provide sufficient cooling to the internal space throughout the occupied period.

6.3.3.2 Predicted ACR values, N_{pr}

Figure 6.5 includes four separate distributions. These are developed based on the data for each of the three possible configurations, RS.02, RS.03 & RS.04 along with the normal distribution in

TABLE 6.3: Summary statistics of N_{re} (VC mode 2, see equation B.8) for each month individually calculated using equation B.7 in the VC potential analysis tool

Month	Mean	SD	Max
Jan	1.6	0.87	3.2
Feb	1.7	0.88	3.5
Mar	2.1	1.05	4.2
Apr	2.7	1.08	5.1
May	3.3	1.17	5.6
Jun	3.8	1.33	7.7
Jul	4.1	1.65	11.0
Aug	4.0	1.47	9.4
Sep	3.3	1.19	5.7
Oct	2.4	1.03	4.4
Nov	2.0	0.87	3.7
Dec	1.6	0.83	3.0
Annual	2.7	1.50	11.0

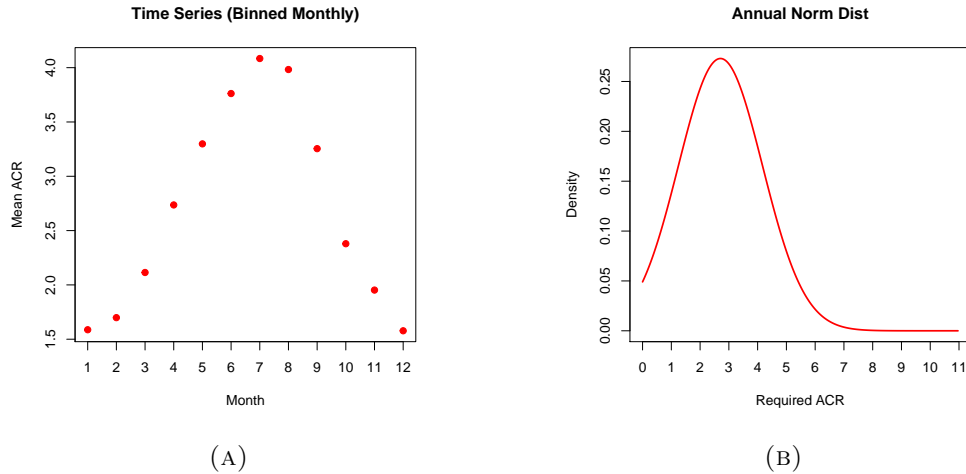
FIGURE 6.4: Mean monthly required ACR values, $\hat{N}_{re}(i)$ for month i including all 12 months in the annual calendar, (A) Mean monthly ACR, (B) Annual normal distribution for \hat{N}_{re}

Figure 6.4(B) which represents the annual distribution of N_{re} . While the distributions are idealisations of real data, effectively Gaussian representations of the discrete data, they nonetheless provide a convenient tool for studying the probable range of values taking moments equal to those derived from the real data. At any point where one of the three slot louvre system distributions, each a separate distribution of N_{pr} , shaded in blue, does not incorporate the N_{re} distribution, coloured in red, then the ventilative cooling system cannot deliver the entire number of counts for N_{re} at that value. Supplementary cooling is required for this part of the distribution. As previously mentioned, a thermal comfort study completed at the building for the system demonstrated a real risk of over-cooling when using RS.04 when it was $12^{\circ}C$ outside, even though the internal air temperature, T_i , was $25^{\circ}C$. For this reason a restriction was adopted where RS.04 was only available when $T_e \geq 13^{\circ}C$.

We see from the adjusted distribution for RS.04 a more realistic range of N_{pr} values available for offsetting cooling demand at times when there is a cooling need, i.e., without the inclusion of

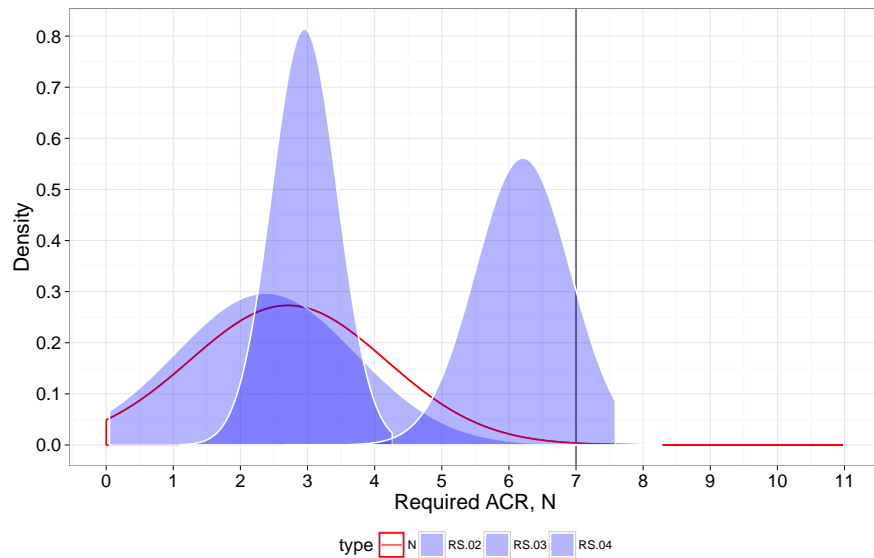


FIGURE 6.5: mean monthly required ACR values, \hat{N}_i for month i including all months in the annual calendar

ACR values during periods where there was a risk of over-cooling due to the combination of flow rates and temperature of the air used for aeration of the space. RS.02 has a shape that most closely resembles that of N_{re} . RS.02 is a manual occupancy level opening and its ACR values are calculated using a wind driven correlation. It can satisfy the requirements for ventilative cooling entirely until about 3 ACH is required. Beyond this, depending on N_{re} , somewhere between about 15% and 40% of the time RS.02 cannot meet the demand. RS.03 has the narrowest distribution with many of the available ACR values in the range 2 to 4 ACH. However, beyond around 3.7 ACH almost 100% of the time that an ACR value of greater than 3.7 ACH is needed RS.03 is unable to meet the demand. Above 4.8 ACH RS.04 can provide 100% of N_{re} . When we consider June, July and August in isolation (as these are the peak cooling periods) RS.04 has an ACR value greater than 7 ACH for only 9% of the occupied hours, has an ACR value of greater than 5 for 89% of the occupied hours and has a mean ACR value of 6.1 ACH. Revisiting Figure 4.7 and Table 4.5 (page 105) RS.04 was measured as having a mean of 3.8 ACH and a maximum of 5.8 ACH. This would suggest ACR values lower than those predicted, even though an mape of 18.9% was achieved using the correlation selected for this study. However, even if the values are somewhat lower, the comparison of distributions show that there is potential in the system to provide the required flow rates, given differing boundary conditions. The challenge seems to be delivering these at the time in which they are needed, i.e. at certain limited times a mismatch exists between when a given flow rate is required and when it is actually available based on the performance and capacity of the opening.

6.4 Analysis

With the combination of all three configurations it is clear that only a narrow range of incompatibility exists. Was the system to rely on any of the individual configurations in isolation,

there would be both under-cooling issues and over-cooling issues depending on the configuration selected and time of year.

6.4.1 ACR profile matching, N_{re} vs N_{pr}

As discussed previously, to identify the specific times of the annual occupied hours where each configuration can meet the demand a comparison for each hour was made between N_{re} and N_{pr} . Figures 6.6 to 6.8 show the results of this comparative analysis for each of the three configurations. Each figure contains three plots, plotting time of day as a function of day of the year, in three different 4 month periods (Jan-Apr, May-Aug, Sep-Dec), one period for each Figure. The coloured tiles represent whether a given condition is met or otherwise. A grey tile means N_{pr} for the particular configuration (RS.02, RS.03 or RS.04) is less than N_{re} for that hour. An orange tile means the N_{pr} for the particular configuration meets N_{re} for VC. Finally, a red tile shows hours that no configuration was able to meet N_{re} and therefore presents a limitation of the system.

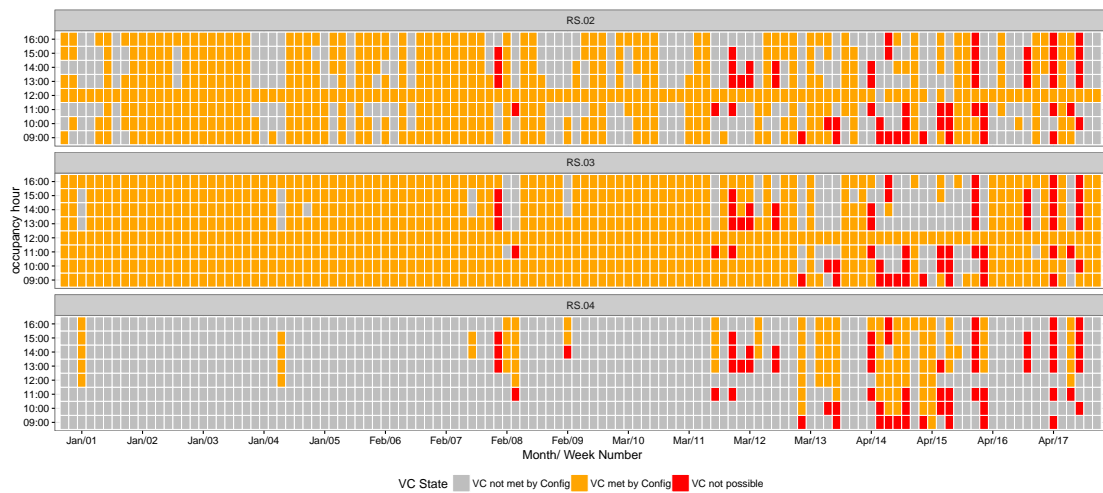


FIGURE 6.6: Ventilative Cooling State for January to April

From January to April RS.03 appears to meet the criteria in many instances until the last week in March where there is a period of about 3 weeks where N_{re} values are not met for both morning and evening. During this period RS.04 can offset some of the demand. In almost every instance from January until March RS.04 also provides the required ACR when RS.03 cannot. RS.02 can provide N_{re} during this period for many of the same hours as RS.03 and is complimentary in that, at certain times, it provides N_{re} when RS.03 cannot. RS.04 has only a limited potential during these months given the constraints to its availability based on the risk of over-cooling. There are only a minor number of instances where N_{re} is in-sufficient. Even in these instances there is still an ACR available that can provide cooling and although this would result in an indoor temperature beyond the upper thermal comfort limit, it does not mean no cooling could take place during this period (the plots have a binary condition; 1 if N_{re} meets N_{pr} and 0 if not. However, even when it does not meet N_{pr} , which is the ACR required to maintain the space at the upper thermal comfort limit, an airflow rate is still available). However, as we are mapping

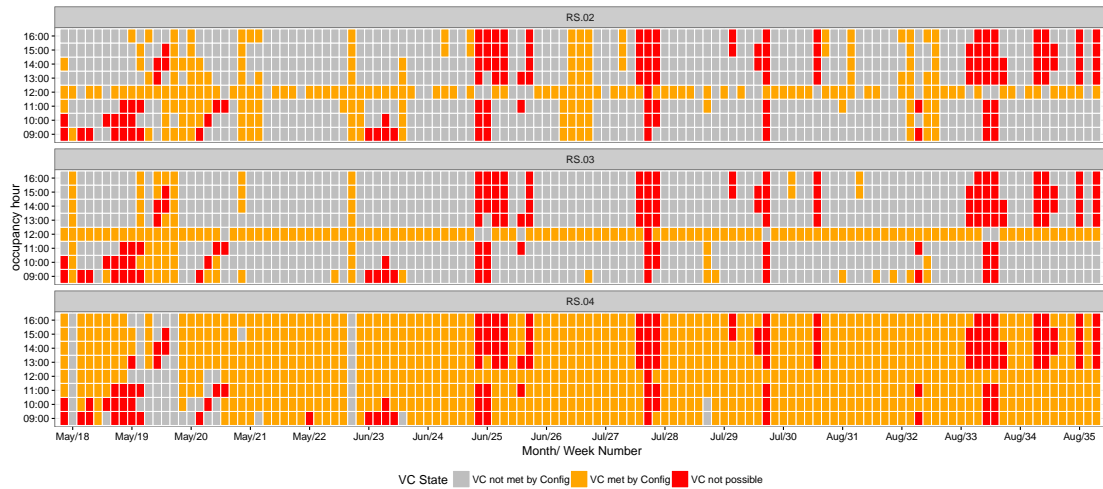


FIGURE 6.7: Ventilative Cooling State for May to August

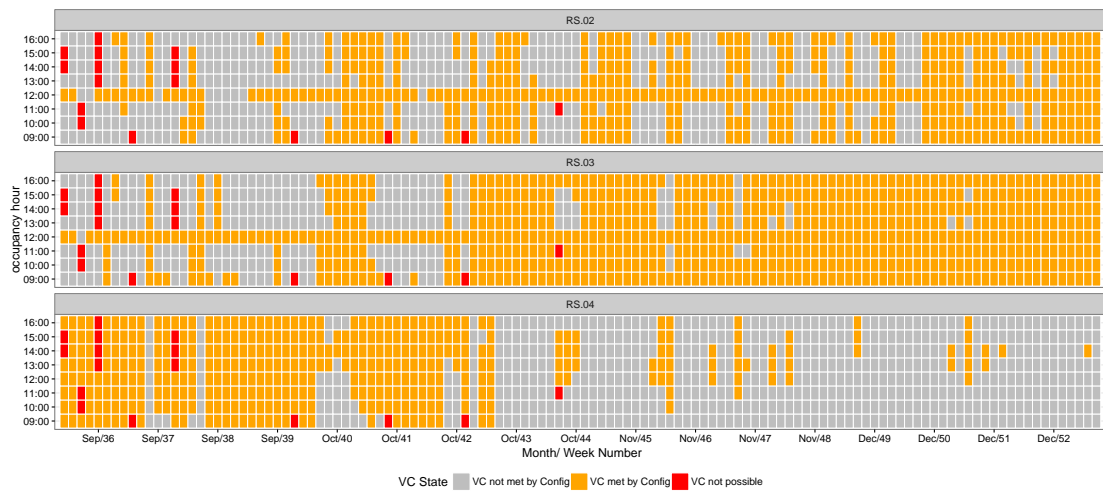


FIGURE 6.8: Ventilative Cooling states for September to December

the potential to meet a particular criteria we have chosen to retain the binary or discrete nature of the approach. Towards the end of the first 4 month period a modal shift appears to take place during week 13 (End of March) suggesting both a step change on the magnitude of the required ACR values and a change in external ambient temperatures.

During May to August there is a reversal regarding the availability and suitability of the three configurations. RS.04 now provides the bulk of the required ACR throughout the 4 months. Only during the designated lunch break, where there is no occupant heat gains and the lighting and small power heat gains are also not present, can RS.02 and RS.03 satisfy the requirements reasonably well. During week 18 and 19 there is a period where RS.04 cannot meet the target values, due more to the availability constraint from the 12°C ambient external temperature threshold. Many of these can be met by RS.03 with some remaining without the target ACR. There is a 4 day period in week 25, a 3 day period at the beginning of week 28 and a 5 day period in week 33 where no VC can be supplied by any of the three configurations. These are demonstrable of the critical limit of the slot louvre system to provide adequate VC.

During September to December we experience a modal shift at week 43 with the first third of the period displaying similar patterns to the May-August plot previously. From week 43 onwards there is a marked shift back to the January-April pattern of RS.02 and RS.03 providing much of the required ACR.

The inability of RS.02 and RS.03 to consistently supply N_{re} values until week 43 suggests the required cooling ACR rates are still relatively high. RS.04 satisfies the requirements generally until week 43 but beyond this external ambient temperatures must be regularly below the 12°C as RS.04 is largely unavailable. This pattern of a modal shift in week 43 could be seen as the shift from peak cooling season into the shoulder season. Recalling the modal shift around week 13, this would support the argument of an extended cooling season from late March until late October. It should be noted that the TMY3 file type is being used to assess the climate cooling potential. This is a statistically aggregated dataset based on 30 years of weather data and does not include for elevated temperatures for extended periods in a way that for example, CIBSE DSY weather file would. Unfortunately the CIBSE DSY file type is unavailable for Cork and many locations within Ireland.

Understandably, when considering the three 4-month periods above, where the ACR requirement is not met by any of the configurations this will have a negative effect on the subsequent hours with an additional heat gain remaining to be dealt with during the following hour. However, to account for this would require a more advanced modelling approach and the VC Potential analysis tool from Annex 62 has been adopted for the purposes of demonstrating the component cooling potential. Another area that can improve the accuracy of both the estimation of ACR as well as climate cooling potential is the inclusion of the effects of thermal mass, particularly in heavyweight structures with high levels of thermal performance. However, extending the capabilities of the tool is outside the current scope of work.

6.4.2 Optimum Opening Schedule

Figure 6.9 presents the percentage of hours in each month where N_{re} can be delivered by the slot louvre system, categorised according to opening configuration. During summer months (May to September) RS.02 and RS.03 are very similar. RS.03 performs better than RS.02 during winter months. This is largely due to the large envelope temperature difference that is undoubtedly present at this time and is the basis for the RS.03 ACR calculation. However, the reduced opening area, combined with the elevated height allows the introduction of cooler air above the occupancy zone and some mixing can take place, introducing the cooler air with potentially lower risk of thermal discomfort. This principle was confirmed recently in a thermal comfort field study at the zero2020 building [72]. RS.04 provides between 80% and 90% of the required cooling ACR during June, July & August. This still leaves an average of 16% of occupied hours during these months where there is insufficient cooling available. In September this reduces to 13%, still a significant shortcoming.

In order to maximise the available cooling potential from the overall slot louvre ventilation system supplying the office space it was necessary to combine the different ACR contributions available,

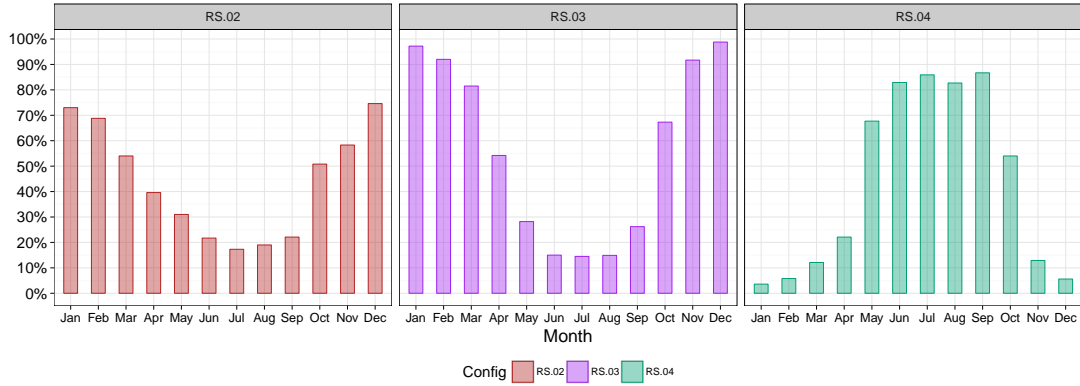


FIGURE 6.9: Percentage of monthly occupied hours where the required ventilative cooling ACR rate is met with the predicted ACR for the particular configuration

N_{pr} , from each of the configurations to ensure the best possible opening scenario at each time step had been selected. Where one configuration was able to provide VC another was not and this leads to a need to select the most suitable opening configuration to match N_{re} at each time step. By doing this we can produce a schedule of which configuration should be active for each of the occupied hours assessed. As the weather file used for the analysis is statistically aggregated over 30 years the resulting schedule is not necessarily the basis for a recommended control strategy. Rather it compliments the previous section outlining the climate cooling potential by providing a system level optimised opening pattern. This is required primarily because there are three possible options for ventilation at each time step. Were there is only one opening then this would be a much simplified process and a plot similar to those in figure 6.6 to 6.8 would be sufficient. A sequential hierarchy was adopted for identifying suitable configurations at each time step. This is summarised in equation 6.14 below. We then use the integers 0-3 to categorise each time step accordingly. We set RS.03 as the default system where possible. This is because of its automated nature and it can reliably be set as the configuration that would respond as a base option. RS.02 was then chosen where RS.03 was unable to meet the required ACR value. Finally RS.04 was selected when available and neither RS.03 or RS.02 could satisfy requirements. Understandably the dynamic interaction between the occupant and the system is neglected to be taken into account here. This is because we are assessing the potential of the system to respond to the ventilative cooling requirements in an optimized sequence of operation. This is a system capacity sizing exercise more than a operational performance exercise.

$$\text{ACR mode} = \begin{cases} 0 & \text{if } [N_{pr,rs02}, N_{pr,rs03}, N_{pr,rs04}] \leq N_{re}, \\ 1 & \text{if } N_{pr,rs03} \geq N_{re}, \\ 2 & \text{if } N_{pr,rs03} \leq N_{re} \ \& \ N_{pr,rs02} \geq N_{re}, \\ 3 & \text{if } N_{pr,rs03} \leq N_{re} \ \& \ N_{pr,rs02} \leq N_{re} \ \& \ N_{pr,rs04} \geq N_{re} \ \& \ T_e \geq 12^\circ C, \\ 0 & \text{if } N_{pr,rs03} \leq N_{re} \ \& \ N_{pr,rs02} \leq N_{re} \ \& \ N_{pr,rs04} \geq N_{re} \ \& \ T_e \leq 12^\circ C, \end{cases} \quad (6.7)$$

This results in an optimised combination of each of the configurations to give the operating pattern in figure 6.10, 6.11 & 6.12, depending on the 4 month period of interest. As expected

RS.03 provides the bulk of the ACR during January to March. RS.02 and RS.04 provide some of the needs during April. During May we see an increasing contribution from RS.04 as expected. RS.02 provides a substantial contribution during week 26 and week 27. In Week 40 we see a return to the dominant contribution from RS.03.

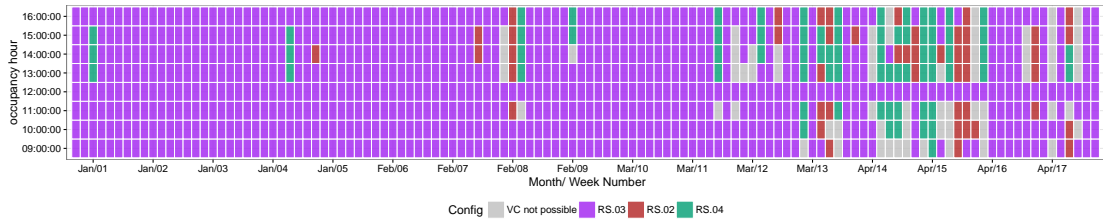


FIGURE 6.10: Percentage of monthly occupied hours where the required ventilative cooling ACR rate is met with the predicted ACR for the particular configuration

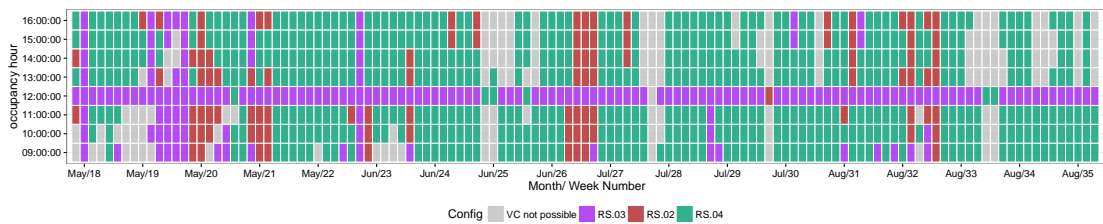


FIGURE 6.11: Percentage of monthly occupied hours where the required ventilative cooling ACR rate is met with the predicted ACR for the particular configuration

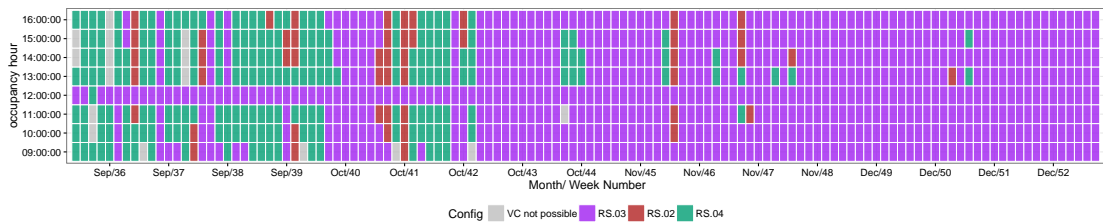


FIGURE 6.12: Percentage of monthly occupied hours where the required ventilative cooling ACR rate is met with the predicted ACR for the particular configuration

6.4.3 Parametric Analysis

Figure 6.13 (A) presents the total percentage of hours in each month where ventilative cooling is satisfied for the system inclusive of all configurations, based on the methodology above. In every month there are some hours where cooling cannot be met. This is to some extent due to the external ambient temperature constraint imposed on the system to avoid thermal discomfort when cooling during shoulder seasons. When we consider the effect of setting this constraint we see in Figure 6.14 that even with a value of $T_{e,lim} = 0^{\circ}C$ we still have 115 hours, or approximately 4% of the occupied period, with no ventilative cooling possible.

Figure 6.13 (B) show that these hours are distributed almost entirely across June, July & August. This highlights an inability of the current system to generate large enough flowrates during certain periods of the peak summer season.

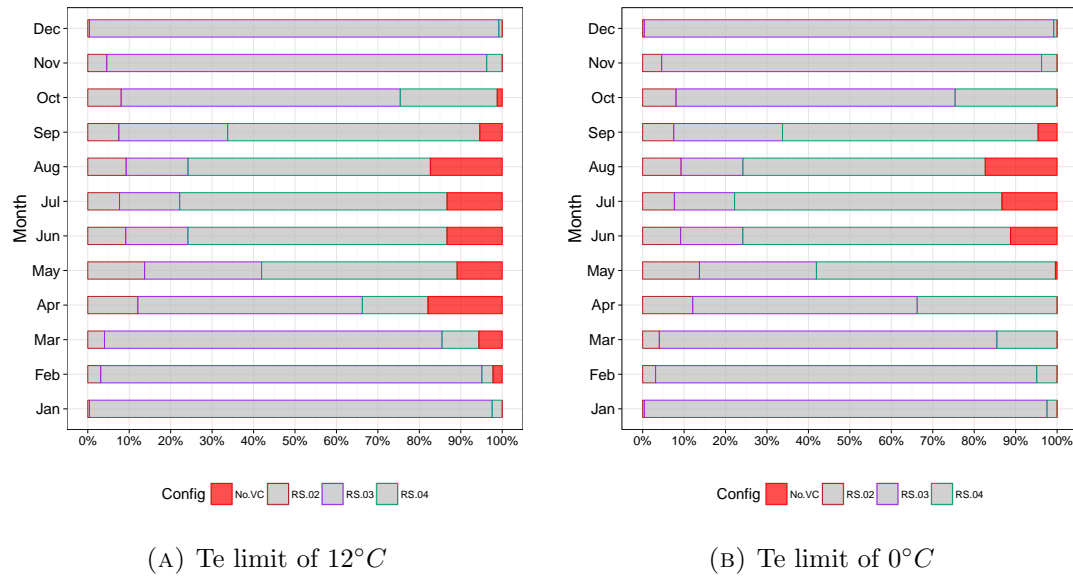


FIGURE 6.13: Total percentage hours with N_{re} either met (grey) or not met (red) for the integrated system using optimum N_{pr} values from each configuration. Two scenarios shown, one incorporating a low limit constraint for T_e of $12^\circ C$ for RS.04, the other with a constraint of $0^\circ C$ (Note: individual configuration contributions shown with shaded borders)

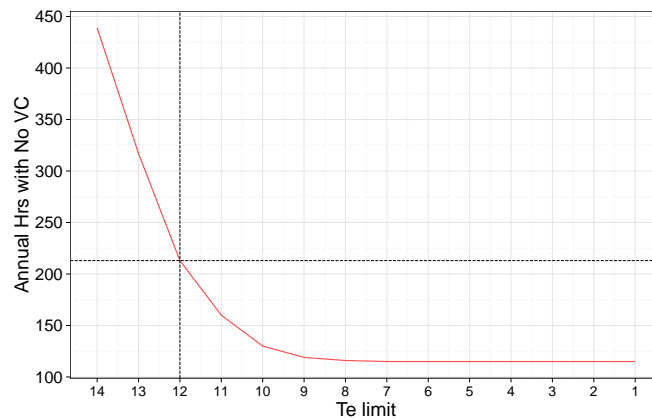


FIGURE 6.14: Effect the external ambient temperature limit has on the number of hours where no VC is possible due to the un-availability of RS.04

Figure 6.15 plots the distribution of values for the percentage difference in N_{pr} for RS.04 when compared with N_{re} for instances when RS.04 was not able to meet the demand. In fact the maximum under supply from the system during June - August was 73% with a mean under supply of 21.6%. Given the uncertainty ranges of the correlations used to predict ACR for the system the mean is generally within the bounds of uncertainty. However, an extension of the systems capacity is required to provide this additional supply and meet N_{pr} year round. One solution may be to introduce a hybrid VC solution with a local mechanical fan installed into the opening, potentially within the automated upper insulated door. This door could then close when conditions were within the critical range between T_{cr} and T_{cu} where passive VC is no longer able to maintain an acceptable indoor environment. The mechanical fan would provide for the estimated under supply. The maximum under supply was 7.9 ACR for an hour and using a fan with a specific fan power of $2.0 \text{ W l}^{-1} \text{ s}^{-1}$ it would require 143 Wh to provide this

ventilation rate, a very small load. This would scale up with the number of offices and building size. Using the passive VC approach alone, in some under supply instances the required redesign would be impractical. Figure 6.16 presents ACR performance as a function of opening height and envelope temperature difference. The current opening width of 0.6m (2 louvre banks at 0.3m each) is shown in black while an opening width increased by 30% is shown in red.

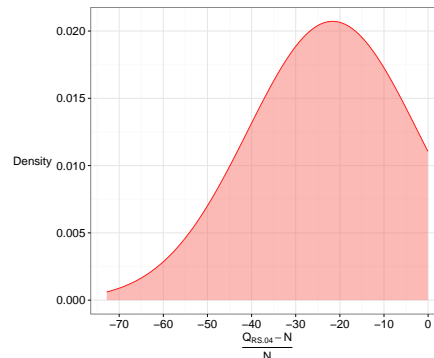


FIGURE 6.15: Density distribution of Percentage difference between the required ACR values and the predicted ACR values for RS.04 during the months of June, July & August, (**Only instances where the predicted ACR value was less than the required ACR value are shown**)

The maximum measured ACR for RS.04 across a range of boundary conditions was 5.8. 6.0 ACH is marked in orange on Figure 6.15. Considering the same opening geometry as is currently installed, ($H = 1.6m$, $Cd = 0.52$) a ΔT of 10K will only give around 6.5 ACH. This value is potential possible during night time hours where there are large diurnal swings but very unlikely during summer day time periods. A height of 2.0m and a reasonable ΔT of 6K can provide around 6.8 ACH. Extending the height to 2.0m becomes challenging due to the issues around draughts and increased air movement within the space. However, the nature of the slot louvre means this is less of a problem as the full opening height is available but comprised of a composite of smaller openings. Extending the opening height to 2.0m increases ACR performance by 40% compared with the current arrangement. Further, by increasing the ΔT from 2K to 6K provides a 70% for the 2.0. opening. It is difficult to artificially produce this increased in temperature difference and 2.0m is a very tall opening. However, these two effects combined mean a maximum ACR value of 6.8 ACH is possible which is excellent performance for Single Sided ventilation. It still does not meet all the required ACR values to maintain conditions below the thermal comfort range year round. Extending the opening width for the 2.0m high opening as shown in Figure 6.16, produces an ACR of 8.8 ACH. In fact leaving the opening height at 1.6m and extending the width produces an ACR of 6.3 ACH. It is difficult to see how the system can be reasonably extended to deal with all values of N_{pr} .

In general, 7.0 ACH would be perceived as nearing the upper limit of practical performance for single sided ventilation strategies. Beyond this, consideration should be given to alternative solutions that could still incorporate the slot louvre system but use an alternative exhaust locations making use of the extended performance of cross flow ventilation strategies. Openings of this height are usually difficult to accommodate in practice and they ultimately rely on a different theoretical approach to predict their performance. However the nature of the slotted design facilitates large opening heights while preventing excessive bulk air movement within the

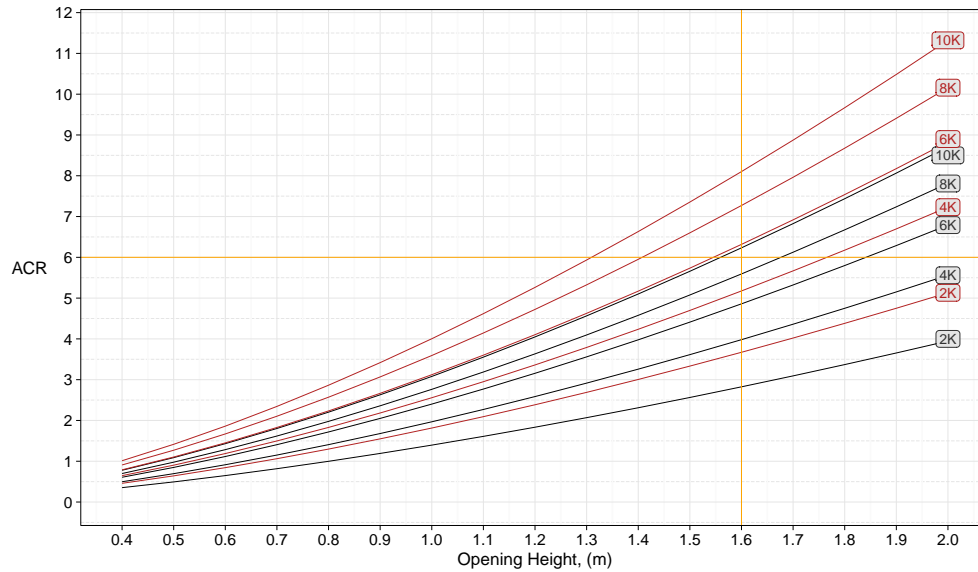


FIGURE 6.16: N_{pr} as a function of both opening height, H and envelope temperature difference, ΔT . N_{pr} vs H curves shown for two different slot louvre section opening widths, 0.3m and 0.4m, Effectively a 30% increase in available opening area. Proposed Upper limit for ACR shown in orange based on measurements. Current opening height also shown in orange.

space. They are an alternative to positioning a smaller opening at high level and one at low level giving similar area within an increased amount of slotted openings.

Further, thermal mass has not been included in the current demonstration methodology. This will likely reduce the peak day time temperatures in the space resulting in slightly lower peak value for N_{pr} . In this scenario the system may be able to deliver the required performance across the full spectrum of conditions.

6.5 Conclusion

The aim of this section of the thesis was to demonstrate the cooling performance of the slot louvre system. Having empirically investigated the macroscopic ACR performance of a number of different configurations, the aim was to investigate the ability of the system to deliver an ACR, calculated to maintain indoor temperatures within the comfort range defined by the adaptive approach in EN15251. The analysis was completed for a 12 month calendar year and the extent of cooling needed for the low energy retrofit space was also quantified. It was found that there was a need for enhanced ventilation for ventilative cooling above the minimum IAQ values in every month of the year, with for example, 60% of the occupied hours in January requiring enhanced ventilation and over 90% of occupied hours in July. A significant cooling demand is needed for the low energy retrofit with year round cooling. 80% of annual occupied hours required some enhanced ventilative cooling. This highlighted the extension of the cooling season in the space into the shoulder seasons, beyond the traditional 4 month summer period in Ireland. The cooling potential of Ireland's climate outside the core summer months should mean passive ventilation is a suitable option for cooling, thus offsetting the increased cooling energy demand

from the inherent nature of the low energy building. The component cooling potential was also estimated by comparing the required ACR to maintain comfortable conditions, calculated using the approach outlined, with ACR values estimated using correlations based on empirical measurements. The individual opening configurations had limitations in their ability to supply adequate ACR year round, the summer being overly demanding on the small openings RS.02 and RS.03 and the over-cooling constraint on RS.04 limiting its usefulness in shoulder seasons. When all configurations were combined, obtaining a composite of openings to achieve the required ACR, the requirements were satisfied in all but a short range. There were 223 hours, mainly concentrated in summer months, where the system capacity was incapable of providing sufficient cooling. The system as a whole was able to satisfy the ventilative cooling ACR requirements for 93% of the annual occupied hours. When the external ambient temperature limit was removed this was increased to 96% with the remaining 4% concentrated in June, July & August.

Chapter 7

Overall Conclusion & Future Work

7.1 General Overview

This thesis has presented the scope, methodologies and results of research that sought to quantify what is the effect to the aeration performance (and subsequent cooling potential) of a single sided, natural ventilation opening when using a MCSL solution designed to prevent rain ingress and burglary during night cooling. While these types of systems are increasingly popular amongst architects and low energy building designers there was a lack of empirical measurement data in the literature regarding their cooling performance and their ability to provide sufficient airflow to prevent overheating. To investigate this a number of experimental field studies were completed using an isolated office space employing the MCSL in a retrofitted building at Cork Institute of Technology, Cork, Ireland. The office space was vacant and used solely for the field studies. This is usually difficult to obtain in real buildings given all spaces are generally occupied. This is one of the unique aspects of the research, having the opportunity to complete ACR measurements over an extended period in a real building while exposed to a range of boundary conditions. It can also be challenging to obtain good quality ACR measurement data in occupied office spaces owing to the invasive nature of the test method.

The MCSL system performs well as a single sided ventilation solution. The system provided good performance across a range of boundary conditions. The internal thermal environment was relatively stable at times when VC was employed. This was not the case in the pre retrofit space where extreme levels of overheating were observed even when VC was active with night cooling. The decision to design the MCSL system with different opening sections resulted in varying levels of aeration of the space depending on the configuration adopted, which was largely a consequence of how each opening interacted differently with the external boundary conditions. In particular the slot louvre increases the wind dominant airflow rate for small opening heights while for larger heights buoyancy is dominant. This can be exploited as an effective strategy if there is some knowledge about the typical boundary conditions observed at a given building location. By

way of example the open plan office in the building has nine separate louvre banks each with an upper and lower opening section. When conditions are known to be wind dominant, multiple low level openings can be employed with potentially greater ACR than using the high level openings. When conditions favour buoyancy driven flow a smaller quantity of full height openings might suffice without the risk of over cooling, particularly during shoulder seasons. The MSCL system displayed good performance with some ACR values as high as 5 ACH, which is at the upper end of the single sided ventilation range. When in full VC mode it achieved comparable ACR performance to the existing window arrangement with many additional advantages (night cooling opportunities, improved thermal envelope performance etc). The non-dimensional airflow rate was found to be higher than for a plain opening, although slotted louvre systems will have lower ACR values compared with a plain opening with equivalent opening dimensions and this must be recognised when developing the architectural design of faades.

In general these opening types are able to use large opening heights, promoting good buoyancy driven airflow rates, without the additional problems associated with very large opening areas. This is indicative by the acceptable levels of air movement observed at a typical occupant location when using the lower opening configuration, the system not producing excessive draughts or air movement characteristics. Reduced turbulence levels at the occupant location were observed when the slot louvre was used compared with a plain opening as well as no significant difference in the distribution of sampled air speeds at this location. This means that the ability to extend the thermal comfort range using enhanced air movement is potentially limited by the MCSL system. However, even with the plain opening air movement was quite low suggesting the highly decoupled thermal environment may contribute to this situation. Air flow characteristics were measured when only 1 of the 4 opening sections were activated and this is also potentially a contributing factor (equates to a POF of 1.1% for the slot louvre and 2.3% for the plain opening). More research in this area is needed. The MCSL system has good cooling potential even when used with day time VC only. It should be considered as a realistic alternative to traditional window solutions given its improved thermal performance compared with glazing approaches. However, due to the limitations of single sided ventilation as a strategy there is an upper limit to the capacity of the system without imposing impractical physical dimensioning. For this reason the MCSL in SS mode is best suited to low energy spaces that required reasonable levels of ventilation. In reviewing the original objectives of the work we can make the following key conclusions:

7.1.1 Primary Conclusions

There are five key conclusions. These are presented addressing the original five objectives of the research work along with a supporting summary.

Conclusion 1: *All rooms in the retrofitted building complied with all three of the criteria set out by CIBSE TM52 using an adaptive thermal comfort approach.*

Occupancy was low during the cooling season given the academic nature of the office spaces. This no doubt contributed to the very low results in the assessment when considering the sensitivity to

occupant heat gain in low energy spaces. A night cooling strategy was in place which was shown to assist with heat removal. The internal thermal stratification was effectively eliminated by the retrofit space. Only with the full height opening configuration was there still some appreciable temperature difference present. From the analysis of over 1000 hours of measurement data the space generally complied with category A of ISO 7730 under vertical temperature difference criteria. It is possible to radically transform the thermal environment in an existing building with a deep external retrofit upgrade. This environment is more stable, less likely to overheat and has lower peak indoor temperatures requiring less outdoor air for cooling.

Conclusion 2: *The MCSL system demonstrated comparably good aeration and internal environmental performance. Depending on configuration employed it modifies the contribution from driving forces to the airflow rate compared with the pre retrofit building.*

Although a lower mean and spread of ACR values was observed for the MCSL system in the retrofit space compared with the existing control space, the results still showed good aeration performance. The free area of the combined full height configuration, RS.04, was 30% greater than the control space window and when these are compared directly ACR values are comparable. ACR values for the full height configuration of the MCSL was shown to be strongly correlated with high envelope temperature differences and wind speed, while no clear trend was evident for the window in the control space. The other MCSL configurations also exhibited a dependency between ACR and wind speed with a weaker relationship for envelope temperature difference. Envelope temperature difference and magnitude of ACR appeared to also depend on wind direction for both the window and MCSL. A non dimensional study highlighted similar non-dimensional ACR values for the MCSL and window opening. It also highlighted buoyancy as the dominant force producing ACR for the full height MCSL system. For the low level MCSL configuration wind was the dominant force and for the high level opening it appeared less well defined. This suggests a relationship exists between opening height, position of the opening in the envelope and whether or not buoyancy will dominate. The opening height and opening position are important parameters influencing nature of airflow at the opening. The opening position is not considered in any existing correlations. This suggests different correlations should be considered for different opening configurations.

Conclusion 3: *The slotted louvre has a higher non-dimensional airflow rate, at low opening heights increases the wind dominance of the flow through the opening and reduces the fluctuating component of air movement at the occupant location but not the mean or average conditions.*

The same opening was investigated with and without a slotted louvre in place and for the same free opening area there was between 75% and 100% improvement in ACR using the slot louvre. For the same opening dimensions (the slot louvre having less than 50% of the opening area) there is a reduction in ACR of between 16% and 30%. There is a 53% increase in wind driven non dimensional flow through the slot louvre when compared with a plain aperture of the same free area. This includes results from all wind directions. However, this increase is mainly attributable to windward wind directions with similar non-dimensional flow numbers observed for leeward conditions. The non-dimensional flow measured through the plain opening was larger than other laboratory and lab studies. However this can be attributed to the increased turbulence in

the boundary conditions. The louvre appears to enhance further the air exchange mechanism present when the wind is dominant and the direction is windward. The local wind direction at the opening was measured as always parallel. It is likely that, depending on wind direction, the slot louvre is either guiding the shear mixing layer into the room in a way that is promoting further entrainment than would otherwise happen without the curved louvre profile, or, some venturi effect is present enhancing the mean pressure driven flow. The opening type had little impact on the airflow characteristics within the room.

Conclusion 4: *Existing single sided airflow correlations under predicted ACR values for the slotted louvre system. A new non-dimensional flow number is proposed to better account for wind dominant ACR*

Existing single sided airflow correlations had a mean error in prediction of 41% across all slotted louvre tests when compared with the measurement data. These all under predicted on average. The leeward tests had lower prediction errors. The same correlations had a mean error of 28% for the plain opening tests. Warrens correlation performed best for the slotted louvre with an MAPE of 36% while Argiriou performed best for the plain openings at 21% (though Warren was at 22%). For the plain opening measurements most of the correlations performed in line with other published studies. A simplified wind driven model based on Warrens approach is proposed for the slot louvre when at heights generally $\leq 1.0\text{m}$. A higher F_r value is proposed for wind dominant situations, in the range of 0.04 - 0.07. There was a pattern of lower non-dimensional flow when conditions were leeward. When comparing the same opening dimensions there was approximately a 53% increase in the non dimensional flow with the slotted louvre.

Conclusion 5: *The system and retrofitted building displayed good VC potential with indoor conditions remaining within the adaptive thermal comfort range for 93% of the annual hours assessed*

The annual component cooling potential of the system installed in the retrofit building was investigated for an Irish climate. Overall, 82% of annual occupied hours required an enhanced VC airflow rate. In July and August this was as high as 90%. Of the hours where an enhanced air flow rate was required, using a combination of opening configurations, the system was able to provide the required airflow rate for 93% the time maintaining comfortable conditions in the space. For the hours where VC could not be provided this is based on the proposed ACR not meeting the required ACR. The average difference in these when the proposed ACR was insufficient was 22% (with up to 70% in some instances), so some cooling is still available though it does not maintain temperatures within the thermal comfort range. Following a parametric analysis the system was still not able to provide sufficient year round cooling 100% of the time within the constraints set by the study. This could be remedied by employing a night cooling strategy. The solution performs well overall and is limited by the aeration potential of single sided ventilation. 60% of occupied hours in January required an airflow rate larger than that provided by the minimum to meet IAQ standards. This seemed unreasonable for this time of year and incorporating the effects of thermal mass to the study may reduce this further.

7.2 Practical Implications for Designers and Researchers

The information presented in this thesis can be used by designers when considering the use of multi-configuration slotted louvre designs which are increasing in popularity. Making use of the improved wind driven performance should be accounted for when sizing openings as this will provide a more realistic estimate of the VC system performance. Low energy retrofit designers can benefit from gaining insight into how the solution adopted for CIT has performed and aspects of this approach are transferable to other designs. Removing openable windows in lieu of dedicated PPO strategies such as the MCSL have been demonstrated to work well and it is realistic to have very high performance thermal envelopes and low levels of overheating. This information should inform future design of low energy retrofit and VC systems. Consideration must also be given to the upper threshold of the systems performance capability and in some instances a hybrid solution may be preferable if no overheating is tolerable.

Researchers can benefit by having more confidence regarding the in situ real performance of MCSL systems. They can contribute to advancing further knowledge regarding performance and dimensioning of such systems by considering the proposed future research below.

7.3 Future Work

7.3.1 Future Research ideas

There are a number of opportunities to extend the research work further. These are summarised as follows:

Interrelationship between driving forces and opening height

Using a laboratory experiment an investigation into the inter relationship between wind speed, temperature difference, opening height and ACR for the slot louvre would be useful to compare against field measurement data. Different ACR performance will result from the different combinations of the relative strength of wind and buoyancy driven forces. The opening height, as well as the relative height in the room/building, are key variables in determining when airflow through the louvre transitions from being wind driven to buoyancy driven. What is the height at which this transition takes place, is it different to conventional openings, is it a variable and what does it depend on, for example temperature difference, slot dimensioning etc. This can inform better prediction and dimensioning of systems. Using a laboratory set up to isolate certain phenomena and investigate more closely different characteristics observed in the field studies can support louvre design development and allow a better understanding of field data. It can also inform future field studies.

Effect of opening depth on jet deflection

Previous researchers demonstrated how jet momentum was affected through deflection arising from deep openings. The depth of openings may increase with increasing wall thickness from

retrofitting external wall insulation of existing structures. The slot louvre or similar airflow guiding components may be an effective solution to overcome this and provide increased ventilation in single sided spaces. Modifying the shearing effect at the boundary of the jet with the acquiescent room air may assist in reducing the effect of jet deflection. Using a laboratory/wind experiment and Computational Fluid Dynamics simulations (CFD) a study could be undertaken investigating the effect of the opening depth on the ACR performance with and without the louvre system to establish whether this in fact does relate to performance enhancements. The louvre profile design may be a variable in this situation.

Airflow guiding nature of the Concave Louvre Profile

This is closely connected to the previous study. The profile of slotted louvres can be optimised using aerodynamic and fluid mechanics theory. An investigation into the concave louvre profile for wind driven flow and buoyancy driven flow separately in the laboratory should be completed. Quantification of the contribution to ACR from the curved shape needs to be identified and compared with traditional angled slat type louvres. Clarification of the underlying physics contributing to the louvre performance needs to be further investigated given its demonstrated performance under real building boundary conditions.

Design Chart

There is potential to investigate the concept of a new design chart for single sided natural ventilation systems based on the warren plot. The concept has not been fully developed yet but warrants some further investigation. Using the empirically derived F_r value along with a range of Ar values defined within realistic wind driven and buoyancy driven ranges, different opening height and width combinations can be defined that deliver a target ACR value, depending on whether the design should be wind driven or buoyancy driven. This would involve defining an F_b and Ar_b combination initially. This can be done using the warren plot. Then keeping F_b as a constant allows for Ar values above Ar_b to be all buoyancy dominant designs while values below this are all wind driven. The buoyancy dominant designs rely on differing combinations of ΔT_{ie} , velocity due to buoyancy, U_b and opening height, H . The wind dominant designs rely on the wind speed, U_w , opening area, A_o and keeping F_r constant and equal to F_b . While F_r is a function of wind direction and wind speed it has shown to perform well when taken as a constant of somewhere around 0.03 for plain openings. Working with this and using a realistic range of Ar values could allow the definition of specific combinations of opening heights and $C_d A_o$ combinations giving different ACR values. Using design and U_r values could allow the creation of design charts giving resulting dimensioning. The charts would be based on empirical measurements taken from existing field studies as well as lab measurements for various openings and boundary conditions. The idea is still in its infancy but it is planned to develop this further. The charts would be developed from measurements of ACR through multiple combinations of opening shapes and boundary conditions. Dimensional analysis and design of experiment would be essential to reduce the parameter space and number of experiments needed. However, these could be useful charts for designers at early stage design. It is still unclear whether they can improve current approaches to single sided ventilation opening design.

Improved Cooling Potential Analysis

The effect of thermal mass on the estimation of the required ACR, N_{re} , to improve the current approach to predicting the VC potential in the IEA-EBC Annex 62 tool should be further considered. Further, the effect of allowing for the calculated ACR even when it does not meet N_{re} should be added. An energy indicator can be used to provide the 'supplementary' mechanical cooling or mechanical ventilation needed to meet the target thermal comfort conditions in the space. The tool should also be able to consider single sided and cross flow strategies.

Climate Cooling Potential for Ireland

A study is required extending the cooling potential to different locations and building types throughout Ireland and incorporating the latest probabilistic weather data where available. VC is under represented in the Irish Building regulations and industry generally. Better knowledge surrounding the conditions that enhance VC potential is needed.

References

- [1] European Union. Directive 2012/27/EU on energy efficiency, amending Directives 2009/125/EC and 2010/30/EU and repealing Directives 2004/8/EC and 2006/32/EC. *Official Journal of the European Union*, (October): 1–56, 2012. URL <http://kspu.karelia.ru/attach.php/id/20171/name/{%}E2{%}E0{%}EA{%}E0{%}ED{%}F1{%}E8{%}E8{%}E2{%}CC{%}CE{%}D3{%}ED{%}E014.11.2012.doc>.
- [2] Chris Marnay, Michael Stadler, Sam Borgeson, Brian Coffey, Ryoichi Komiyama, and Judy Lai. A Buildings Module for the Stochastic Energy Deployment System. In *2008 ACEEE Summer Study on Energy Efficiency in Buildings, Scaling Up: Building Tomorrows Solution*, number May, page 16, Calif, 2008.
- [3] IEA. Energy Performance Certification of Buildings. Technical report, 2010.
- [4] Martin Howley and Mary Holland. Energy in Ireland 1990–2015. Technical report, Sustainable Energy Authority Ireland, 2016.
- [5] Kevin J. Lomas and Stephen M. Porritt. Overheating in buildings: lessons from research. *Building Research & Information*, 45(1-2):1–18, 2017. ISSN 0961-3218. doi: 10.1080/09613218.2017.1256136. URL <https://www.tandfonline.com/doi/full/10.1080/09613218.2017.1256136>.
- [6] Robert S. McLeod and Michael Swainson. Chronic overheating in low carbon urban developments in a temperate climate. *Renewable and Sustainable Energy Reviews*, 74 (July 2016):201–220, 2017. ISSN 13640321. doi: 10.1016/j.rser.2016.09.106. URL <http://linkinghub.elsevier.com/retrieve/pii/S1364032116305925>.
- [7] Anna Mavrogianni, Paul Wilkinson, Michael Davies, Phillip Biddulph, and Eleni Oikonomou. Building characteristics as determinants of propensity to high indoor summer temperatures in London dwellings. *Building and Environment*, 55:117–130, 2012. ISSN 03601323. doi: 10.1016/j.buildenv.2011.12.003. URL <http://dx.doi.org/10.1016/j.buildenv.2011.12.003>.
- [8] Kevin Lomas and T Kane. Summertime temperatures and thermal comfort in UK homes. *Building Research and Information*, 41(3):259–280, 2013. ISSN 0961-3218. doi: 10.1080/09613218.2013.757886. URL <http://www.scopus.com/inward/record.url?eid=2-s2.0-84876211342&partnerID=40&md5=689ba31d894e461c921725e56066eeaa>.

- [9] N. Artmann, H. Manz, and P. Heiselberg. Climatic potential for passive cooling of buildings by night-time ventilation in Europe. *Applied Energy*, 84(2):187–201, feb 2007. ISSN 03062619. doi: 10.1016/j.apenergy.2006.05.004. URL <http://linkinghub.elsevier.com/retrieve/pii/S0306261906000766>.
- [10] Mattheos Santamouris and Dionysia Kolokotsa. Passive cooling dissipation techniques for buildings and other structures: The state of the art. *Energy and Buildings*, 57:74–94, feb 2013. ISSN 03787788. doi: 10.1016/j.enbuild.2012.11.002. URL <http://linkinghub.elsevier.com/retrieve/pii/S0378778812005762>.
- [11] Guilherme Carrilho da Graça and Paul Linden. Ten questions about natural ventilation of non-domestic buildings. *Building and Environment*, 107:263–273, 2016. ISSN 03601323. doi: 10.1016/j.buildenv.2016.08.007. URL <http://dx.doi.org/10.1016/j.buildenv.2016.08.007>.
- [12] IPCC. Climate Change 2014 Synthesis Report Summary Chapter for Policymakers. Technical report, 2014.
- [13] T. Psomas, P. Heiselberg, K. Duer, and E. Bjørn. Overheating risk barriers to energy renovations of single family houses: Multicriteria analysis and assessment. *Energy and Buildings*, 117:138–148, 2016. ISSN 03787788. doi: 10.1016/j.enbuild.2016.02.031. URL <http://linkinghub.elsevier.com/retrieve/pii/S0378778816300883>.
- [14] Robert S. McLeod, Christina J. Hopfe, and Alan Kwan. An investigation into future performance and overheating risks in Passivhaus dwellings. *Building and Environment*, 70:189–209, dec 2013. ISSN 03601323. doi: 10.1016/j.buildenv.2013.08.024. URL <http://linkinghub.elsevier.com/retrieve/pii/S0360132313002503>.
- [15] Maria Kolokotroni, Per Heiselberg, Lorenzo Pagliano, Jie Han, Regina Bokel, Peter Holzer, and Annamaria Belleri. IEA EBC Annex 62 Ventilative Cooling - State of the Art review. Technical Report October, International Energy Agency, 2015. URL venticool.eu/wp-content/uploads/2013/09/SOTAR-Annex-62-FINAL.pdf.
- [16] A. C. Sever and D. Rockwell. Oscillations of shear flow along a slotted plate: small- and large-scale structures. *Journal of Fluid Mechanics*, 530:213–222, 2005. ISSN 0022-1120. doi: 10.1017/S0022112005003721. URL [http://www.journals.cambridge.org/abstract_{_}S0022112005003721](http://www.journals.cambridge.org/abstract/_jS0022112005003721).
- [17] A. Ekmekci and D. Rockwell. Self-sustained oscillations of shear flow past a slotted plate coupled with cavity resonance. *Journal of Fluids and Structures*, 17(8):1237–1245, 2003. ISSN 08899746. doi: 10.1016/S0889-9746(03)00073-2.
- [18] Ben Richard Hughes, John Kaiser Calautit, and Saud Abdul Ghani. The development of commercial wind towers for natural ventilation: A review. *Applied Energy*, 92:606–627, 2012. ISSN 03062619. doi: 10.1016/j.apenergy.2011.11.066. URL <http://dx.doi.org/10.1016/j.apenergy.2011.11.066>.

- [19] Toshikazu Nakanishi, Tamotsu Nakamura, Youichirou Watanabe, Katsumasa Handou, and Takahiro Kiwata. Technical Paper: Investigation of Air Flow passing through Louvers. Technical Report 160, Komatsu, 2007.
- [20] NSAI. ISEN 15251:2007 -Indoor Environmental Input Parameters for design and Assessment of Energy performance of Buildings addressing Indoor Air. Technical report, 2007.
- [21] Fergus Nicol and Brian Spires. CIBSE TM52: The Limits of Thermal Comfort. Technical report, CIBSE, London, 2013.
- [22] Better Buildings: A National Renovation Strategy for Ireland. Technical report, Department of Communications Energy and Natural Resources, Dublin, 2014.
- [23] European Union. Directive 2010/31/EU. pages 13–35, 2010.
- [24] National Energy Efficiency Action Plan 2014. Technical report, Department of Communications Energy and Natural Resources, Dublin, 2013. URL <http://www.dcenr.gov.ie/energy/SiteCollectionDocuments/Energy-Efficiency/NEEAP3.pdf>.
- [25] DCENR. Maximising Irelands Energy Efficiency - National Energy Efficiency Action Plan. Technical report, 2009.
- [26] SEAI. Annual Report 2016 on Public Sector Energy Efficiency Performance. Technical report, Department of Communications, Climate Action & Environment, 2015. URL http://www.seai.ie/Publications/Your_{_}Business_{_}Publications/Public_{_}Sector/Annual-Report-2015-on-Public-Sector-Energy-Efficiency-Performance.pdf.
- [27] Alex (Minister for Communications Energy White and Natural Resources). Statutory Instrument No. 426 of 2014 - European Union (Energy Efficiency) Regulations 2014, 2014.
- [28] SEAI. Extensive survey of the commercial buildings stock in the Republic of Ireland Final report for The Research Perspective. Technical Report November, Sustainable Energy Authority Ireland, 2015.
- [29] Jim Scheer, Emrah Durusut, and Sam Foster. Unlocking the Energy Efficiency Opportunity. Technical Report June, Sustainable Energy Authority Ireland, 2015.
- [30] Andrew. J. Hoffman and Rebecca Henn. Overcoming the Social and Psychological Barriers to Green Building. *Organization & Environment*, 21(4):390–419, 2008. ISSN 1086-0266. doi: 10.1177/1086026608326129.
- [31] Marianne Ryghaug and Knut H. Sørensen. How energy efficiency fails in the building industry. *Energy Policy*, 37(3):984–991, 2009. ISSN 03014215. doi: 10.1016/j.enpol.2008.11.001.
- [32] Constantine E. Kontokosta. Modeling the energy retrofit decision in commercial office buildings. *Energy and Buildings*, 131:1–20, 2016. ISSN 03787788. doi: 10.1016/j.enbuild.2016.08.062. URL <http://dx.doi.org/10.1016/j.enbuild.2016.08.062>.

- [33] Z. Ma, P. Cooper, D. Daly, and L. Ledo. Existing building retrofits: Methodology and state-of-the-art. *Energy and Buildings*, 55:889–902, aug 2012. ISSN 03787788. doi: 10.1016/j.enbuild.2012.08.018. URL <http://linkinghub.elsevier.com/retrieve/pii/S0378778812004227>.
- [34] E. Dascalaki and M. Santamouris. On the potential of retrofitting scenarios for offices. *Building and Environment*, 37(6):557–567, 2002. ISSN 03601323. doi: 10.1016/S0360-1323(02)00002-1.
- [35] US Green Building Council. Leadership In Energy and Environmental Design. URL <http://www.usgbc.org/leed>.
- [36] BRE. Building Research Establishment Environmental Assessment Method. URL <http://www.breeam.com/>.
- [37] Stuart Barlow and Dusan Fiala. Occupant comfort in UK offices-How adaptive comfort theories might influence future low energy office refurbishment strategies. *Energy and Buildings*, 39(7):837–846, 2007. ISSN 03787788. doi: 10.1016/j.enbuild.2007.02.002.
- [38] Olli Seppanen, William. J. Fisk, and Q H Lei. Effect of Temperature on Task Performance in Office Environment. Technical report, Lawrence Berkeley National Laboratories, 2006.
- [39] Li Lan, Pawel Wargocki, and Zhiwei Lian. Quantitative measurement of productivity loss due to thermal discomfort. *Energy and Buildings*, 43(5):1057–1062, may 2011. ISSN 03787788. doi: 10.1016/j.enbuild.2010.09.001. URL <http://linkinghub.elsevier.com/retrieve/pii/S0378778810003117>.
- [40] Tanabe Shin-ichi, Iwahashi Yuko, Tsushima Sayana, and Naoe Nishihara. Thermal comfort and productivity in offices under mandatory electricity savings after the Great East Japan earthquake. *Architectural Science Review*, 56(1):4–13, 2013. ISSN 0003-8628. doi: 10.1080/00038628.2012.744296.
- [41] Chien-fei Chen, Xiaojing Xu, and Julia K. Day. Thermal comfort or money saving? Exploring intentions to conserve energy among low-income households in the United States. *Energy Research & Social Science*, 26:61–71, 2017. ISSN 22146296. doi: 10.1016/j.erss.2017.01.009. URL <http://dx.doi.org/10.1016/j.erss.2017.01.009>.
- [42] Yufan Zhang and Hasim Altan. A comparison of the occupant comfort in a conventional high-rise office block and a contemporary environmentally-concerned building. *Building and Environment*, 46(2):535–545, 2011. ISSN 03601323. doi: 10.1016/j.buildenv.2010.09.001. URL <http://dx.doi.org/10.1016/j.buildenv.2010.09.001>.
- [43] a. M.R. Aminuddin, S. P. Rao, and Hong Wan Thing. Thermal comfort field studies in two certified energy efficient office buildings in a tropical climate. *International Journal of Sustainable Building Technology and Urban Development*, 3(2):129–136, 2012. ISSN 2093-761X. doi: 10.1080/2093761X.2012.696324.
- [44] Public Health England NHS. Heatwave plan for England. *Heatwave plan for England & Wales*, (May):4, 2015. URL <https://www.gov.uk/>

government/uploads/system/uploads/attachment_data/file/429572/
Heatwave-plan-Making-the-case-2015.pdf.

- [45] A. Beizaee, K. J. Lomas, and S. K. Firth. National survey of summertime temperatures and overheating risk in English homes. *Building and Environment*, 65:1–17, 2013. ISSN 03601323. doi: 10.1016/j.buildenv.2013.03.011. URL <http://dx.doi.org/10.1016/j.buildenv.2013.03.011>.
- [46] Pieter de Wilde and Wei Tian. The role of adaptive thermal comfort in the prediction of the thermal performance of a modern mixed-mode office building in the UK under climate change. *Journal of Building Performance Simulation*, 3(March 2015):87–101, 2010. ISSN 1940-1493. doi: 10.1080/19401490903486114.
- [47] M. Kolokotroni, X. Ren, M. Davies, and a. Mavrogianni. London’s urban heat island: Impact on current and future energy consumption in office buildings. *Energy and Buildings*, 47:302–311, apr 2012. ISSN 03787788. doi: 10.1016/j.enbuild.2011.12.019. URL <http://linkinghub.elsevier.com/retrieve/pii/S0378778811006293>.
- [48] Salvatore Carlucci and Lorenzo Pagliano. A review of indices for the long-term evaluation of the general thermal comfort conditions in buildings. *Energy and Buildings*, 53:194–205, 2012. ISSN 03787788. doi: 10.1016/j.enbuild.2012.06.015. URL <http://dx.doi.org/10.1016/j.enbuild.2012.06.015>.
- [49] NSAI. IS EN ISO 7730:2006 - Ergonomics of the thermal environment - analytical determination and interpretation of thermal comfort using calculation of the pmv and ppd indices and local thermal comfort criteria. Technical report, National Standards Authority of Ireland, 2006.
- [50] Pawel Wargocki and David P. Wyon. Ten questions concerning thermal and indoor air quality effects on the performance of office work and schoolwork. *Building and Environment*, 112:2–9, 2016. ISSN 03601323. doi: 10.1016/j.buildenv.2016.11.020. URL <http://linkinghub.elsevier.com/retrieve/pii/S0360132316304449>.
- [51] Weilin Cui, Guoguang Cao, Qin Ouyang, and Yingxin Zhu. Influence of dynamic environment with different airflows on human performance. *Building and Environment*, 62:124–132, 2013. ISSN 03601323. doi: 10.1016/j.buildenv.2013.01.008.
- [52] G. Chiesa and M. Grosso. Geo-climatic applicability of natural ventilative cooling in the Mediterranean area. *Energy and Buildings*, 107:376–391, 2015. ISSN 03787788. doi: 10.1016/j.enbuild.2015.08.043. URL <http://dx.doi.org/10.1016/j.enbuild.2015.08.043>.
- [53] A. Aflaki, N. Mahyuddin, and M. R. Baharum. The influence of single-sided ventilation towards the indoor thermal performance of high-rise residential building: A field study. *Energy and Buildings*, 126:146–158, 2016. URL <http://dx.doi.org/10.1016/j.enbuild.2016.05.017>.

- [54] A. Belleri, R. Lollini, and S. M. Dutton. Natural ventilation design: An analysis of predicted and measured performance. *Building and Environment*, 81:123–138, nov 2014. ISSN 03601323. doi: 10.1016/j.buildenv.2014.06.009. URL <http://linkinghub.elsevier.com/retrieve/pii/S0360132314001954>.
- [55] L. Moosavi, N. Mahyuddin, N. Ab Ghafar, and M. Azzam Ismail. Thermal performance of atria: An overview of natural ventilation effective designs. *Renewable and Sustainable Energy Reviews*, 34:654–670, 2014. ISSN 13640321. doi: 10.1016/j.rser.2014.02.035.
- [56] Q. Chen. Ventilation performance prediction for buildings: A method overview and recent applications. *Building and Environment*, 44(4):848–858, apr 2009. ISSN 03601323. doi: 10.1016/j.buildenv.2008.05.025. URL <http://linkinghub.elsevier.com/retrieve/pii/S0360132308001510>.
- [57] Gwelen Paliaga, Lawrence J Schoen, Peter F Alspach, Edward a Arens, Richard M Aynsley, Robert Bean, Josh Eddy, Thomas B Hartman, Daniel Int-hout, Michael a Humphreys, Essam Eldin Khalil, Michael P O Rourke, Peter Simmonds, John L Stoops, Stephen C Turner, Kenneth W Cooper, William F Walter, Douglass S Abramson, Charles S Barnaby, Steven J Emmerich, Julie M Ferguson, Richard L Hall, and Rita M Harrold. ASHRAE 55: Thermal Environmental Conditions for Human Occupancy. Technical report, 2013.
- [58] DEHLG. Irish Building Regulations - Technical Guidance Document L - Conservation of fuel and energy - buildings other than dwellings. Technical report, 2008.
- [59] Fergus Nicol and Michael Humphreys. Maximum temperatures in European office buildings to avoid heat discomfort. *Solar Energy*, 81(3):295–304, mar 2007. ISSN 0038092X. doi: 10.1016/j.solener.2006.07.007. URL <http://linkinghub.elsevier.com/retrieve/pii/S0038092X06001964>.
- [60] Don T Stevens, Paul Francisco, Steven J Emmerich, David A Baylon, Terry M Brennan, Roy R Crawford, David C Delaquila, Lance L Delaura, S Craig Drumheller, Philip W Fairey, Dwight H Heberer, Roger L Hedrick, Thomas P Heidel, Mark C Jackson, David E Jacobs, Glenn P Langan, Joseph W Lstiburek, Jane Malone, Stephany I Mason, James C Moore, Amy B Musser, John P Proctor, Paul H Raymer, Max H Sherman, Iain S Walker, Eric D Werling, and Charles S Barnaby. ASHRAE 62.1 Ventilation and Acceptable Indoor Air Quality. Technical report, ASHRAE, 2013.
- [61] Maria Kolokotroni, V Kukaïda, and E Perera. NATVENT - European project on overcoming technical barriers to low-energy natural ventilation. In *Proceedings CIBSE/ASHRAE Joint National Conference*, number Sept, pages 36–41, Harrogate, UK, 1996.
- [62] Maria Kolokotroni and Peter Warren. Building Advent: Building Advanced Ventilation technological examples to demonstrate materialised energy savings for indoor air quality and thermal comfort. In *Proceedings Indoor Air*, Copenhagen, Denmark, August 2008.
- [63] P Blondeau, M Spérandio, and F Allard. Night ventilation for building cooling in summer. *Solar Energy*, 61(5):327–335, 1997. URL <http://www.sciencedirect.com/science/article/pii/S0038092X97000765>.

- [64] S.A. et al Klein. TRNSYS 18: A Transient System Simulation Program, Solar Energy Laboratory,, 2017. URL <http://sel.me.wisc.edu/trnsys>.
- [65] G.A Florides, S.A Tassou, S.A Kalogirou, and L.C Wrobel. Measures used to lower building energy consumption and their cost effectiveness. *Applied Energy*, 73(3-4):299–328, 2002. ISSN 03062619. doi: 10.1016/S0306-2619(02)00119-8. URL <http://www.sciencedirect.com/science/article/pii/S0306261902001198>.
- [66] Lina Yang and Yuguo Li. Cooling load reduction by using thermal mass and night ventilation. *Energy and Buildings*, 40(11):2052–2058, jan 2008. ISSN 03787788. doi: 10.1016/j.enbuild.2008.05.014. URL <http://linkinghub.elsevier.com/retrieve/pii/S0378778808001308>.
- [67] Adams Rackesa and Michael S. Waring. Alternative ventilation strategies in U.S. offices: Comprehensive assessment and sensitivity analysis of energy saving potential. *Building and Environment*, 116:30–44, 2017. ISSN 03601323. doi: 10.1016/j.buildenv.2017.01.027. URL <http://linkinghub.elsevier.com/retrieve/pii/S0360132317300446>.
- [68] Ivan Oropeza-Perez and Poul Alberg ??stergaard. Potential of natural ventilation in temperate countries - A case study of Denmark. *Applied Energy*, 114:520–530, 2014. ISSN 03062619. doi: 10.1016/j.apenergy.2013.10.008. URL <http://dx.doi.org/10.1016/j.apenergy.2013.10.008>.
- [69] T. van Hooff, B. Blocken, L. Aanen, and B. Bronsema. A venturi-shaped roof for wind-induced natural ventilation of buildings: Wind tunnel and CFD evaluation of different design configurations. *Building and Environment*, 46(9):1797–1807, sep 2011. ISSN 03601323. doi: 10.1016/j.buildenv.2011.02.009. URL <http://linkinghub.elsevier.com/retrieve/pii/S0360132311000576>.
- [70] Yeong Sik Kim, Dong Hun Han, Hanshik Chung, Hyomin Jeong, and Soon-Ho Choi. Experimental study on Venturi-type natural ventilator. *Energy and Buildings*, 139:232–241, 2017. ISSN 03787788. doi: 10.1016/j.enbuild.2017.01.016. URL <http://linkinghub.elsevier.com/retrieve/pii/S0378778817300580>.
- [71] Naghman Khan, Yuehong Su, and Saffa B. Riffat. A review on wind driven ventilation techniques. *Energy and Buildings*, 40(8):1586–1604, jan 2008. ISSN 03787788. doi: 10.1016/j.enbuild.2008.02.015. URL <http://linkinghub.elsevier.com/retrieve/pii/S0378778808000443>.
- [72] Adam O’ Donovan, Paul. D. O’ Sullivan, and Michael D Murphy. A field study on the thermal comfort performance of a ventilative cooling system in a retrofitted low energy building. *Energy and Buildings*, 135:1–12, 2016. ISSN 03787788. doi: 10.1016/j.enbuild.2016.11.049. URL <http://dx.doi.org/10.1016/j.enbuild.2016.11.049>.
- [73] Cristian Ghiaus. Free-running building temperature and HVAC climatic suitability. d: 405–411, 2003.
- [74] Cristian Ghiaus and Francis Allard. Potential for free-cooling by ventilation. *Solar Energy*, 80(4):402–413, 2006. ISSN 0038092X. doi: 10.1016/j.solener.2005.05.019.

- [75] Christian Inard, Jens Pfafferott, and Christian Ghiaus. Free-running temperature and potential for free cooling by ventilation: A case study. *Energy and Buildings*, 43(10): 2705–2711, oct 2011. ISSN 03787788. doi: 10.1016/j.enbuild.2011.06.017. URL <http://linkinghub.elsevier.com/retrieve/pii/S0378778811002660>.
- [76] James W. Axley and Steven J. Emmerich. A Method to Assess the Suitability of a Climate for Natural Ventilation of Commercial Buildings. *Indoor Air 2002, 9th International Conference on Indoor Air Quality and Climate*, 2(December 2015):854–859, 2002.
- [77] D Bourgeois, A Potvin, and F. Haghghat. Hybrid Ventilation of Canadian non Domestic Buildings :A Procedure For Assessing IAQ , Comfort and Energy Conservation. In *Proceedings Of RoomVent 2002*. Elsevier Ltd, 2000.
- [78] Kevin John Lomas and Yingchun Ji. Resilience of naturally ventilated buildings to climate change: Advanced natural ventilation and hospital wards. *Energy and Buildings*, 41(6): 629–653, 2009. ISSN 03787788. doi: 10.1016/j.enbuild.2009.01.001.
- [79] Pieter de Wilde and David Coley. The implications of a changing climate for buildings. *Building and Environment*, 55:1–7, 2012. ISSN 03601323. doi: 10.1016/j.buildenv.2012.03.014.
- [80] Mat Santamouris. Cooling the buildings ??? past, present and future. *Energy and Buildings*, 128:617–638, 2016. ISSN 03787788. doi: 10.1016/j.enbuild.2016.07.034. URL <http://dx.doi.org/10.1016/j.enbuild.2016.07.034>.
- [81] Ana Tejero-Gonzalez, Manuel Andres-Chicote, Paola Garcia-Ibanez, Eloy Velasco-Gomez, and Francisco Javier Rey-Martinez. Assessing the applicability of passive cooling and heating techniques through climate factors: An overview. *Renewable and Sustainable Energy Reviews*, 65:727–742, 2016. ISSN 18790690. doi: 10.1016/j.rser.2016.06.077.
- [82] T. Kershaw, M. Eames, and D. Coley. Assessing the risk of climate change for buildings: A comparison between multi-year and probabilistic reference year simulations. *Building and Environment*, 46(6):1303–1308, jun 2011. ISSN 03601323. doi: 10.1016/j.buildenv.2010.12.018. URL <http://linkinghub.elsevier.com/retrieve/pii/S0360132310003707>.
- [83] C. Liu, T. Kershaw, M. E. Eames, and D. A. Coley. Future probabilistic hot summer years for overheating risk assessments. *Building and Environment*, 105:56–68, 2016. ISSN 03601323. doi: 10.1016/j.buildenv.2016.05.028. URL <http://dx.doi.org/10.1016/j.buildenv.2016.05.028>.
- [84] Sandhya Patidar, David Jenkins, Phil Banfill, and Gavin Gibson. Simple statistical model for complex probabilistic climate projections: Overheating risk and extreme events. *Renewable Energy*, 61:23–28, 2014. ISSN 09601481. doi: 10.1016/j.renene.2012.04.027.
- [85] Z. T. Ai and C. M. Mak. From street canyon microclimate to indoor environmental quality in naturally ventilated urban buildings: Issues and possibilities for improvement. *Building and Environment*, 94:489–503, 2015. ISSN 03601323. doi: 10.1016/j.buildenv.2015.10.008.

- [86] M. Santamouris, N. Papanikolaou, I. Koronakis, I. Livada, and D. Asimakopoulos. Thermal and air flow characteristics in a deep pedestrian canyon under hot weather conditions. *Atmospheric Environment*, 33(27):4503–4521, 1999. ISSN 13522310. doi: 10.1016/S1352-2310(99)00187-9.
- [87] Ch Georgakis and M. Santamouris. Experimental investigation of air flow and temperature distribution in deep urban canyons for natural ventilation purposes. *Energy and Buildings*, 38(4):367–376, 2006. ISSN 03787788. doi: 10.1016/j.enbuild.2005.07.009.
- [88] T. van Hooff and B. Blocken. On the effect of wind direction and urban surroundings on natural ventilation of a large semi-enclosed stadium. *Computers and Fluids*, 39(7):1146–1155, 2010. ISSN 00457930. doi: 10.1016/j.compfluid.2010.02.004. URL <http://dx.doi.org/10.1016/j.compfluid.2010.02.004>.
- [89] M. Kolokotroni, I. Giannitsaris, and R. Watkins. The effect of the London urban heat island on building summer cooling demand and night ventilation strategies. *Solar Energy*, 80(4):383–392, 2006. ISSN 0038092X. doi: 10.1016/j.solener.2005.03.010.
- [90] Steve Irving, David Etheridge, and Brian Ford. *Natural Ventilation in Non-domestic Buildings CIBSE AM10*. CIBSE, 2005. ISBN 1903287561.
- [91] David W. Etheridge and Mats . Sandberg. *Building ventilation: theory and measurement*. Wiley, 1996. ISBN 047196087 X.
- [92] Steve Sharples and Nelson Chilengwe. Performance of ventilator components for natural ventilation applications. *Building and Environment*, 41(12):1821–1830, dec 2006. ISSN 03601323. doi: 10.1016/j.buildenv.2005.08.012. URL <http://linkinghub.elsevier.com/retrieve/pii/S0360132305003343>.
- [93] W. G. Brown and K.R. Solvason. Natural convection through rectangular openings in partitions - 1: Vertical partitions. *International Journal of Heat and Mass Transfer*, 5:859–868, 1962. ISSN 00179310.
- [94] T. Yamanaka, H. Kotani, K. Iwamoto, and M. Kato. Natural, wind-forced ventilation caused by turbulence in a room with a single opening. *International Journal of Ventilation*, 5(1):179–187, 2006. ISSN 14733315.
- [95] J. P. Cockroft and P. Robertson. Ventilation of an enclosure through a single opening. *Building and Environment*, 11(1):29–35, 1976. ISSN 03601323. doi: 10.1016/0360-1323(76)90016-0.
- [96] H. Malinowski. Wind Effect on the air movement inside buildings. In *Third International Conference on Wind on Buildings and Structures*, pages 125–134, Tokyo, 1971.
- [97] P. R. Warren and L. M. Parkins. Single-sided ventilation through open windows. *ASHRAE SP49*, (1), 1985. URL <http://www.ornl.gov/sci/buildings/2012/1985B3papers/015.pdf>.

- [98] Masaya Narasaki, Toshio Yamanaka, and Masaaki Higuchi. Influence of Turbulent Wind on the Ventilation of an Enclosure with a single opening. *Environment International*, 15: 627–634, 1989.
- [99] RD Crommelin and EMH Vrins. Ventilation through a single opening in a scale model. *Air Infiltration Review*, 9(3):11–15, 1988.
- [100] Fariborz Haghighat, Jiwu Rao, and Paul Fazio. The influence of turbulent wind on air change rates—a modelling approach. *Building and Environment*, 26(2):95–109, 1991. ISSN 03601323. doi: 10.1016/0360-1323(91)90017-6.
- [101] J Rao, F Haghighat, and D Bienfait. Fluctuating airflow in buildings. In *Proc. of die 5th Int. Indoor Air Quality*, 1992.
- [102] H. Wang and Q. Chen. A new empirical model for predicting single-sided, wind-driven natural ventilation in buildings. *Energy & Buildings*, 54:386–394, 2012. ISSN 0378-7788. doi: 10.1016/j.enbuild.2012.07.028. URL <http://dx.doi.org/10.1016/j.enbuild.2012.07.028>.
- [103] J Van der Mass. Airflow through large openings in buildings (subtask 2): IEA Annex 20 : Air Flow Patterns within Buildings:. Technical report, 1992.
- [104] C. R. Chu, Y. H. Chiu, Y. T. Tsai, and S. L. Wu. Wind-driven natural ventilation for buildings with two openings on the same external wall. *Energy and Buildings*, 108:365–372, 2015. ISSN 03787788. doi: 10.1016/j.enbuild.2015.09.041. URL <http://dx.doi.org/10.1016/j.enbuild.2015.09.041>.
- [105] F. H. Champagne, Y. H. Pao, and I. J. Wygnanski. On the two-dimensional mixing region. *Journal of Fluid Mechanics*, 74(02):209, 1976. ISSN 0022-1120. doi: 10.1017/S0022112076001778.
- [106] P. E. Dimotakis. Turbulent Mixing. *Annual Review of Fluid Mechanics*, 37(1):329–356, 2005. ISSN 0066-4189. doi: 10.1146/annurev.fluid.36.050802.122015. URL <http://www.annualreviews.org/doi/abs/10.1146/annurev.fluid.36.050802.122015>.
- [107] K. Adams, E. Arens, D. Banks, S. Brunswick, G. Carrilho da Graca, N. Daish, S. Dutton, M. Fountain, B. Fisk, R. Gerard, F. Gillan, G. Gross, P. Haves, M. Hill, A. Honnekeri, M. Hovanec, T. Lawton, P. Linden, M. Pigman, P. Switenki, G. Szakats, R. Thomas, and Zhang H. Natural Ventilation For Energy Savings In California Commercial Buildings. Technical report, University of California, UC San Diego, California, 2014.
- [108] T. S. Larsen and P. Heiselberg. Single-sided natural ventilation driven by wind pressure and temperature difference. *Energy and Buildings*, 40(6):1031–1040, jan 2008. ISSN 03787788. doi: 10.1016/j.enbuild.2006.07.012. URL <http://linkinghub.elsevier.com/retrieve/pii/S0378778807002137>.
- [109] Rubina Ramponi, Adriana Angelotti, and Bert Blocken. Energy saving potential of night ventilation: Sensitivity to pressure coefficients for different European climates. *Applied Energy*, 123:185–195, 2014. ISSN 03062619. doi: 10.1016/j.apenergy.2014.02.041. URL <http://dx.doi.org/10.1016/j.apenergy.2014.02.041>.

- [110] C. R. Chu, R. H. Chen, and J. W. Chen. A laboratory experiment of shear-induced natural ventilation. *Energy and Buildings*, 43(10):2631–2637, oct 2011. ISSN 03787788. doi: 10.1016/j.enbuild.2011.06.014. URL <http://linkinghub.elsevier.com/retrieve/pii/S0378778811002635>.
- [111] M. Caciolo, P. Stabat, and D. Marchio. Full scale experimental study of single-sided ventilation : Analysis of stack and wind effects. *Energy & Buildings*, 43(7):1765–1773, 2011. ISSN 0378-7788. doi: 10.1016/j.enbuild.2011.03.019. URL <http://dx.doi.org/10.1016/j.enbuild.2011.03.019>.
- [112] David Etheridge. *Natural Ventilation of Buildings: Theory, Measurement and Design*. Wiley-Blackwell, 2011. ISBN 047066035X. URL <http://www.amazon.co.uk/Natural-Ventilation-Buildings-Theory-Measurement/dp/047066035X>.
- [113] E. Dascalaki, M. Santamouris, A. Argiriou, C. Helmis, D.N. Asimakopoulos, K. Papadopoulos, and A. Soilemes. On the combination of air velocity and flow measurements in single sided natural ventilation configurations. *Energy and Buildings*, 24(2):155–165, 1996. URL <http://www.sciencedirect.com/science/article/pii/S0378778896009735>.
- [114] A. A. Argiriou, C. A. Balaras, and S. P. Lykoudis. Single-sided ventilation of buildings through shaded large openings. *Energy*, 27(2):93–115, 2002. ISSN 03605442. doi: 10.1016/S0360-5442(01)00058-5.
- [115] W. De. Gids and H. Pfaff. Ventilation rates and energy consumption due to open windows: A brief overview of research in the Netherlands. *Air Infiltration Review*, 4(1):4–5, 1982.
- [116] M. Caciolo, S. Cui, P. Stabat, and D. Marchio. Development of a new correlation for single-sided natural ventilation adapted to leeward conditions. *Energy & Buildings*, 60:372–382, 2013. ISSN 0378-7788. doi: 10.1016/j.enbuild.2013.01.024. URL <http://dx.doi.org/10.1016/j.enbuild.2013.01.024>.
- [117] Y. Tang, X. Li, W. Zhu, and P. Lun Cheng. Predicting Single-sided Airflow Rates Based on Primary School Experimental Study. *Building and Environment*, 98:71–79, 2016. ISSN 03601323. doi: 10.1016/j.buildenv.2015.12.021. URL <http://www.sciencedirect.com/science/article/pii/S0360132315302195>.
- [118] Tine S. Larsen, Christoffer Plesner, and Valerie Leprince. Calculation methods for single-sided natural ventilation - simplified or detailed? In *CLIMA 2016 - proceedings of the 12th REHVA World Congress*, volume 5, page 11, 2016. URL http://vbn.aau.dk/files/233778874/paper_{ }753.pdf.
- [119] M Kolokotroni and a Aronis. Cooling-energy reduction in air-conditioned offices by using night ventilation. *Applied Energy*, 63(4):241–253, 1999. ISSN 03062619. doi: 10.1016/S0306-2619(99)00031-8.
- [120] Jong Hoon Kang and Sang Joon Lee. Improvement of natural ventilation in a large factory building using a louver ventilator. *Building and Environment*, 43(12):2132–2141, 2008. ISSN 03601323. doi: 10.1016/j.buildenv.2007.12.013.

- [121] Ben Richard Hughes and S. a a Abdul Ghani. A numerical investigation into the effect of Windvent louvre external angle on passive stack ventilation performance. *Building and Environment*, 45(4):1025–1036, 2010. ISSN 03601323. doi: 10.1016/j.buildenv.2009.10.010. URL <http://dx.doi.org/10.1016/j.buildenv.2009.10.010>.
- [122] J. Koffi, M. El Mankibi, E. Gourdon, and R. Issoglio. Assessment of single-sided ventilation with acoustic shutters on windows. *Building Simulation*, 8(6):689–700, 2015. ISSN 1996-3599. doi: 10.1007/s12273-015-0246-3. URL <http://link.springer.com/10.1007/s12273-015-0246-3>.
- [123] D. S. Lee, S. J. Kim, Y. H. Cho, and J. H. Jo. Experimental study for wind pressure loss rate through exterior venetian blind in cross ventilation. *Energy and Buildings*, 107:123–130, 2015. ISSN 03787788. doi: 10.1016/j.enbuild.2015.08.018. URL <http://linkinghub.elsevier.com/retrieve/pii/S0378778815302036>.
- [124] T. G. Mara. Influence of Solid Area Distribution on the Drag of a Two-Dimensional Lattice Frame. *Journal of Engineering Mechanics*, 140(3):644–649, 2014. ISSN 0733-9399. doi: 10.1061/(ASCE)EM.1943-7889.0000681. URL <http://www.scopus.com/inward/record.url?eid=2-s2.0-84894058474{&}partnerID=tZ0tx3y1>.
- [125] Nicole Carpman. Turbulence Intensity in Complex Environments and its Influence on Small Wind Turbines. (219):219, 2011. ISSN 1650-6553.
- [126] Stephen B Pope. *Turbulent flows*, 2001.
- [127] Peter Bradshaw. *An introduction to turbulence and its measurement: thermodynamics and fluid mechanics series*. Elsevier, 2013.
- [128] G. I. Taylor. The Spectrum of Turbulence. In *Proceedings of the Royal Society of London Series A, Mathematical and Physical Sciences*, pages 476–490. The Royal Society, 1938.
- [129] Erwin Kreyszig. *Advanced engineering mathematics*. John Wiley & Sons, 2010.
- [130] Robert H Shumway and David S Stoffer. *Time series analysis and its applications: with R examples*. Springer Science & Business Media, 2006.
- [131] J. W. Cooley and J. W. Tukey. An Algorithm for the Machine Computation of the Complex Fourier Series. *Mathematics of Computation*, 19:297, 1965. ISSN 00255718. doi: 10.2307/2003354.
- [132] Q. Ouyang, W. Dai, H. Li, and Y. Zhu. Study on dynamic characteristics of natural and mechanical wind in built environment using spectral analysis. *Building and Environment*, 41:418–426, 2006. ISSN 03601323. doi: 10.1016/j.buildenv.2005.02.008.
- [133] R. Gao, W. Zhang, Y. Zhang, and A. Li. Statistical Characteristics and Frequency Spectrum Analysis of Fan Induced Airflow Compared with Natural Winds. *International Journal of Ventilation*, 14(3):273–288, 2015.

- [134] X. Zhou, Q. Ouyang, G. Lin, and Y. Zhu. Impact of dynamic airflow on human thermal response. *Indoor Air*, 16:348–355, 2006. ISSN 09056947. doi: 10.1111/j.1600-0668.2006.00430.x.
- [135] A. Kolmogorov. The Local Structure of Turbulence in Incompressible Viscous Fluid for Very Large Reynolds' Numbers. *Akademiia Nauk SSSR Doklady*, 30:301–305, 1941.
- [136] Edward Arens, Tengfang Xu, Katsuhiko Miura, Zhang Hui, Marc Fountain, and Fred Bauman. A study of occupant cooling by personally controlled air movement. *Energy and Buildings*, 27:45–59, 1998. ISSN 03787788. doi: 10.1016/S0378-7788(97)00025-X.
- [137] P. O. Fanger, A. K. Melikov, H. Hanzawa, and J. Ring. Air turbulence and sensation of draught. *Energy and Buildings*, 12(1):21–39, 1988. ISSN 03787788. doi: 10.1016/0378-7788(88)90053-9.
- [138] Tyler Hoyt, Hui Zhang, and Edward Arens. Draft or breeze? preferences for air movement in office buildings and schools from the ASHRAE database Draft or Breeze? Preferences for air movement in office buildings and schools from the ASHRAE database. *Healthy Buildings*, pages 1–4, 2009. URL <http://escholarship.org/uc/item/99q2f4cf>5Cn<http://www.escholarship.org/help{ }copyright.html{#}reuse>.
- [139] J Toftum. Air movement—good or bad? *Indoor air*, 14 Suppl 7(Suppl 7):40–45, 2004. ISSN 0905-6947. doi: 10.1111/j.1600-0668.2004.00271.x. URL <http://www.ncbi.nlm.nih.gov/pubmed/22396505>5Cn<http://www.ncbi.nlm.nih.gov/pubmed/15330770>.
- [140] Marc Fountain, Edward Arens, Richard de Dear, Fred Bauman, and Katsuhiko Miura. Locally Controlled Air Movement Preferred in Warm Isothermal Environments. In *ASHRAE Annual General Meeting*, volume 100, pages 937–952, Orlando, 1994. ASHRAE Transactions.
- [141] Yingxin Zhu, Maohui Luo, Qin Ouyang, Li Huang, and Bin Cao. Dynamic characteristics and comfort assessment of airflows in indoor environments: A review. *Building and Environment*, 91:5–14, 2015. ISSN 03601323. doi: 10.1016/j.buildenv.2015.03.032. URL <http://www.sciencedirect.com/science/article/pii/S036013231500150X>.
- [142] Li Huang, Edward Arens, Hui Zhang, and Yingxin Zhu. Applicability of whole-body heat balance models for evaluating thermal sensation under non-uniform air movement in warm environments. *Building and Environment*, 75:108–113, 2014. ISSN 03601323. doi: 10.1016/j.buildenv.2014.01.020. URL <http://dx.doi.org/10.1016/j.buildenv.2014.01.020>.
- [143] E. Mayer. Physical causes for draft: Some new findings. volume 93, pages 540–548, 1987. URL <https://www.scopus.com/inward/record.uri?eid=2-s2.0-0023535679&partnerID=40&md5=6a7889be82bd201d5441126b556cc09d>. cited By 13.
- [144] Li Huang, Qin Ouyang, and Yingxin Zhu. Perceptible airflow fluctuation frequency and human thermal response. *Building and Environment*, 54:14–19, 2012. ISSN 03601323. doi: 10.1016/j.buildenv.2012.02.004. URL <http://dx.doi.org/10.1016/j.buildenv.2012.02.004>.

- [145] CIBSE. *CIBSE Guide A Environment Design*. 2010. ISBN 9780240812243. doi: 10.1016/B978-0-240-81224-3.00016-9.
- [146] NSAI. IS EN ISO 6946:2007 - Building components and building elements - thermal resistance and thermal transmittance - calculation method (ISO 6946:2007). Technical report.
- [147] UNI EN ISO 13786. Thermal performance of building components - Dynamic thermal characteristics - Calculation methods. page 42, 2007. URL <https://www.iso.org/obp/ui/{#}iso:std:iso:13786:dis:ed-3:v1:en>.
- [148] UNE-EN ISO 6946. Building components and building elements- Thermal resistance and thermal transmittance. page 36, 2012.
- [149] NSAI. ISO 10077-2:2012 Thermal performance of windows, doors and shutters - Calculation of thermal transmittance - Part 2 : Numerical method for frames. Technical report, 2012.
- [150] NSAI. IS EN 13779:2007 - Ventilation for non residential buildings - performance requirements for ventilation and room-conditioning systems. Technical report, National Standards Authority of Ireland, 2007.
- [151] Lawrence Berkeley National Laboratory. NFRC Simulation Manual, 2011.
- [152] B Knoll, JC Phaff, and WF De Gids. Pressure simulation program. In *DOCUMENT-AIR INFILTRATION CENTRE AIC PROC*, pages 233–233. OSCAR FABER PLC, 1995.
- [153] Claude-Alain Roulet. *Ventilation and Airflow in Buildings: Methods for Diagnosis and Evaluation (BEST (Buildings, Energy and Solar Technology))*. Routledge, 2007. ISBN 184407451X. URL <http://www.amazon.co.uk/Ventilation-Airflow-Buildings-Evaluation-Technology/dp/184407451X>.
- [154] AK Persily. Evaluating Building IAQ and Ventilation with Indoor Carbon Dioxide. *ASHRAE Transactions*, 103:4072, 1997. URL <http://fire.nist.gov/bfrlpubs/build97/PDF/b97044.pdf>.
- [155] Max Sherman. Tracer Gas Techniques for Measuring Ventilation in a Single Zone. *Building and Environment*, 25(4):365–374, 1990.
- [156] ASTM. ASTM E741-11 Standard Test Method for Determining Air Change in a Single Zone by Means of a Tracer Gas Dilution. *ASTM International*, 00(2006):1–18, 2011. doi: 10.1520/E0741-11.Copyright.
- [157] S. Cui, M. Cohen, P. Stabat, and D. Marchio. CO₂ tracer gas concentration decay method for measuring air change rate. *Building and Environment*, 84:162–169, jan 2015. ISSN 03601323. doi: 10.1016/j.buildenv.2014.11.007. URL <http://linkinghub.elsevier.com/retrieve/pii/S0360132314003606>.

- [158] H. Okuyama and Y. Onishi. Uncertainty analysis and optimum concentration decay term for air exchange rate measurements: Estimation methods for effective volume and infiltration rate. *Building and Environment*, 49(1):182–192, 2012. ISSN 03601323. doi: 10.1016/j.buildenv.2011.09.018. URL <http://dx.doi.org/10.1016/j.buildenv.2011.09.018>.
- [159] K.V. Mardia, Z.W. Birnbaum, and E Lukacs. *Statistics of Directional Data*. Elsevier B.V., 1972.
- [160] Z.T. Ai and C.M. Mak. Determination of single-sided ventilation rates in multistory buildings: Evaluation of methods. *Energy and Buildings*, 69:292–300, feb 2014. ISSN 03787788. doi: 10.1016/j.enbuild.2013.11.014. URL <http://linkinghub.elsevier.com/retrieve/pii/S0378778813006968>.
- [161] P Karava, T Stathopoulos, and AK Athienitis. Wind driven flow through openings a review of discharge coefficients. *International Journal of Ventilation*, 3(3), 2004. URL <http://www.ijoint.org/doi/abs/10.5555/ijov.2004.3.3.255>.
- [162] P. Heiselberg, Kjeld Svidt, and PV Nielsen. Characteristics of airflow from open windows. *Building and Environment*, 36:859–869, 2001. URL <http://www.sciencedirect.com/science/article/pii/S0360132301000129>.
- [163] Y-H. Chiu and D.W. Etheridge. External flow effects on the discharge coefficients of two types of ventilation opening. *Journal of Wind Engineering and Industrial Aerodynamics*, 95(4):225–252, apr 2007. ISSN 01676105. doi: 10.1016/j.jweia.2006.06.013. URL <http://linkinghub.elsevier.com/retrieve/pii/S0167610506000857>.
- [164] Jörn Von Grabe. Flow resistance for different types of windows in the case of buoyancy ventilation. *Energy and Buildings*, 65:516–522, 2013. ISSN 0378-7788. doi: 10.1016/j.enbuild.2013.06.035. URL <http://dx.doi.org/10.1016/j.enbuild.2013.06.035><http://www.sciencedirect.com/science/article/pii/S0378778813003848>.
- [165] Jörn von Grabe, Petr Svoboda, and Armin Bäumler. Window ventilation efficiency in the case of buoyancy ventilation. *Energy and Buildings*, 72:203–211, apr 2014. ISSN 03787788. doi: 10.1016/j.enbuild.2013.10.006. URL <http://linkinghub.elsevier.com/retrieve/pii/S037877881300652X>.
- [166] DJ Pinnock. *An investigation into the influence of wind in single-sided natural ventilation*. PhD thesis, Loughborough University, 2000. URL <https://dspace.lboro.ac.uk/xmlui/handle/2134/7465>.
- [167] T Lumley. *leaps: regression subset selection*, 2009. URL <https://CRAN.R-project.org/package=leaps>. R package version 2.9, using Fortran code by Alan Miller.
- [168] T. Hasama, S. Kato, and R. Ooka. Analysis of wind-induced inflow and outflow through a single opening using LES & DES. *Journal of Wind Engineering and Industrial Aerodynamics*, 96:1678–1691, 2008. ISSN 01676105. doi: 10.1016/j.jweia.2008.02.005.
- [169] H. Thomann. Effect of streamwise wall curvature on heat transfer in a turbulent boundary layer. *Journal of Fluid Mechanics*, 33:283–292, 8 1968. ISSN 1469-7645.

- doi: 10.1017/S0022112068001308. URL http://journals.cambridge.org/article_S0022112068001308.
- [170] C. Gau and C. M. Chung. Surface Curvature Effect on Slot-Air-Jet Impingement Cooling Flow and Heat Transfer Process. *Journal of Heat Transfer*, 113(4):858, 1991. ISSN 00221481. doi: 10.1115/1.2911214.
- [171] M. Choi, H. S. Yoo, G. Yang, J. S. Lee, and D. K. Sohn. Measurements of impinging jet flow and heat transfer on a semi-circular concave surface. *International Journal of Heat and Mass Transfer*, 43(10):1811–1822, 2000. ISSN 00179310. doi: 10.1016/S0017-9310(99)00257-4.
- [172] Paul D O’Sullivan, Adam O’Donovan, Guoqiang Zhang, and Guilherme Carrilho da Graca. Design and performance of ventilative cooling : a review of principals , strategies and components from International case studies. In *38th AIVC - 6th Tightvent - 4th Venticool*, 2017.
- [173] Marie Laure Delignette-Muller and Christophe Dutang. fitdistrplus: An R package for fitting distributions. *Journal of Statistical Software*, 64(4):1–34, 2015. URL <http://www.jstatsoft.org/v64/i04/>.
- [174] Annamaria Belleri, Theofanis Psomas, and Per Heiselberg. Evaluation Tool of Climate Potential for Ventilative Cooling. In *Proceeding of: 36th AIVC - 5th TightVent- 3rd venticool: "Effective ventilation in high performance buildings"*, pages 53–66, Madrid, 2017. AIVC.
- [175] S VanBuggenhout, A VanBrecht, S ErenOzcan, E Vranken, W Van Malcot, and D Berckmans. Influence of sampling positions on accuracy of tracer gas measurements in ventilated spaces. *Biosystems Engineering*, 104:216–223, 2009. doi: 10.1016/j.biosystemseng.2009.04.018.
- [176] Haojie Wang, Panagiota Karava, and Qingyan Chen. Development of simple semiempirical models for calculating airflow through hopper, awning, and casement windows for single-sided natural ventilation. *Energy and Buildings*, 96:373–384, 2015. ISSN 03787788. doi: 10.1016/j.enbuild.2015.03.041. URL <http://dx.doi.org/10.1016/j.enbuild.2015.03.041>.
- [177] Matthieu Labat, Monika Woloszyn, Géraldine Garnier, and Jean Jacques Roux. Assessment of the air change rate of airtight buildings under natural conditions using the tracer gas technique. Comparison with numerical modelling. *Building and Environment*, 60:37–44, feb 2013. ISSN 03601323. doi: 10.1016/j.buildenv.2012.10.010. URL <http://linkinghub.elsevier.com/retrieve/pii/S0360132312002752>.

Appendix A

Single Sided Ventilation Measurement Techniques

measuring volume flow rates is generally a straight forward task in ducted air systems. When the flow is bounded and unidirectional, flow measurement is achieved exploiting the relationship between different forms of energy in a stream of fluid and the Bernoulli principle. Introducing a reduction in cross sectional area of the duct causes a decrease in fluid pressure to accommodate the in velocity or kinetic energy of the fluid. The venturi tube or meter is an example of this approach. A pitot traverse is also sometimes employed which measures the dynamic pressure at a number of locations and calculates the velocity of the fluid with the results integrated to give the volume flow rate. Given that the airflow in a ducted system is created by a mechanical fan the flow is in one direction and this makes measurement convenient. However, a sufficient length of straight duct is needed upstream of the measuring location to ensure a developed velocity profile. These approaches are less suited to measurement of airflow rates in single sided naturally ventilated spaces. When using a single opening to ventilate a space flow across the opening will be bidirectional with fresh air entering and vitiated air exiting the space. In a situation with no wind the flow will be gravity driven with a s-shaped velocity profile figure below. When wind is simultaneously present the velocity pattern at the opening becomes more complicated. For this reason it is difficult to use velocity measurements in the opening alone to estimate the average ventilation rate as the velocity profile is unsteady and non-isotropically distributed making it difficult to obtain a sufficient number of measuring locations to calculate the net airflow exchange across the opening. Normally directional anemometers will be required, either 2D or 3D to ensure when a speed reading is recorded its direction is also known. Further, turbulent diffusion will be a dominant air exchange mechanism at certain wind directions and this again make it difficult to correctly estimate the ventilation rate using velocity measurement alone. Often tracer gas dilution techniques are employed to compliment velocity readings. This approach involves marking the internal air with a tracer gas. Once the gas is injected and uniformly mixed the ventilation opening is activated and a suitable method for monitoring and recording the evolution of the gas concentration with time is used. Various strategies are available for estimating the

TABLE A.1: Characteristics of commonly used tracer gases [157]

Tracer Gas	σ_{O_2}	Advantages	Disadvantages
Krypton-85 ^{85}Kr	2.93	-1 ppm in air	-Heavy -Expensive
Nitrous Oxide N_2O	1.53	-Low cost -Density similar to air	-Interacts with H_2O & CO_2
Sulfur Hexafluoride SF_6	5.11	-Not present in air -Not harmful	-Very heavy -Expensive -High GHG effect
Carbon Dioxide CO_2	1.53	-Easily available -Very low cost -Max 30000 ppm	-Exists in air

airflow rates; monitoring the gas concentration decay having stopped the injection, monitoring the concentration when injecting at a constant rate or monitoring the tracer gas concentration

A.1 Properties of Tracer Gases

Various gases have been used or proposed as tracers with different properties that make them attractive. A good tracer gas should be easily analysable with readily available equipment. Ideally there should be a low background concentration to avoid additional sources of noise in the sampled data. The gas should be neither flammable nor explosive and also be non toxic. To ensure good mixing and reduce additional uncertainty in the data from imperfect mixing and non representative sampling the density of the gas should be close to that of air. Of course this is not always possible and once the gas is actively mixed and suspended in the internal air this can often be acceptable. It should not be absorbed by furnishings as this will lead to erroneous results. Finally, it should be cheap and easily available with inexpensive transport and handling methods. Table 2.2 below, adapted from Cui et al [157], summarises some characteristics of common tracer gases.

Carbon Dioxide, CO_2 is probably the most commonly used tracer gas for assessing airflow in buildings. It is cheap, readily available, safe to use and a range of options exist for equipment to monitor its concentration in air. However, its main disadvantage is the high background concentration of CO_2 in air. This requires additional monitoring equipment, higher levels of CO_2 injection when marking the air and modification of the mass balance equations when estimating ventilation rates. SF_6 is also commonly used as a tracer gas and while it is not present in air is specialised and the gas itself is expensive. The advantages of using CO_2 as a tracer gas is the usefulness of the sensing equipment in other areas outside of airflow measurements, for example in occupancy monitoring and long term CO_2 monitoring of indoor air quality amongst others.

A.2 Mixing

Perfect mixing of the tracer gas in the air of the measured space is essential when determining airflow rates. This ensures that sampled data from individual locations give a good representation of the average concentration decay for the space and are not affected by non isotropic distribution of the tracer gas at the outset of the test, giving higher and lower concentration values over time in specific location not due to ventilation alone. Mixing is often achieved by positioning the gas injection nozzle upstream of a small mechanical desk fan. This disperses the gas as it enters the room, entraining it with the room air. Excellent mixing can be achieved within a couple of minutes using this approach. The number of sampling locations is also important for estimating airflow rates. Cui et al investigated the influence the number and position of in-situ sensors have on the measured airflow rate in a test chamber using CO₂ [157]. They found that locating sensors near the boundary walls or too low down resulted in larger measurement discrepancies. Keeping closer to the centre of the room and at heights above mid-height produced more accurate results. Buggenhout et al investigated how individual sensor locations can give erroneous results when predicting airflow rates using the 2 point decay technique [175]. They compared 36 different sensor locations and found errors as high as 86% in some instances. They didn't consider airflow rates estimated by averaging data from multiple sensor locations. The ventilation system was mechanical and they found best agreement with the between the fan airflow rate and the airflow rate calculated from the decay method using the outlet sensor position. However in single sided ventilation it is not possible to locate a sensor at the outlet as both the turbulent exchange process and the inflow/outflow regime through the single opening prevent any reasonable assessment of the average space air exchange rate.

A.3 Tracer Gas Analysers

There are a number of different options available for analysing tracer gas concentrations. They include infra-red (IR) absorption spectrometry, photo-acoustic detectors, mass spectrometry and chemical tube indicators. The choice of which to use is generally based on sensitivity to tracer gas quantity, selectivity of the analyser so as not to be sensitive to other gases present in air, speed of the analysis and accuracy of the results. Both dispersive and non dispersive Infra-red (NDIR) spectrometry sensors are commonly used as in-situ sensors but other techniques are also employed. The decision is often related to the availability of equipment or funding budget etc. For example, Caciolo et al used photo-acoustic detectors with SF₆ [111], Cui et al used two different types of NDIR detectors, in-situ and sampling based [157], Buggenhout used a BINOS 100 2M NDIR gas analyser [175], Larsen and Heiselberg used an Innova 3429A fast response Triple-gas photo-acoustic Monitor [108]. Tang et al used CO₂ and dry ice as a stable release method and thermo-hygrographs to analyse the gas [117]. Wang and Chen used SF₆ in combination with an INNVA 1309 multi point sampler and an INNOVA 1312 photo-acoustic analyser [176], Labat used CO₂ and IR analysers, a sampling based and an in-situ based [177]. Dascalaki used N₂O and IR analysers [113]. There are a number of additional methods for sampling during the test such as active grab sampling, passive grab sampling and using networks of tubes for multi zone

but these are not covered here. NDIR sensor, both in-situ and sampling based analysers along with photo-acoustic analysers seem to be the preferred option for most researchers. in-situ NDIR alphasense CO₂ sensors were used in this research. More information is provided in Section 3.3.

A.4 Analytical Methods

Before considering different analytical approaches to determining the airflow rate in a single zone using the concentration of a tracer gas we must first consider the continuity equation or the conservation of mass of tracer gas and air.

The change in the amount of air inside a zone is related to the net inflow, m_{ie} and outflow, m_{ei} :

$$\frac{d}{dt}\rho_i V = m_{ie} - m_{ei} \quad (\text{A.1})$$

Similarly the conservation of tracer gas will have an analogous expression with the air exchange weighted by the concentration ratios and include a term for the tracer gas mass flow:

$$\rho_i V \frac{dC_i}{dt} = m_{ie}C_i - m_{ei}C_e + m_t \quad (\text{A.2})$$

For mass conservation of air in the measurement space, $m_{ie} = m_{ei}$ and so:

$$\frac{d}{dt}\rho_i V C_i = m_{ei}(C_e - C_i) + m_t \quad (\text{A.3})$$

Transforming the mass flows and mass injections to their equivalent volumetric form using the respective density and setting:

$$C = C_i - C_e \quad (\text{A.4})$$

we can rewrite the above as:

$$V \frac{dC_i}{dt} + QC = Q_t \quad (\text{A.5})$$

In principle we can solve this equation directly to provide the airflow rate.

$$Q = \frac{Q_t - V \frac{dC_i}{dt}}{C} \quad (\text{A.6})$$

However, due to measurement problems, mixing and random concentration variations due to turbulence etc the calculation of an instantaneous ventilation rate can be highly inaccurate

and instead a time average value should be taken. We can integrate equation 2.49 for a given measurement time period:

$$\int_t^{t+\Delta t} Q dt = \int_t^{t+\Delta t} \frac{Q_t}{C} dt - V \int_t^{t+\Delta t} \frac{dC_i}{C} \quad (\text{A.7})$$

Therefore:

$$\int_t^{t+\Delta t} Q dt = \int_t^{t+\Delta t} \frac{Q_t}{C} dt - V[\ln(\Delta C(t)) - \ln(\Delta C(t + \Delta t))] \quad (\text{A.8})$$

Dividing both side by ΔT :

$$\bar{Q} = \left(\frac{\bar{Q}_t}{C} \right) - \frac{V}{\Delta t} \ln \left(\frac{\Delta C(t)}{\Delta C(t + \Delta t)} \right) \quad (\text{A.9})$$

There are a number of approaches to solving for the ventilation rate, Q or the air change rate, N , (h^{-1}), directly, depending in the specific experimental technique adopted. We present 3 different techniques. These are known as transient techniques and depend on different ways of characterising the change in tracer gas concentration in the room. They all measure N :

$$N = \frac{Q}{V} \quad (\text{A.10})$$

A.4.1 Tracer Decay, Two Point Average Decay Method

For the 2 point average tracer decay approach with no continuous injection during the measurement period a suitable quantity of gas is injected to achieve an initial concentration, $C_i(t_0)$. At time, t_0 , the injection is stopped and $Q_t = 0$ thereafter. From equation 2.49 we can show that the concentration decays with time according to

$$C = C(0) e^{-Nt} \quad (\text{A.11})$$

Since $Q_t = 0$ equation 2.53 becomes:

$$\bar{Q} = -\frac{V}{\Delta t} \ln \left(\frac{\Delta C(t)}{\Delta C(t + \Delta t)} \right) \quad (\text{A.12})$$

We can use this method with two measurements of the internal and background concentration, an initial concentration at the beginning of the measurement period when the tracer gas injection has stopped and the tracer gas is fully mixed with the internal air in the space, and a final concentration at the end of the measurement period. According to Sherman if the ventilation air change rate varies over the measurement period this technique assures an unbiased estimate of the average [155]. However, it is a less precise technique than the others.

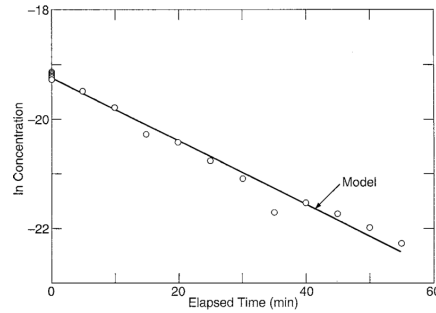


FIGURE A.1: concentrations and estimate of concentrations plotted logarithmically against elapsed time. [156]

A.4.2 Tracer Decay, Regression Method

Again, as above, if there is no tracer gas injection during the measurement period and we allow the tracer to decay from some initial concentration, the concentration decay should be according to equation 2.55. Taking the natural log of the normalised concentration linearises the decay data, equation 2.57. See Figure 2.20 adapted from [156] for an example of this approach.

$$C_n = \ln \frac{C(t) - C_e}{C(0) - C_e} \quad (\text{A.13})$$

Using a linear regression least squares fit of the data we can obtain N from equation 2.58. This gives a value for N that best fits the measurement data.

$$\ln C(t) = -Nt + \ln C(0) \quad (\text{A.14})$$

Measurement Uncertainty - Decay Technique

There are a number of sources of uncertainty when using tracer gas techniques, namely (1) tracer gas injection and distribution procedures, (2) tracer gas sampling and storage (3) changes in wind, temperature and zonal operation regimes and (4) tracer gas concentration determination. ASTM741-11 states that where its procedures are followed an overall uncertainty of 10% can be expected in the ACR measurement results [156]. Caciolo estimated the uncertainty based on error propagation analysis with full scale measurement data to be $\pm 25\%$ [111] while Cui et al suggested uncertainty could be up to $\pm 15\%$ using in-situ CO_2 sensors based on their laboratory study [157]. Larsen estimates uncertainty of $\pm 5\%$ in their tracer decay ACR measurements [108] while Etheridge and Sandberg calculated error measurements of $11\% \pm 6\%$ based laboratory investigations [91]. For this research we summarise tracer gas concentration determination (i.e. gas sensor precision and bias) along with uncertainty due to injection and distribution (i.e. improper mixing) in sections 3.3.2.2 and 3.3.3.2. Tracer gas sampling and storage is not relevant with the in-situ gas sensor approach. Changes in wind and temperature will result in an unsteady ACR value during testing and an uncertainty is associated with the assumption the ACR is constant during testing.

The degree to which sampled data points conform to the model predicted by a smooth tracer gas decay can be an indication of the uncertainty with the assumption of steady state conditions. The spread of data about the model can be used to estimate this uncertainty [156]. As discussed it is convenient to linearise the TGCD data using a log of the values as shown in Figure 2.20. When using linear regression to estimate the ACR, N , equation 2.58, from a sample of the population, the Students t -distribution is proposed to represent possible values for N depending on the level of confidence. Using the t -distribution we can establish the confidence in N . From ASTM741-11 we can use equation 2.59 for this purpose:

$$\epsilon_N(t) = N \pm \sigma_N t(n - 2, 1 - \alpha) \quad (\text{A.15})$$

We have two degrees of freedom (slope and intercept). We use this formula to calculate the uncertainty for each test to obtain knowledge about the uncertainty in the measurement data. We calculate the standard error of estimate for the linear fitted model predicting ACR, σ_N , using the following formula:

$$\sigma_N = \frac{\sigma_c}{\sqrt{n}} \quad (\text{A.16})$$

σ_c is estimated using equation 4.2, chapter 4, page 124, n represents the number of data points used in the regression model to predict ACR, N . Uncertainty in the ACR measurement data is presented along with the results in Chapter 4 and 5.

Optimum Decay Time

When using the TGCD technique it is important to select a test duration that minimises uncertainty in the result. Table 2 of ASTM741-11 presents minimum decay durations for various ACR based on a 10% uncertainty at the 95% confidence level in the determination of ACR and a TGCD measurement precision error of 5% of reading [156]. The equation used for estimating the minimum decay time in Table 2, depending on the ACR value, N , and the measurement uncertainty is:

$$T_{op} \geq \frac{20}{N} \epsilon_{meas} \quad (\text{A.17})$$

The difficulty with this approach is the need to estimate N in advance of knowing the decay time given the decay time is needed to calculate N . It is useful when a reasonably acceptable approximate for N can be chosen at the outset.

Sherman [155] suggested for the two point decay technique that the test duration should be only as long as the decay time. He proposed that the ACR uncertainty can be estimated from equation 2.61 below and setting $t_{op} \approx 1/N$ we have a limit for ACR uncertainty of equation 2.62.

$$\epsilon_N \approx \frac{\sqrt{1 + e^{2Nt_{op}}}}{t_{op}} \frac{\epsilon_C}{C(0)} \quad (\text{A.18})$$

$$\frac{\epsilon_N}{N} \geq 3 \frac{\epsilon_C}{C_i} \quad (\text{A.19})$$

Okuyama and Onishi stated that if the measurement error of each measurement data point is the same then there exists an uncertainty propagation in concentration measurements and applying an optimum decay time can minimise the errors associated with the estimation of ACR [158]. Based on their equation for ACR, the uncertainty propagation law for the estimated error variance and the decay model they developed a recurrence relation for the lumped parameter term Nt_{op} which can be solved iteratively. The lumped parameter Nt_{op} gives the optimum decay time for a given N . They showed through numerical analysis that this product has a value of 1.23 for 30 measurement points and converges to 1.25 for 60 measurement points or greater. When N is unknown the lumped parameter Nt_{op} must be solved for iteratively by first calculating N for an initial time period, t , then assessing the value of Nt to establish if it is in the asymptotic range. This is repeated with increasing time intervals until a value close to 1.25 is obtained giving the optimum decay time and minimising the error due to measurement error propagation. This approach is adopted in Chapter 5 and the numerical script used to solve the equation is described therein.

A.4.3 Constant Concentration

In the constant concentration approach some form of mass flow controller is employed along with the tracer gas analyser to maintain the tracer concentration constant in the measurement space. This approach adjusts the flow of tracer continuously in response to changes in the amount of tracer in the space from the ventilation rate. The time derivative of tracer concentration is subsequently zero and the ventilation rate can be calculated from equation 2.63 as:

$$Q = \frac{Q_t}{C} \quad (\text{A.20})$$

This method requires additional equipment and a mass flow meter control strategy compared with the tracer decay methods. It also provides an unbiased estimate of the ventilation rate.

A.4.3.1 Constant Injection Rate

If the injection rate, Q_t , is constant we can solve the differential equation as:

$$C(t) = \frac{Q_t}{Q} + \left(C - \frac{Q_t}{Q} e^{-Nt} \right) \quad (\text{A.21})$$

However, after a sufficiently long time, assuming a constant airflow rate, with steady state conditions achieved the exponential term disappears and equation 2.64 becomes:

$$Q = \frac{Q_t}{C} \text{ for } e^{-Nt} \ll 1 \quad (\text{A.22})$$

The result will be biased if the ventilation rate is not constant. The result will not be biased however if the following condition is met:

$$\left| \ln \left(\frac{C_{final}}{C_{initial}} \right) \right| \ll NT \quad (\text{A.23})$$

Appendix B

IEA-EBC Annex 62 VC Potential Analysis

In this appendix the method developed within Subtask A of IEA-EBC Annex 62 for predicting the ACR required for ventilative cooling of a given internal space at a given location is outlined. This method is utilised herein for the purposes of estimating the required ACR for ventilative cooling of the experimental test space at zero2020, described in Chapter 3. The theoretical underpinning of the VC potential tool is based on the method proposed by Axley and Emmerich [76] and further developed within IEA-EBC Annex 62.

The method proposes the calculation of a heating balance point temperature, T_{bp} , for a given building which defines the external ambient temperature, T_e , at which no heating or cooling is required to maintain a defined internal set-point temperature, T_{sp} . Below this temperature supplementary heat energy is required to maintain the desired set-point temperature. Above this value heat energy will need to be removed (cooling mode) to maintain the desired set-point temperature. Adjusting the set-point temperature based on a particular criteria (for example using the adaptive thermal comfort model) will result in a different heating balance point temperature. T_{bp} can be defined mathematically as:

$$T_{bp} = T_{sp} - \frac{E_T(t)}{\dot{m}_{mn} \cdot c_p + \sum UA} \quad (\text{B.1})$$

Equation 6.1 shows that T_{sp} is adjusted according to the net energy balance between total internal gains, E_T , and the energy exchanges due to the minimum indoor air quality ventilation rate requirement, \dot{m}_{mn} , and the thermophysical properties of the envelope, $\sum UA$. According to Axley and Emmerich [76] this equation derives from the energy balance of a well mixed single zone delimited by heat transfer at the boundary surfaces and relies on the assumption that the accumulation term of the energy balance can be negligible, which is reasonable if the thermal mass in the space is small or the indoor temperature is regulated to remain constant. Under these assumptions the model is steady state and can give an approximate means to characterising the ventilative cooling potential of a climate. As explained below, E_T is a variable quantity and

so T_{bp} will also vary at each time step. This means recalculating T_{bp} at each time step also. In principal a calculation is completed at each time interval based on the granularity of weather data used in the assessment. In this instance hourly data was used. The step by step approach at each time step, t , can be summarised as follows:

- Calculate individual and total heat gains
- Calculate balance point temperature, T_{bp}
- Calculate thermal comfort upper and lower limit temperatures T_{cu} and T_{cl}
- Assess VC mode criteria
- Determine required mass flowrate (and in turn the required ACR)

These are detailed further below.

B.1 Calculate Heat Gains

Heat gains are calculated at each time step individually and as functions of floor area, A_f , before being summed to establish the total gain to the space at time, t . Firstly, calculate the total casual internal heat gain to the space, $E_c(t)$, at a given time step, t , inclusive of occupancy sensible heat gain, lighting and PC heat gains. $E_{ci}(t)$ are individual casual gains, anything from steady heat production from lighting and equipment in the zone to sensible heat generation from occupants. The total heat gain associated with all static or process loads, $E_c(t)$ can be defined as:

$$E_c(t) = \sum_{i=1}^n \frac{n_i(t) \cdot E_{ci}(t) \cdot h_i(t)}{A_f} \quad (\text{B.2})$$

Where n is the quantity of casual gain type i , (i.e. lets say casual gain i is occupant sensible heat gain in our model), E_{ci} is the specific gain in $\frac{W}{m^2}$ and A_f is the floor area of the zone in m^2 . h_i represents the hourly profile for the heat gain, i.e. active or otherwise. The heat generation rate from these are usually calculated separately and summed as shown above. Typically these are provided based on a given load per zone floor area, W/m^2 . If not they are adjusted prior to calculation.

Once casual gains have been determined then calculate the solar gain contribution, E_s , taking into account the shading performance of the fenestration system. This is based on the hourly global horizontal irradiation and is adjusted for inclination and azimuth angles of the faade. The solar gains are calculated as follows:

$$E_s(t) = \frac{G(t) \cdot A_g}{A_f} \cdot S_G \quad (\text{B.3})$$

Both solar heat gains, $E_s(t)$ and total casual heat gains, $E_c(t)$, are summed at time step, t , to give $E_T(t)$. Once this has been calculated the balance point temperature can then be established

which allows assessment of whether or not some ventilative cooling is needed at the give time step, t , depending on criteria outlined as follows. Fabric gains are incorporated to the energy balance calculation when establishing T_{bp} and are not included in the specific heat gains calculations above.

B.2 Thermal Comfort Threshold Temperatures

Having established the balance point temperature at a given time step, t , the next task is to define the upper and lower temperature limit of the acceptable comfort range for the conditions at the particular time step of interest. This is generally calculated using the adaptive thermal comfort model in EN 15251 with equations 6.4 and 6.5 below:

$$T_{cu}(t) = 0.33 \cdot T_{rm}(t) + 18.8 + K \quad (\text{B.4})$$

$$T_{cl}(t) = 0.33 \cdot T_{rm}(t) + 18.8 - K \quad (\text{B.5})$$

T_{rm} is taken as the outdoor running mean calculated initially using the last 7 days in the previous year as follows, i.e. for $n = 7$.

$$T_{rm}(t) = \frac{T_{e(t-1)} + 0.8 \cdot T_{e(t-2)} + 0.6 \cdot T_{e(t-3)} + \sum_{i=4}^n 0.9 - (0.1 \cdot i) \cdot T_{e(t-i)}}{3.8} \quad (\text{B.6})$$

Where $T_{rm}(t)$ is below 10°C , the upper temperature limit is set as the upper limit for heating recommended by EN 15251:2007, in the case of an office space, 24°C . Where $T_{rm}(t)$ is below 15°C , the lower temperature limit is set as the lower limit for heating recommended by EN 15251:2007, in the case of an office space 20°C . Lower and upper temperature limits are calculated at each time step, t , in order to define the acceptable indoor temperature range for comfort. These values can then be used to determine whether cooling is needed and if so what is the required ventilative cooling ACR value to achieve these conditions. \dot{m}_{vc} is the airflow rate adjusted above the minimum value required for IAQ, \dot{m}_{mn} , calculated using the following equation:

$$\dot{m}_{vc}(t) = \frac{E_T(t)}{c_p \cdot (T_{cu}(t) - T_e(t))} \quad (\text{B.7})$$

Whether or not ventilative cooling is required and to what magnitude the airflow rate will be is based on the an assessment of indoor and outdoor conditions at each time step as follows.

B.3 VC modes

To determine when ventilative cooling is needed and whether; (a) the minimum IAQ airflow rate will be sufficient, (b) an enhanced airflow rate \dot{m}_{vc} is needed or, (c) no VC is possible at the time step, the following conditional arguments are tested at each time step, t :

$$\text{VC mode} = \begin{cases} 0 & \text{if } T_e \leq T_{bp}, \\ 1 & \text{if } T_{bp} \leq T_e < T_{bp} + (T_{cu} - T_{cl}), \\ 2 & \text{if } T_{bp} + (T_{cu} - T_{cl}) \leq T_e < T_{cu} - T_{cr}, \\ 3 & \text{if } T_e \geq T_{cu} - T_{cr} \end{cases} \quad (\text{B.8})$$

If T_e is below T_{bp} this is Mode 0 and represents the heating mode for the space and as such no ventilative cooling takes place. The minimum mass airflow rate is factored into the calculation of T_{bp} for IAQ purposes is not deemed to be providing cooling due to the value of T_e , but is still required. The next sequential conditional argument assesses whether T_e is above T_{bp} , identifying a cooling need, but is below the lower limit of the comfort range, meaning that only a minimum airflow rate is available for cooling due to the external ambient conditions being outside the acceptable comfort range. If T_e is above the lower limit temperature range and below the upper limit, including an offset for the fact that no valuable contribution can be made if the ambient temperature is too close to the upper limit temperature, then enhanced ventilative cooling is possible and mode 2 is selected. When T_e is above the upper limit temperature, no VC is possible and mode 3 is allocated. Where conditions are evaluated as mode 1 at the given time step, t , then the VC airflow rate is calculated as \dot{m}_{mn} . When conditions are evaluated as mode 2 the VC airflow rate is calculated as \dot{m}_{vc} , a larger airflow rate required to maintain the internal space temperature at the upper limit value given the net heat gains to the space.

The process of calculating $T_{bp}(t)$, $Q_T(t)$, $T_{cl}(t)$, $T_{cu}(t)$, VC mode and \dot{m} is repeated sequentially for all 8760 time steps in the model. Once these have been calculate it is then possible to identify the percentage of annual occupied hours in the year that ventilative cooling is available and has the potential to provide comfortable conditions. The results are influenced by the building properties, usage profiles and boundary conditions.